Development and Characterization of Collagen type I and Hyaluronic acid (HA) based Interlaced Scaffolds for Tissue Engineered Heart Valves (TEHVs)

RABIA NAZIR

ST PETER'S COLLEGE



A THESIS SUBMITTED FOR THE DEGREE OF

DOCTOR OF PHILOSOPHY

DEPARTMENT OF MATERIALS

UNIVERSITY OF OXFORD

MICHAELMAS TERM 2017

Abstract

An ideal scaffold for the regeneration of valvular tissue should replicate the natural heart valve extracellular matrix (ECM) in terms of microstructure and properties. Tissue engineers have achieved limited success so far in designing an ideal scaffold; scaffolds lack in mechanical compatibility, appropriate degradation rate, and microstructural similarity. This thesis, therefore, is the first attempt to develop interlaced scaffolds from collagen type I and hyaluronic acid (HA), polymers found in the natural valve, via a modified carbodiimide based crosslinking technique. Scanning electron micrographs (SEM) and images of Alcian blue – Periodic acid Schiff (PAS) stained samples suggested that our crosslinking technique yielded an ECM mimicking microstructure with interlaced bands of collagen and HA in the hybrid scaffolds. Hybrid scaffolds also offered a wide range of pore size (66 – 126 μm) which fulfilled the criteria for valvular tissue regeneration. Swelling studies revealed that crosslinking densities of parent networks increased with increasing the concentration of the crosslinking agents whereas crosslinking densities of hybrid scaffolds averaged from those of parent collagen and HA networks. Fourier transform infrared spectroscopy (FTIR) and thermogravimetric analysis (TGA) showed that this technique could crosslink collagen type I and HA without denaturation. Also, no intermediate phase formation between collagen and HA could be detected.

Elastic moduli increased with increasing crosslinking densities, in the dry and wet state, for parent networks whereas those of interlaced scaffolds were higher than either network alone. Compressive, bending, and storage moduli ranged from 35 ± 5 kPa to 95 ± 5 kPa, 154 ± 12 kPa to 1660 ± 7 kPa, and 16 ± 2 kPa to 113 ± 6 kPa respectively in the dry state. Corresponding wet mechanical moduli ranged from 1 ± 0.3 kPa to 5 ± 0.1 kPa, 7 ± 2 kPa to 55 ± 4 kPa, and 2 ± 0.4 to 9 ± 2 respectively. Bending and storage moduli, in the dry state, matched and exceeded those of human aortic valve leaflets (HAVL). Similarly, degradation resistance increased with increasing the crosslinking densities for collagen only and HA only scaffolds. Interlaced scaffolds showed partial degradation in the presence of either collagenase or hyaluronidase as compared to when exposed to both enzymes together. These results agreed with FTIR and SEM that interlaced scaffolds were composed of independent collagen and HA networks without crosslinking between them.

Cardiosphere derived cells (CDCs) attached and proliferated on all scaffolds in cell culture experiments as confirmed by AlamarBlue® assay and SEM images. The increase in crosslinking density, however, affected the cell affinity because of the engagement of the cell-attachment sites in the crosslinking process. CDCs seeded scaffolds also showed 50 % increase in bending modulus after 28 days of culture. While evaluated against the criterion for tissue engineered heart valve (TEHV), S-3 and S-4 among interlaced scaffolds/compositions not only matched mechanically but also showed high degradation resistance which potentially made them as **'close-fit'** candidates. Findings from this thesis indicated that collagen/HA interlaced scaffolds have the potential to fill in the niche for designing an ideal TEHV. Furthermore, the properties of the interlaced scaffolds, fabricated by our crosslinking technique, can be tailored by controlling the crosslinking density which can also widen the scope of these scaffolds for other tissue engineering applications such as bone, cartilage etc.

Preface

The research described in this thesis was carried out by the author in the Department of Materials at the University of Oxford between October 2013 and March 2016, under the supervision of Dr. Jan. T. Czernuszka. No part of this thesis has been submitted or accepted for any other degree at this university or elsewhere.

Part of this work has been peer-reviewed and published in Journals, or presented at international conferences as follows:

1. [*] Rabia Nazir, Collagen–hyaluronic acid based interpenetrating polymer networks as tissue engineered heart valve, *Materials Science and Technology*, 32:871-882, 2016.
2. Arne Bruyneel, Rabia Nazir, Qi Chen, Colleen Lopez, Jan Czernuszka, and Carolyn Carr, Cardiosphere-derived cell-seeded porous collagen scaffolds for cardiac repair, *Heart*, 2016 (Accepted).
3. Rabia Nazir, Collagen–Hyaluronic acid (HA) based Interpenetrating Polymer Networks (IPNs) as Tissue Engineered Heart Valve (TEHV), *27th European Conference on Biomaterials*, Krakow, Poland, 2015.

[*]The review article won first prize in 'Postgraduate Literature Review Competition 2015' organized by Institute of Material, Minerals, and Mining (IOM^3).

Acknowledgements

I would like to acknowledge the following supports from all the generous people, without them this thesis would never have been completed. Regrettably, but inevitably, the list of names will be incomplete, and I hope that those who are missing will forgive me and will still accept my sincere appreciation of their influence on my work.

I would like to express my special appreciation and thanks to my advisor Professor Dr. Jan. T. Czernuszka. You have been a tremendous mentor for me. I would like to thank you for encouraging my research and for allowing me to grow as an independent research scientist. I appreciate the valuable suggestions by my examiners Dr. Keven Shoksheff and Dr. Nicole Grobert to improve this thesis.

I would like to thank COMSATS Institute of Information Technology (CIIT), Pakistan for funding my D.Phil studies at the University of Oxford and giving me a life-changing experience. I am grateful to all my colleagues at IRCBM for their moral support.

My sincere gratitude goes to Dr. Carolyn Carr, Dr. Arne Bruyneel and Colleen Lopez from the Cardiac Metabolism Research Group in the Department of Physiology, Anatomy and Genetics for a fruitful collaboration, particularly Arne for training me on the cell culture techniques. I had a great time there while sharing office space with Collen, Sophia, Hiba, and Jack.

I deeply appreciate the support from the technical staff at Oxford Materials. I would like to thank Dr. Paul Warren and Chris Akinola for their patience with the breakdowns of my laptop. Thanks to Dr. Colin Johnston, Dr. Alison Crossley, Gabriella Chapman (Late), Chris Salter, and Susan Warren for their technical support with scanning electron microscope (SEM), Fourier transform infrared spectroscopy (FTIR), and thermogravimetric analysis (TGA).

Thanks to my former and current group mates in Biomaterials group at Oxford; Dr. Qi Chen, Dr. Jessica Smith, Xue Min, Narjes Rashidi, Fang Li, Sonia Iftikhar, and Jim Yang for the inspiring discussions and valuable knowledge shared.

Special thanks to Dr. Rafaqat Hussain for investing time in proofreading this thesis word by word.

It was great to know a bunch of wonderful souls at Oxford; Fozia, Bo, Shifali, Kokil, Momina, Gustawo, Huma, Ping, Rachita, Viviana, Pedro, and Karan. Thank you, Shaista Siddique and Maria Tahir Azam for always being there with open arms. Thank you Syrul Hussain and Tasneem Johra for feeding me loads of delicious Asian food and playtimes with your little angel 'Araa Sushmeen'.

Thanks to my host family in Oxford; Kelston Chorley, Asima Rafath-Chorley, Ayesha, and Rafi for all the love and care. You made me feel living in a home away from home.

Finally, special thanks to my beloved family: My parents, Nazir Ahmad and Shahida Nazir for giving birth to me in first place and then raising me as I am today. My brothers, Aneel Ahmad and Arhum Nazir, have always been strong pillars of support for me. I am also thankful to my aunts Rashida Tariq and Asma Aftab for their endless love and prayers.

Rabia Nazir, Oxford, 2017.

Table of Contents

Abstract i

Preface iii

Acknowledgment iv

Chapter No.1. Introduction and Literature Review

1.1 Background 1

1.2 Thesis proposal 5

1.2.1 Problem statement 5

1.2.2 Objectives of thesis 6

1.2.3 Outline of thesis 8

1.3 Anatomy of the aortic heart valve 9

1.3.1 Aortic root 10

1.3.2 Ascending aorta 11

1.3.3 Aortic valve leaflets 12

1.3.3.1 Fibrosa 13

1.3.3.2 Spongiosa 14

1.3.3.3 Ventricularis 14

1.3.4 Cellular makeup of the aortic valve leaflet 15

1.3.4.1 Valvular endothelial cells (VECs) 15

1.3.4.2 Valvular interstitial cells (VICs) 15

1.3.4.3 Neurons 16

1.3.5 Biomechanics of the aortic heart valve 16

1.3.5.1 Inter-layer load transition during systole-diastole 16

1.3.5.2 Modelling of aortic valve leaflet 18

1.3.5.3 Viscoelastic behaviour of valvular tissue 20

1.3.6 Collagen and Hyaluronic acid (HA) as potential materials for tissue engineered heart valve (TEHV) 21

1.3.6.1 Molecular structures 23

1.3.6.2 Collagen/HA based hybrid scaffolds in heart valve tissue engineering 27

1.3.6.3 Crosslinking routes for the fabrication of collagen-HA based hybrid scaffolds 31

1.3.6.4 Biocompatibility of collagen/HA-based hybrid scaffolds 39

1.4 Conclusion 45

Chapter No.2. Fabrication and Microstructural Characterization of Collagen/HA Hybrid Scaffolds

2.1 Introduction 47
2.2 Materials and methods 48
2.2.1 Synthesis of collagen network 48
2.2.2 Synthesis of HA network 49
2.2.3 Synthesis of collagen/HA hybrid scaffolds 50
2.2.4 Crosslinking density and swelling behaviour 53
2.2.5 Scanning electron microscopy (SEM) 54
2.2.6 Alcian blue-periodic acid (PAS) differential staining 55
2.2.7 Fourier transform infrared spectroscopy (FTIR) 56
2.2.8 Thermogravimetric analysis (TGA) 57
2.2.9 Statistical analysis 57
2.3 Results 58
2.3.1 Crosslinking density and swelling behaviour 58
2.3.2 SEM and pore size analysis 60
2.3.3 Alcian blue-periodic acid (PAS) differential staining 64
2.3.4 Fourier transform infrared spectroscopy (FTIR) 66
2.3.5 Thermogravimetric analysis (TGA) 70
2.4 Discussion 72
2.5 Conclusion 77

Chapter No.3. Mechanical Properties of Collagen/HA Hybrid Scaffolds

3.1 Introduction 79
3.2 Materials and methods 80
3.2.1 Compression test 80
3.2.2 Bending test 81
3.2.2.1 Three-point bend test (dry condition) 81
3.2.2.2 Self-deflection bending test (wet condition) 82
3.2.3 Dynamic mechanical properties 83
3.2.4 Rheology test 84
3.2.5 Statistical analysis 84
3.3 Results 85
3.3.1 Compression test 85
3.3.2 Bending test 88
3.3.2.1 Three-point bend test (dry condition) 88

3.3.2.2 Self-deflection bending test (wet condition) 91
3.3.3 Dynamic mechanical properties 93
3.3.4 Rheology testing 99
3.4 Discussion 100
3.4.1 Effect of crosslinking density and interlacing on E_{comp} 100
3.4.2 Effect of crosslinking density and interlacing on E_{bend} 102
3.4.3 Effect of crosslinking density and interlacing on dynamic mechanical properties 103
3.4.4 Effect of crosslinking density on the mechanical properties of collagen network under wet conditions 105
3.4.5 Effect of crosslinking density and interlacing on the mechanical properties of hybrid scaffolds under wet conditions 105
3.4.6 Comparison of mechanical properties of hybrid scaffolds with the human aortic valve leaflet (HAVL) 106
3.5 Conclusion 109

Chapter No.4. Degradation Behvaiour of Collagen/HA Hybrid Scaffolds

4.1 Introduction 111
4.2 Materials and methods 112
4.2.1 Degradation behaviour under non-enzymatic conditions 112
4.2.2 Degradation behaviour under enzymatic conditions 113
4.2.3 Statistical analysis 113
4.3 Results 114
4.3.1 Degradation behaviour under non-enzymatic conditions 114
4.3.1.1 Collagen scaffolds 114
4.3.1.2 HA scaffolds 116
4.3.1.3 Collagen/HA hybrid scaffolds 118
4.3.2 Degradation behaviour under enzymatic conditions 121
4.4 Discussion 124
4.5 Conclusion 131

Chapter No.5. Cell Response of Collagen/HA Hybrid Scaffolds

5.1 Introduction 132
5.2 Materials and methods 133
5.2.1 CDCs harvest and isolation 133
5.2.2 CDCs culture on scaffolds 134
5.2.3 Assessment of CDCs attachment and proliferation 134
5.2.4 Scanning electron microscopy (SEM) 136

5.2.5 Self-deflection bending test 136
5.2.6 Statistical analysis 137
5.3 Results 138
5.3.1 CDCs attachment 138
5.3.2 CDCs proliferation 139
5.3.3 Scanning electron microscopy (SEM) 143
5.3.4 Self-deflection bending test 145
5.4 Discussion 145
5.5 Conclusion 151

Chapter No.6. Summary and Conclusions

6.1 Overview 152
6.2 Summary 152
6.3 Conclusions 159
6.3.1 Assessment of hybrid scaffolds as TEHV 159
6.3.2 Achievements of the thesis 160
6.3.2.1 Development of a new crosslinking approach 160
6.3.2.2 Aortic valve leaflet ECM mimicking scaffolds 160
6.3.2.3 Mechanically matching scaffolds 161
6.3.2.4 Tailorable properties 161
6.3.2.5 Understanding the microstructure-property relationship for hybrid scaffolds 162
6.3.2.6 A preliminary model for an ideal TEHV 162

Chapter No.7. Future Work

7.1 Mimicking the native valve 163
7.2 Anisotropic mechanical properties 165
7.3 Restoring the cell-attachment sites 166
7.4 Cell-culture under dynamic conditions 167

References 168

Chapter 1

Introduction and Literature Review

This chapter is comprised of two parts; the first part is the introduction which will focus on the background and motivations for the research work presented in this thesis followed by a brief description of the scope of each chapter. The second part is the literature review which will discuss the potential of collagen type I and hyaluronic acid (HA) based hybrid scaffolds for designing a tissue engineered heart valve (TEHV).

Part I: Introduction

While tissue engineering has come up with the prospect of developing TEHVs, the research presented in this thesis has been motivated by the concept of natural polymer-based hybrid scaffolds with interlaced microstructures. Such scaffolds have the potential to overcome the current challenges of TEHV such as biocompatibility, microstructural heterogeneity, and survival in physiological fluids. Key objectives of the research work and outline of the thesis are also presented.

1.1 Background:

Having a healthy heart ensures a high quality of life. The heart valve disease arises either because of age-related degeneration or congenital defects [1, 2]. Heart diseases such as stenosis (valves narrowing), regurgitation or insufficiency (leak or disturbed blood flow pattern), and prolapse (inability to close properly) result in a high death toll worldwide [3, 4]. More than 100,000 patients in the US alone receive a replacement for diseased heart valve annually [5]. The demand for heart valve replacements in the health industries has also been increasing

because of an increase in the average life expectancy. The estimated number of required bioprosthetic heart valves worldwide is expected to reach more than 850,000 a year by 2050 [6].

The history of heart valve replacement dates back to 1960 when Harken replaced a diseased heart valve with a mechanical valve (a ball-in-cage design) [7, 8]. The surgical techniques developed slowly over time as the design of mechanical valves evolved from the simple ball-in-cage design to bi-leaflet and tri-leaflet designs [9, 10]. In addition to the mechanical prostheses, homografts (where donor and acceptor of the tissue graft are of the same species) became popular in the late 60's. The Ross procedure has been considered as an important advancement in autografting (where grafted tissue is borrowed from the same individual) when the diseased aortic valve of a patient was replaced by his own pulmonary valve. The pulmonary valve was, in turn, replaced by either a xenograft (where donor and acceptor of the tissue graft are from different species) or cardiac tissue from the same patient [11]. Xenografts have also been developed, the first porcine aortic valve treated with glutaraldehyde was implanted successfully in 1965 [12, 13, 14].

There are now above 80 designs [15]. However, none of these have met the ideal conditions completely. For instance, a mechanical implant is not capable of remodeling over time, the patients may need a replacement and they will need to take anti-coagulating drugs. On the other hand, biological prostheses (xenograft, homograft, and autograft) may involve the risk of infection transfer and have also been reported to fail because of a mechanical mismatch [16-18]. In addition, biological implants are only available in limited quantities and require a perfect tissue match between donor and recipient [16, 19]. Examples of mechanical and biological heart valves are shown in figure 1.1. Advantages and the limitations of all types of heart valve implants currently in clinical use have been summarized in table 1.1.

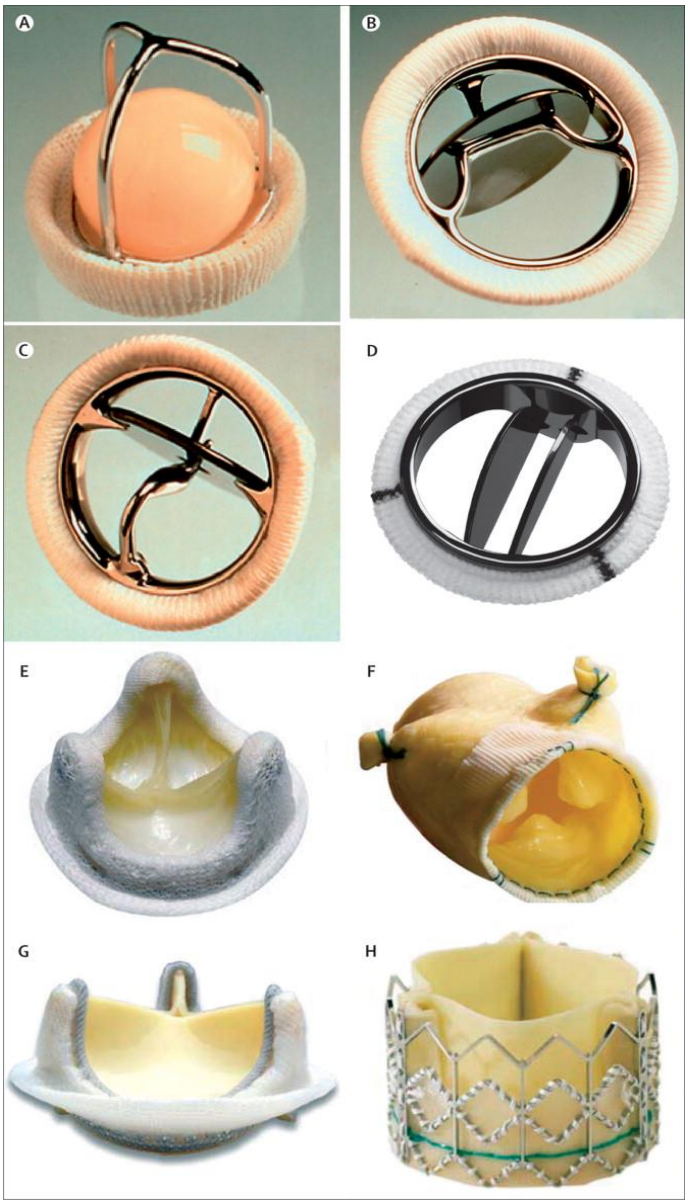


Figure 1.1: Different models of prosthetic heart valves. Mechanical heart valves include caged-ball valve (A), tilting-disk valve (B, C), bi-leaflet valve (D). Porcine valve (E, F), bovine pericardial valve (G), pericardial aortic valve (H) are examples of biological heart valves [20].

Table 1.1: Summary of advantages and limitations of biological and mechanical heart valve implants[21].

Type of Prosthesis	Advantages	Limitations
Allografts/Autografts	Identical to the original valve, similarity in structure and dimensions	Risk of degeneration, limited availability, limited shelf life, challenging surgical procedure involved
Xenografts	Biological source, abundantly available, resistance to degradation, thrombosis, and hemolysis	Transmission of disease, inferior mechanical properties, limited service life
Mechanical Implants	Cheap, unlimited supply, mechanical strength	Non-biocompatibility, lifetime anticoagulation treatment, drug side effects, Inability to grow and remodel for pediatric patients

Tissue engineering uses a scaffold made of a suitable material carrying cells, usually from the patient, that generates the new and healthy heart tissue over time [22]. Natural and synthetic polymers are under extensive experimentation. Among synthetic polymers, FDA-approved biocompatible polymers such as polyurethane (PU), polylactic acid (PLA), polyglycolic acid (PGA), and poly fumarates (PF) have already found their way into heart valve construction. Natural polymers such as silk, fibrin, gelatin, collagen, and glycosaminoglycans (GAGs) are

also in use. Each group of polymers has its advantages. For instance, synthetic polymers offer a vast range of mechanical properties, while natural polymers guarantee the permissible degradation rates and *in-vivo* biocompatibility [23, 24]. Advantages and limitations of synthetic and natural polymer based TEHVs are summarized in table 1.2. However, it is necessary to combine both the desirable mechanical and biological features in a single construct. The ideal scaffold should mimic the mechanical and biological properties of the heart valve tissue. Initial clinical trial on small animal models and humans have shown promising results[22, 24, 25].

Table 1.2: Summary of advantages and limitations of synthetic and natural polymer based TEHVs[21].

Type of Scaffold	Advantages	Limitations
Synthetic Polymer Scaffolds	Abundantly available, cheap, ease of fabrication, and mechanical strength	Non-biocompatible, high degradation rate
Natural Polymer Scaffolds	Biocompatible, no danger of calcification and antigenicity, controlled degradation	Limited resources, poor mechanical strength

1.2 Thesis proposal:

1.2.1 Problem statement:

An ideal scaffold for heart valve regeneration should have a biocompatible surface to permit *in-vivo* cellular activities, has the adequate biomechanical strength to provide necessary support to the new growing tissue, and degrade at a rate compatible with the rate of formation of new tissue[26, 27]. Development of a scaffold capable of mimicking the natural heart valve

in terms of microstructure, desirable mechanical and biological properties is challenging[28, 29]. To date, little success has been achieved with mechanical matching scaffolds showing a controlled degradation rate[30, 31]. In addition, homogeneous/single-polymer scaffolds are not able to mimic the heterogeneous microstructure of natural heart valve extracellular matrix (ECM) [22, 32]. Therefore, a hybrid scaffold with heterogeneous microstructure taking advantage of its constituent natural polymers has the potential to meet these challenges.

1.2.2 Objectives of thesis:

Polymers that are found in the heart valve such as collagen type I and hyaluronic acid (HA) have been selected for this study due to their known biocompatibilities. A scaffold made from these polymers is expected to minimize the chances of rejection by human tissue. This thesis has following objectives:

Objective 1: Fabrication of collagen type 1 and HA based hybrid scaffolds with interlaced microstructure*

This will be achieved through a modified crosslinking route based on carbodiimide chemistry i.e. (1-ethyl-3-(3-dimethylaminopropyl) carbodiimide hydrochloride) [EDC] / (N-hydroxy succinimide) [NHS].

Objective 2: Studying the effect of interlaced microstructure on the mechanical properties of collagen/HA hybrid scaffolds

This will be achieved by varying the concentration of crosslinking agents (EDC/NHS) to prepare interlaced compositions with varying crosslinking densities. The resultant hybrid

*Terms ‘hybrid scaffolds’ and ‘interlaced scaffolds’ have been used interchangeably throughout the thesis.

scaffolds are expected to show different mechanical properties as compared to the parent networks. These scaffolds will be characterized by compression, bending, and viscoelasticity tests under wet and dry conditions.

Objective 3: Studying the effect of interlaced microstructure on the degradation resistance of collagen/HA hybrid scaffolds

It is proposed that variation in the crosslinking densities of the individual networks will allow the close control over the degradation behaviour of the resulting hybrid scaffolds. Thus, scaffolds with a range of degradation behaviours could be prepared. The increase in crosslinking density could slow down the degradation rate which should increase the *in-vivo* stability of these scaffolds.

Objective 4: Studying the effect of interlaced microstructure on the cell response of collagen/HA hybrid scaffolds

EDC/NHS crosslinking could affect the cell attachment and proliferation behaviours of interlaced scaffolds. Therefore, it is important to examine the effect of crosslinking density on their cell response. An appropriate mechanism will also be proposed.

Objective 5: Comparison of collagen/HA hybrid scaffolds with natural valves and choosing 'close-fit' composition.

Properties (mechanical strength, degradation rate, and cell response) of hybrid scaffolds will be compared with those of the biological valves (porcine and human) to choose the most suitable hybrid composition for designing a TEHV.

1.2.3 Outline of thesis:

Chapter 2 covers the synthesis scheme/crosslinking route for the fabrication of individual networks as well as the resultant hybrid scaffolds. The effect of crosslinking technique on the molecular bonding, thermal stability, and microstructure has been analyzed.

Chapter 3 describes the effect of variation in the crosslinking density and the microstructure on the mechanical response of individual networks as well as the hybrid scaffolds. The mechanical response has been studied under different modes of stress such as compression, flexural, and shear in dry and wet states.

Chapter 4 focuses on the effect of crosslinking density and interlaced microstructure on the degradation behaviour of the parent networks as well as the hybrid scaffolds. The degradation behaviour has been studied under non-enzymatic and enzymatic conditions.

Chapter 5 discusses the effect of variation in crosslinking density/microstructure as a means of tailoring the cell response of hybrid scaffolds.

Chapter 6 summarizes the key results from previous chapters and concludes the main achievements of the thesis.

Chapter 7 provides limitations of the thesis and outlines the directions for future research.

Part II: Literature Review

The anatomy and biomechanics of the aortic heart valve and its surrounding tissue have been described for the basic understanding in the beginning. The molecular structures and properties of collagen type I and HA as potential polymers to design TEHV have also been assessed. Furthermore, current state-of-the-art including fabrication techniques and

crosslinking approaches for the development of collagen and HA hybrid scaffolds have been discussed.

1.3 Anatomy of the aortic heart valve:

Two types of heart valves can be found in the heart; atrioventricular (AV) and semilunar valves (SV). The AV is present in the middle of the heart and ensures unidirectional flow of blood from the arteries to the ventricles. The AV valve on the right side of the heart is made of three cusps and hence called the tricuspid valve. Similarly, the AV valve on the left side of the heart has two cusps and is called the mitral or bicuspid valve as shown in figure 1.2A. The AV valves are attached to the ventricular side through threads called chordae tendineae. The chordae tendineae prevent the AV valves from folding backward during the valve opening. The semilunar valves are situated between the ventricles and the arteries carrying the oxygenated blood ready to enter the body. The semilunar valves located on the right and left side of the heart are called the pulmonary valve and the aortic valve respectively. The pulmonary valve prevents the backflow of blood from the pulmonary trunk into the right ventricle as shown in figure 1.2B. Similarly, the aortic valve limits the aorta from regurgitating blood back into the left ventricle [33, 34].

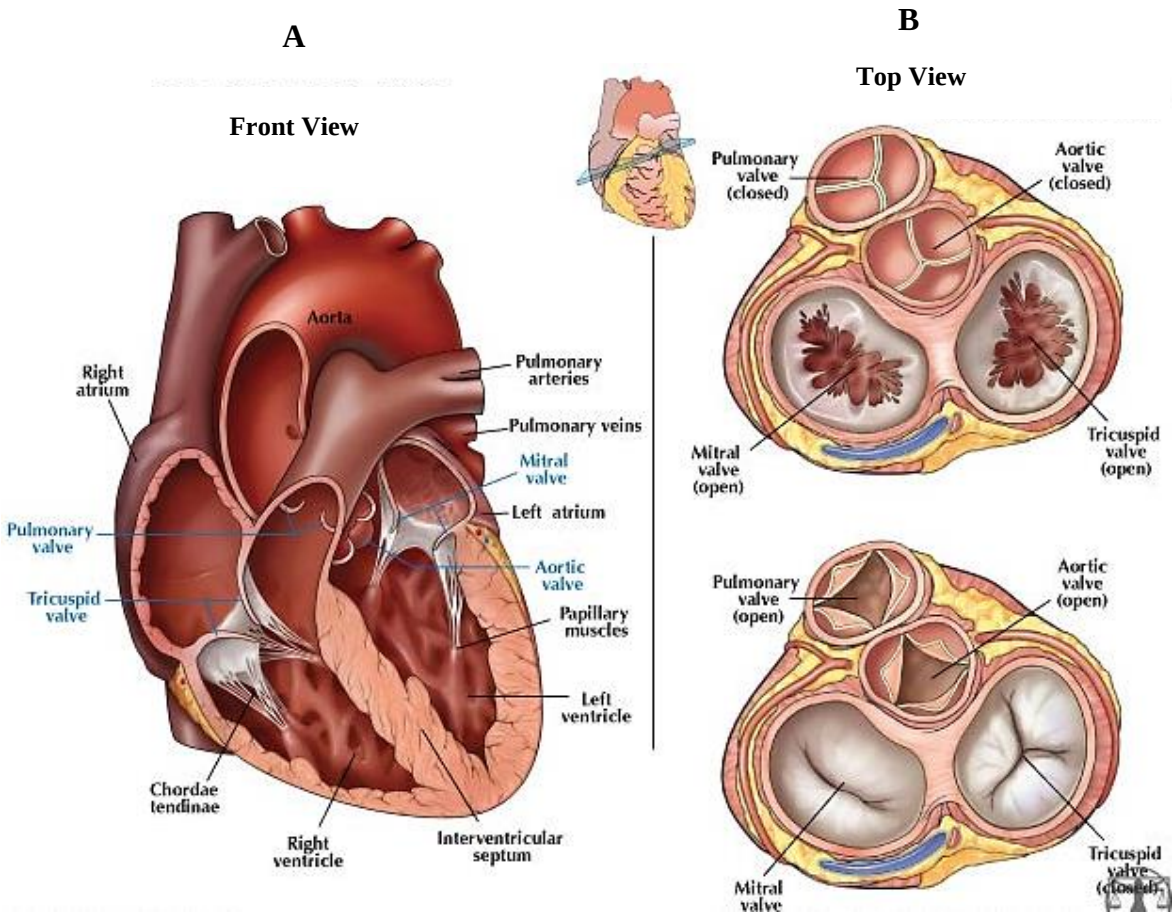


Figure 1.2: Anatomy of the heart valves (A) front view (B) top view [35].

1.3.1 Aortic root:

This thesis will focus on the aortic heart valve because aortic valve diseases are the most common and serious among the valvular heart diseases [36]. The aortic valve is supported by the outflow tract of the left ventricular known as aortic root (figure 1.3). The aortic root is a complex structure and consists of the sinutubular junction, commissure, sinus of Valsalva, aortic valve leaflets, and interleaflet triangles. Sinutubular junction (blue ring) forms the top plane whereas ventriculo-aortic junction (green ring) forms the basal plane in the aortic root as shown in figure 1.3. Heart leaflets are supported within the aortic root between these two planes and are attached to the bulgy portion of aortic wall known as sinus of Valsalva (brown plane). Sinuses are made up of the wall of the aorta where two of the three sinuses have

coronary arteries. These coronary arteries feed oxygenated blood to the myocardium and are called right and left coronary aortic sinuses with respect to the position of each coronary. The third sinus does not have a coronary artery and is called the non-coronary aortic sinus[37, 38].

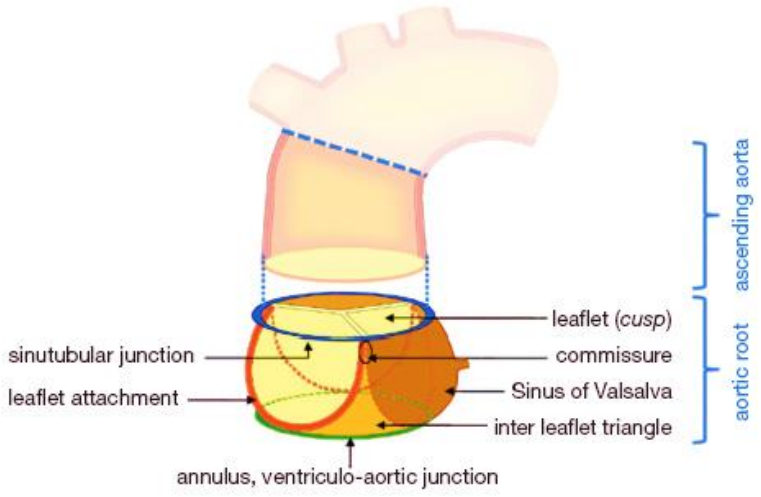


Figure 1.3: Anatomy of the aortic root [39].

The points where leaflets attachments run parallel in the upward direction towards ascending aorta are called commissures (black ring). Each commissure forms the top of each inter-leaflet triangle (yellow) [40, 41]. Blood vessels are sparsely distributed through the aortic valve structure and diffusion through the bloodstream has been generally accepted as a major source for the metabolic activities of the valve[42].

1.3.2 Ascending aorta:

The initial part of the aorta, known as the ascending aorta, emerges from the sinutubular junction in the aortic root and extends to the aortic arch through aortic valve[43, 44]. Three layers can be distinguished in the microscopic anatomy of the aortic wall: intima, media, and adventitia (figure 1.4). The intima is composed mainly of a single layer of endothelial cells, a sub-endothelial layer of collagen fibrils and a thin basal membrane. The media is the

thickest layer and provides structural support and elasticity. It is composed of smooth muscle cells, elastin, and collagen fibers. The adventitia is made up of loose connective tissue. The primary constituents of the adventitia are thick bundles of collagen fibrils arranged in helical structures. Vasa vasorum are small blood vessels that supply blood to the media and adventitia whereas intima is in direct contact with bloodstream to feed itself [45, 46]. The thickness of the wall of ascending aorta is greater than wall thickness in aortic root (sinus of Valsalva) [38].

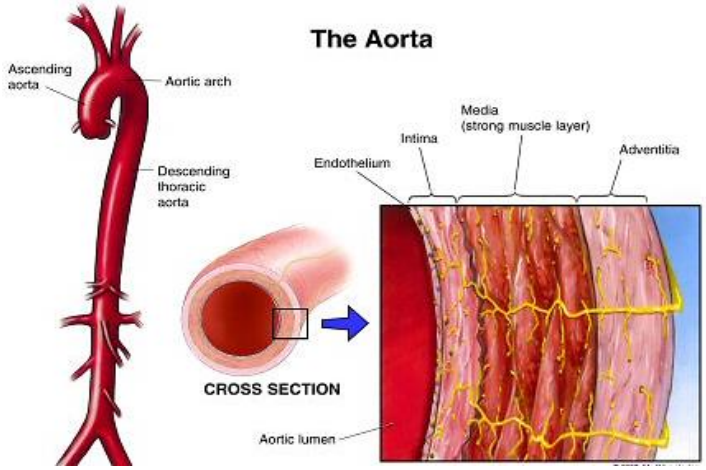


Figure 1.4: Architecture of the aortic wall [47].

1.3.3 Aortic valve leaflets:

The thickness of the human heart leaflet is around 1 mm which varies slightly during opening and closing of the valve[48]. Structurally, the cross-section of a leaflet of aortic valve consists of the following three layers as shown in figure 1.5. Mechanical properties of fibrosa, spongiosa, and ventricularis have also been compared in table 1.3.

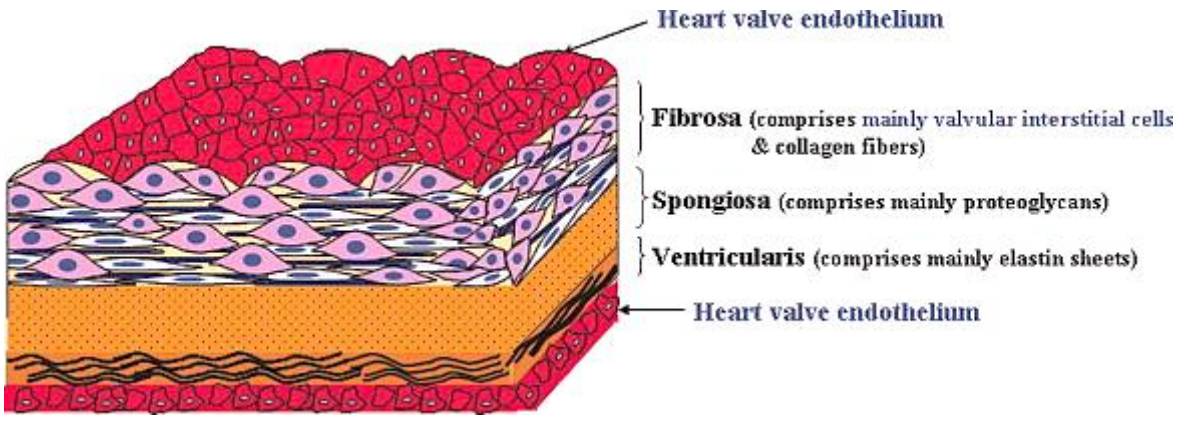


Figure 1.5: A cross-sectional view of the aortic valve leaflet [49].

1.3.3.1 Fibrosa:

This is the thickest and the most identifiable layer in the human heart valve leaflet with a thickness ranging from 80 – 170 μm, located on the outflow side (facing aorta)[50, 51]. Mathematical modeling and mechanical characterization have shown that the fibrosa is the main load bearing layer (E_{circum} = 13.8 ± 5 kPa[52]) and extends through the entire length of the leaflet[53]. The fibrosa is composed of circumferentially arranged densely packed collagen type I fibers and organized elastin fibers as shown in figure 1.5. Circumferentially aligned collagen fibers in fibrosa can support radial loads by extending up to 27.8 %. Table 1.3 shows the mechanical properties of fibrosa which indicates that fibrosa is responsible for the biaxial tensile response of the aortic valve[54, 55]. The presence of low molecular weight proteoglycans (PGs) is found to interact with the D-period of collagen fibrils. This feature gives rise to a tissue-level viscoelastic behaviour in fibrosa and facilitates stress relaxation (slope of stress relaxation curve varies from -6.5 to -8.7) under physiological conditions [56]. Also, the shear modulus of fibrosa has been estimated around 160 kPa[54].

Table 1.3: Comparison of biaxial mechanical properties of fibrosa, spongiosa, and ventricularis (based on human aortic valve leaflet).

	Young's Modulus, E, (kPa)		Extensibility (%)		Slope of stress relaxation curve	
	Circumferential	**Radial**	**Circumferential**	**Radial**	**Circumferential**	**Radial**
Fibrosa	13.8 ± 5.0 kPa[57]	4.6 ± 2.3[58]	19.4%[59]	27.8%[59]	-6.5 ± 1[58]	-8.7 ± 2[58]
Spongiosa	6.1 ± 1 kPa[57]	-	-	-	-	-
Ventricularis	7.1 ± 1.6 kPa[57]	3.7 ± 0.5[58]	21.8%[59]	62.7%[59]	-8.2 ± 2[58]	-9 ± 1.3[58]

1.3.3.2 Spongiosa:

Spongiosa is the middle sandwich layer between fibrosa and ventricularis with a thickness in the range of 58 – 108 μm[50]. It is rich in PGs and glycosaminoglycans (GAGs) as shown in figure 1.5[60]. These components make spongiosa a highly hydrated and incompressible gel phase (E_{circum} = 6.1 ± 1 kPa[52]) which provides lubrication and smooth load transition during valve systole-diastole cycle. From a biomechanical prospect, the functional role of spongiosa can be described as 'delamination resistant layer' between fibrosa and ventricularis due to the interconnectivity of collagen fibers through the tri-layer structure[54, 55].

1.3.3.3 Ventricularis:

Ventricularis (E_{circum} = 7.1 ± 1.6 kPa) is situated on the inflow side (ventricle facing) and is the thinnest of three layers with a thickness in the range of 21 – 48 μm[61]. Fibrosa and ventricularis have similar radial elastic moduli (table 1.3) which indicated similar

proportions of collagen fibers in both layer[58]. Radially arranged elastin fibers, as shown in figure 1.5, are believed to form a honeycomb structure around collagen fibers in ventricularis. Such a microstructure gives allowances for fiber stretching during full valve opening (62.7 %) and their rapid return to the initial state after the load is released[60, 62]. The physiological function of elastin fibers is to minimize large radial strains and bear compressive loads during systole[54].

1.3.4 Cellular makeup of the aortic valve leaflet:

The heart valve also contains various types of cells. The two most distinct are:

1.3.4.1 Valvular endothelial cells (VECs):

These cells serve as a lining for the surface of the leaflet valves as shown in figure 1.5. VECs are usually aligned in a direction parallel to the underlying circumferentially arranged tissue and perpendicular to the direction of blood stream[63]. VECs are involved in physiological processes such as regulation of coagulation, interaction with other cell types in the valve, and transportation of nutrients through the blood stream [64].

1.3.4.2 Valvular interstitial cells (VICs):

VICs are a heterogeneous population of cells[65]. Five major phenotypes have been identified in VICs including embryonic progenitor, quiescent VICs (qVICs), activated VICs (aVICs), progenitor VICs (pVICs), and osteoblastic VICs (oVICs) as shown in figure 1.6. Embryonic progenitor VICs undergo a transformation in valve development stages in the embryo. qVICs are generally static and maintain normal valve functioning. aVICs and pVICs are responsible for the repair in case of disease or injury whereas oVICs control osteogenesis and are thought to be responsible for the calcification of the heart valve [66].

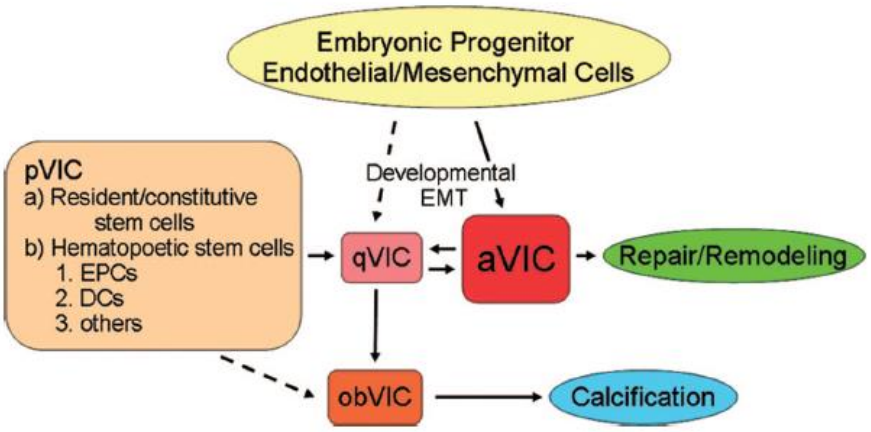


Figure 1.6: Various phenotypes identified for VICs and their functions in valvulogenesis[66].

1.3.4.3 Neurons:

Neurons are found in varying degrees across different heart valves. The neurons present in the heart valve are believed to regulate the pathological functioning by communicating with VICs and VECs. However, the role of neurons in the heart valve functioning is far complex and is not completely understood[67].

1.3.5 Biomechanics of the aortic heart valve:

Each of the above components has a specific role in the heart cycle where they cooperate to the overall biomechanical functioning of the heart valve.

1.3.5.1 Inter-layer load transition during systole-diastole:

The anisotropic structure of the aortic valve leaflet is intimately related to the displacement of the valve itself during the opening (unloading) and closing (loading) of the heart valve as shown in figure 1.7. The leaflets work under the complex stress cycle of flexure (valve opening), shear (flow of blood), flexure (valve closing), and tension (backward flow of bloodstream on the closed valve)[68].

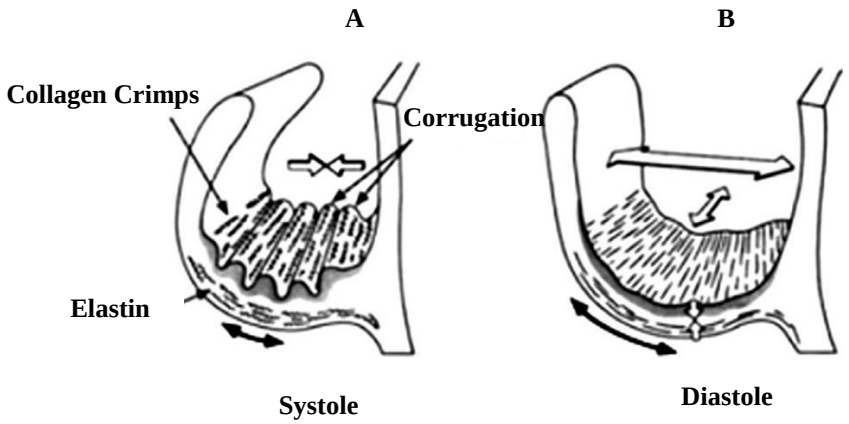


Figure 1.7: Schematic of the elastin and collagen microstructure in different layers during systolic and diastolic cycles [69].

During systole, elastin fibers present in the ventricularious in the form of coils unfold allowing the inward flow of blood through the valve opening (orifice) as shown in figure 1.7A. At the same time, collagen bundles in the fibrosa are deformed circumferentially. Elastin is responsible for load bearing during systole. The load transfer from elastin fibers in ventricularious to collagen bundle in fibrosis during diastole. Collagen bundles in the valve expand radially during diastole as shown in figure 1.7B. Various studies have estimated the total stresses in the leaflets in systole (50 – 200 kPa) and diastole (400 – 500 kPa)[70, 71].

Rego *et al* have used the analogy of 'functionally graded material (FGM)' to study the heterogeneous biomechanics of the aortic heart valve. Based on the FGM model, they proposed that the fibrosa is responsible for supporting the circumferential stress whereas radial stress is equally shared between fibrosa and ventricularis (figure 1.8). Table 1.3 also supports FGM model where fibrosa has a higher E (13.8 kPa) than ventricularis (7.1 kPa) in the circumferential direction but E in radial directions is similar to both layers. The role of spongiosa in load bearing is almost negligible [72].

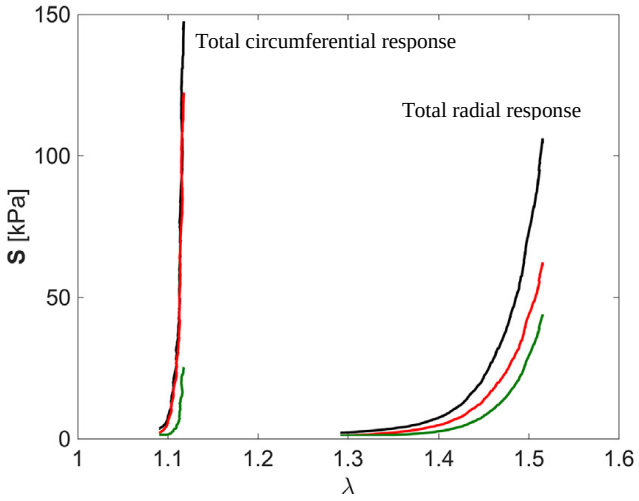


Figure 1.8: Equibiaxial tension response of fibrosa (red) and ventricularis (green) based on FGM model for aortic heart valve[72].

1.3.5.2 Modelling of aortic valve leaflet:

Aortic heart valve leaflet has been described as a parabolic structure which enables it to support the blood volume (3 – 5 lit/min) and transvalvular pressure (80 mmHg)[73, 74]. Finite element analysis (FEA) using triangular thin shell elements was applied to a parabolic model by Phillip *et al*[75] as shown in figure 1.9A. The geometry of each triangular element was approximated by the following quadratic equation:

$$Z_{(x,y)} = h_1 + h_2x + h_3y + h_4x^2 + h_5xy + h_6y^2 \qquad Eq.\ 1.1$$

Where $Z_{(x, y)}$ represented the coordinate normal to the base triangle and h_1-h_6 were the coefficients determined from the grid point data. Stress analysis of this model showed that the principal load is supported in the circumferential direction during diastole and compressive forces are confined only to the boundaries[75] as shown in figure 1.9B.

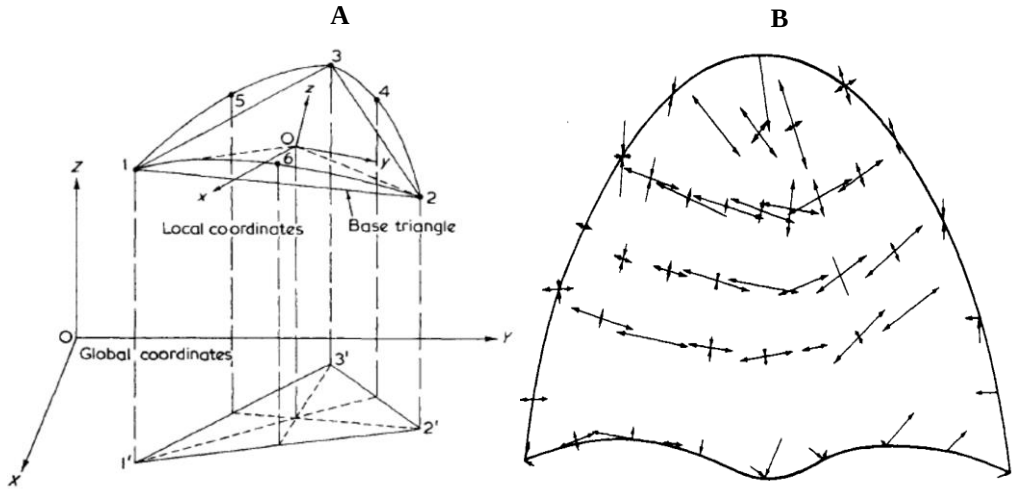


Figure 1.9: (A) finite element analysis applied to parabolic model (B) resultant stress distribution[75].

Yaghoub *et al* compared the computational models for leaflets with varying angles and curvatures as shown in table 1.4. Results showed that the pressure gradients and stresses depend on the leaflet curvatures and the parabolic model did not fit the data using FEA as shown in figure 1.10A. This could be due to the reason that basal attachments take rather a circular shape during valve opening (systole) as shown in figure 1.10B. Therefore, a better model based on a circular circumferential leaflet curvature and linear leaflet radius curvature have been proposed[76]. While mathematical models are helpful despite discrepancies, standardized testing methods need to be developed to establish successful designs for TEHVs.

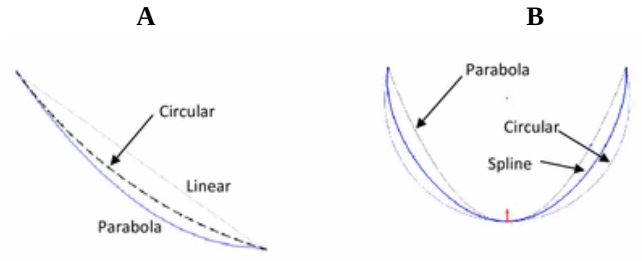


Figure 1.10: Comparison of parabolic and circular approach applied to (A) radial direction (B) vertical direction.

Table 1.4: Specifications of the 10 cases investigated by Yagoub *et al*[76].

Case number	Leaflet angle (degree)	Radial curvature	Circumferential curvature
1	54.4	Linear	Parabola
2	54.4	Linear	Spline
3	54.4	Linear	Circular
4	–	Parabola	Circular
5	–	Circular	Circular
6	45.0	Linear	Circular
7	47.85	Linear	Circular
8	50.97	Linear	Circular
9	58.14	Linear	Circular
10	62.22	Linear	Circular

1.3.5.3 Viscoelastic behaviour of valvular tissue:

While GAGs are generally responsible for the intrinsic viscoelastic behaviour and their depletion due to aging results in the reduction of tissue hysteresis and stress relaxation behaviour[55, 77]. This concept of viscoelasticity was challenged by John *et al*. They studied the time-dependent mechanical properties of porcine aortic valves and observed significant anisotropic directional stress-relaxation (figure 1.11a) whereas a low hysteresis behaviour (17%) with negligible creep (in 3-hour long experiment) could be measured under

physiological conditions[56] as shown in figure 1.11b. These results suggest that the valvular tissue is intrinsically viscoelastic, however, it does not contribute much to the functional biomechanics. This is a unique behaviour as compared to other tissues such as bone, cartilage etc and redefines the valvular tissues as 'functionally anisotropic, quasi-elastic biological materials' [54].

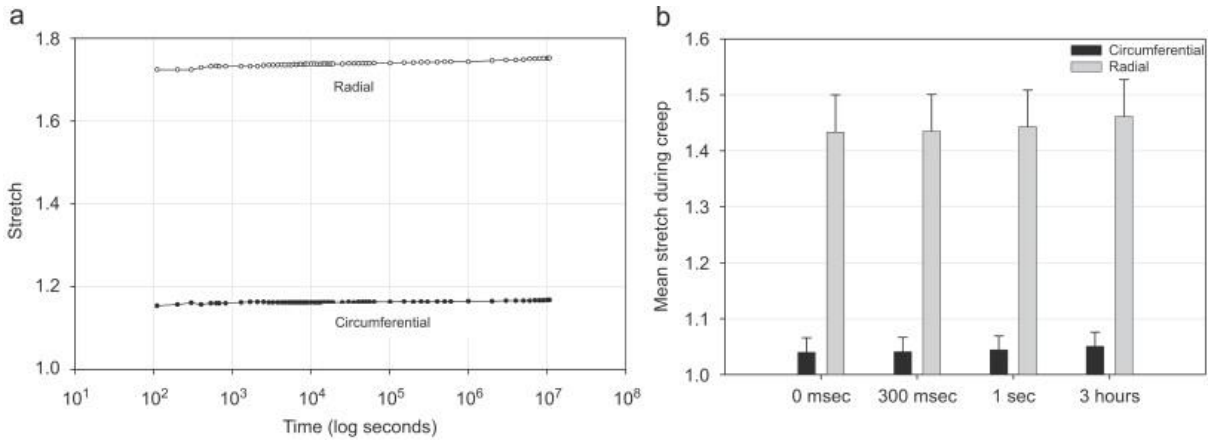


Figure 1.11: (a) Biaxial creep behaviour of the porcine aortic valve in the circumferential and radial directions over the 3 h test (b) The mean stretch observed during creep tests (*n* = 6), indicating that creep in both the circumferential and radial axes, was negligible for all time points[56].

1.3.6 Collagen and Hyaluronic acid (HA) as potential materials for tissue engineered heart valve (TEHV):

The aortic valve leaflets and supporting tissues (aortic root and ascending aorta) are made up of collagen, GAGs, and elastin with variations in compositions and conformations, as discussed in section 1.3.3 Collagen is a major component of the heart valve as 74 % type I, 24 % type III, and 2 % type V collagen [78]. GAGs are the second most abundant ingredient (60 % collagen, 20 % GAGs, and 10 % elastin) by the dry mass [79], of which HA is the most abundant. Other GAGs present in minor quantities dermatan sulphate (DS), chondroitin-4-sulphate (CS-4), and chondroitin-6-sulphate (CS-6) [80]. Table 1.5 compares the mechanical

properties of collagen type I and HA with those of human aortic leaflet. It also shows that collagen type I fibrils have higher elastic modulus (2.9 – 7.4 GPa[81, 82]) as compared to the leaflet (20 – 100 kPa[83]) and has the potential to mechanically match with the target tissue. However, collagen type I alone could not match the viscoelasticity requirements of the leaflet ($G^{`}$ = 0.545 – 10.5 kPa[84], δ = 0.1 – 0.4 [85]) and therefore, it would be desirable to combine it with a viscoelastic natural polymer such as HA (δ = 0.04 – 0.78[86, 87]). Thus, an ideal TEHV aiming to mimic the human aortic leaflet should be built from collagen type I and HA.

Table 1.5: Comparison of mechanical properties of the human aortic leaflet, collagen type I, and HA.

Mechanical Property	Circumferential	Radial	Collagen type I (bovine Achilles tendon)	HA
Elastic modulus (E)	20 – 100 MPa[83]	2 – 10 kPa[83]	2.9 – 7.4 GPa[81, 82]	0.2 – 70 kPa[88, 89]
Maximum strain (ε_{max})	22 %[90]	30 % [90]	10 – 33 %[91]	15 – 18 %[92]
Ultimate tensile strength (σ_{UTS})	2 – 4 MPa[83]		25 – 210 MPa[93, 94]	-
Maximum stress (σ_{max}) in leaflet	0.1 MPa[95]		-	-
Flexural/bending modulus (E_{bend})	1220 kPa in systole, 710 kPa in diastole[96]		1.0 – 3.0 GPa[97]	-
Storage modulus ($G^{`}$)	0.545 – 10.5 kPa (aortic leaflet + sinus)[84]		10 – 140 GPa[85]	0.3 – 2.20 kPa[86, 87]
Loss tangent (δ)	0.3 – 0.4[84]		0.1 – 0.4 [85]	0.04 – 0.78[86, 87]

[a] Represent values for collagen fibrils (d = 125 µm) measured by Atomic Force Microscopy (AFM). [b] Represent values for HA hydrogels modified with polyethylene glycol (PEG) with varying degrees of modification.

1.3.6.1 Molecular structures:

a) Collagen:

Collagen is the major component of human heart ECM comprising about 50% by mass on the dry basis [98]. The collagen molecule has a triple helix structure. The individual chains are known as α-chains. Each α-chain has a characteristic repeating sequence of 3 amino acids G-X-Y (figure 1.12) [99].



Figure 1.12: Triple-helix structure of collagen [99].

Collagen can be further subdivided into 29 types depending on the nature of the three chains and the distribution of X and Y amino acids [100]. Being the smallest amino acid, glycine always occupies a central position in the α-chain facing the axis of the triple helix, leaving the other two amino acid residues pointing outwards as shown in figure 1.13a [99]. The backbone -NH- of the glycine forms hydrogen bonds with the backbone -CO- of the Y residue on the right-hand side α-chain [101]. This stabilizes the triple helix [99]. Once assembled, the triple helix is secreted out of the cell and then tailored into a molecule of approximately 300 nm in length and 1.5 nm in diameter, which becomes a tropocollagen, as the precursor to collagen as shown in figure 1.13b. Five tropocollagens then aggregate to form a microfibril about 4nm in diameter [102], in which they are staggered longitudinally from each other by around 67 nm, referred to as the D-period.

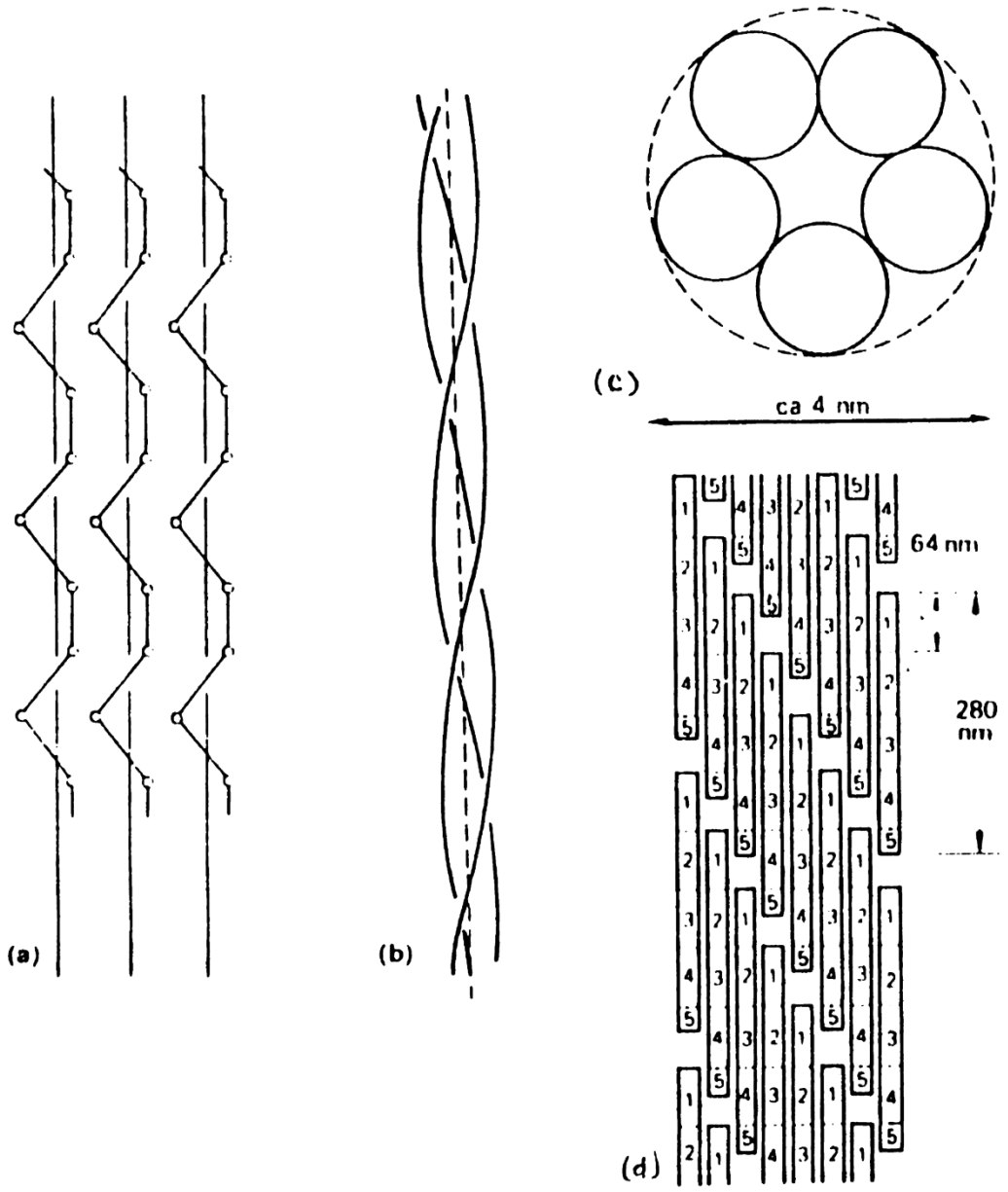


Figure 1.13: Building blocks of collagen fibrils (a) three polypeptide chains around a minor axis (b) about a single central axis (c) five tropocollagen molecules aggregate to form a microfibril (d=4nm) (d) longitudinal section of quarter staggered arrangement tropocollagen helices [103].

As can be seen in figure 1.13c, each D-period contains one segment with all the five tropocollagens in the cross-section and the other segment with only four. This results in the overlap-gap structure which can be observed as the characteristic banding pattern with the periodic length of the D-period under electron microscopes [102] (figure 1.13d). The microfibrils are then assembled into fibrils, with various diameters ranging from 30 to 500

nm (30-50 nm for human heart valve collagen fibrils) [102]. The fibrils are further bundled up to collagen fibers with the aid of glycoproteins and PGs, which bridge the fibrils and further strengthen the collagen fibers [104, 105]. Due to this complex hierarchical structure, collagen fibers have a high Young's modulus of 0.1 – 1 GPa [106]. However, the collagen fibers are longitudinally crimped with a periodicity of approximately 20 µm (figure 1.14), which can give them an extensibility of approximately 10% (table 1.5) [107, 108].

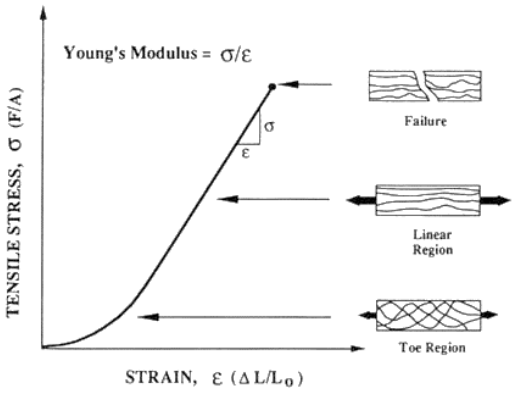


Figure 1.14: the Non-linear stress-strain curve of collagen [109].

b) Hyaluronic acid (HA):

Hyaluronic acid (HA) or hyaluronan is a linear polysaccharide that consists of alternating units of repeating disaccharide, β-1,4- D -glucuronic acid – β -1,3- *N* -acetyl- D – glucosamine [110]. It is found in the human body in the form of hydrophilic sodium hyaluronate. It occurs in connective tissue ECM, joints, skin, and eye. The HA molecule can absorb and retain large amounts of water. Therefore, its principal role in the human body is to give support to ECM structure and cushioning against impacts. It has also been known to take part in cellular activities like migration, adhesion, wound repair, and ECM assembly [111, 112].

HA is an attractive biological molecule for a broad spectrum of biological applications e.g. tissue engineering, drug delivery, ocular surgery, visco-supplementation for arthritis, and wound healing[113-115]. Chemical modification of HA provides a means to modify its

degradation and mechanical properties for a specific application [116, 117]. The HA molecule has the following potential sites for chemical modification (figure 1.15).

I. —COOH group:

The – COOH group is usually modified by amidation [carbodiimide, 2-chloro-1-methylpyridinium (CMPI), 2-chloro-dimethoxy-1,3,5-triazine (CDMT), carbonyldiimidazole], Ugi condensation, ester formation [using alkyl halides, tosylate activation, diazomethane, epoxides] [118]. Other functionalization routes include modification with dialdehyde [116] and disulphide [119]. Metahcrylamide modified carboxylic groups have been photo-cross-linked [120].

II. –OH group:

This group can be modified into ether (epoxide [121], divinyl sulfone [122] and ethylene sulphide [123]), hemiacetal [124], ester (octenyl succinic anhydride, methacrylate anhydride and activated compounds [118]), and carbamate [125]. Also, OH group can be oxidized with sodium periodate.

III. –$NHCOCH_3$ group:

An amino group can be yielded by deacetylation of N-acetyl group. This amino group is capable of reacting with acid leading to the similar modifications to amidation [126].

Each of the above set of reactions has a specific mechanism and yields a different HA derivative.

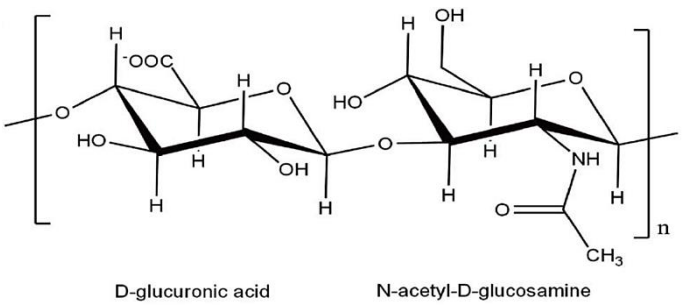


Figure 1.15: Molecular structure of HA monomer [127, 128].

1.3.6.2 Collagen/HA hybrid scaffolds in heart valve tissue engineering:

Single polymer based scaffolds are less likely to meet the criterion of regenerating the heart valve tissue as discussed in section 1.2.1. In heart valve tissue engineering, multicomponent hybrid scaffolds may not only serve as analogous to natural heart valve ECM but also allow the exploitation of optimum properties of individual components [129, 130]. Hybrid scaffolds also allow the incorporation of biological motifs and drugs to widen the potential applications in regenerative medicines [131].

a) Mechanical matching between collagen and HA:

Collagen has been utilized in tissue engineering because of its excellent biocompatibility and cell attachment characteristics [132]. Similarly, HA is a non-sulfated glycosaminoglycan and offers properties favorable for tissue regeneration such a slow immunogenicity, superior swelling characteristics, and biodegradability. HA-based products are also being used in optics, orthopedics, and wound healing aids [133]. However, both polymers individually show inadequate mechanical properties for valvular tissue growth as shown in table 1.5[134]. Also, HA hydrogels have also been reported for rapid *in-vivo* degradation (completely digested in 10 hours) in the presence of hyaluronidase [135]. A hybrid scaffold based on decellularized ECM has been reported where Young's modulus of decellularized ECM has increased from 5 Pa to 32 kPa when fabricated in the form of hybrid scaffolds with fibrin. C-kit+ cardiovascular progenitor cells from pediatric patients with congenital heart defects seeded on ECM-fibrin hybrid scaffold have been able to interact and remodel the ECM [136]. Hence, hybrid scaffolds based on collagen and HA could be a solution to overcome the challenges of controlled degradation rates and suitable mechanical properties.

b) Effect of fabrication/crosslinking route on the resulting properties:

Collagen/HA combination could also be used to synthesize hybrid microstructures in a number of ways. Collagen could be taken as the primary network and HA could be taken as

a secondary network or vice versa. In either way, various properties could be achieved. For example, two sophisticated techniques of salt leaching and electrospinning have been combined to produce collagen/HA scaffolds. This could result in combining both mesoporous and nano-porous features in a single material [137]. Such multi-scale pattern of porosity could be favorable for blood and tissue vascularization. A limiting factor in the study was the low concentration of collagen (5, 10%). HA fibers could have a thin coating of collagen at low concentrations rather than forming a hybrid microstructure.

Shapira et al discussed synthetic-natural polymer composite scaffolds for cardiac tissue engineering. They showed that tunability of the mechanical/physical properties of a given polymer-polymer composite system depends on the fabrication route [138]. An attempt to mimic the heart valve ECM with multicomponent polymer blend based on collagen, gelatin, elastin, and PCL showed compatibility with adipose-derived cells [139]. Although FDA approved synthetic polymers such as PCL, PGA, and PLA have shown great potential for TEHVs, mathematical modeling studies have also shown that these polymers, due to their isotropic mechanical properties, are not appropriate for designing anisotropic structures such as aortic heart valve [140].

The stiffness of either collagen or HA could be improved by the incorporation of secondary polymeric networks such as poly (ethylene glycol) diacrylate (PEGDA) and alginate [141, 142]. Collagen and gelatine based hybrid hydrogels with GAGs have shown potential in regenerating skin, nerves, and orthopedic tissues [143]. HA-based hybrid scaffolds have been shown to hold promising properties for myocardial repair by encouraging cell activities with reduced immunogenic response [144]. Although the above-discussed studies have shown the influence of crosslinks, simple crosslinking of collagen in the presence of HA does not guarantee the formation of an interlaced hybrid microstructure. Also, unmodified HA is not recommended for tissue engineering application because of its poor handling properties [142,

[145]. This problem could be solved by introducing various pendent groups on HA backbone as discussed in section 1.3.6.1. One such study reported the modification of HA and CS to yield Methacrylated HA (MeHA) and methacrylated chondroitin sulfate (MeCS). MeHA and MeCS were combined with self-assembled collagen to form an interpenetrating microstructure for cartilage tissue repair. Collagen was assumed to be self-assembled (physical bonds) in this study, and HA/CS were chemically crosslinked. These structures showed cytocompatibility and cell attachment with tunable degradation rates and swelling ratios (varying the ratio of MeHA and MeCS) [146].

c) Novel combinational fabrication techniques:

Novel fabrication techniques or a combination of different techniques have been developed for the fabrication of combinational scaffolds [147]. Recently, Shaohua *et al* have exploited the conventional textile weaving technique to prepare a polyacrylonitrile (PAN) based micro-nano fabric laid up with HA based hydrogels. The resulting composite scaffolds showed elastic modulus up to 20MPa in the micro-fiber direction which matched the elastic modulus of the human heart valve in the circumferential direction [148]. Another report has discussed the fabrication of alginate based shape-memory scaffolds for cartilage repair. Alginate shape-memory scaffolds were subsequently coated with collagen type I, collagen type II, and CS which not only resulted in an increase in elastic modulus (15MPa) but also promoted stem cell recruitment [149]. Nano-micro fabrication techniques could be applied to natural polymers such as collagen and HA to develop robust composite scaffolds with anisotropic mechanical properties and to meet the requirements of viable TEHVs [150, 151].

d) Interpenetrating polymer networks (IPNs):

Interpenetrating polymer networks (IPNs) is a special case of polymer blends where the two or more polymers are at least partially interlaced at the molecular level. Some IPNs based on the natural polymers such as protein (collagen, fibrin, silk, and gelatin), polysaccharides

(hyaluronic acid, chondroitin sulphate, dextran, agarose, and chitosan) and DNA have been recently developed. Initial in-vitro trials have indicated their potential for skin, bone, cartilage, and nerve tissue regeneration[133, 146, 152-155]. An attempt to make a semi-interpenetrating polymer network (sIPN) based on unmodified HA with different molecular weights has been reported. Low molecular weight HA (LMHA) showed promising results as compared to high molecular weight (HMHA). Collagen fibers were made to penetrate LMHA network followed by fibrillogenesis [142]. Active molecular interactions between LMHA and collagen fibers established the characteristic networking for a sIPN. Recently, linear low-density polyethylene (LLDPE)/HA IPN prepared by solvent infiltration technique has been reported. IPN has been shown to have anti-thrombogenicity properties with bending stiffness (26 – 12.93 nN m^2) matching to that of the human heart valve (13.87 nN m^2) [156]. However, the material needs to be tested further for its *in-vivo* anti-calcification potential [157]. Incorporation of poly (N – isopropylacrylamide) (PNIPAM) to the collagen matrix yielded a broad spectrum of shear moduli ranging from 10^5Pa to 10^2Pa. PNIPAM-collagen blend resulted in a range of microstructures which were found highly sensitive to the cell fate [158]. Several fabrication techniques are being studied for the development of collagen and HA based hybrid scaffolds for many tissue engineering applications. There is still much to explore regarding innovative techniques for the fabrication of collagen-based hybrid microstructures. Simple and relatively straightforward approaches capable of utilizing non-toxic, cheap, and readily available precursors need to be developed. The ideal synthesis route should yield such microstructures without compromising the useful biological and mechanical properties of natural polymers such as collagen and HA.

1.3.6.3 Crosslinking routes for the fabrication of collagen-HA based hybrid scaffolds:

a) Physical crosslinking:

Dehydrothermal treatment (DHT), irradiation techniques, and photo-crosslinking methods can introduce physical crosslinks in proteins. Conventional heat treatment in a simple drying oven at 100°C under vacuum increased Young's modulus of heat treated collagen films due to crosslinking[159]. In DHT, an amide bond is formed by a condensation reaction between –COOH and $–NH_2$ group in neighboring collagen α-chains[160] as shown in figure 1.16.

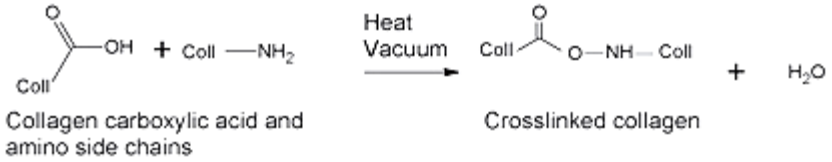


Figure 1.16: Condensation reaction takes place between adjacent carboxylic acid and amine groups of neighboring collagen chains during DHT.

Experimental parameters such as DHT temperature, exposure time, and vacuum levels can be controlled to get the desired properties in scaffolds[161]. Higher DHT temperatures result in higher crosslinking densities in shorter exposure times and vice versa[162]. It has been found that post-DHT increase in crosslinking density is correlated with the increase in compressive strength and tensile strength up to several folds in collagen-GAG scaffolds[163]. DHT is a slow and time-consuming process which typically takes 3 – 5 days for completion depending upon the DHT temperature. It also involves the risk of denaturation of collagen triple helix structure at higher temperature[162-164].

Exposure of collagen to irradiations such as gamma (γ) rays results in the formation of physical crosslinks[165, 166]. The extent of crosslinking achieved through irradiation techniques depends on the γ-rays dosage (100 – 400 Gy is capable to form crosslinks). Higher dosage of γ-rays (dosage ≥ 1 kGy) involves degradation of collagen triple helix structure through

peptide bond cleaving[167] as shown in figure 1.17. While the use of low-intensity γ-rays for the sterilization of collagen scaffolds is still in use, however, the risk of collagen chain scission cannot be completely avoided even at low dosage. This is the reason that the utilization of γ-rays has been abandoned for collagen crosslinking[168-170].

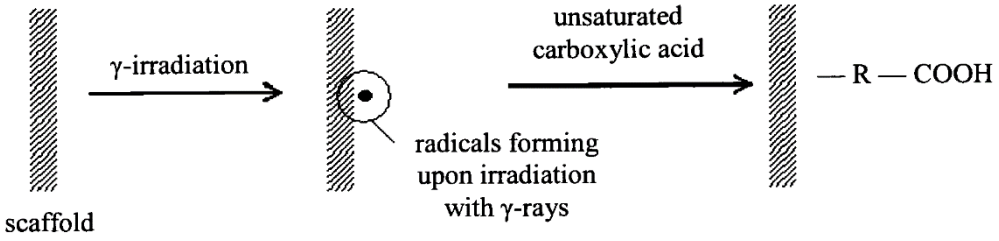


Figure 1.17: γ-rays treatment of collagen scaffold result in the formation of unsaturated carboxylic acid (breakdown of peptide bond).

Ultra-violet (UV) light-mediated physical crosslinks are formed between bulky aromatic groups (tyrosine and phenylalanine) through free-radical mechanism[171, 172]. UV intensity and exposure time are the key parameters to control in determining the degree of crosslinking. A typical set-up has been shown in figure 1.18A. The number of crosslinks formed is also limited by the number of available aromatic groups (figure 1.18B)[173]. UV-treated collagen films are found to be mechanically robust (increase in tensile strength and stiffness) and resistant to enzymatic degradation [160]. For example, tensile stress has been reported to reach maxima (60 kPa) at an exposure time of around 4 hours at a UV intensity of 1.66 mW/cm^2 [174].

UV-irradiation technique has also been applied to crosslink the photo-cross-linkable pendant groups on HA backbone chain such as glycidalmethacrylated coupled HA (GMHA) [175]. This technique has been widely applied to synthesize collagen/HA hybrid scaffolds for various potential tissue engineering applications. Briefly, MeHA modified pre-polymer solution was combined with collagen solution in different mass ratios along with a photo-initiator. This mixture was then exposed to UV light for a few minutes to establish crosslinks [133, 176, 177].

The technique was modified to establish domains with various crosslinking densities which can facilitate localized IPN and sIPN regions in a single sample [133]. The resulting IPNs not only showed compatibility with fibroblasts but also showed G` up to 800 Pa [176].

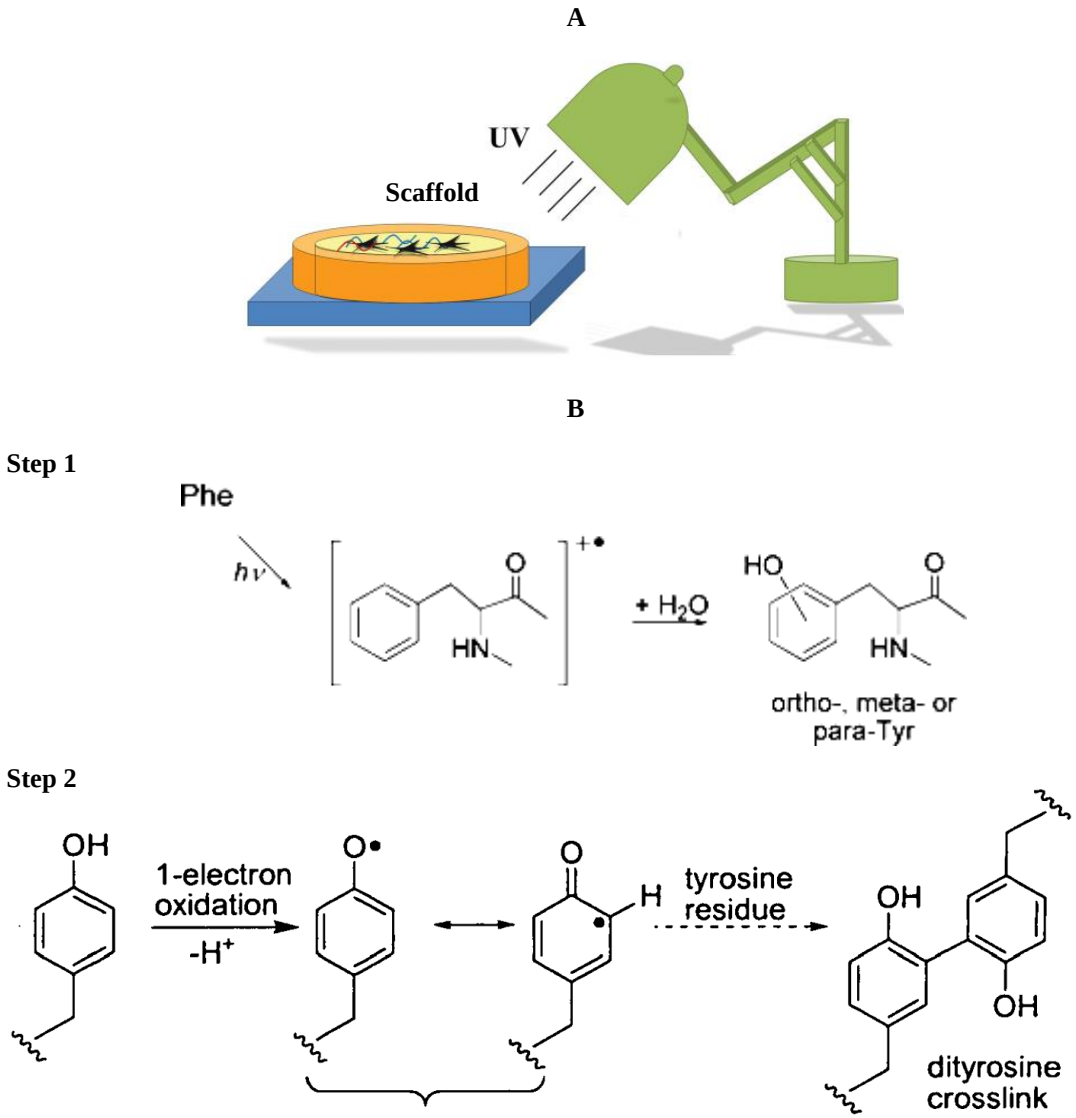


Figure 1.18: (A) set-up for UV treatment of collagen scaffolds (B) UV-assisted crosslinking mechanism; step 1 shows the conversion of phenylalanine to tyrosine whereas step 2 shows crosslinking between two tyrosine free radicals[178].

As compared to DHT, UV crosslinking has certain advantages such as better control of parameters and much shorter exposure times e.g. 15 min of exposure to UV source can produce the same effect that is achieved with DHT within 3-5 days [160]. A serious disadvantage of this technique is the use of cytotoxic photo-initiators and UV light [179, 180].

Also, longer exposure time to either high temperature or high-intensity UV light can induce the deterioration of properties due to the denaturation of collagen structure [174].

The freeze-thawing technique can be categorized as a non-thermal physical crosslinking of collagen. It has been found that traces of secondary polymer such as polyvinyl acetate (PVA) as well as ice crystals formed during freezing act as small crystallites (physical interaction) in the freeze-thawed collagen matrix[181] as shown in figure 1.19.

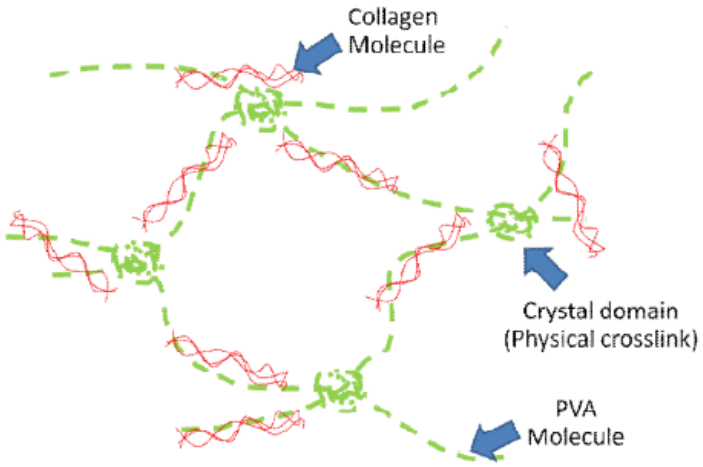


Figure 1.19: PVA crystallites act as physical crosslinks for collagen network[181].

b) Chemical crosslinking:

A wide range of crosslinking agents has been used for chemical crosslinking of collagen and HA based materials. Chemical crosslinking of collagen using different crosslinking agents has been given in figure 1.20. Glutaraldehyde (GA) is the most used crosslinking agent, also used as a disinfectant for the fixation and sterilization of biological valves [182, 183]. GA introduces Schiff base structures while reacting with the amino acids of proteins as shown in figure 1.20a. Schiff base structures enhance thermal (shrinkage temperature increases from 56º C to 78º C) and mechanical strength (elastic modulus increases from 20 MPa to 60 MPa) of the collagen [184]. As the concentration of GA increases, GA is substituted as a pendant group on the backbone chain of collagen rather than as a crosslinking agent. This

increase in GA concentration switches the crosslinking mechanism in collagen from intra-fibrillar to inter-fibrillar [185]. Furthermore, physical properties of GA-crosslinked HA hydrogels such as dimensional stability in physiological solutions and controlled degradation were increased [184]. The mechanism of GA crosslinking reaction is fast and complex but poorly understood [184]. Also, it imparts an undesirable pale yellow to brown colour in collagen (due to the side reaction with primary amines) and toxic byproducts are also difficult to control [186, 187]. Genipin is a plant-derived non-toxic and water-soluble crosslinker for proteins [188, 189]. It has low toxicity as compared to glutaraldehyde, however, it is expensive to extract and gives low crosslinking densities[190].

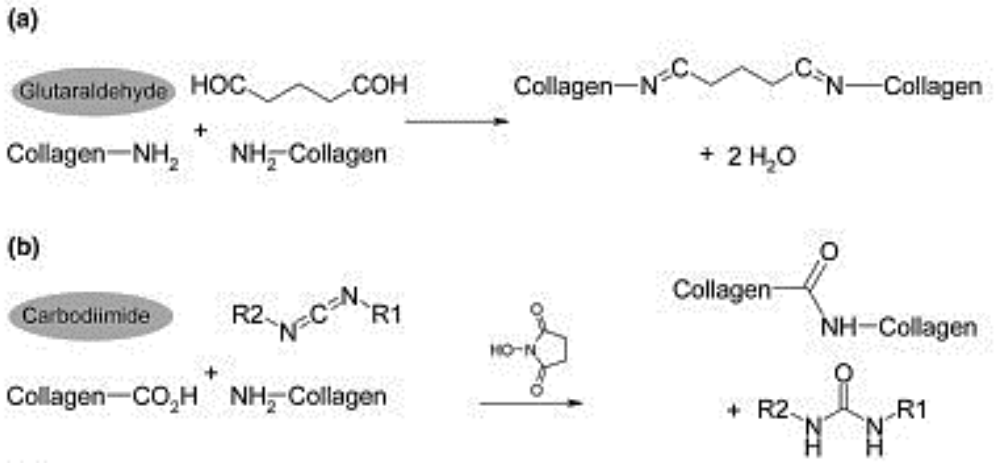


Figure 1.20: Chemical crosslinking of collagen using (a) glutaraldehyde, (b) carbodiimide, and (c) genipin.

Carbamide chemistry is a popular and well-established approach [127, 191]. 1-ethyl-3-(3-dimethylaminopropyl) carbodiimide (EDC)/ *N*-hydroxysuccinimide (NHS) have been studied extensively. In a typical reaction, EDC/NHS attacks the carboxylic group in a molecule in acidic media which reacts with amine group from another molecule thus forming an amide bond as shown in figure 1.20b. An increment in either the EDC/NHS ratio or incubation time for a given ratio results in an increase in crosslinking density[192, 193]. Various studies have confirmed that the EDC/NHS crosslinked collagen shows increase in mechanical strength and denaturation temperature. These are also resistant to enzymatic

degradation, have high cell attachment potential, and controlled swelling characteristics with least cytotoxicity as compared to GA. Unlike GA and genipin, EDC/NHS form zero-length crosslinks with water-soluble by-products[194-197].

A combination of physical and chemical crosslinking methods has been attempted to take the advantage of both techniques. DHT treatment of collagen is followed by chemical crosslinking with either GA [198] or EDC/NHS [199, 200]. However, the sequence of application of physical and chemical crosslinking techniques did not seem to affect the results. Such hybrid techniques could be very attractive for producing graded crosslinking densities in hydrogel as drug delivery vehicle for a controlled drug release or in scaffolds for tissue culture. A comparison of physical and chemical crosslinking techniques has been given in table 1.6.

Table 1.6: Comparison of physical and chemical crosslinking techniques[21].

Physical Crosslinking	Chemical Crosslinking
Mechanical strength is increased as compared to un-crosslinked samples e.g. DHT treated collagen scaffolds showed compressive modulus of 0.5 kPa[201].	The mechanical strength of collagen is increased as compared to physical crosslinking e.g. EDC crosslinked collagen scaffolds showed 4 times increase (2.0 kPa) in compressive modulus[201].
Collagen structure may get denatured as a result of exposure to high-temperature ≥ 80°C or gamma rays[174].	Collagen structure remains preserved[202].
Short reaction times e.g. 15min exposure to UV light introduces crosslinks[160].	Long reaction times e.g. crosslinking with EDC takes 3 – 4 hr[203].
Use of photo-initiators in UV crosslinking may leave toxic residues[179].	Water-soluble by-products are formed in EDC/NHS crosslinking[204].

c) Enzymatic crosslinking:

Enzymes catalyze the specific chemical reaction of polymers including crosslinking [205]. Transglutaminase (TGs), lysyl oxidase, and horseradish peroxidase (HRP) are non-toxic and biocompatible crosslinkers for collagen and HA as shown in figure 1.21[206]. Enzymatically crosslinked scaffolds showed low elastic modulus (10 – 30 kPa), which limited their application to injectable hydrogels only [181, 185, 207].

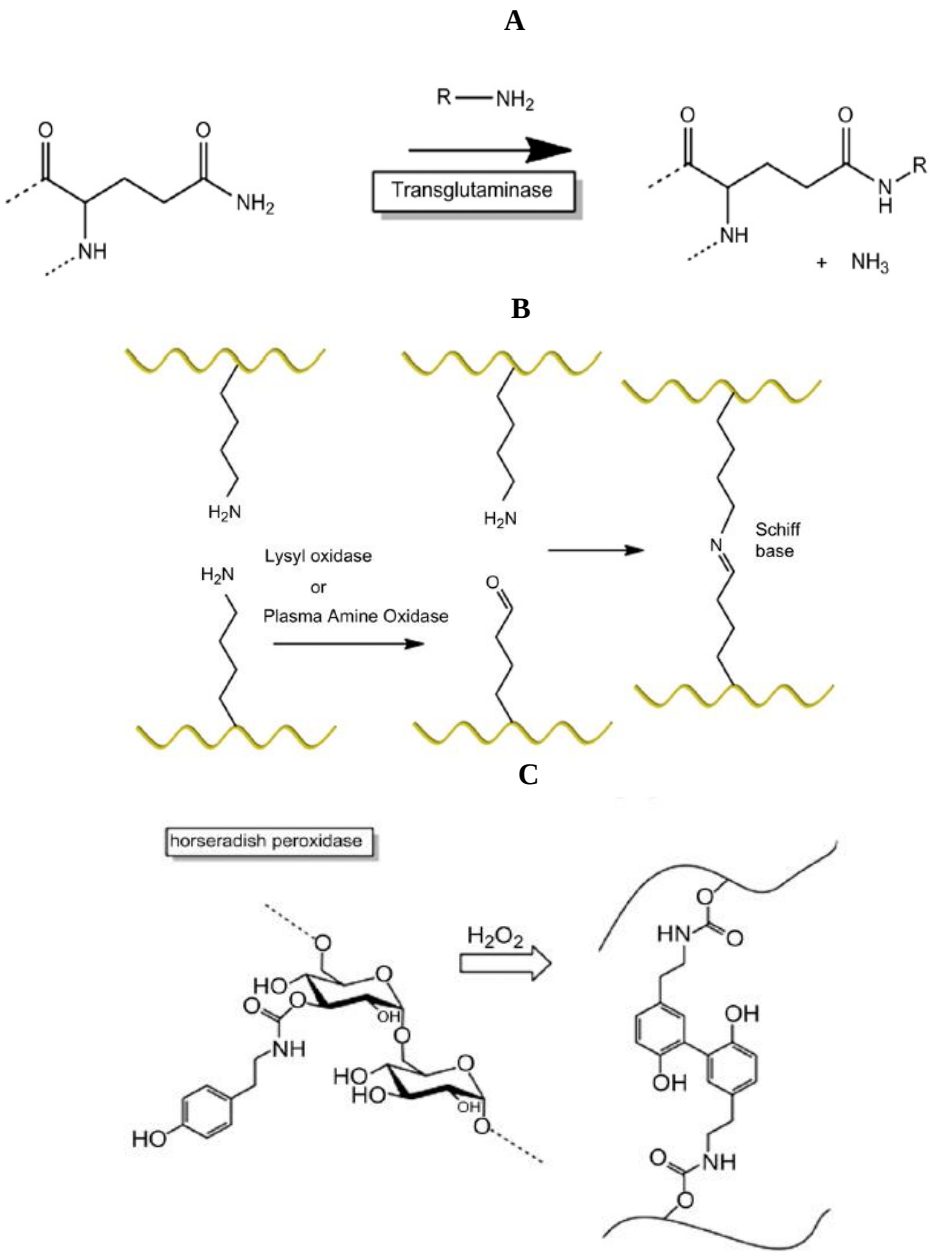


Figure 1.21: Mechanisms of (A) TGs-assisted (B) lysyl oxidase-assisted, and (C) HRP-assisted crosslinking reactions[206, 207].

HRP has also been applied to yield a hyaluronic acid-tyramine (HA-Tyr) network as shown in figure 1.21C. The network was further combined by simultaneous crosslinking with fibrin to yield a macro scale hybrid microstructure [208]. A double enzymatic crosslinking technique for gelatine/chitosan hybrid hydrogel showed an increase in stiffness (up to 1 MPa) and degradation resistance (35% drug release in 10 hours)[209]. In another study, cytocompatibility of enzymatically crosslinked gelatine-HA-CS hydrogel has been endorsed [143].

The mechanisms for establishing the crosslinks by physical, chemical and enzymatic routes are shown in figure 1.22. Although no enzymatically crosslinked collagen-HA based scaffolds have been reported till date, the above studies suggest that both collagen and HA have potential functional groups for enzymatic crosslinking. Enzymatic crosslinking can be successfully applied to any biopolymer, which will further extend the existing library of biomaterials.

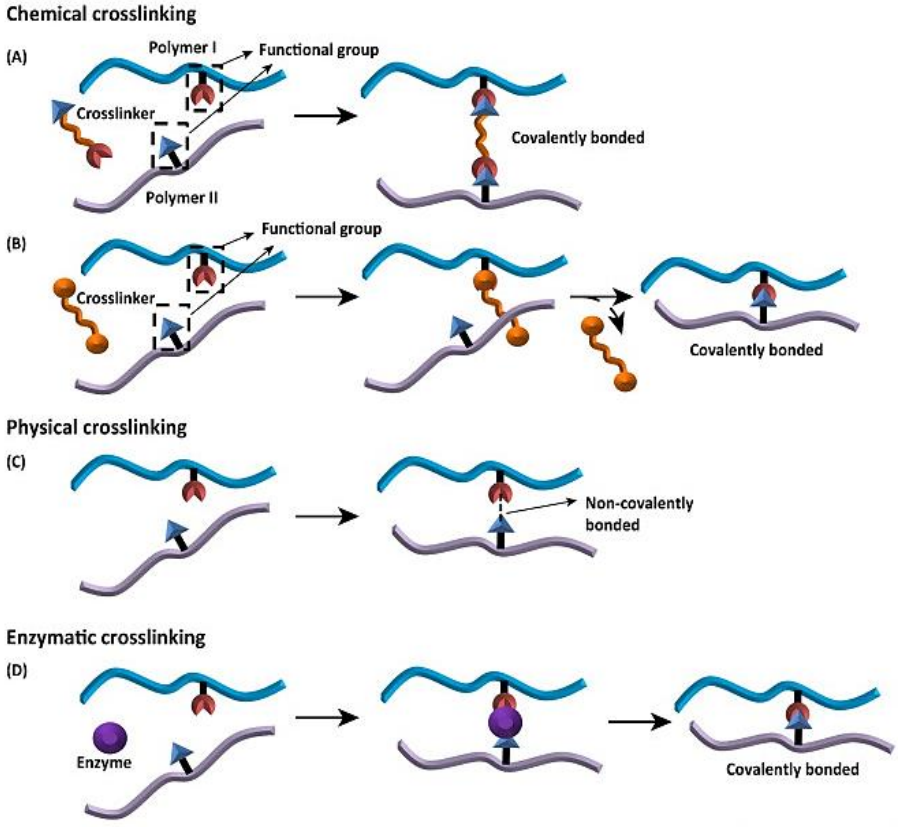


Figure 1.22: (A, B) Chemical, (C) Physical, and (D) Enzymatic crosslinking routes [210].

1.3.6.4 Biocompatibility of collagen/HA-based hybrid scaffolds:

a) Degradation behaviours of crosslinked collagen-HA scaffolds in physiological fluids:

Evaluating *in-vitro* degradation of collagen/HA is based on the mass loss in physiological fluids like phosphate buffer saline (PBS) at 37°C over a given period with or without

enzymes (collagenase for collagen and hyaluronidase for HA) [191, 211, 212]. Degradation in non-enzymatic physiological fluids (*in-vitro*) occurs through hydrolysis whereas polymer chain cleavage in the presence of enzymes further accelerates the degradation under *in-vivo* conditions [213, 214]. The degree of crosslinking also affects the degradation rate and the overall mass loss of collagen/HA based materials. The higher the crosslinking density, the slower will be the degradation rate [215]. The chemistry of crosslinks assisted by a certain crosslinking agent also affects the degradation behaviour of collagen e.g. zero-length crosslinks formed by EDC/NHS are more resistant to degradation as compared to Schiff based structures formed by GA as shown in figure 1.20 (a, b)[215]. The addition of a high molecular mass pendant group such as glycidyl methacrylate (GMA) or palmitoyl on the HA backbone increased the hydrophobicity of HA [127, 216, 217]. Increase in hydrophobicity increased the degradation resistance of GMA substituted HA hydrogels as shown in figure 1.23[218].

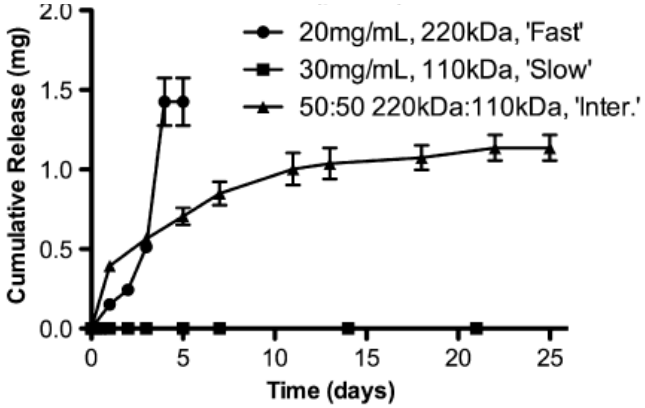


Figure 1.23: Hydrolytic degradation of different GMA-HA hydrogels formulations targeting slow, intermediate, and fast degradation rates[218].

The degradation mechanism of HA hydrogel is also influenced by the pH of the medium. Acid and base-catalyzed hydrolysis cleave the 1→3 and/or 1→4 glycosidic bond of HA as shown in figure 1.15. Deacetylation of the N-acetyl group also occurs at basic medium which results in rapid degradation rates as shown in figure 1.24[216, 219]. Collagen/HA based scaffolds could have potential with tunable degradation properties to allow enough time for the heart

tissue to regenerate completely. Their degradation resistance can be increased by introducing chemical bonds (crosslinks) in both the components as well as ensuring maximum interlocking between the two networks.

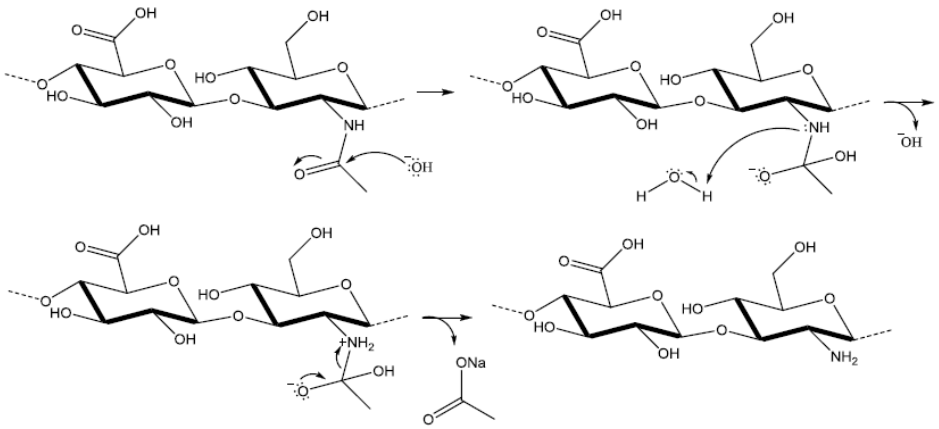


Figure 1.24: Mechanism of deacetylation of N-acetyl group of HA in basic medium[219].

b) Cell compatibility of crosslinked collagen-HA based hybrid scaffolds:

The choice of cell source plays a crucial role in the success of a tissue-engineered graft[220, 221]. Various cell sources, from human and animals, have been compiled by Jana *et al* and given in table 1.7[222]. Allogenic (derived from another individual of the same species) and xenogenic (derived from different species) cells involve risk of immunogenic response[223]. Therefore, patient-specific cells could be the most compatible choice for TEHV. Duan *et al* have attempted to seed the human aortic valve interstitial cells (HAVICs) on bio-printed methacrylated HA (Me-HA) and methacrylated gelatin (Me-Ge) hybrid scaffolds. HAVICs showed viability potential on Me-HA/Me-Ge hybrid scaffolds by the deposition of collagen and GAGs [224].

Table 1.7: Cell sources for TEHVs[222].

Cell type	Organ source (tissue/animal)
Valvular interstitial cell	Aortic valve/porcine
Valvular endothelial cell	Aortic valve/bovine
Endothelial cell	Carotid artery/lamb
Bone marrow progenitor cell	Bone marrow/lamb
Myofibroblast	Aortic wall/porcine
Mesenchymal stem cell	Bone marrow
	Adipose tissue
	Umbilical cord matrix
	Umbilical cord blood
	Amniotic fluid
	Chorionic villi
Endothelial progenitor cell	Amniotic fluid
	Peripheral blood
	Umbilical cord blood
Valvular interstitial cell	Aortic valve
Induced pluripotent stem cell	Skin (fibroblasts)

It has also been shown that HAVICs exhibited better fibroblastic phenotype on combinational scaffolds as compared to homogenous scaffolds [148]. However, the procedure to take a biopsy from a human valve is challenging due to its critical location and there is a need to look for alternative cell sources[225]. Recent research at the University of Oxford has shown a uniform distribution of cardiosphere-derived cells (CDCs) on novel bi-layer collagen/elastin scaffolds indicating their potential for TEHV [226]. The emergence of induced pluripotent stem cells (iPSCs) has also opened new possibilities for tissue engineering and can be alternative cell source for TEHVs[227, 228].

c) Cardiac tissue culture on natural polymer based crosslinked scaffolds in a bioreactor:

A further step in the experimental development towards *in-vitro* tissue engineering is the evolution of bioreactors to culture an actual tissue outside the body. Bioreactors can mimic the physiological conditions such as using growth factors, mechanical, and electrical stimuli but also yield an actual graft[229, 230]. A summary of various factors involved in cardiac tissue regeneration under *in-vitro* and *in-vivo* environments is given in table 1.8[231]. Smooth muscle cells (SMC) have been cultured on collagen-elastin scaffolds under pulsatile flow conditions. In addition to the uniform distribution of cells, cultured grafts also exhibited increased mechanical properties as compared to those cultured under static conditions as shown in table 1.9[232]. Microfabricated poly (glycerol sebacate) (PGS) scaffolds have been cultured with supplemental insulin-like growth factor-1 (IGF-1) and electrical stimuli (to mimic heart beat). The results showed that the use of electrical signals resulted in 10 times enhancement of matrix metalloproteinase-2 (MMP-2) gene expression [233].

Table 1.8: A biomimetic approach to cardiac tissue engineering; main factors of the *in-vivo* myocardial environment and their *in-vitro* counterparts [231].

	In-vivo	*In-vitro*
Cells	High density (~10^8cells/cm^3) Multiple cell types (cardiac myocytes, fibroblasts, endothelial cells)	High density (~0.3×10^8cells/cm^3) Multiple cell types (cardiac myocytes, fibroblasts, endothelial cells)
Geometry	Capillary network (~7 µm diameter, ~20 µm spacing)	Parallel channel array (100-300 µm diameter 100-300 µm spacing)
Mass transport	Convection: Blood flow ~500µm/s Diffusion in tissue space	Convection: Medium flow at velocities ~50-500 µm Diffusion in construct space
Oxygen carrier	Hemoglobin (arterial blood) O_2 dissolved in plasma 130 µM O_2 as oxyhemoglobin 8,500 µM O_2 total 8630 µM	PFC emulsion (at 160mm Hg and 37° C) O_2 dissolved in aqueous phase 220 µM O_2 in PFC particles 230 µM O_2 total 450 µM
Physical signals	Excitation (by electrical signals from pacer cells), Synchronous contractions and electro-mechanical cell coupling (functional gap junctions, contractile apparatus)	Electrical stimulation (by pacing) of cultured constructs, Synchronous contractions, and electro-mechanical cell coupling

Table 1.9: Mechanical properties of crosslinked and uncrosslinked collagen/elastin scaffolds after culture with SMC for 7 days under static or dynamic conditions[232].

Culture environment	Crosslinking method	Stiffness at low strain (kPa)	Stiffness at high strain (kPa)	Yield stress (kPa)	Yield strain (%)
Static	None	2.00 ± 0.01	18.0 ± 1.0	4.0 ± 0.1	160 ± 10
	EDC/NHS	10.0 ± 0.5	16.0 ± 1.0	15 ± 1	160 ± 30
Dynamic	None	10.0 ± 0.01	35.0 ± 1.0	20 ± 10	220 ± 20
	EDC/NHS	10.0 ± 0.01	35.0 ± 1.0	40 ± 10	130 ± 30

Natural polymer based scaffolds such as fibrin-cultured with neonatal rat heart cells in a dynamic environment produced a fully functional graft after four weeks in a rat model [234]. On-going attempts with bioreactors to furnish TEHVs showed satisfactory performance on the pilot scale but the debate on the feasibility of cultured implants on human heart scale is still unresolved [157, 235, 236]. The potential of cardiac tissue culture using human stem cells in a bioreactor is also debatable [237].

1.4 Conclusion:

Natural polymers such as collagen type I and HA offer advantages such as existence in the natural heart valve ECM, abundant availability from natural sources, and biocompatibility. In addition, a single polymer alone cannot fulfill all the requirement for the design of a heterogeneous scaffold for TEHV due to the tri-layer (heterogeneous) microstructure of the heart valves leaflets. Therefore, these polymers have been selected for study in this thesis

because collagen/HA based hybrid scaffolds are expected to have the potential to overcome the current challenges such as microstructural heterogeneity, maintaining the mechanical strength in the physiological environment, and controlled degradation rate.

While collagen/HA based hybrid scaffolds have been developed for various tissue engineering applications such as bone, skin, and eye; fundamentals of this approach could be extended for the fabrication of TEHVs. Current crosslinking strategies such as DHT and use of irradiation yield scaffolds with inferior mechanical properties and require careful handling of processing parameters to avoid the alterations in protein structures. EDC/NHS crosslinking not only reduces the risk of collagen denaturation but also have the potential to produce hybrid scaffolds with heterogeneous microstructure. Furthermore, the concentration of EDC/NHS can be closely controlled to develop hybrid scaffolds with varying crosslinking densities and hence tailorable properties can be achieved. Therefore, chapter 2 will focus on a modified fabrication route based on EDC/NHS, adopted in this thesis, for the synthesis of collagen/HA hybrid scaffolds.

Chapter 2

Fabrication and Microstructural Characterization of Collagen/HA Hybrid Scaffolds

2.1 Introduction:

Three-dimensional porous scaffolds with tailorable properties capable of mimicking the extracellular matrix (ECM) should be 'ideal' for growing tissue [238, 239]. Collagen type I and hyaluronic acid (HA), together making around 70 % by mass of the heart valve ECM, have been selected in this study [240, 241]. Porous hybrid scaffolds have been prepared by using the freeze-drying method. Freeze-drying is a well-proven fabrication technique for the development of uniformly porous biocompatible materials. The greatest advantage of freeze-drying is the use of water rather than any organic chemicals [215, 242]. Ice-crystals produced as a result of freezing process act as the porogen (pore creators) [243].

Chemical crosslinking techniques have advantages over physical crosslinking methods as discussed in chapter 1 (see table 1.6). 1-Ethyl-3-(3-dimethylaminopropyl)-carbodiimide / N-Hydroxysuccinimide (EDC/NHS) chemistry offers incentives such as the minimal chance of depolymerization, zero-length crosslinking, preservation of protein structure, and easy removal of water-based by-products[244-247]. It has been hypothesized that hybrid scaffolds with interlaced microstructure could be developed using a multi-step chemical crosslinking technique based on EDC/NHS. A sequential approach to the crosslinking technique is expected to minimize crosslinking between collagen type I and HA networks.

This chapter outlines the experimental scheme adopted for the synthesis of collagen network, HA network, and the resultant hybrid scaffolds. A wide range of samples has been prepared by using different concentrations of EDC/NHS. Crosslinking density for all the compositions has been estimated by the Flory-Rehner equation. In addition, the effect of variation in EDC/NHS concentration (or crosslinking density) on properties of the parent networks as well as hybrid scaffolds has been examined. FTIR has been employed to draw information about the changes in chemical bonding resulted from the crosslinking process. Also, FTIR spectra along with TGA have been used to study possible interactions between the networks. Microstructural changes and variations in pore size have been studied through scanning electron microscopy (SEM). Differential staining has been used to map the mutual distribution of the parent networks.

2.2 Materials and methods:

This section will discuss the synthesis of type I collagen network, HA network, and the resultant hybrid scaffolds.

2.2.1 Synthesis of collagen network:

Type I collagen (from bovine Achilles tendon) was purchased from Sigma-Aldrich, UK. 1%w/v suspension of collagen was prepared by dispersing collagen fibrils in 0.05M acetic acid (pH 3.2) [248, 249]. The suspension was homogenized using a blender (HR1611/01, 650 W, Philips, UK). The process was performed in an ice-bath to reduce the chance of denaturation that could have been caused by heat generated during blending. The suspension was then transferred to polytetrafluoroethylene (PTFE) moulds (15mm diameter, 10mm height) as shown in figure 2.1A, frozen overnight at -20^{o}C (EU7120C, Electrolux, UK), and freeze-dried in a Christ I-5 freeze-dryer (Martin Christ Gefriertrocknungsanlagen GmbH, Germany)

for 24 hours under a vacuum of 5Pa. This process resulted in the removal of ice crystals by sublimation leaving behind the three-dimensional porous collagen scaffolds as shown in figure 2.1B [226].

Several scaffolds were left uncrosslinked at this stage. The remaining scaffolds were cross-linked by N-(3-Dimethylaminopropyl)-N′-ethylcarbodiimide hydrochloride (EDC) (Sigma-Aldrich, UK) and N-Hydroxysuccinimide (NHS) (Sigma-Aldrich, UK) at various concentrations (table 2.1). The ratio of EDC: NHS was fixed at 2:1. EDC/NHS were dissolved in a 50:50 ethanol-phosphate buffer saline (PBS) [193, 250]. Scaffolds were placed in the solution and shaken gently for 4 hours. They were then washed in 1M NaCl solution for 2 hours followed by washing in deionized water for 2 hours, then carefully removed from the water and allowed to drain on a wire mesh for 1min. Finally, scaffolds were frozen at -20^{o}C overnight followed by freeze-drying [251].

Table 2.1: Concentration of EDC/NHS used for crosslinking collagen networks.

Sample ID	Conc. of EDC (mM)	Conc. of NHS (mM)
C0	0	0
C25	25	12.5
C40	40	20
C60	60	30

2.2.2 Synthesis of HA network:

0.2 g of sodium hyaluronate ($C_{14}H_{22}NNaO_{11}$), SHA, (95%, ACROS organics) was dissolved in 50 ml of distilled water (equivalent to 4mg/ml) with continuous stirring at room

temperature. 3.5 g (30 times molar excess) of adipic dihydrazide (ADH, 98%, Sigma-Aldrich) was added to the above solution, resulting in the formation of a clear and slightly viscous solution [252]. The pH of the solution was adjusted to 4.75 by adding few drops of 0.1 N HCl. 0.02 g of EDC (2mM) was added to the above solution while maintaining the pH at 4.75. The reaction was stirred for 24 hours, then stopped by increasing the pH to 7.0 by the addition of 1N NaOH. The reaction mixture was transferred to a dialysis tube (Mw cut-off = 14,000, Sigma-Aldrich). The mixture was dialyzed for 24 hours against 150 mM NaCl and then for 24 hours against deionized water to remove any residues, then poured into PTFE molds and put in -20 ^{o}C freezer for 24 hours. The frozen scaffolds were lyophilized for 24 hours. The final product (ADH modified HA) in the form of a white and soft material was removed from the molds as shown in figure 2.1C. The above procedure was repeated with 4 mM (HA4), 10 mM (HA10), and 20 mM (HA20) of EDC to prepare HA networks with different crosslinking densities.

2.2.3 Synthesis of collagen/HA hybrid scaffolds:

Collagen/HA hybrid scaffolds were prepared by combining the two networks together. HA solutions with two different concentration of EDC (i.e. HA2 and HA20) were prepared as described in section 2.2.2. Un-crosslinked and crosslinked collagen scaffolds (i.e. C0 and C60, see table 2.1) prepared according to the protocol described in section 2.2.1 were placed in each of the HA solutions for 24 hours with gentle stirring as shown in figure 2.1D. HA formed the secondary network through the primary collagen network. The resulting hybrid scaffolds were removed from the HA reaction mixture after 24 hours and washed according to the protocol described in section 2.2.1. The various types of hybrid compositions are listed in table 2.2. Preparation of S-1 and S-2 did not involve crosslinking of collagen networks and the scaffolds were immersed in the HA solution straightaway after the first cycle of

freeze drying. For S-3 and S-4, collagen network had been crosslinked with 60mM EDC/30mM NHS. Finally, they were frozen at -20^{o}C overnight and freeze-dried for 24 hours as shown in figure 2.1E. A schematic of the process is presented in figure 2.2.

Table 2.2: Nomenclature and composition details of collagen/HA hybrid scaffolds.

Sample ID	Primary collagen network Conc. of EDC (mM)	Secondary HA network Conc. of EDC (mM)
S-1	0	2
S-2	0	20
S-3	60	2
S-4	60	20

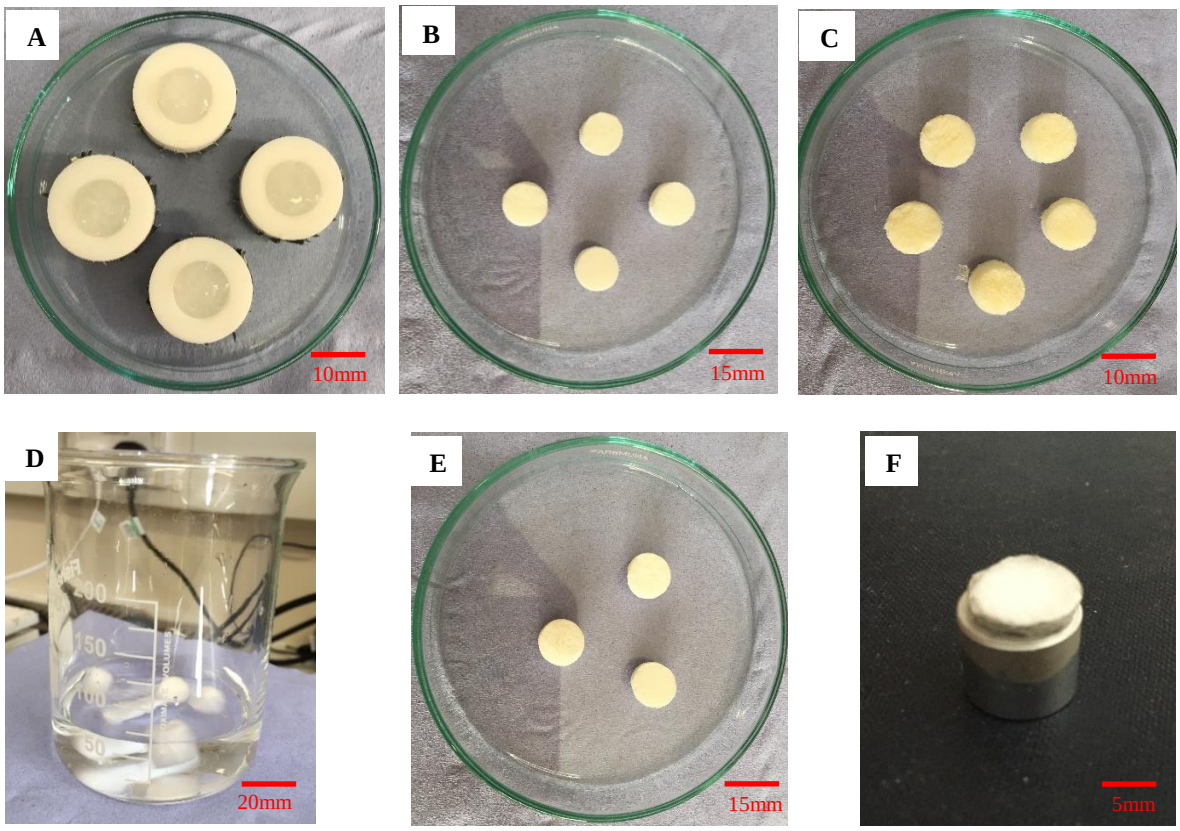


Figure 2.1: (A) Collagen suspension in PTFE molds, (B) Freeze-dried collagen scaffolds, (C) Freeze-dried HA scaffolds, (D) Collagen scaffolds in crosslinking HA solution, (E) Freeze-dried collagen/HA hybrid scaffolds, and (F) Platinum coated collagen/HA scaffold sample for SEM.

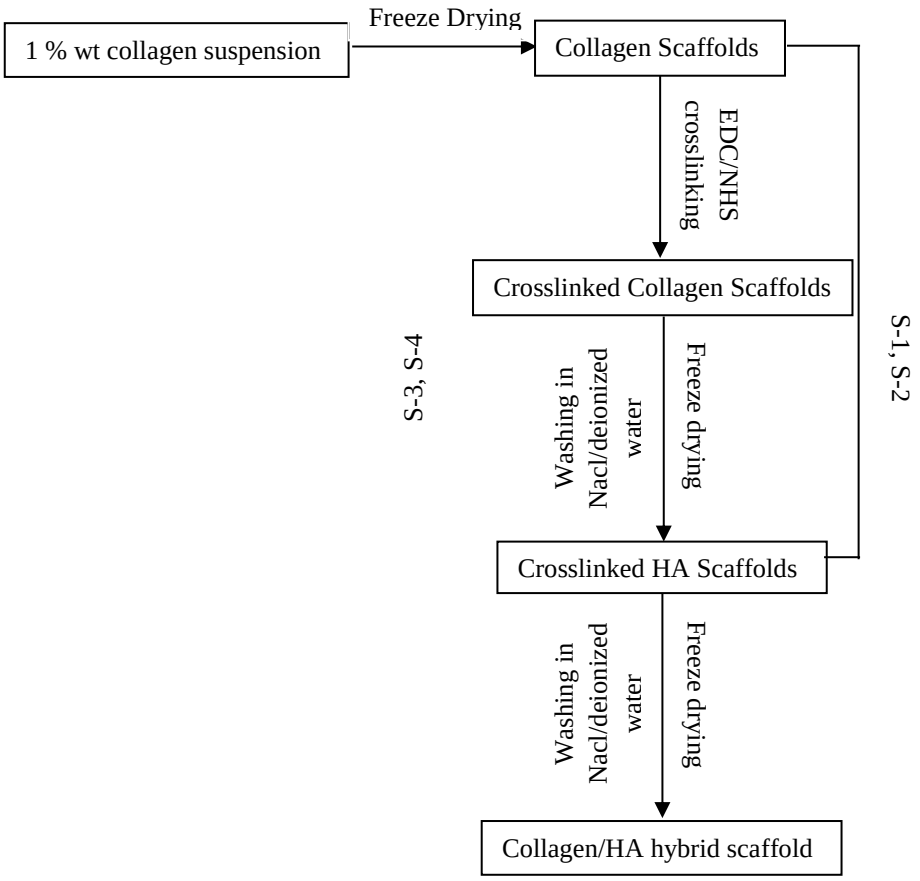


Figure 2.2: Schematic diagram for the fabrication of collagen/HA hybrid scaffolds through sequential EDC/NHS crosslinking route.

2.2.4 Crosslinking density and swelling behaviour:

All swelling experiments were performed in deionized water at 37 ^{o}C for 24 hours and repeated three times. The degree of mass swelling (Q_M) is simply the ratio of mass gain (M_2-M_1) to initial mass (M_1) of samples. Volumetric swelling ratio, $Q_{v,}$ is related to the degree of mass swelling, Q_M, through Eq. 2.1 [253]:

$$Q_v = 1 + \rho_p/\rho_s (Q_M - 1) \qquad \textit{Eq. 2.1}$$

Where ρ_p = Density of the dry polymer (1.229 gm/cm^3 for HA, 1.35 gm/cm^3 for collagen)

ρ_s = Density of water

Average molecular weight between the two crosslinks (M_c) for collagen network, HA network, and hybrid scaffolds was estimated by using a simplified version of the Flory-Rehner equation [254]:

$$Q_v^{5/3} = vM_c / V_1 (0.5\text{-}X) \qquad \textit{Eq. 2.2}$$

Where Q_v = Volumetric swelling ratio

v = Specific volume of dry polymer (m^3/kg)

M_c= Average molecular weight between the two crosslinks (kg/mol)

V_1=Molar volume of the solvent ($18cm^3/mol$ for water)

X= Flory polymer-solvent interaction parameter (0.473 for HA, 0.495 for collagen [255])

Finally, the effective crosslinking density, v_e, was calculated from M_c using Eq. 2.3 [175]:

$$v_e = \rho_p / M_c \qquad (kmol/m^3) \qquad \textit{Eq. 2.3}$$

The degree of crosslinking is defined as the reciprocal of the average of the molecular mass between two crosslinks (M_c) and given by [256]:

$$X_c = 1/M_c \qquad (mol/kg) \qquad \textit{Eq. 2.4}$$

Similarly, the distance between sequential crosslink points, ξ, is given by [254, 256]:

$$\xi = 0.1748 \sqrt{M_c} (Q_v)^{1/3} \quad (nm) \qquad \textit{Eq. 2.5}$$

2.2.5 Scanning electron microscopy (SEM):

The scanning electron microscope utilizes a beam of electrons directed at the surface of the specimen (provided by tungsten or LaB_6 filament or a field emission gun, (FEG))[257]. The secondary electrons emitted from the sample surface are detected and amplified by a

scintillator-photomultiplier system, and the signal is converted into a grey scale image to obtain the surface topography and microstructure image. SEM can provide a higher resolution than a light microscopy by utilizing an electron beam. In addition, one of the major advantages of SEM is the large depth of field, which is especially useful for obtaining an image of a highly porous structure such as scaffolds[258].

Scanning electron microscopy (SEM, JEOL JSM-840F) was employed for imaging of surfaces of scaffolds fixed on a conducting stub with carbon tape. Samples were sectioned with a sharp razor blade and mounted onto 12mm diameter aluminum stubs using adhesive carbon tabs. All samples (n = 5) were coated with 3.0 nm platinum coating using a 208HR sputter coater (Cressington Scientific Instruments Ltd, UK) as shown in figure 2.1F. SEM images of scaffolds (5 images/sample) were taken at an accelerating voltage of 10 kV. Pore size analysis was performed by measuring the diameters of the pores (25 measurements/image) by ImageJ software (National Institute of Health, USA).

2.2.6 Alcian blue-periodic acid (PAS) differential staining *:

Alcian blue-periodic acid (PAS) belong to the family of basic dyes which are used to stain acidic polysaccharides such as proteoglycans (PGs) and glycosaminoglycans (GAGs) in connective tissues such as cartilage and mucus [259, 260]. Parent networks, as well as hybrid scaffolds (n = 3), were processed using ShandonTM ExcelsiorTM ES Tissue Processor (Thermo Scientific, UK). All samples were dehydrated by exposing it to a gradient of ethanol (VWR chemicals, UK) 70%, 80%, 90%, and 100% for 90 minutes in each followed by treatment with histoclear II (National Diagnostics, UK) for 90 minutes. Next, the samples were treated with Fibro wax TM (VWR chemicals, UK) for 4 hours using a wax embedding

* performed by Richard Stillion, Sir William Dunn School of Pathology, University of Oxford.

machine (Surgipath Medical Industries, UK). Wax-embedded samples were cut into 5µm thick slices using LEICA DSC1 microtome cutter (Mercedes Medical, UK). The samples were mounted onto the glass slides and were dried overnight at 37ºC. Samples were then dewaxed in histoclear II solution for 10 minutes followed by rehydration in an ethanol gradient 70%, 80%, 90% and 100% for 30 seconds in each. Collagen/HA hybrid scaffolds were stained using alcian blue-PAS kit (Clin-Tech Kit, UK, Cat no: 631045) according to the standard procedure to examine the spatial distribution of HA within the samples [261]. Samples were examined under a 'DSS1' Nikon Slide Scanner at various magnifications.

2.2.7 Fourier transform infrared spectroscopy (FTIR):

Fourier transform infrared spectroscopy (FTIR) is a widely-used technique in industry and research to determine the presence of a specific chemical bond. It utilizes an infrared beam, which interacts with the chemical bonds present in the material, to determine the state of the bonds, such as bending, stretching or contracting[262]. The technique involves passing an infrared beam through a thin specimen sandwich between two potassium bromide (KBr) discs. The absorbance of the infrared light by specific bonds at specific wavelengths is recorded against background scan every hour. KBr discs are transparent to infrared radiation between 40,000 cm^{-1} and 400 cm^{-1}, and thus, are used for sample preparation[263].

In this study, any potential changes in the molecular structures of both collagen and HA, as well as hybrid scaffolds (n = 3) during the manufacturing process, were studied using a Varian FTIR spectrometer (UMA600, Palo Alto, CA). Spectra of infra-red absorbance were collected in the mid-infrared region (wavenumber 4000 – 400 cm^{-1}) with a resolution of 8 cm^{-1} averaging 64 scans per sample.

2.2.8 Thermogravimetric analysis (TGA):

Thermogravimetric analysis (TGA) is the technique which measures the change of mass of a material, either as a function of temperature or isothermally as a function of time, in an inert atmosphere. TGA is employed to draw information about the thermal profile of a material (degradation temperature, glass-transition temperature, and other phase changes)[264, 265]. Thermal degradation profiles for the individual networks, as well as hybrid scaffolds (n = 3), were determined. The samples, weighing between 6 – 8 mg, were analyzed in open ceramic pans on a Pyris Diamond TG/DTA under an N_2 purge (60 ml/min) and at a scan rate of 10^{o}C/min up to 500^{o}C.

2.2.9 Statistical analysis *:

All data have been reported as means, with the standard deviations as the errors. One-way analysis of variance (ANOVA) followed by Tukey's test has been used to compare groups of samples, with a probability value of 95% ($p < 0.05$) to determine statistical significance. Two-tailed Pearson's correlation tests have been performed to examine the correlation between calculated crosslinking density and FTIR relative peak intensity ratio. Pearson product-moment correlation coefficient (R^2) has been used to measure the linear correlation (dependence) between the crosslinking density and FTIR peak intensity ratios. *p* values less than 0.05 have been considered significant.

* performed by Carolyn Carr, Department of Physiology, University of Oxford.

2.3 Results:

2.3.1 Crosslinking density and swelling behaviour:

Table 2.3A shows that both mass swelling ratio (Q_M) and the volumetric swelling ratio (Q_v) of collagen network, HA network, and hybrid scaffolds decrease with increasing EDC concentration. Table 2.3B shows the values of average molecular weight between the two crosslinks (M_c), effective crosslinking density (v_e), the degree of crosslinking (X_c), and the distance between crosslinks (ξ) for collagen network, HA network, and hybrid scaffolds. Crosslinking densities for both collagen and HA networks increase gradually with an increase in the concentration of EDC. Similarly, crosslinking densities also increase gradually from S-1 to S-4. The values of crosslinking densities for all hybrid scaffolds are higher than their parent collagen network and lower than their parent HA network.

Table 2.3A: Effect of EDC concentration on the mass swelling ratio (Q_M) and the volumetric swelling ratio (Q_v) of collagen network, HA network, and hybrid scaffolds. [a] and [b] represents statistically significant values within collagen networks as compared to C0 and C25 respectively. [c], [d], and [e] represent statistically significant values within HA networks as compared to HA2, HA4, and HA10 respectively. [f], [g], and [h] represent statistically significant values within hybrid scaffolds as compared to S-1, S-2, and S-3 respectively.

Sample ID	Mass swelling ratio (Q_M)	Volumetric swelling ratio (Q_v)
C0	82 ± 5	28 ± 3
C25	78 ± 7	22 ± 5
C40	78 ± 5	20 ± 5
C60	46 ± 8 [a, b]	12 ± 3 [a, b]
HA2	40 ± 7	18 ± 3
HA4	42 ± 5	14 ± 1
HA10	30 ± 8 [c]	11 ± 4 [c, d]
HA20	32 ± 3 [c, d]	8 ± 3 [c, d, e]
S-1	43 ± 6	7 ± 2
S-2	34 ± 7	5 ± 1 [f]
S-3	35 ± 5	5 ± 1 [f]
S-4	33 ± 8	4 ± 1 [f]

Table 2.3B: Effect of EDC concentration on swelling properties of collagen network, HA network, and hybrid scaffolds. [a] and [b] represents statistically significant values within collagen networks as compared to C0 and C25 respectively. [c], [d], and [e] represent statistically significant values within HA networks as compared to HA2, HA4, and HA10 respectively. [f], [g], and [h] represent statistically significant values within hybrid scaffolds as compared to S-1, S-2, and S-3 respectively.

Sample ID	Average molecular weight between the two crosslinks (M_c, $\times 10^2$ kg/mol)	Degree of crosslinking (X_c, $\times 10^{-3}$mol/kg)	Effective crosslinking density (v_e, kmol/m^3)	Distance between crosslinks points (ξ, nm)
C0	32 ± 2.5	0.3 ± 0.03	0.4 ± 0.03	37 ± 1
C25	10 ± 1 [a]	1 ± 0.1	1.3 ± 0.2	19 ± 1[a]
C40	6.7 ± 2.5 [a]	1.8 ± 0.09 [a]	2 ± 1 [a]	15 ± 3 [a]
C60	4.1 ± 0.5 [a, b]	2.4 ± 0.3 [a, b]	3.3 ± 0.4 [a, b]	11 ± 1 [a, b]
HA2	6.4 ± 0.9	1.6 ± 0.3	2 ± 0.3	9.7 ± 1
HA4	5.2 ± 0.2	2 ± 0.08	2.5 ± 0.1	8.3 ± 0.2
HA10	3.3 ± 0.6 [c]	3.2 ± 0.7	4.3 ± 0.1	6.0 ± 0.6 [c, d]
HA20	0.8 ± 0.2 [c, d, e]	12 ± 0.3 [c, d, e]	17 ± 4 [c, d, e]	2.4 ± 0.3 [c, d, e]
S-1	16 ± 2.1	0.6 ± 0.09	0.8 ± 0.1	13 ± 1
S-2	14 ± 2.4	0.7 ± 0.01	0.9 ± 0.1	10 ± 1 [f]
S-3	7 ± 0.2 [f, g]	1.4 ± 0.05 [f, g]	5.0 ± 0.6 [f, g]	8.2 ± 0.1 [f]
S-4	5 ± 0.1 [f, g]	2 ± 0.05 [f, g, h]	6.8 ± 0.7 [f, g, h]	7.3 ± 0.1[f, g]

2.3.2 SEM and pore size analysis:

Figure 2.3 shows representative SEM images of (A) C0, (B) C25, (C) C40, and (D) C60. These images of crosslinked collagen networks indicate that multiple cycles of freeze-drying involved in the fabrication process did not affect the pore shape. The mean pore sizes within primary collagen network are summarized in table 2.4. It shows that the mean pore size tends

to decrease from C0 to C60 as a result of increasing EDC concentration. The difference between the mean pore sizes of C40 and C60 is not statistically significant. Figure 2.3E shows a SEM image of the HA network (HA20). The freeze-drying process has introduced micropores in HA network. No specific pattern for pore shape and pore size was observed in all the HA network samples regardless of the concentration of EDC. The mean pore size is calculated to be 10 μm (S.D = ±5 μm).

Figure 2.4 (A-D) shows SEM images for S-1, S-2, S-3, and S-4, respectively. The thickness of the fine mesh (t), spacing between mesh (d), and primary network pore size (p) are listed in table 2.4. The secondary HA network appears as fine parallel mesh across the diameter of primary collagen pores in S-1 and S-2 (figure 2.4A and figure 2.4B). There is no significant difference between the pore sizes of S-1 and S-2. Figure 2.4C shows the HA threads forming an incomplete network in S-3, whereas S-4 (figure 2.4D) shows a more tightly packed microstructure. In comparison with parent collagen scaffolds, the pore diameter of primary collagen network tends to decrease with the incorporation of secondary HA network in the hybrid scaffolds (table 2.4).

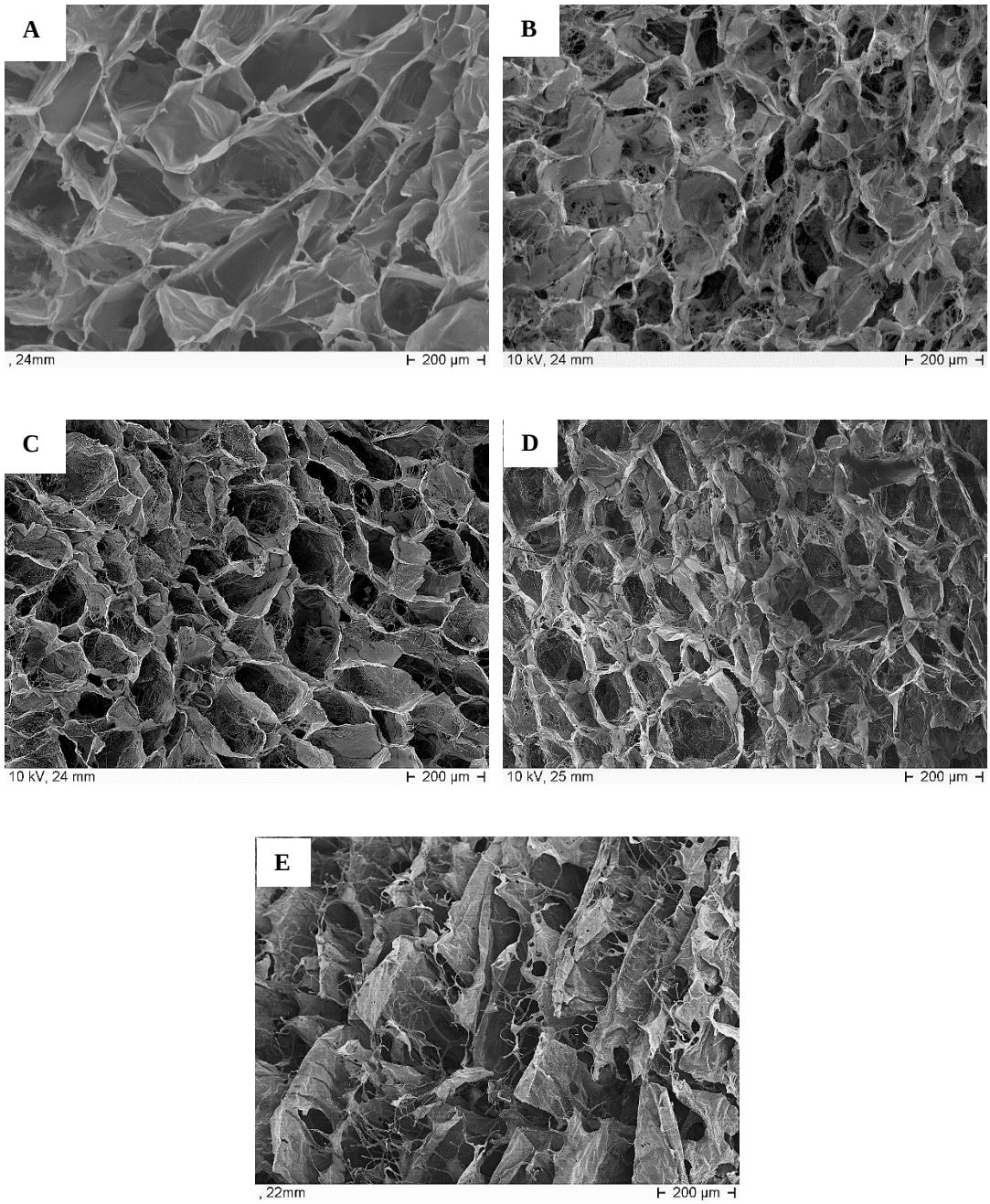


Figure 2.3: SEM images of (A) C60, (B) C25, (C) C40, (D) C60, and (E) HA20.

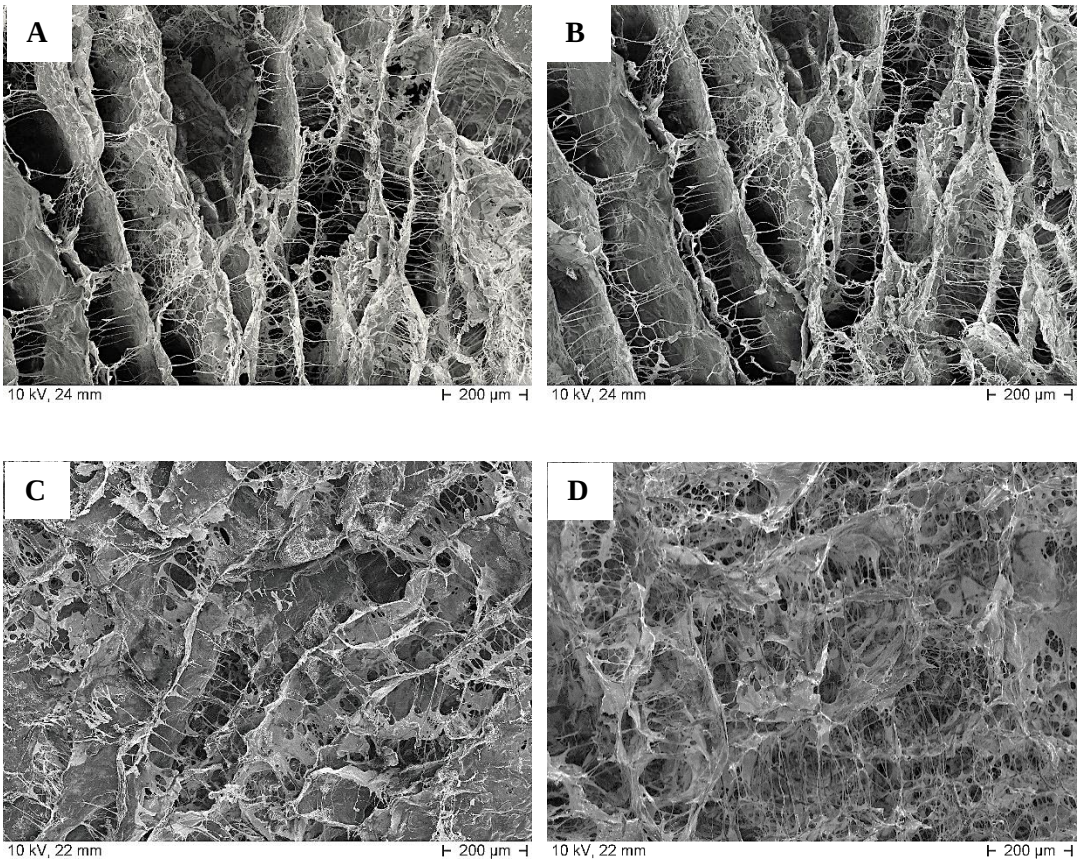


Figure 2.4: SEM images of (A) S-1, (B) S-2, (C) S-3, and (D) S-4.

Table 2.4: Pore dimensions for primary collagen networks and hybrid scaffolds. [a] and [b] represent statistically significant values within collagen networks as compared to C0 and C25 respectively. [c], [d], and [e] represent statistically significant values within hybrid scaffolds as compared to S-1, S-2, and S-3 respectively.

Sample ID	Mean diameter (µm)	Spacing between fibers (d, µm)	Fibre Thickness (t, µm)
C0	170 ± 19	-	-
C25	148 ± 25 [a]	-	-
C40	120 ± 10 [a, b]	-	-
C60	109 ± 13 [a, b]	-	-
S-1	126 ± 4	33.4 ± 1.5	4
S-2	125 ± 5	25 ± 0.9	4
S-3	84 ± 16 [c, d]	-	-
S-4	66 ± 9 [c, d, e]	-	-

2.3.3 Alcian blue-periodic acid (PAS) differential staining:

Alcian blue-PAS staining is able to differentiate between the collagen network (appear grey) and HA network (appear blue) as shown in figure 2.5A and 2.5B. Bands of collagen and HA are present in all hybrid scaffolds. HA network is interlaced with collagen network on microscale as shown in figure 2.5C, 2.5D, 2.5E, and 2.5F. S-3 and S-4 show well-arranged bands of collagen and HA in the microstructure as compared to S-1 and S-2. Figure 2.5G and 2.5H showed zoom-in images of S-1 and S-2 respectively.

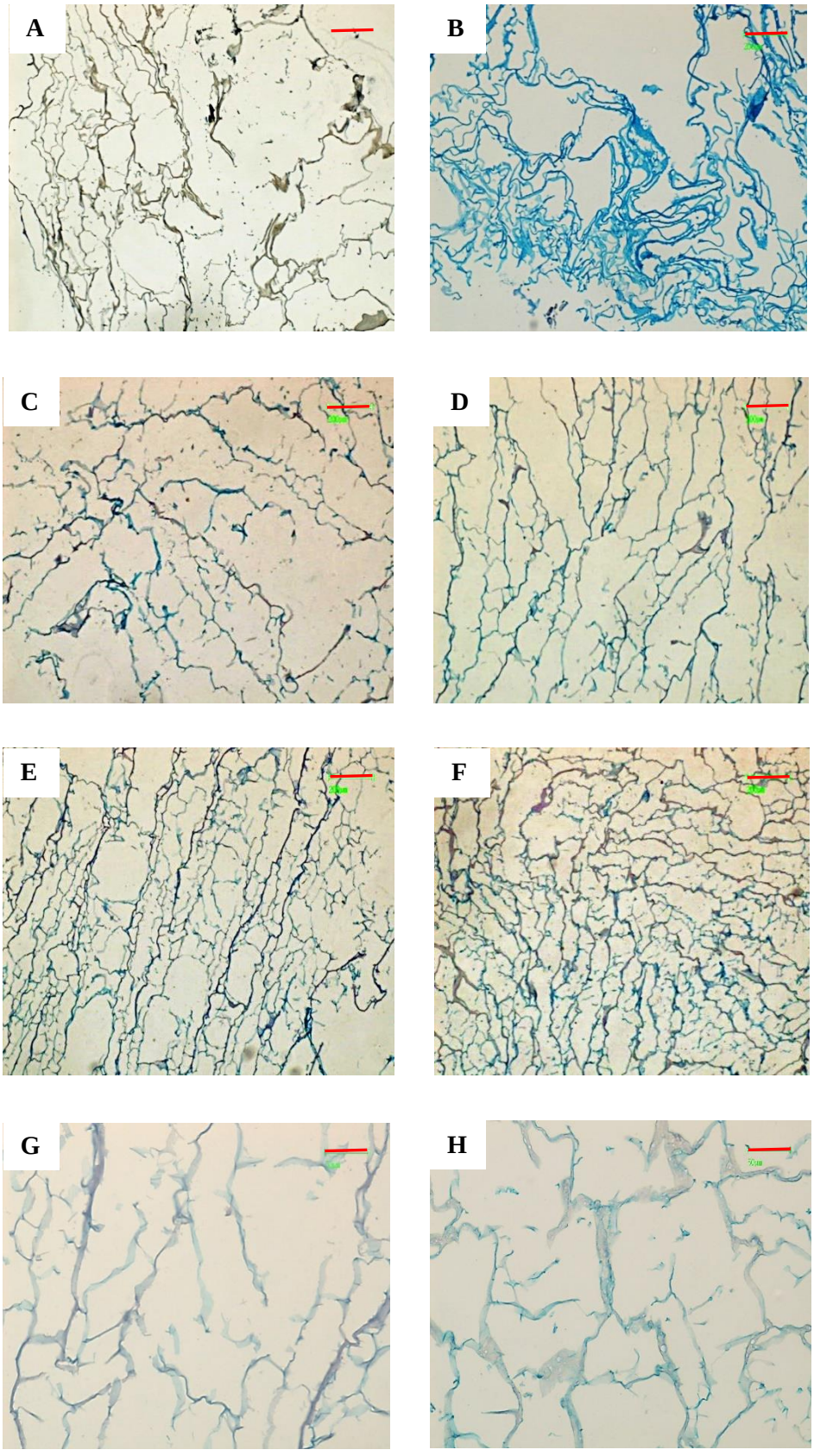


Figure 2.5: Histology images of alcian blue-PAS stained samples (A) C60, (B) HA20, (C) S-1, (D) S-2, (E) S-3, (F) S-4, (G) S-1, and (H) S-2. Image A-F (100X, scale bar = 200 µm) and image G-H (50X, scale bar = 50 µm).

2.3.4 Fourier transform infrared spectroscopy (FTIR):

Figure 2.6 presents the FTIR spectra of C0, C25, C40, and C60 (table 2.1). FTIR of C0 shows the four characteristic amide bands of pure collagen at frequencies of 3307, 3051, 1633, and 1546 cm^{-1}. 1633 cm^{-1} has been assigned to amide I bands resulting from C=O stretching vibrations coupled to N–H bending vibration. Amide II bands at 1546 cm^{-1} arise from the N–H bending vibrations coupled to C–N stretching vibrations. The remaining two peaks at 3307 and 3051 cm^{-1} arise from the stretching vibrations of N—H group [266]. After crosslinking with EDC/NHS, an increase in the intensity of the amide bands (1633, 1546, 1240 cm^{-1}) and ester band (1164 cm^{-1}) has been observed (figure 2.6). Relative peak intensities in FTIR spectra reveal information about the extent of crosslinking. In this case, the peak at 1164 cm^{-1} is assigned to C—O stretch in the ester carbonyl[267-269] and its relative intensity gives a direct indication of the amount of ester crosslinking. Similarly, amide formation can be estimated by amide II peak at 1544 cm^{-1} corresponding to –NH in the amide bond [203, 266]. All spectra have been normalized against absorption at 2925 cm^{-1}, assigned to the CH_2 group. This peak remains unchanged during the crosslinking reaction [270]. The relative peak intensities associated with ester and amide bonds are summarized in table 2.5. These values suggest that more and more ester and amide crosslinks are introduced as the concentration of EDC/NHS is gradually increased from 0/0mM to 60/30mM. A correlation is found between the crosslinking densities (table 2.5) and relative peak intensities (table 2.5) for collagen networks. Correlation for amide bond (R^2 = 0.9039, p = 0.0492) is stronger than for ester bond (R^2 = 0.8965, p = 0.0532) as shown in figure 2.7.

Figure 2.8 shows that EDC assisted crosslinking of ADH modified HA has resulted in the formation of new peaks at 1624 cm^{-1}, 1531 cm^{-1}, and 1273 cm^{-1}. The cross-linked hydrogel shows the appearance of twin peaks at 3282 cm^{-1} and 3300 cm^{-1}. Figure 2.9 shows the FTIR

for S-4 as a representation for collagen/HA hybrid scaffolds. FTIR spectrum of S-4 can be seen as the summation of the spectra of parent networks as it shows the presence of characteristic peaks of both collagen and HA. While comparing spectra for C60, HA20 and S-4 in figure 2.9; twin peaks, 3282 cm^{-1} and 3300 cm^{-1} for crosslinked HA network are superimposed on the 3600-3100 cm^{-1} band for collagen.

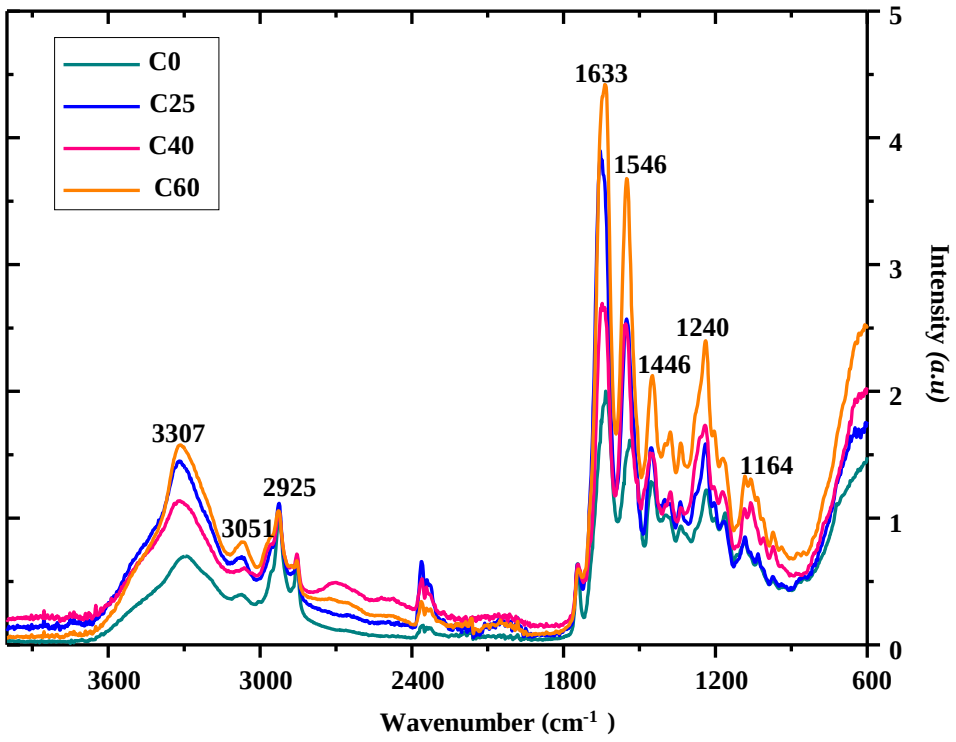


Figure 2.6: FTIR spectra of collagen networks.

Table 2.5: Relative peak intensities (ester and amide bands) of EDC/NHS treated collagen scaffolds.

	Amide Bond	Ester Bond
Sample ID	**1546cm^{-1}/2925cm^{-1}**	**1164cm^{-1}/2925cm^{-1}**
C0	1.23 ± 0.02	0.8 ± 0.01
C25	1.63 ± 0.04	0.82 ± 0.03
C40	3.29 ± 0.03	1.29 ± 0.04
C60	3.34 ± 0.01	1.32 ± 0.02

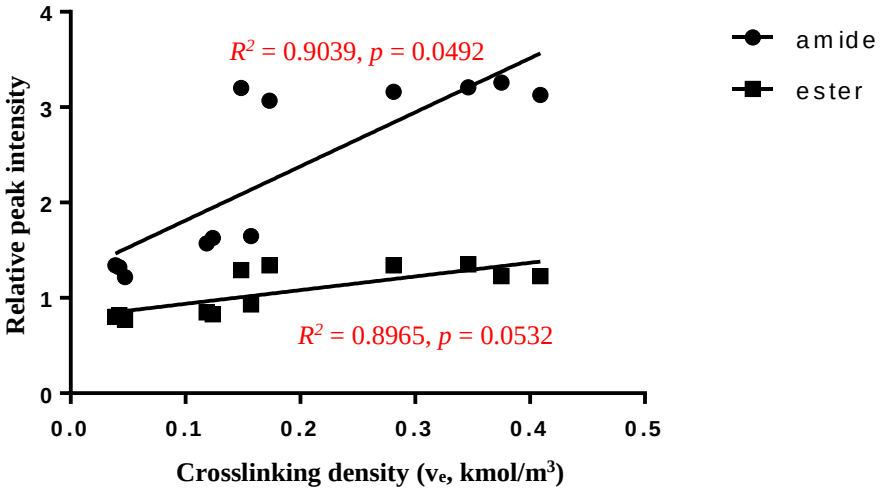


Figure 2.7: Pearson's correlation model between the crosslinking densities and relative peak intensities for collagen networks.

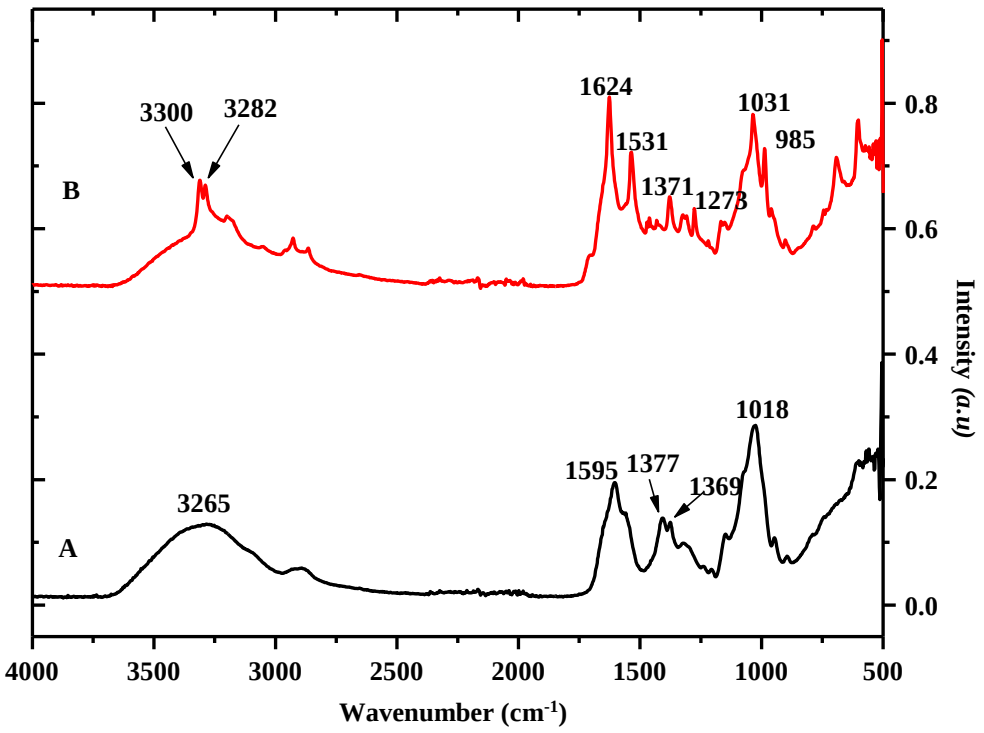


Figure 2.8: FTIR spectra of (A) sodium hyaluronate (B) and adipic dihydrazide modified hyaluronic acid hydrogel.

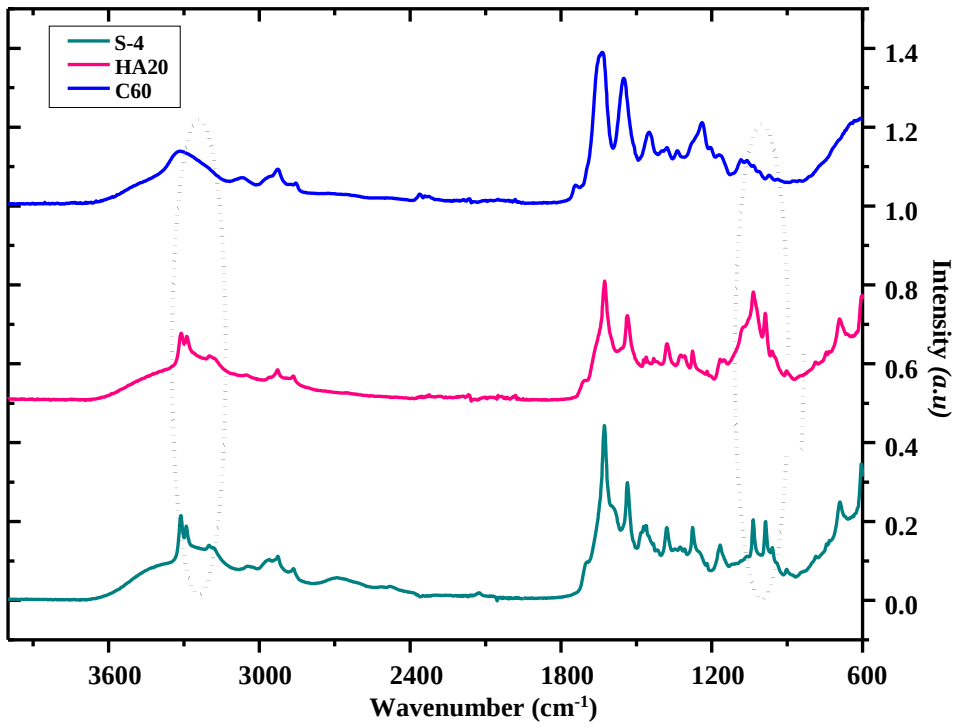


Figure 2.9: FTIR spectra of the collagen network (C60), HA network (HA20), and the resultant hybrid scaffold (S-4).

2.3.5 Thermogravimetric analysis (TGA):

Figure 2.10 compares the mass derivative curves against temperature for SHA and HA20. Two dips are observed for SHA at 80ºC and 241.28ºC. Broad dip around 220ºC (lower than corresponding SHA peak) is observed for HA20. Figure 2.11 presents the mass derivative curve for C60. Mass loss is observed to start around 80ºC and continued up to 120ºC. The second phase of mass loss is observed in the range 280-450ºC. Figure 2.12 shows the mass derivative curve against temperature for S-4 up to 500ºC as a representative sample. As the temperature is increased and approaches around 80ºC, the first mass loss is observed as a dip. A second dip is seen around 230ºC followed by the final and major loss around 300ºC.

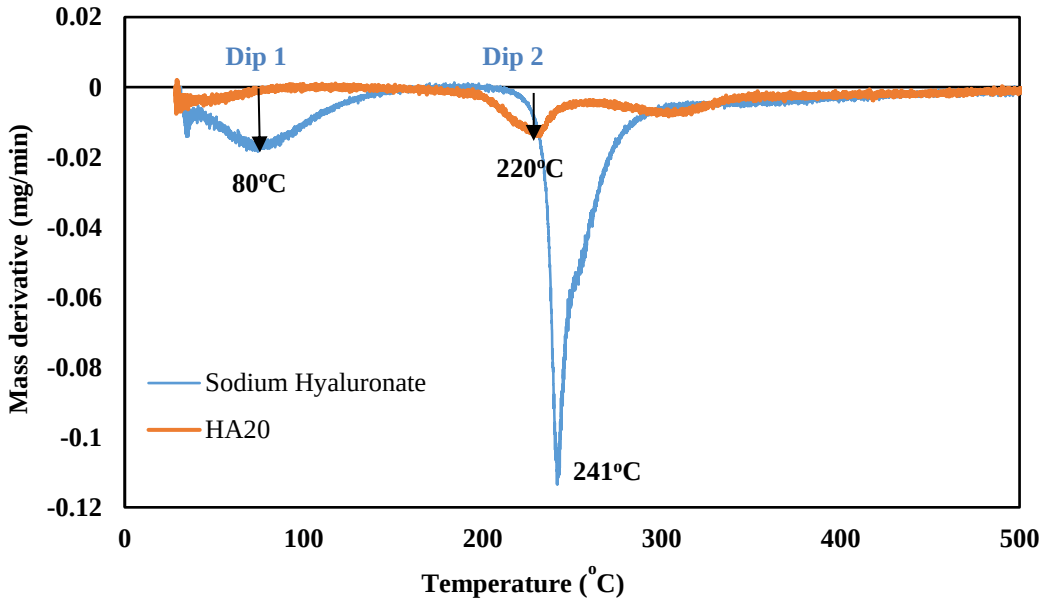


Figure 2.10: Comparison of mass derivative profiles of sodium hyaluronate (SHA) and HA20.

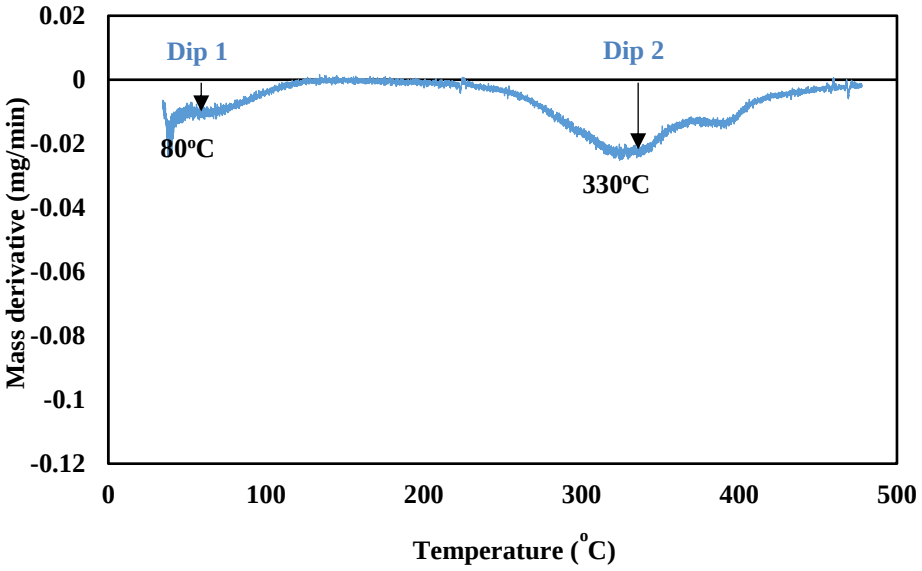


Figure 2.11: Mass derivative profile of collagen network (C60).

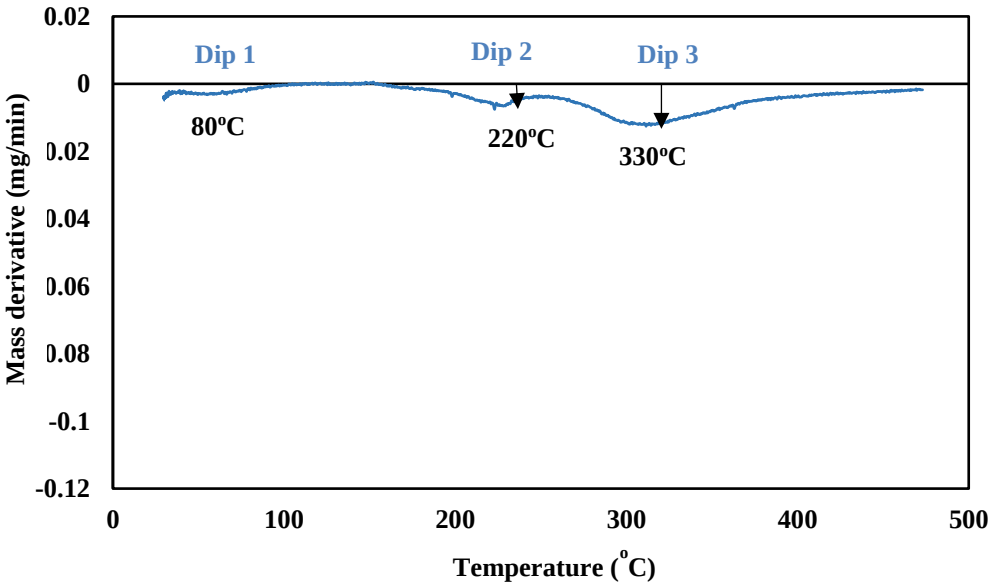


Figure 2.12: Mass derivative profile for S-4 up to 500ºC.

2.4 Discussion:

A sequential crosslinking approach based on EDC/NHS for the synthesis of collagen/HA hybrid scaffolds has been demonstrated in this chapter. Physical crosslinking routes for the crosslinking of collagen-based scaffolds resulted in denaturation of protein structure and inferior mechanical properties[21, 271] as discussed in chapter 1 (section 1.2.3.3). In addition, previous attempts to synthesize collagen/HA hybrid scaffolds involved single-step crosslinking techniques that yielded single phase/homogeneous microstructures[202, 272]. The sequential crosslinking technique (figure 2.2), adopted in this thesis, is based on carbodiimide chemistry which offers advantages such as zero-length crosslinks, preservation of triple helix structure, close control over reaction conditions, and water-soluble by-products [273, 274].

The ratio of EDC: NHS is an important parameter in the crosslinking reaction. This ratio is fixed at 2:1 in this study as it has been known to result in the highest crosslinking density and the greatest increase in denaturation temperature of collagen (T_d)[275, 276]. Table 2.3B shows that crosslinking densities of the parent networks increase with increasing the EDC concentration. With increasing crosslinking density (v_e), more and more crosslinks are formed between adjacent polymer (collagen or HA) strands, the struts are brought closer together and the distance between polymer chains (ξ) decreases. This could result in an increase in net volumetric shrinkage (Δv) of the scaffold as shown in figure 2.13[277-279]. Δv could lead to a reduction in pore size for collagen network as shown in table 2.4. There is also an increase in crosslinking density for the HA network as shown in table 2.3, however, the effect of crosslinking density on the pore size for HA networks could not be studied, this is probably because of the random orientation of the modified HA chains in a frozen state as shown in figure 2.3E. For any given interlaced composition, the pore size of scaffold further

decreases by the incorporation of the HA network (table 2.4). It can also be seen that the mean pore size is not affected by the crosslinking density of HA network. For instance, there is no the difference between the mean pore sizes for S-1 and S-2 whereas those of S-3 and S-4 are also quite similar. Overall, the mean pore size range of hybrid scaffolds, 66 – 126 µm, is useful for the vascularization of valvular tissue [280]. A decrease in the vascularization process occurs if the pore size is increased much beyond 100 µm [281]. Thus, the crosslinking route adopted in this thesis can be exploited to prepare scaffolds with tailorable pore sizes for a number of tissue engineering applications.

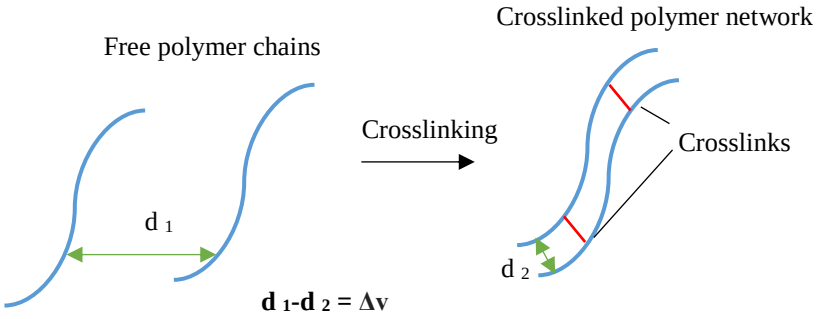


Figure 2.13: Schematic diagram showing a decrease in the interchain distance between the polymer chains as a result of crosslinking.

SEM images of hybrid scaffolds (figure 2.4) show a biphasic microstructure where HA network appears as mesh sitting inside the pores of collagen network. Histology images of alcian blue-PAS stained samples (figure 2.5) support the observations from SEM images and reveal interlaced bands of collagen (grey) and HA (blue) networks. S-4 and S-3 show tightly packed microstructures as compared to S-1 and S-2. It can be explained in terms of the crosslinked state of both collagen and HA in S-3 and S-4 whereas only HA is crosslinked in S-1 and S-2. Interlacing between the collagen network and the HA network has been assisted by the *in-situ* crosslinking of HA in the presence of the collagen network.

EDC/NHS crosslinking of collagen type I resulted in the formation of the amide and ester bonds, also confirmed by FTIR spectra (figure 2.6). This can be explained by EDC-activated carboxylic groups on aspartic and glutamic acid moieties in collagen to form the O-

acylisourea group. O-acylisourea has a tendency to convert into stable N-acylurea, which does not form a crosslink. The coupling of NHS with EDC not only suppresses the formation of N-acylurea but also increases the rate of reaction [276]. This intermediate is then attacked by the free amine group of (hydroxy) lysine to form an amide bond. For the collagen network, EDC/NHS establishes a crosslink through the formation of an amide bond between the carboxylic group and the amine group of neighboring collagen chains as shown in figure 1.20[270, 282, 283]. The intensities of the peaks corresponding to amide (1633, 1546, 1240 cm^{-1}) and ester bands (1164 cm^{-1}) increase with increasing the EDC concentration providing further evidence of this mechanism (table 2.5). Pearson's correlation model between crosslinking density and relative peak intensities for collagen scaffolds shows that correlation is stronger for amide band as compared to ester band as shown in figure 2.7. This indicates that population of amide bonds is greater than ester bonds and hence amide bonds have majorly contributed to the overall increase in crosslinking density in collagen scaffolds. In addition, no shift in either the peak position in FTIR could be seen for collagen network after crosslinking. This indicates that EDC/NHS crosslinking is capable of crosslinking collagen without denaturation. The chemical reaction involved in the crosslinking of collagen network is shown in figure 2.14.

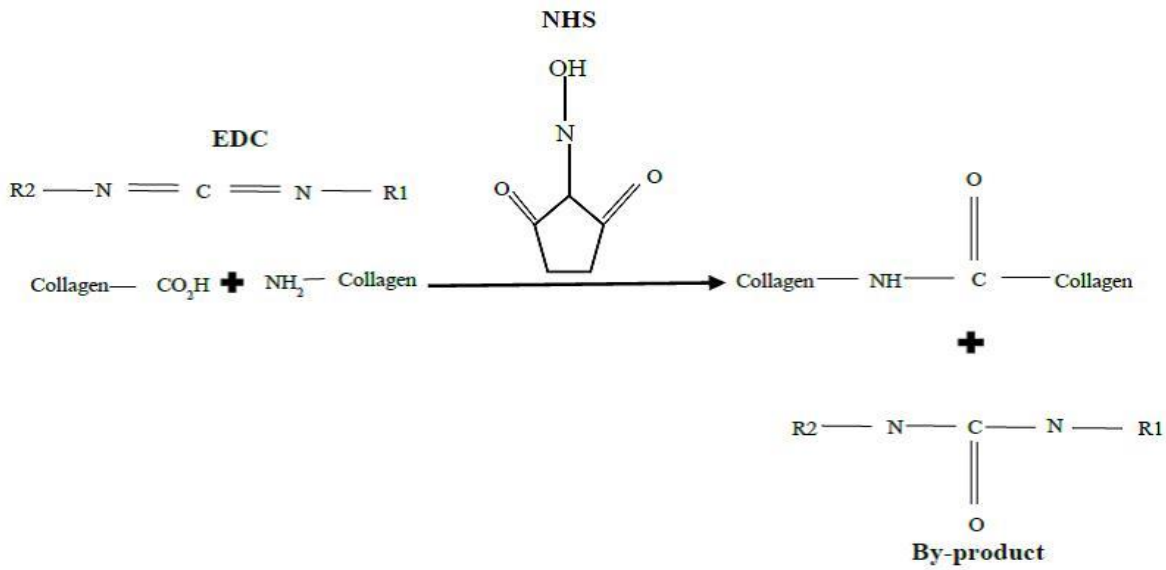


Figure 2.14: Schematic crosslinking reaction for crosslinking of collagen using EDC/NHS chemistry [249].

The HA molecule has three potential sites for chemical modification *viz* –COOH, –OH, and –$NHCOCH_3$. Each of these sites can be modified in many ways [118, 284] as discussed in chapter 1 (section 1.2.4.1). In this thesis, the modification of the –COOH group has been performed with EDC in the presence of ADH. The double peaks at 3300 and 3282 cm^{-1} which are associated with the primary amine of the ADH provide an evidence of this crosslinking reaction [285]. Formation of an amide bond has been confirmed by FTIR (1624, 1531, and 1273 cm^{-1}) of the EDC-crosslinked HA network (figure 2.8). However, this is a two-step reaction which is highly pH-sensitive. In the activation step, acidic pH is desirable whereas amide formation is favored at higher pH whereas higher pH can hydrolyze the EDC at the same time. Therefore, amines with high *pKa* values are difficult to conjugate to the HA molecule [173]. *pKa* can be shifted towards lower values by replacing diamines with dihydrazides. The addition of ADH results in functionalization and dihydrazide bond formation [286]. The chemical reaction involved for crosslinking of HA network is given in figure 2.15.

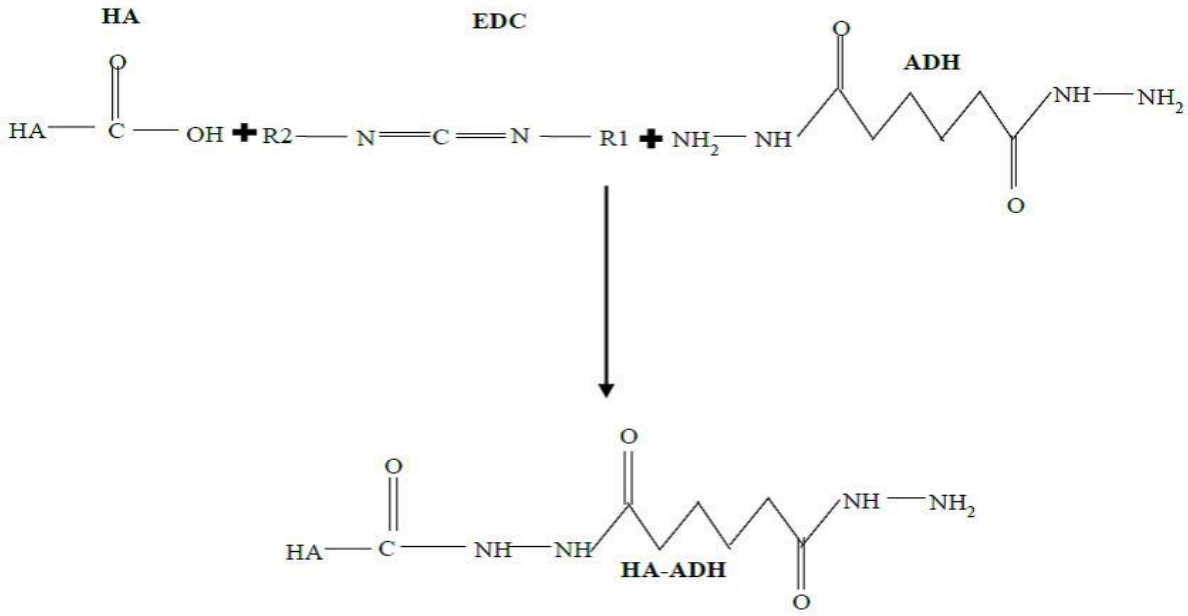


Figure 2.15: Schematic crosslinking reaction for the amidation of HA with EDC and adipic dihydrazide (ADH) [241].

It is important to note that although both collagen and HA have similar functional groups such as carboxylic acid, however, sequential crosslinking approach as adopted in this work could minimize the chances of crosslinking between the two polymers. EDC/NHS chemistry has also been used to attach HA to collagen[287]. For example, - COOH of collagen could attach to the $–NH_2$ from the HA instead of $–NH_2$ from another collagen chain to form an amide bond or vice versa. In S-1 and S-2, this is possible because non-crosslinked collagen has free –COOH and $–NH_2$ moieties which can react with $–NH_2$ and –COOH from functionalized HA. In the case of S-3 and S-4, 60mM of EDC has been selected to maximize the engagement of these functional groups in the collagen network[288, 289]. Thus, the possibility of attachment of HA to collagen is highly reduced. The FTIR spectrum of S-4 where characteristic peak positions of collagen and HA remain unchanged (figure 2.9) provides support for the above hypothesis.

The first stage of degradation shown in the TGA curves (figure 2.10 and 2.11) of HA and collagen networks occurs as a dip around 80^{o}C, which is attributed to the loss of physically

attached water within the polymer chains [290]. Figure 2.10 shows a sharp peak for SHA at 241^{o}C, whilst a broad peak at 220^{o}C is shown by the HA network indicating that HA has become amorphous after modification [291]. The mass loss for the collagen network at 300^{o}C is due to the cleavage of the organic fractions formed as a result of the decomposition of collagen (figure 2.11) [292]. Figure 2.12 also shows the presence of two distinct phases in S-4 corresponding to two different degradation temperatures at 220^{o}C (T_d of HA network) and 330^{o}C (T_d of collagen network), respectively. FTIR (figure 2.9) and TGA (figure 2.12) results taken together imply that no new chemical bond or intermediate phase has been formed between collagen network and HA network. These observations also suggest that the HA network is not only able to penetrate through the collagen network but also maintains its identity as an independent network. Such hybrid scaffolds with interlaced microstructures could have the potential to closely mimic the natural heart valve ECM due to the structural similarity.

2.5 Conclusion:

In this chapter, an EDC/NHS based sequential crosslinking technique has been demonstrated for the fabrication of collagen type I and HA hybrid scaffolds. Swelling studies showed that crosslinking densities of the parent networks, as well as the resultant hybrid scaffolds, increased with increasing the concentration of EDC/NHS. SEM and alcian blue-PAS stained images of hybrid scaffolds revealed their biphasic interlaced microstructures. Image analysis suggested that pore sizes of the collagen network and hybrid scaffolds decreased with an increase in the crosslinking density. The effect of crosslinking density on pore size for HA networks could not be studied because of irregular chain orientations in the microstructure.

FTIR relative peak intensities and crosslinking densities were found to be statistically correlated suggesting that amide bonds contributed towards the overall increase in

crosslinking density. The co-existence of the characteristic peaks in FTIR and TGA, from both collagen type I and HA, indicated the formation of two independent networks with no mutual interaction.

While affecting the microstructural properties of the hybrid scaffolds, crosslinking density can also play an important role in deciding their mechanical response under various types of stresses, which will be discussed in chapter 3.

Chapter 3

Mechanical Properties of Collagen/HA Hybrid Scaffolds

3.1 Introduction:

The '*tissue engineering triad'* consists of scaffolds, cells, and growth factors[293-295]. Scaffolds are seeded with cells before implantation and can be considered as the structural backbone of the resulting TEHV[296]. Therefore, the mechanical properties of the scaffold play a crucial role in the post-implantation performance of the resulting TEHV. TEHV and target tissue should mechanically match so that TEHV can serve as a substitute for the target tissue until the development of new tissue is completed [297, 298]. This need can be reduced because the implant can gain structural and a mechanical similarity with the host tissue through remodeling over a period after implantation. The heart valve, however, is a dynamic tissue which requires an immediate fully functional TEHV[299].

The heart valve experiences different types of stresses such as flexure, bending, and tension during each cycle, as discussed in chapter 1 (section 1.3.5.1). A scaffold aiming at the restoration of the traumatized tissue should be able to withstand 30 million cycles a year [54, 69, 300]. Comparison of mechanical properties of human aortic valve leaflet (HAVL) with those of collagen type I and HA, given in chapter 1 (table 1.5), have shown that these polymers have the potential to replicate the mechanical properties of HAVL provided that they are fabricated into hybrid scaffolds.

An EDC/NHS based sequential crosslinking protocol, to create collagen/HA based hybrid scaffolds with interlaced microstructure, has been elucidated in chapter 2. It is hypothesized that microscale interlacing between collagen type I and HA, as shown in SEM and histology

images in chapter 2 (figure 2.4 and figure 2.5), could affect the mechanical properties of the resulting scaffolds. Hence, this chapter is focused on the mechanical characterization of the parent networks (collagen type I and HA) and hybrid scaffolds. Scaffolds have been characterized under simple compression and flexural modes. The dynamic mechanical properties have also been investigated.

The TEHV will come in contact with physiological fluids e.g. cell culture medium and/or blood which could affect its mechanical properties[301, 302]. Therefore, the ability of scaffold to absorb fluids and its effect on the mechanical properties is worth investigating. Flexural and dynamic mechanical properties have been studied under wet conditions. Compression testing could not be performed under wet conditions due to the sensitivity limit of the testing equipment.

3.2 Materials and methods:

3.2.1 Compression test:

A schematic stress-strain curve for collagen fibres in fibrosa and elastin fibres in elastin during valve cycle has been shown in figure 3.1A. As it has already been discussed in chapter 1 (figure 1.7A) that collagen bundles in fibrosa experience compression during systole. Hence, it is important to quantify the effect of crosslinking and interlacing on the comressive modulus of the crosslinked collagen scaffolds as well as hybrid scaffolds. Unidirectional compression tests, with a 50N load cell, were conducted using a DMA7 (PerkinElmer, MA) as shown in figure 3.1B. Cylindrical samples (d, h = 15 mm) were compressed between parallel plates at a constant strain rate of 0.5 mm/min. All samples (n = 5) were tested at room temperature in the dry state.

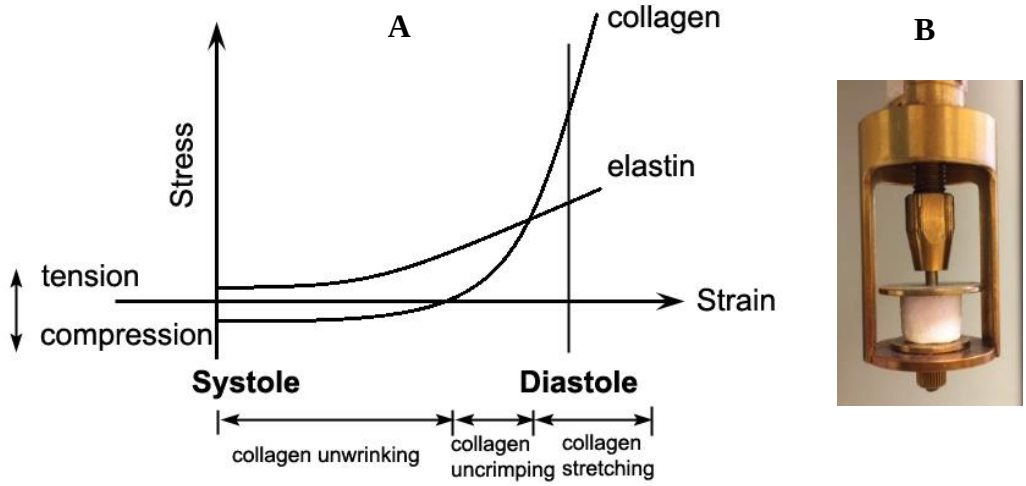


Figure 3.1: (A) schematic stress-strain curve for aortic valve leaflet[303] (B) compression test set-up.

3.2.2 Bending test:

3.2.2.1 Three-point bend test (dry condition):

The aortic valve leaflet experiences a bending moment in the direction of curvature during diastole as shown in figure 3.2A. Loading mechanism (center loaded) in three-point bending test matches more closely to the physiological bending moment of the leaflet as compared to other available bending tests such as four-point bending test. Therefore, it was selected for the evaluation of the bending modulus of the scaffolds. In our three-point bend set-up, rectangular samples (40 mm×12 mm×5 mm) were characterized using a DMA7 (PerkinElmer, MA) with a 50N load cell. Samples (n = 5) were loaded with a cross-head speed of 0.5mm/min using a span of 20 mm as shown in figure 3.2B.

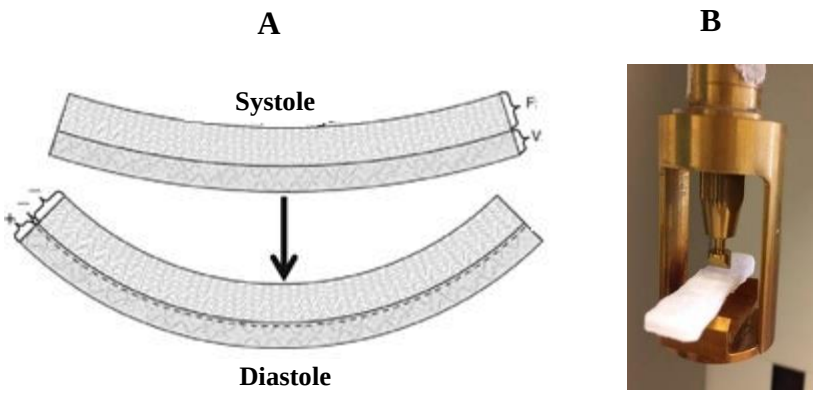


Figure 3.2: (A) bending moment in the leaflet (top view) during diastole (B) three-point bend set-up.

3.2.2.2 Self-deflection bending test (wet condition):

The extremely low load required to characterize the hydrated scaffolds in a three-point bend test made it infeasible and scaffolds were characterized by a self-deflection bending test developed by a previous member of the group[304]. For the self-deflection test, the scaffolds (n = 5) were weighed (AB204, Mettler Toledo, UK) in the dry state (M_{dry}) and soaked in 0.1M Phosphate Buffer Saline (PBS) for 1 hour at room temperature before the test. Scaffolds were then allowed to drain on a wire mesh for 1 min to drain excessive PBS, after which these were weighed again (M_{wet}). Water uptake ratio (U) was calculated using the Eq. 3.1 as follows:

$$U = [(M_{wet} - M_{dry})/M_{dry}] \times 100\ \%\ ^{305} \qquad Eq.\ 3.1$$

Hydrated scaffolds were then clamped over a span of 20 mm and allowed to self-deflect as shown in schematic in figure 3.3. The weight of the PBS absorbed by the scaffold was considered as uniformly distributed load acting over the entire length of the scaffold. The deflection was recorded by a camera (450D, 50mm, F1.8, Canon, Japan) and measured with the aid of Image J (National Institutes of Health, USA)[306].

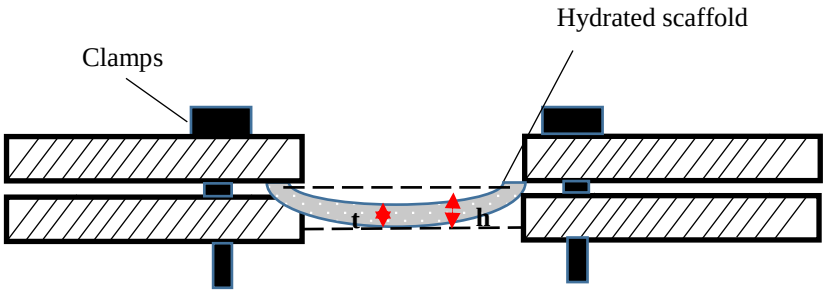


Figure 3.3: Schematic of self-deflection bending test (wet condition).

3.2.3 Dynamic mechanical properties*:

It has been shown in chapter 1 (section 1.3.5.1) that the gross mechanical response of tissue is 'elastic' and GAGs play little role in functional biomechanics as shown in figure 1.11. Investigation of viscoelastic properties of hybrid scaffolds is of interest to completely understand and compare their mechanical properties with leaflet tissue. Dynamic mechanical properties of collagen network and the resultant collagen/HA hybrid scaffolds (n = 5), under dry and wet conditions, were measured using a DMA7 (PerkinElmer, MA). Cylindrical samples (d, h = 15 mm) were subjected to cyclic forces (0 and 10% compressive strain) in the frequency range 0.01 – 100 Hz at 37^{o}C. For wet testing, samples were tested under same conditions while immersed in PBS bath.

*Dynamic mechanical tests were conducted in collaboration with the University of Malaya, Malaysia.

3.2.4 Rheology test*:

It has been shown in chapter 2 (table 2.3) that there is an increase in the crosslinking density of HA networks with increasing EDC concentration. Like collagen and hybrid scaffolds, the effect of increase in crosslinking density on the mechanical properties of HA network could be informative. However, compression and bending tests could not be conducted on HA networks due to the sensitivity limit of the testing equipment and fragile nature of the samples.

Study of the rheological properties of HA networks could reveal the effect of crosslinking on their viscoelastic properties. Samples were characterized with an Anton Paar Physica MCR 301 compact rheometer using oscillatory shear stress test conditions. The tests were performed using parallel plate geometry (25 mm) with a gap size of 1 mm. Constant values of deformation, 0.1 – 1 mrad, were maintained throughout each frequency sweep of 1 – 10 Hz. Four samples from each group were soaked in PBS for 1 hour before the test.

3.2.5 Statistical analysis #:

All data have been reported as means of at least four samples, with the standard deviations as the errors. One-way analysis of variance (ANOVA) with a Bonferroni's post-hoc test has been used to compare groups of samples with a probability value of 95 % ($p < 0.05$) to determine statistical significance.

*Rheology tests were conducted in collaboration with Department of Engineering, University of Oxford.

#performed by Prof. Carolyn Carr, Department of Physiology, University of Oxford.

3.3 Results:

3.3.1 Compression test:

Figure 3.4 shows a representative compressive stress-strain curve for a collagen scaffold. The curve consists of a linear region, stress plateau, and densification sections which indicate the typical behaviour of an elastomeric foam [307, 308]. The linear elastic portion represents the pore edge bending. As the stress is further increased, the walls of the pores start to buckle and curve shows a monotonous rise in strain appearing as stress plateau. Finally, pores start to collapse throughout the scaffold with further increase in stress appeared as densification. The compression moduli (E_{comp}, kPa) for all samples have been calculated from the slope of the linear section of the stress-strain curve as shown in figure 3.4 and are given in table 3.1.

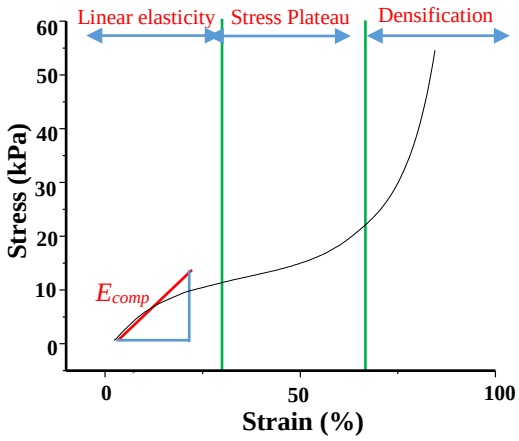


Figure 3.4: Stress-strain profile of scaffolds in compression predominantly behaving as an elastomeric foam. The curve shows characteristic regions of linear elasticity, stress plateau, and densification. Compressive modulus, E_{comp}, is calculated as slop of linear elasticity region.

Table 3.1: Compressive modulus (E_{comp}, kPa) of collagen networks and hybrid scaffolds. [a] and [b] represent statistically significant values ($p < 0.05$) within collagen networks as compared to C0 and C25 respectively. [c], [d], and [e] represent statistically significant values within hybrid scaffolds as compared to S-1, S-2, and S-3 respectively.

Sample ID	Effective crosslinking density (v_e, kmol/m^3)	Compression Modulus (E_{comp}, kPa)
C0	0.4 ± 0.03	35 ± 5
C25	1.3 ± 0.2	56 ± 6 [a]
C40	2 ± 1 [a]	63 ± 5 [a]
C60	3.3 ± 0.4 [a, b]	68 ± 7 [a, b]
S-1	0.8 ± 0.1	41 ± 4
S-2	0.9 ± 0.1	73 ± 5 [c]
S-3	5.0 ± 0.6 [c, d]	68 ± 5 [c]
S-4	6.8 ± 0.7 [c, d, e]	95 ± 4 [c, d, e]

Table 3.1 shows that E_{comp} for collagen networks increases from 35 ± 5 kPa to 68 ± 7 kPa with an increase in v_e, also shown in figure 3.5A. Similarly, E_{comp} for hybrid scaffolds increases from 41 ± 4 kPa to 95 ± 4 kPa as shown in figure 3.5B. Comparison of figure 3.5A and figure 3.5B shows that E_{comp} values of hybrid compositions are 1.4 – 2.0 times higher than those of parent collagen networks. E_{comp} of hybrid compositions is also affected by the crosslinking density of the secondary HA network as can be seen from table 3.1. For instance, HA20 (v_e, 17 ± 4 kmol/m^3) * is the parent HA network in S-2 (E_{comp}, 73 ± 5 kPa) and S-4 (E_{comp}, 95 ± 4 kPa) and these compositions show higher E_{comp} values as compared to S-1 (E_{comp}, 41 ± 4 kPa) and S-3 (E_{comp}, 68 ± 5 kPa) having HA2 (v_e, 2 ± 0.3 kmol/m^3) * as parent HA network.

*Values from table 2.3B (chapter 2).

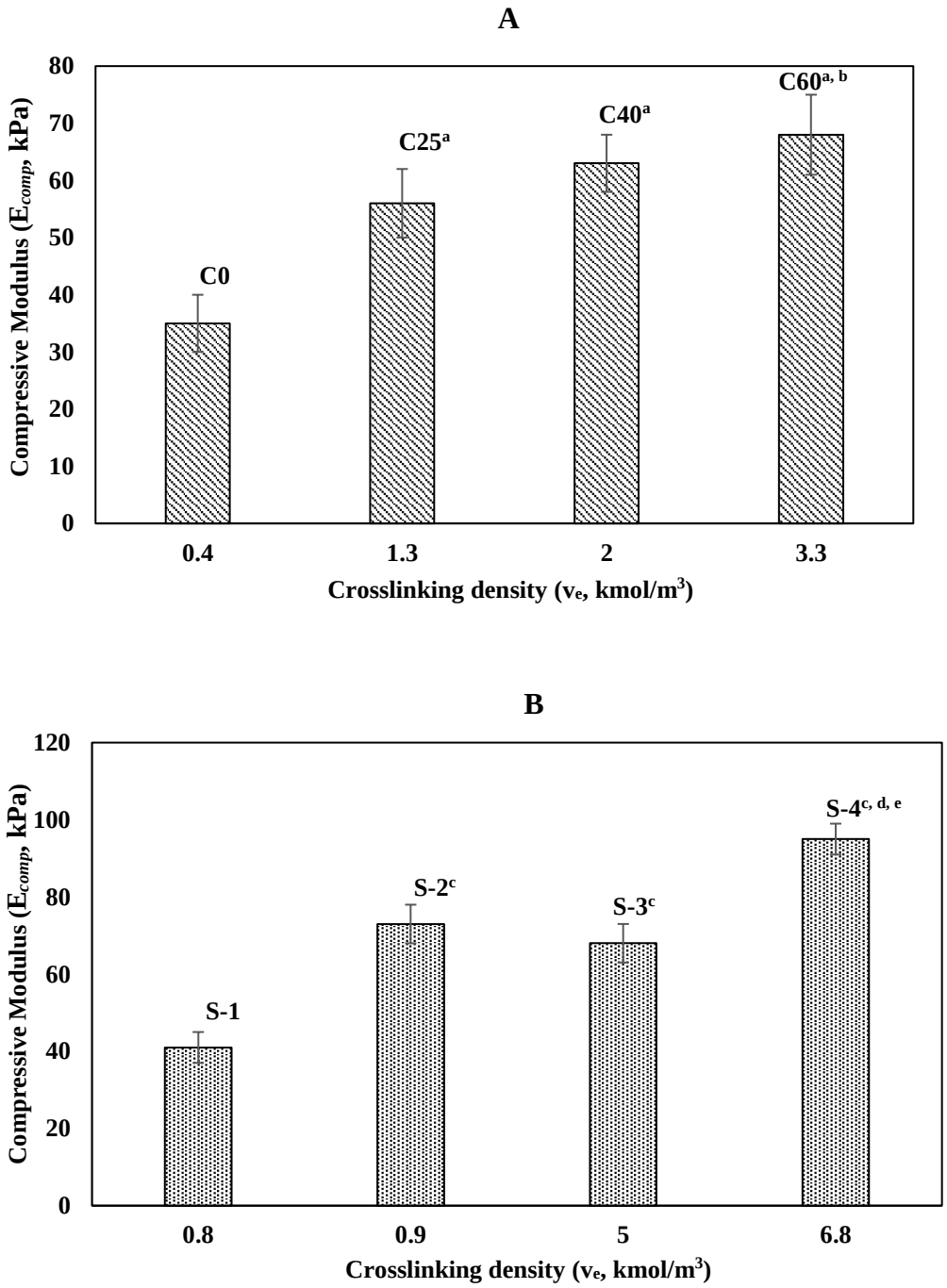


Figure 3.5: Effect of increase in crosslinking density (v_e, kmol/m^3) on the compressive modulus (E_{comp}, kPa) of (A) collagen network and (B) hybrid scaffolds. [a] and [b] represent statistically significant values within collagen networks as compared to C0 and C25 respectively. [c], [d], and [e] represent statistically significant values ($p < 0.05$) within hybrid scaffolds as compared to S-1, S-2, and S-3 respectively.

3.3.2 Bending test:

3.3.2.1 Three-point bend test (dry condition):

A typical load-deflection curve for dry three-point bend test is shown in figure 3.6. The effective bending modulus (E_{bend}) of the scaffold is proportional to the slope ($\delta P/\delta D$) of the load-deflection curve. Applying Euler-Bernoulli's equation for a center-loaded simply supported beam[309] (figure 3.2B), E_{bend} can be calculated from Eq. 3.2 as follows:

$$E_{bend} = (\delta P/\delta D)\, l^3/48I \quad ^{309} \qquad \textit{Eq. 3.2}$$

Where P = load

D = deflection

l = span distance

I = the second moment of inertia (I and l remain constant during the test).

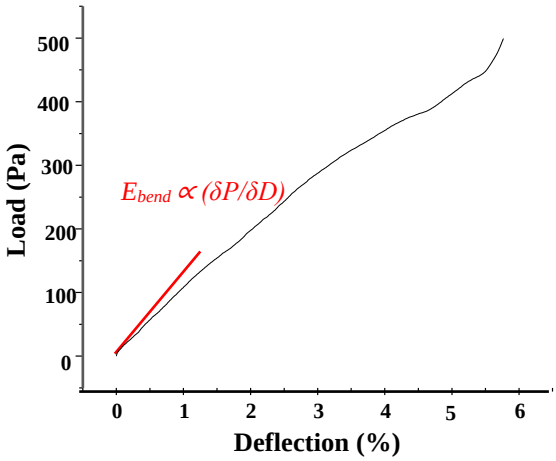


Figure 3.6: Stress-strain profile of a collagen scaffolds under the influence of bending stress. E_{bend} is calculated as the slope of linear elasticity region.

Table 3.2: Dry bending modulus (E_{bend}, kPa) and wet bending modulus ($E_{wet.bend}$, kPa) of collagen networks and hybrid scaffolds. [a], [b] and [c] represent statistically significant values ($p < 0.05$) within collagen networks as compared to C0, C25, and C40 respectively. [d], [e], and [f] represent statistically significant values within hybrid scaffolds as compared to S-1, S-2, and S-3 respectively.

Sample ID	Effective crosslinking density (v_e, kmol/m^3)	Water Uptake Ratio (U) %	Bending Modulus (kPa)	
			Dry E_{bend}	Wet $E_{wet.bend}$
C0	0.4 ± 0.03	2243 ± 45	154 ± 18	2 ± 0.3
C25	1.3 ± 0.2	1352 ± 50 [a]	189 ± 21	3 ± 0.3
C40	2 ± 1 [a]	1042 ± 24 [a, b]	212 ± 16	4 ± 0.1 [a]
C60	3.3 ± 0.4 [a, b]	874 ± 21 [a, b, c]	404 ± 25 [a, b, c]	5 ± 0.3 [a, b]
S-1	0.8 ± 0.1	2039 ± 39	711 ± 29	1 ± 0.2
S-2	0.9 ± 0.1	2011 ± 33	817 ± 17	1 ± 0.3
S-3	5.0 ± 0.6 [d, e]	1097 ± 24 [d, e]	980 ± 20 [d, e]	2 ± 0.3 [d, e]
S-4	6.8 ± 0.7 [d, e, f]	984 ± 24 [d, e]	1660 ± 25 [d, e, f]	3 ± 0.2 [d, e, f]

Table 3.2 shows that E_{bend} for collagen networks increases from 154 ± 18 kPa to 404 ± 25 kPa with an increase in v_e, also shown in figure 3.7A. E_{bend} for hybrid scaffolds also increases from 711 ± 29 kPa to 1660 ± 25 kPa as shown in figure 3.5B. Comparison of figure 3.7A and figure 3.7B shows that E_{bend} values of hybrid scaffolds are 4 – 5 times higher than those of parent collagen networks. E_{bend} of hybrid compositions is also affected by the crosslinking density of the secondary HA network according to table 3.2. For instance, HA20 (v_e, 17 ± 4 kmol/m^3) * is the parent secondary network in S-2 (E_{bend}, 817 ± 17 kPa) and S-4 (E_{bend}, 1660 ± 25 kPa) so these compositions show higher E_{bend} values as compared to S-1 (E_{bend}, 711 ±

29 kPa) and S-3 (E_{bend}, 980 ± 20 kPa) having HA2 (v_e, 2 ± 0.3 kmol/m^3) * as secondary network.

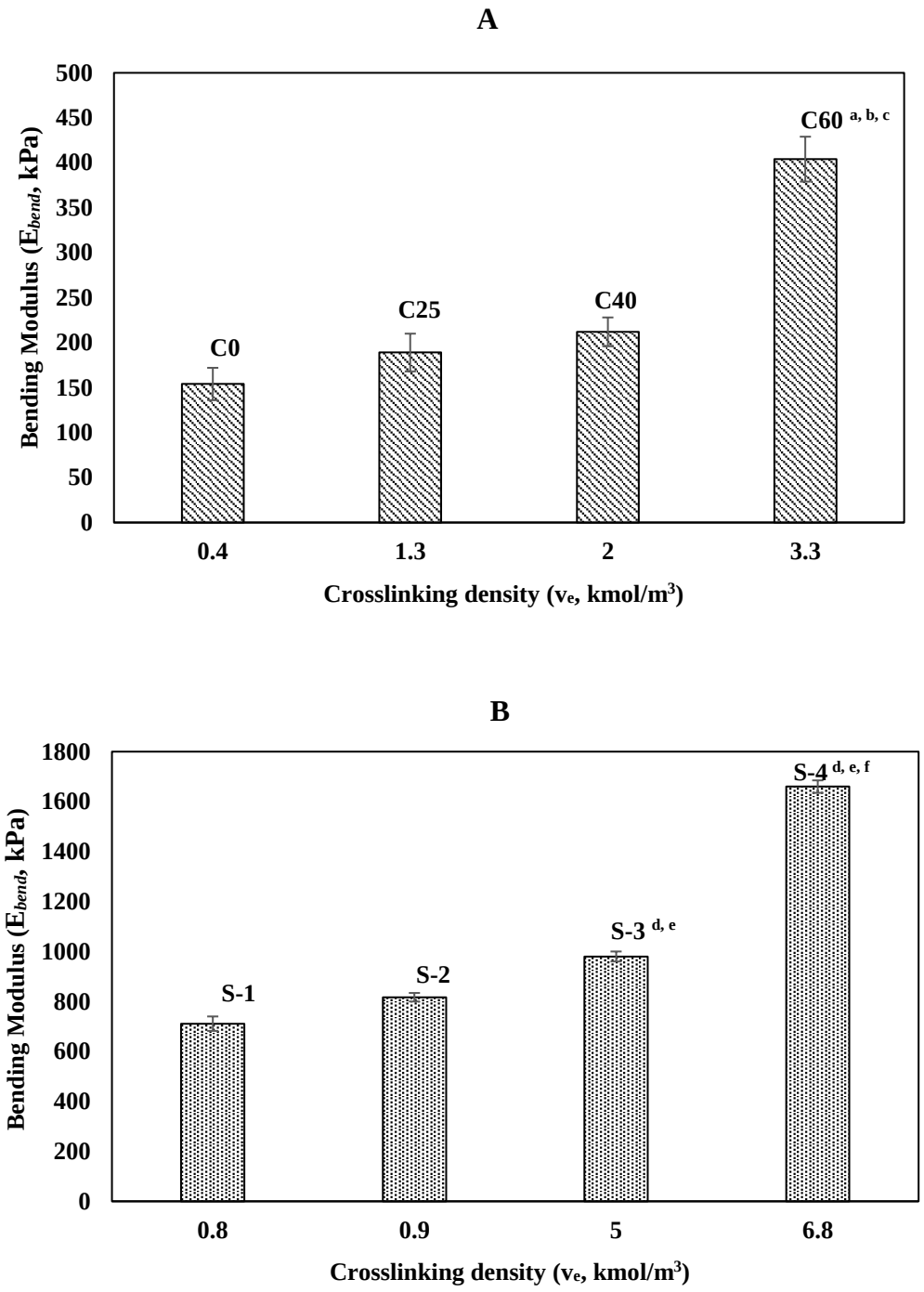


Figure 3.7: Effect of increase in crosslinking density (v_e, kmol/m^3) on the dry bending modulus (E_{bend}, kPa) of (A) collagen network and (B) hybrid scaffolds. [a], [b] and [c] represent statistically significant values within collagen networks as compared to C0, C25, and C40 respectively. [d], [e], and [f] represent statistically significant values ($p < 0.05$) within hybrid scaffolds as compared to S-1, S-2, and S-3 respectively.

3.3.2.2 Self-deflection bending test (wet condition):

The deflection (D) of the hydrated scaffold, as shown in figure 3.3, was determined by Eq. 3.3.

$$D=h-(t/2) \qquad \textit{Eq. 3.3}$$

Where t = thickness of the scaffold

h = distance between the central position of the clamps (i.e., the initial central position of the scaffold) and the lower surface of the deflected scaffold

Applying Euler-Bernoulli's equation for a simply supported beam with uniformly distributed load[309], bending modulus of the hydrated scaffolds can be calculated from Eq. 3.4 assuming the weight of the absorbed PBS as uniformly distributed load over the entire length of the beam ($UM_{dry}g/l$) as follows:

$$E_{bend.wet} = 5ql^4/384DI = 5UM_{dry}gl^3/384DI \ ^{304, 309} \qquad \textit{Eq. 3.4}$$

Where U = water uptake ratio

M_{dry} = dry mass of the scaffold

g = gravitational acceleration

Table 3.2 shows that U values of collagen networks decrease from 2243 ± 45 % to 874 ± 21 % with an increase in their crosslinking densities. S-1 (U, 2039 ± 39 %) and S-2 (U, 2011 ± 33 %) show higher U values as compared to S-3 (U, 1097 ± 24 %) and S-4 (U, 984 ± 24 %). In a hydrated state, bending modulus drops for all the samples as shown in figure 3.8. Comparison of figure 3.7A and figure 3.8A shows that $E_{wet.bend}$ for collagen networks decreases up to 80 times as compared to their E_{bend}. Similarly, comparison of figure 3.7B and figure 3.8B shows that $E_{wet.bend}$ for hybrid scaffolds decreases up to 700 times as

compared to their E_{bend}. Comparison of figure 3.8A and figure 3.8B shows that $E_{wet.bend}$ of hybrid scaffolds (1 – 3 kPa) is lower (50 % reduction) as compared to their parent collagen networks (2 – 5 kPa).

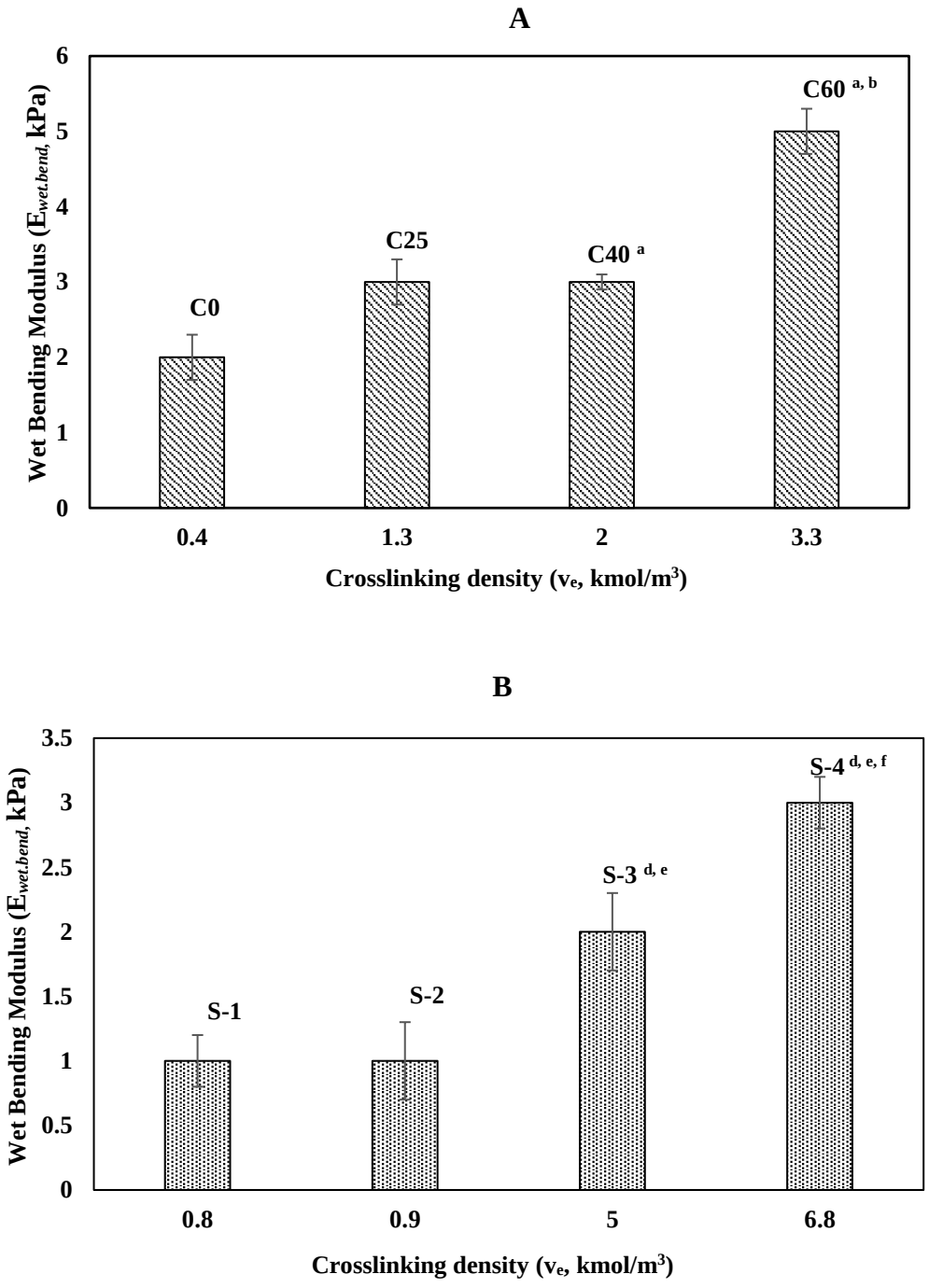


Figure 3.8: Effect of increase in crosslinking density (v_e, kmol/m^3) on the wet bending modulus ($E_{wet.bend}$, kPa) of (A) collagen network and (B) hybrid scaffolds. [a], [b] and [c] represent statistically significant values within collagen networks as compared to C0, C25, and C40 respectively. [d], [e], and [f] represent statistically significant values ($p < 0.05$) within hybrid scaffolds as compared to S-1, S-2, and S-3 respectively.

3.3.3 Dynamic mechanical properties:

Figure 3.9 shows the representative frequency sweep test for non-crosslinked collagen in the dry state at 37 ºC. Similar tests have been run for collagen networks as well as the resultant hybrid scaffolds. The storage modulus, G´, represents the elastic character whereas loss modulus, G´´, accounts for the viscous behaviour of the material under given oscillatory conditions. Loss tangent, tan δ, shows material's internal friction and is defined as is the ratio of G´´/G´. Figure 3.9 suggests that G´ is independent of the frequency, f. At low frequencies, G´´ and tanδ are nearly constant, whereas they tend to increase slightly towards the end of the test. Overall, all parameters show a monotonous behaviour in the range f = 10^{-1} – 10^{1}. The frequency of a healthy adult human heart (assuming 70 beats per minute) is 1 Hz [310]. Therefore, taking it as a reference point, the values of G´, G´´, and tan δ for collagen networks and hybrid scaffolds are given in table 3.3 and 3.4 for dry and wet conditions, respectively.

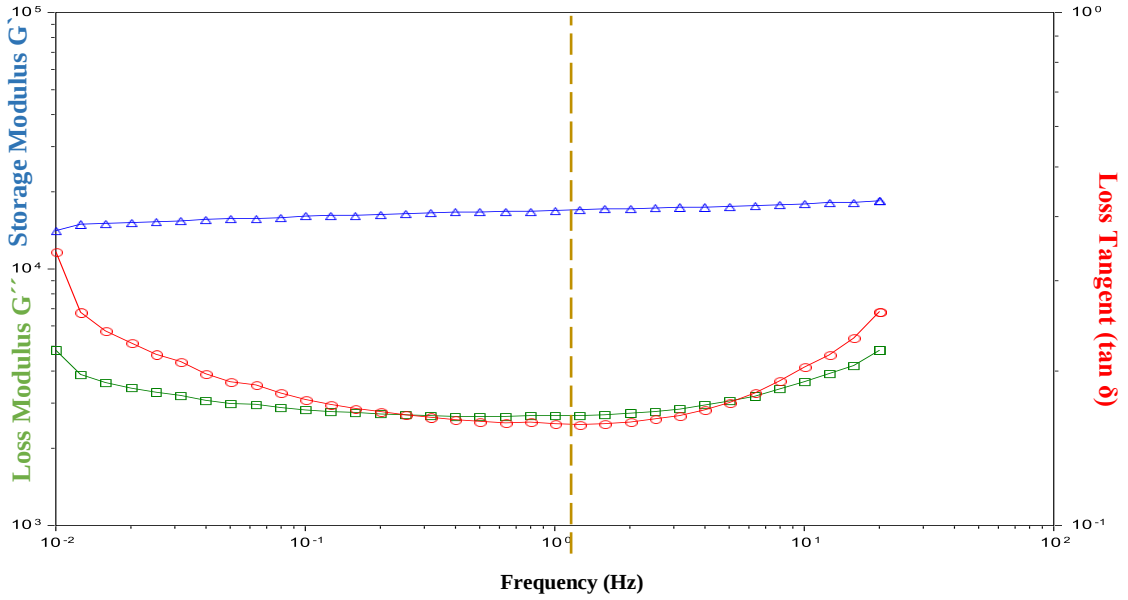


Figure 3.9: Variation of storage modulus G´ (Pa), loss modulus G´´ (Pa) and loss tangent (tan δ) of the collagen network in the dry state at 37 ºC. G´ > G´´ suggests that collagen scaffold behaves as elastic solid. The dashed line indicates the reference point for the values of G´, G´´ and tan δ as presented in table 3.3 and table 3.4.

Table 3.3 shows that the dynamic moduli, G´ and G´´, increase with increasing the crosslinking density for collagen networks and hybrid scaffolds. G´> G´´ and tanδ < 1 for all samples. There is a five-fold increase in G´ and a three-fold increase in G´´ from C0 to C60 as shown in figure 3.10A. G´ and G´´ also increase steadily from S-1 to S-4 as shown in figure 3.10B. For instance, S-4 (G`, 113 ± 6 kPa) is almost two times more elastic than S-1(G`, 52 ± 6 kPa) under given conditions. Comparison of figure 3.10A and figure 3.10B shows that dynamic moduli of hybrid scaffolds are 2 – 4 times higher than their collagen networks. For example, S-4 (G', 113 ± 6 kPa) is more elastic than its parent collagen network C60 (G', 74 ± 3 kPa). Tanδ for collagen networks as well as hybrid scaffolds decreases, from 0.17 to 0.12 and from 0.12 to 0.09 respectively, with increasing the crosslinking density as shown in table 3.3. It also indicated that tanδ for hybrid scaffolds are lower than their parent collagen networks.

Table 3.3: Storage modulus G´ (kPa), loss modulus G´´ (kPa), and loss tangent (tan δ) of collagen networks and hybrid scaffolds in the dry state (37°C, 1 Hz). [a], [b], and [c] represent statistically significant values within collagen networks as compared to C0, C25, and C40 respectively. [d], [e], and [f] represent statistically significant values ($p < 0.05$) within hybrid scaffolds as compared to S-1, S-2, and S-3 respectively.

Sample ID	Effective crosslinking density (v_e, kmol/m^3)	Rheology Properties		
		Storage Modulus (G´, kPa)	Loss Modulus (G´´, kPa)	Loss Tangent (tan δ)
C0	0.4 ± 0.03	16 ± 2	3 ± 1	0.17
C25	1.3 ± 0.2	45 ± 3 [a]	7 ± 2 [a]	0.17
C40	2 ± 1 [a]	49 ± 4 [a]	7 ± 2 [a]	0.14
C60	3.3 ± 0.4 [a, b]	74 ± 3 [a, b, c]	9 ± 1 [a]	0.12 [a, b]
S-1	0.8 ± 0.1	52 ± 6	6 ± 1	0.12
S-2	0.9 ± 0.1	64 ± 4	7 ± 2	0.12
S-3	5.0 ± 0.6 [d, e]	68 ± 5	7 ± 2	0.11
S-4	6.8 ± 0.7 [d, e, f]	113 ± 6 [d, e, f]	10 ± 2 [d]	0.09 [d, e]

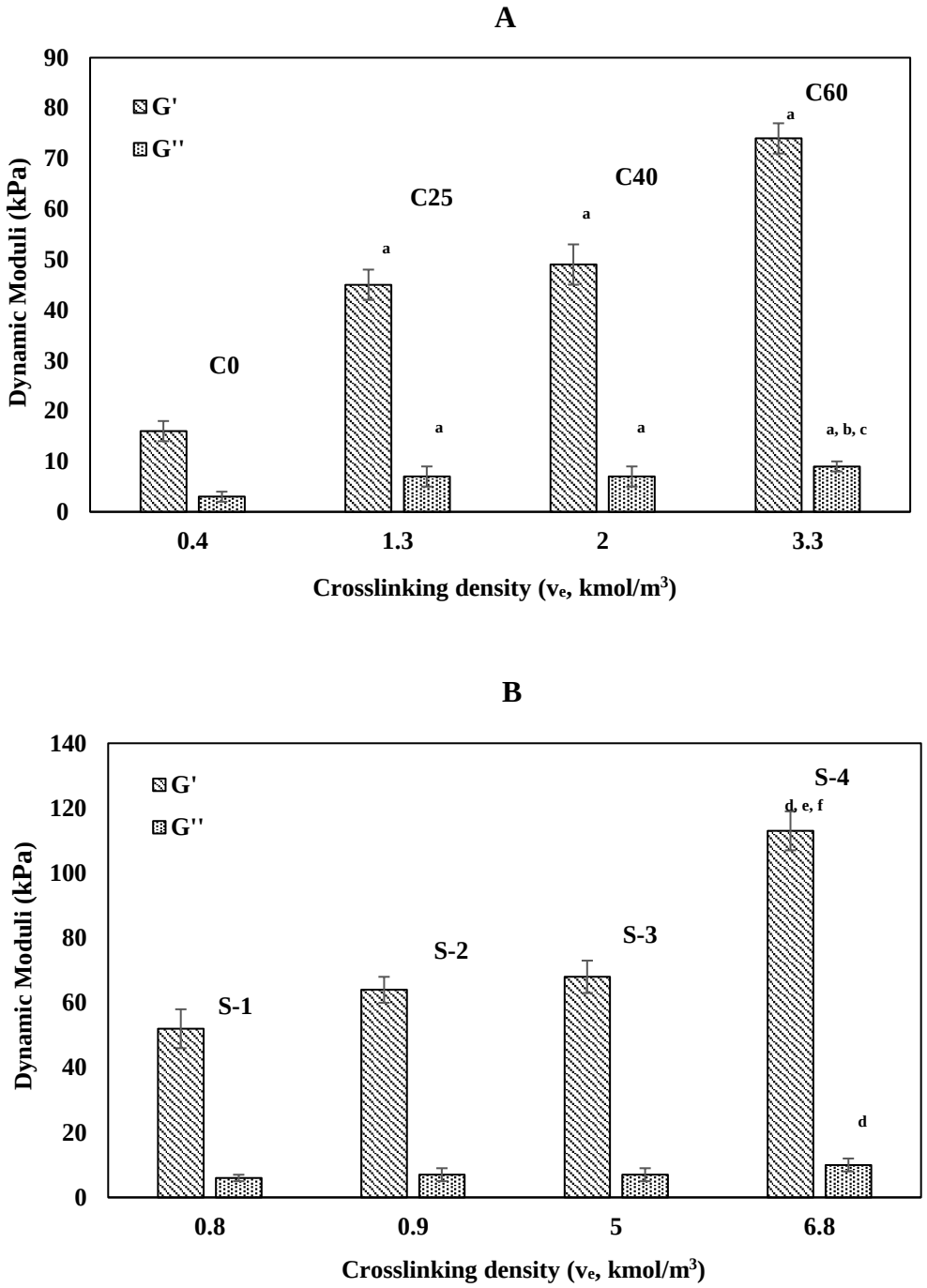


Figure 3.10: Effect of increase in crosslinking density (v_e, kmol/m^3) on dynamic moduli in a dry state (kPa) of (A) collagen network and (B) hybrid scaffolds. [a], [b], and [c] represent statistically significant values within collagen networks as compared to C0, C25, and C40 respectively. [d], [e], and [f] represent statistically significant values ($p < 0.05$) within hybrid scaffolds as compared to S-1, S-2, and S-3 respectively.

Table 3.4 shows that G´´> G´ and tanδ > 1 for sample C0, however, this equilibrium shifts with crosslinking as G´ > G´´ and tanδ < 1 for all other samples as shown in figure 3.9A. Comparison of table 3.3 and table 3.4 indicates that G´´ and G´ for all samples except C0

decrease in the hydrated state 2 – 7 times as compared to those in the dry state. Tanδ increases for all samples in the hydrated state as shown in table 3.4. It also shows that tanδ has lower values for all hybrid scaffolds as compared to collagen networks. Similar to the dry test, scaffolds with higher crosslinking densities have higher G´ and G´´ in wet test or vice versa. For instance, comparison of figure 3.11A and figure 3.11B shows that G´ and G´´ are higher for hybrid scaffolds as compared to their parent collagen networks. The degree of crosslinking of collagen network also affected tanδ in wet condition. For instance, S-1(tanδ, 0.38) and S-2 (tanδ, 0.14), with C0 (tanδ, 1.17) as parent network, have higher values as compared to S-3 (tanδ, 0.1) and S-4 (tanδ, 0.1) which have C60 (tanδ, 0.18) as parent network.

Table 3.4: Storage modulus G´ (kPa), loss modulus G´´ (kPa), and loss tangent (tanδ) of collagen networks and hybrid scaffolds in a hydrated state (37 ºC, 1 Hz). [a], [b], and [c] represent statistically significant values within collagen networks as compared to C0, C25, and C40 respectively. [d], [e], and [f] represent statistically significant values ($p < 0.05$) within hybrid scaffolds as compared to S-1, S-2, and S-3 respectively.

Sample ID	Effective crosslinking density (v_e, kmol/m^3)	Rheology Properties		
		Storage Modulus (G´, kPa)	Loss Modulus (G´´, kPa)	Loss Tangent (tan δ)
C0	0.4 ± 0.03	7 ± 2	9 ± 2	1.17
C25	1.3 ± 0.2	10 ± 3	6 ± 1	0.62 [a]
C40	2 ± 1 [a]	10 ± 3	5 ± 1	0.46 [a]
C60	3.3 ± 0.4 [a, b]	18 ± 3 [a, b, c]	3 ± 1 [a]	0.18 [a, b, c]
S-1	0.8 ± 0.1	11 ± 3	4 ± 1	0.38
S-2	0.9 ± 0.1	15 ± 3	2 ± 0.6 [d]	0.24 [d]
S-3	5.0 ± 0.6 [d, e]	53 ± 4 [d, e]	5 ± 2	0.1 [d]
S-4	6.8 ± 0.7 [d, e, f]	55 ± 3 [d, e]	6 ± 1[e]	0.1 [d]

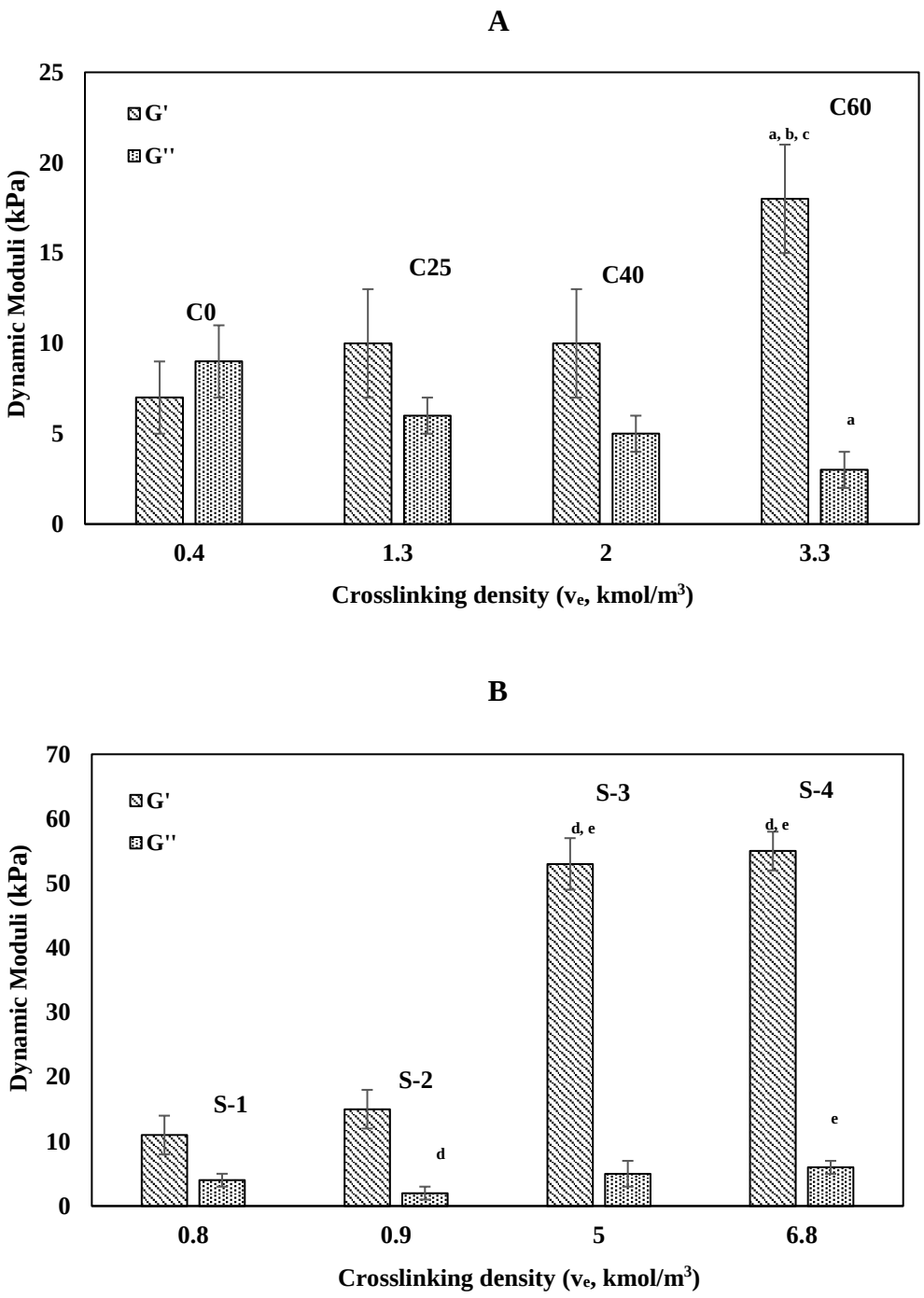


Figure 3.11: Effect of increase in crosslinking density (v_e, kmol/m^3) on dynamic moduli in the wet state (kPa) of (A) collagen network and (B) hybrid scaffolds. [a], [b], and [c] represent statistically significant values within collagen networks as compared to C0, C25, and C40 respectively. [d], [e], and [f] represent statistically significant values ($p < 0.05$) within hybrid scaffolds as compared to S-1, S-2, and S-3 respectively.

3.3.4 Rheology testing:

Table 3.5 shows the effect of an increase in crosslinking density on rheological properties of the HA network. G´ increases with increasing the crosslinking density from 320 ± 24 Pa for HA2 to 870 ± 21 Pa for HA20. Similarly, G`` also increases from 19 ± 6 Pa for HA2 to 33 ± 4 Pa for HA20 with increasing the crosslinking density as shown in figure 3.12. As a result, tanδ decreases from 0.05 to 0.03 (40 % reduction). Comparison of table 3.5 and table 3.4 indicates that G´ and G´´ for collagen networks are up to 20 times higher than HA networks. In addition, the range of tanδ for collagen networks (1.17 – 0.18) is up to 25 times higher than that of HA networks (0.05 – 0.03) in wet condition.

Table 3.5: Storage modulus G´(Pa), loss modulus G´´(Pa), and loss tangent (tanδ) of HA network soaked in PBS at 37°C. [a], [b], and [c] represent statistically significant values ($p < 0.05$) within HA networks as compared to HA2, HA4, and HA10 respectively.

Sample ID	Effective crosslinking density (v_e, kmol/m^3)	Storage Modulus (G´, Pa)	Loss Modulus (G´´, Pa)	Loss Tangent (tanδ)
HA2	2 ± 0.3	320 ± 24	19 ± 6	0.05
HA4	2.5 ± 0.1	480 ± 19 [a]	19 ± 3	0.04
HA10	4.3 ± 0.1	660 ± 23 [a, b]	25 ± 6 [a]	0.04
HA20	17 ± 0.4 [a, b, c]	870 ± 21 [a, b, c]	33 ± 4 [a]	0.03 [a]

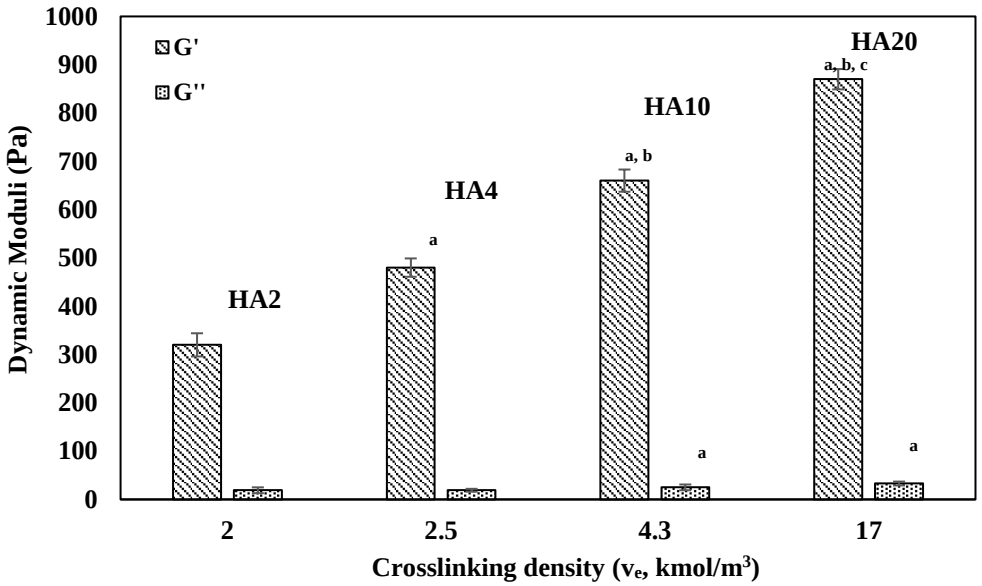


Figure 3.12: Effect of increase in crosslinking density (v_e, kmol/m^3) on rheological properties of the HA networks. [a], [b], and [c] represent statistically significant values ($p < 0.05$) within HA networks as compared to HA2, HA4, and HA10 respectively.

3.4 Discussion:

It has been shown in chapter 2 that increase in the concentration of crosslinking agent (i.e. EDC/NHS) resulted in an increase in the crosslinking density of collagen networks, HA networks and hybrid scaffolds (table 2.3B). It is also evident from SEM and histology images that sequential crosslinking route, adopted in this work, facilitated the formation of interlaced microstructures (figure 2.4 and figure 2.5) in hybrid scaffolds. The effects of these factors on the mechanical properties will be discussed in the following sections.

3.4.1 Effect of crosslinking density and interlacing on E_{comp}:

Increase in E_{comp} of collagen networks with increasing the crosslinking density can be explained by considering the deformation of a single pore within an elastomeric foam (or scaffold). An elastomeric foam deforms by the pore edge bending and pore wall buckling under the effect of compressive stress as shown in figure 3.13A. It has been shown in chapter 2 that pore size of collagen networks tends to decrease with increasing the crosslinking

density (table 2.4) possibly due to the volume shrinkage (Δv) as shown in figure 2.14. A reduction in pore size could increase the resistance towards pore edge deformation and pore wall buckling which would increase the E_{comp} of collagen networks[305, 311, 312]. Comparison of figure 3.5A and figure 3.5B shows that E_{comp} values of hybrid scaffolds are higher than their parent collagen network. It could be due to the effect of interlocking between collagen and HA networks as shown in figure 2.4 and figure 2.5. Figure 3.5B also suggested that incorporation of HA network with higher crosslinking density (HA20) increased the E_{comp} up to 2 times as compared to the one with lower crosslinking density (HA2). The higher crosslinking density of HA20 could result in higher degree of interlocking with collagen network in S-2 and S-4 which could result in higher E_{comp} for these compositions.

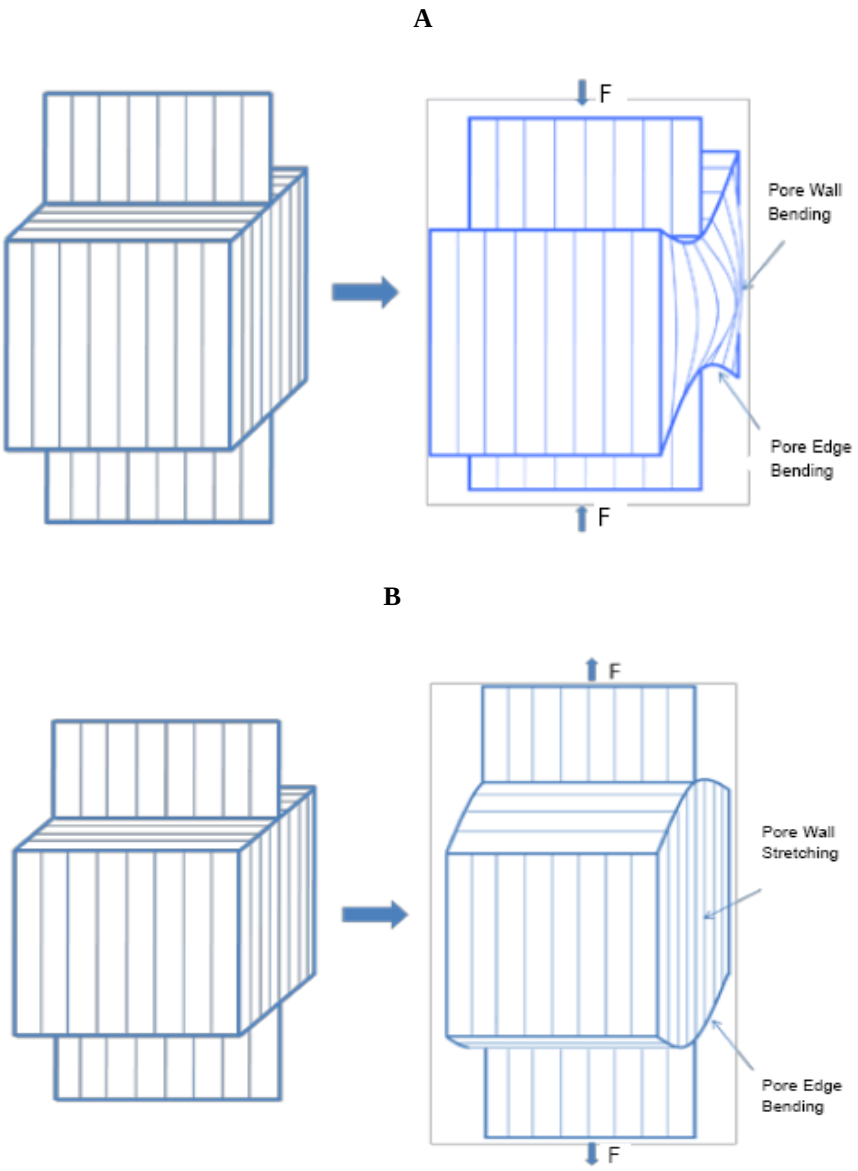


Figure 3.13: Schematic of deformation of an individual pore (A) compression and (B) tension [305].

3.4.2 Effect of crosslinking density and interlacing on E_{bend}:

E_{bend} for collagen networks show a similar trend to E_{comp} i.e. increases with increasing the crosslinking density (figure 3.7A). In addition, hybrid scaffolds show higher E_{bend} values than those of their parent collagen networks as shown in figure 3.7B. Comparison of table 3.1 and table 3.2 shows that E_{bend} is 4 – 18 times higher than those of E_{comp} values. It can be explained by considering a scaffold under the effect of bending force as shown in figure

3.14. When a bending force is applied to the scaffold, different parts of scaffold experience either compression or tension[305]. For a scaffold of uniform composition, E_{bend} is related to E_{comp} by the Eq. 3.5.

$$E_{bend} = 4/(1/\sqrt{E_{ten}}+1/\sqrt{E_{comp}})^2 \quad [304] \qquad \text{Eq. 3.5}$$

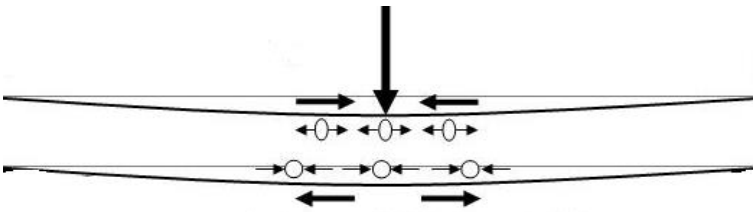


Figure 3.14: Schematic of a scaffold in the three-point bending test. The top surface is in compression whereas the bottom surface is in tension.

E_{ten} of the scaffolds could not be measured experimentally in this study, however, it is likely that E_{ten} could have also increased with increasing the crosslinking density (or decrease of pore size) as shown in figure 3.13B, as the tensile deformation of elastomeric foam is also assisted by pore edge bending and pore wall deformation[304]. Therefore, an increase of both E_{comp} and E_{ten} with increasing the crosslinking density (or with decreasing the pore size) could contribute to the increase in E_{bend}. Similar to E_{comp}, E_{bend} of S-2 and S-4 are higher 1.5 – 2 times higher than those of S-1 and S-3 most likely due to the effect of interlocking between collagen and highly crosslinked HA chains (HA20).

3.4.3 Effect of crosslinking density and interlacing on dynamic mechanical properties:

Dynamic mechanical properties give an insight into microstructural changes resulting from polymer chain movements[313, 314]. Table 3.3 shows that the dynamic moduli (G`, G``) of collagen network increase with increasing the crosslinking density. This could be due to the fact that zero-length crosslinks, formed by EDC/NHS, act as joining points between polymer chains resisting chain slippage[315, 316] as shown in figure 3.15.

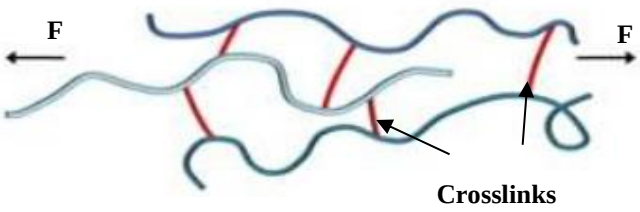


Figure 3.15: Schematic of crosslinked collagen network. Crosslinks (red lines) resist chain slippage.

This increased resistance, due to higher crosslinking density, against slipping under the effect of dynamic forces could explain the increase in G` and G`` for primary collagen networks. Comparison of figure 3.10A and figure 3.10B shows that values of dynamic moduli for hybrid compositions are greater than collagen networks. Increase in G` and G`` for hybrid scaffolds could be due to the incorporation of secondary HA network which is likely to further restrict the polymer chains as shown in figure 3.16A. tanδ < 1 shows that elastic character is dominant for all scaffolds in the dry state and decrease of tanδ with increasing the crosslinking density, as shown in table 3.3, indicates an increase of the elastic character. S-3 and S-4 have lowest tanδ suggesting that polymer chain movement is the most restricted in these compositions due to polymer chain entanglements between collagen type I and HA as shown in figure 2.4 and figure 2.5. It agrees with the observations from E_{comp} and E_{bend} values for hybrid scaffolds in the dry state.

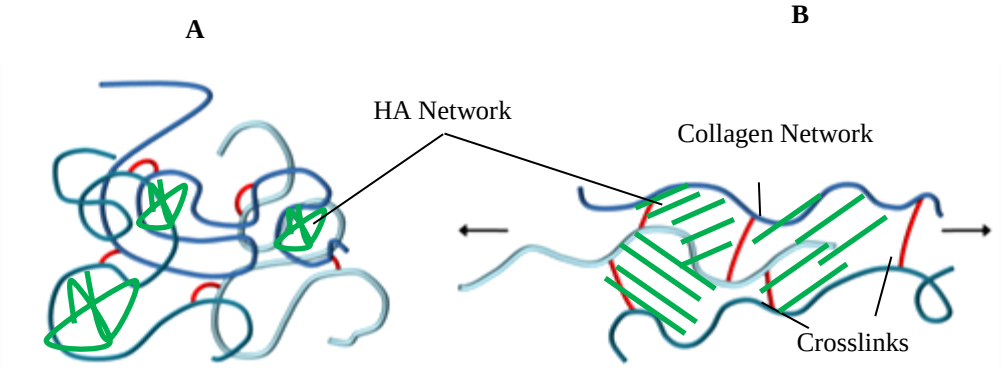


Figure 3.16: Schematic of collagen/HA hybrid scaffold (A) in the dry state and (B) in the wet state.

3.4.4 Effect of crosslinking density on the mechanical properties of collagen network under wet conditions:

Figure 3.8A and figure 3.11A suggest that $E_{wet.bend}$, G`, and G`` for collagen networks decrease significantly in the wet state as compared to those in the dry state. This behaviour can be explained by considering U values, which tend to decrease with increasing the crosslinking density for collagen networks as shown in table 3.2. FTIR studies from chapter 2 (figure 2.6) have shown that – COOH and $–NH_2$ groups form the amide bond during the EDC/NHS crosslinking. The decrease of U is possibly because of the engagement of these water-interacting sites (– COOH, $–NH_2$) in the crosslinking process which could increase the hydrophobicity of collagen network [251]. Increased hydrophobicity could result in taking up less water by the scaffolds with higher crosslinking densities such as C40 and C60 (table 3.2). Over all, water taken up by the scaffolds may act as a lubricant to facilitate chain slipping which explains the decrease of $E_{wet.bend}$, G`, and G`` for collagen networks in wet condition. Comparison of tanδ values from table 3.3 and 3.4 also supports this explanation that collagen chains experience more freedom in the wet state as compared to dry state most likely due to the lubricating effect of the absorbed water.

3.4.5 Effect of crosslinking density and interlacing on the mechanical properties of hybrid scaffolds under wet conditions:

In addition to the effect of crosslinking density, U values of hybrid compositions could also be related to the presence of secondary HA network[175, 317, 318]. Table 3.6 supports this hypothesis as HA chains are capable of absorbing an appreciable amount of water even in the crosslinked state and hence show highly hydrophilic character. Assuming these crosslinked HA chains packed inside collagen network in a hybrid composition as shown in

figure 3.16B. In the hydrated state, HA chains could slip off easily out of the collagen network and the role of primary collagen network becomes important at this stage. The presence of highly crosslinked collagen network (C60) in hybrid compositions (S-3 and S-4) could hold back the hydrated HA chains more efficiently than non-crosslinked collagen network (C0) present in S-1 and S-2. Comparison of figure 3.8A and figure 3.8B shows that $E_{wet.bend}$ values for hybrid scaffolds are lower than those of collagen networks. This suggests that hydrophilic effect of HA chains probably dominates the hydrophobic effect of collagen network, discussed in the section 3.4.4, for hybrid scaffolds in the wet state.

According to table 3.4, the shift from the viscous character for C0 ($G'' > G'$ and $\tan\delta > 1$) to the elastic character ($G'' < G'$ and $\tan\delta < 1$) for all other compositions suggests that crosslinking contributes towards increasing the elastic character of the scaffolds. Comparison of figure 3.11A and figure 3.11B shows that G` values for hybrid scaffolds are higher than those of collagen networks whereas there is no significant difference between G`` values for collagen networks and hybrid scaffolds. It agrees with the observation from $E_{wet.bend}$ values where hydrophilicity of HA network seems to dominate and also contributes to the viscous character (G``) of the hybrid scaffolds in the wet state. Tanδ values for S-1 and S-2 from table 3.4 that presence of HA chains tend to experience more freedom due to the lack of hold from non-crosslinked C0 network. On the other hand, tanδ decreases for S-3 and S-4 where highly crosslinked C60 network could hold back the HA chains from slipping (figure 3.16).

3.4.6 Comparison of mechanical properties of hybrid scaffolds with the human aortic valve leaflet (HAVL):

The heart valve leaflet has a multicomponent hybrid microstructure and exhibits anisotropic mechanical characteristics as discussed in chapter 1 (section 1.3.3). Many research groups

have been investigating the mechanical properties of the heart valve leaflets[319, 320], however, the available data is highly divergent due to the biological diversity and lack of standardization in testing methods [321, 322]. The potential of collagen type I and HA to match the mechanical properties of the human aortic valve leaflet (HAVL) has already been discussed in chapter 1 (table 1.5). Table 3.1 – 3.5 indicate that hybrid scaffolds showed higher mechanical properties as compared to the either network alone. E_{comp} of HAVL has not been reported yet whereas that of the porcine aortic valve leaflet (PAVL) from belly region has been reported in the range of 5 – 6 kPa[323]. E_{comp} of hybrid scaffolds is in the range of 41 – 95 kPa; which exceeds that of PAVL. Given that E_{bend} of HAVL is said to be higher than those for PAVL and E_{bend} is related to E_{comp} (Eq. 3.5), it can be inferred that hybrid scaffolds have the potential to match E_{comp} of the HAVL[69]. Bending and dynamic moduli (dry state) of the collagen/HA hybrid scaffolds, as reported in this chapter, have been compared with those of HAVL in table 3.6. Table 3.6 shows that E_{bend} values of S-1 and S-2 match that of HAVL in diastole whereas E_{bend} values of S-3 and S-4 match that of HAVL in systole. $G^{`}$ values of hybrid scaffolds are 5 – 10 times higher than those of HAVL and sinus. Also, tanδ for HAVL is higher than those of hybrid scaffolds. This comparison suggests that hybrid scaffolds, in a dry state, are stiffer and more elastic than HAVL.

Table 3.6: Comparison of mechanical properties of HAVL and hybrid scaffolds in the dry state.

Mechanical Property	HAVL	Hybrid Scaffolds			
		S-1	S-2	S-3	S-4
Flexural/bending modulus (E_{bend}, kPa)	1220 kPa in systole, 710 kPa in diastole[96]	711 ± 29	817 ± 17	980 ± 20	1660 ± 25
Storage modulus ($G^{`}$, kPa)	0.545 – 10.5 kPa (aortic leaflet + sinus)[84]	52 ± 6	64 ± 4	68 ± 5	113 ± 6
Tanδ	0.3 – 0.4[84]	0.12	0.12	0.11	0.09

Lower G` and higher tanδ of HAVL, from table 3.6, could be due to the hydrated condition of the tissue and therefore, table 3.7 compares the wet mechanical properties of hybrid scaffolds with those of HAVL. Table 3.7 shows that $E_{wet.bend}$ values of hybrid scaffolds are very low as compared to the HAVL. G` and tanδ of S-1 and S-2, in the wet state, match those of HAVL whereas S-3 and S-4 have higher values than those of HAVL.

Table 3.7: Comparison of mechanical properties of HAVL and hybrid scaffolds in the wet state.

Mechanical Property	HAVL	Hybrid Scaffolds			
		S-1	S-2	S-3	S-4
Flexural/bending modulus (E_{bend}, kPa)	1220 kPa in systole, 710 kPa in diastole[96]	1 ± 0.2	1 ± 0.3	2 ± 0.3	3 ± 0.2
Storage modulus (G`, kPa)	0.545 – 10.5 kPa (aortic leaflet + sinus)[84]	11 ± 3	15 ± 3	53 ± 4	55 ± 3
Tanδ	0.3 – 0.4[84]	0.38	0.24	0.1	0.1

Bending is an important mode of deformation of the heart valve[54, 69] and therefore, any scaffold designed to serve as TEHV should match the bending stiffness of the heart valve. Collagen/HA hybrid scaffolds, in a dry state, match the range of bending modulus of the HAVL. Low bending modulus of the hybrid scaffold, in the wet state, could be increased by the incorporation of elastin[26]. In addition, seeding of cells has also been reported to increase the bending stiffness of scaffolds[324], which will be studied in chapter 5. Dynamic mechanical properties of the hybrid scaffolds, in the wet state, match those of HAVL whereas scaffolds, in a dry state, seem more elastic than HAVL. This indicates that hybrid scaffolds could also be optimized for the target tissues stiffer than HAVL such as cartilage.

3.5 Conclusion:

It has been shown that compressive (E_{comp}), bending (E_{bend}), and dynamic moduli (G´, G``) of collagen networks and hybrid scaffolds increase with increasing the crosslinking density under dry as well as wet conditions. However, E_{comp} in the wet condition could not be measured due to the sensitivity limit of the equipment. Increase in mechanical moduli is attributed to the resistance of the crosslinks towards the polymer chain movement as well as a decrease in the pore size resisting pore edge and wall deformation. The mechanical moduli of collagen/HA hybrids are found to be several orders higher, in both dry and wet conditions, than those of their parent collagen network due to the effect of interlacing between collagen and HA networks. The higher the crosslinking density of the HA network, the greater is the increase in the mechanical moduli of collagen/HA hybrid scaffolds.

$E_{wet.bend}$, G´, and G`` for all scaffolds decrease whereas tanδ increase several orders in the wet state due to the lubrication effect of water. Scaffolds with higher crosslinking densities show lower values of water uptake ratio (U) due to the higher number of water-interacting sites engaged in the crosslinking process. In addition to the effect of crosslinking density, wet mechanical properties of hybrid scaffolds are also found to be affected by the hydrophilicity of the HA network.

Bending moduli of collagen/HA hybrid scaffolds, in the dry state, exceed that of PAVL and matched that of HAVL whereas dynamic mechanical properties (G`, tanδ), in the wet state, matched that of HAVL and exceed that of HAVL in the dry state. Therefore, it can be concluded that hybrid scaffolds have the potential to serve as mechanically matching TEHV. Furthermore, mechanical properties of an interlaced hybrid scaffold can be optimized for other tissue engineering applications by changing the crosslinking densities of the parent networks.

While mechanical properties decrease significantly in the wet condition, scaffolds could also have a tendency to degrade. Therefore, degradation behaviour of parent networks and the resultant scaffolds under different conditions will be studied and discussed in chapter 4.

Chapter 4

Degradation Behaviour of Collagen/HA Hybrid Scaffolds

4.1 Introduction:

Scaffolds are designed to house the cells and give them sufficient support until a fully functional tissue can be generated[325-327]. Apart from mechanical strength, the second important parameter for scaffold is the rate at which it degrades inside the body[5, 328, 329]. It should degrade at an appropriate rate into the body friendly by-products, which can be easily washed away by physiological fluids[330-332].

Biocompatible polymers, either synthetic or natural, are usually chosen for making scaffolds for tissue engineering applications[333, 334]. Their degradation behaviours, in turn, depend on various factors such as physical (crystallinity and molecular weight) and chemical properties (nature of bonding) of the polymer[26, 335, 336]. The degradation rate and degradation mechanism are also affected by the host environment[337]. For example, the *in-vivo* degradation rate is usually higher than *in-vitro* degradation rate. Degradation in non-enzymatic physiological fluids (*in-vitro*) occurs through hydrolysis whereas polymer chain cleavage in the presence of enzymes further accelerates the degradation under *in-vivo* conditions [213, 214].

The degradation behaviour is usually studied in phosphate buffer saline (PBS, pH 7.4) at 37^{o}C with or without enzymes [338, 339]. It has been shown in chapter 3 that incorporation of hyaluronic acid (HA) network has significantly increased the mechanical properties of the collagen/HA hybrid scaffolds not only in dry but also in wet conditions. The survival of

scaffolds in physiological fluids is, therefore, is also of interest in this thesis. In this chapter, the degradation behaviour of parent networks and hybrid scaffolds with and without enzymes under the standard condition has been investigated. It is also important to elucidate the degradation behaviour of scaffolds under different pH, where pH 7.4 represents physiological environment and pH 4.0 represents the environment of an infected tissue of body[340, 341]. The non-enzymatic experiments have been replicated under acidic and basic conditions to understand the degradation behaviour on a broader spectrum. Furthermore, the effect of variation in crosslinking density on degradation resistance of parent networks and hybrid scaffolds has also been discussed. Scaffolds have been examined the effect of polymer-specific enzymes e.g. collagenase for collagen and hyaluronidase for HA. Collagen/HA hybrid scaffolds have been exposed to each enzyme individually and together. It is hypothesized that collagenase could attack collagen network only without affecting the HA network and vice versa.

4.2 Materials and methods:

4.2.1 Degradation behaviour under non-enzymatic conditions:

Collagen scaffolds, HA scaffolds, and collagen/HA hybrid scaffolds (d = 12 mm, h = 4 mm) were prepared according to the protocol described in 2.2.1, 2.2.2, and 2.2.3 respectively. Initial mass (M_1) of each scaffold was recorded and the sample was incubated in 0.01M PBS (Sigma-Aldrich, UK, pH 7.4) at 37 ^{o}C. Three scaffolds from each group were removed on day 1, 7, 14, 21, and 28. The samples were washed three times with deionized water to remove residual salts. These were then frozen at -20 ^{o}C overnight, freeze-dried for 24 hours, and final mass (M_2) was recorded. Mass loss in scaffolds at each time point as a result of degradation was calculated using the following equation:

$$Mass\ Loss = [(M_2-M_1)/M_1] \times 100 \qquad Eq.\ 4.1$$

The study was repeated in PBS at pH 4.0 and pH 10.0 to study the effect of pH on the degradation behaviour.

4.2.2 Degradation behaviour under enzymatic conditions:

Collagen/HA hybrid scaffolds (d = 12 mm, h = 4 mm) were exposed to 0.01M PBS (pH 7.4) containing collagenase from *Clostridium histolyticum* (≥ 250 CDU/mg of solid, Sigma-Aldrich, UK) and hyadulronsae from *streptomyces hyalurolyticus* (400-1000 CDU/mg of solid) at a concentration of 10 U/ml of each at 37 ^{o}C for 35 hours. Three scaffolds from each composition were removed after 1, 5, 8, 24, and 35 hours. The samples were washed three times with deionized water to remove residual salts, frozen overnight at -20 ^{o}C, and freeze-dried for 24 hours. Final mass (M_2) was recorded and percentage mass loss was calculated using Eq. 4.1. The experiment was repeated with the only collagenase and also with only hyadulronsae. The parent networks e.g. collagen (C0 and C60) and HA (HA2 and HA20) were degraded in collagenase and hyadulronsae respectively as controls under the same conditions (10 U/ml of each enzyme, 37^{o}C, 35 hours).

4.2.3 Statistical analysis *:

All data for enzymatic degradation have been reported as means, with errors as standard deviations. The data have been analysed using one-way ANOVA with a Bonferroni's post-hoc test. The probability of 95 % ($p < 0.05$) has been taken as statistically significant. At least three samples have been analysed for each group.

* performed by Prof. Carolyn Carr, Department of Physiology, University of Oxford.

4.3 Results:

4.3.1 Degradation behaviour under non-enzymatic conditions:

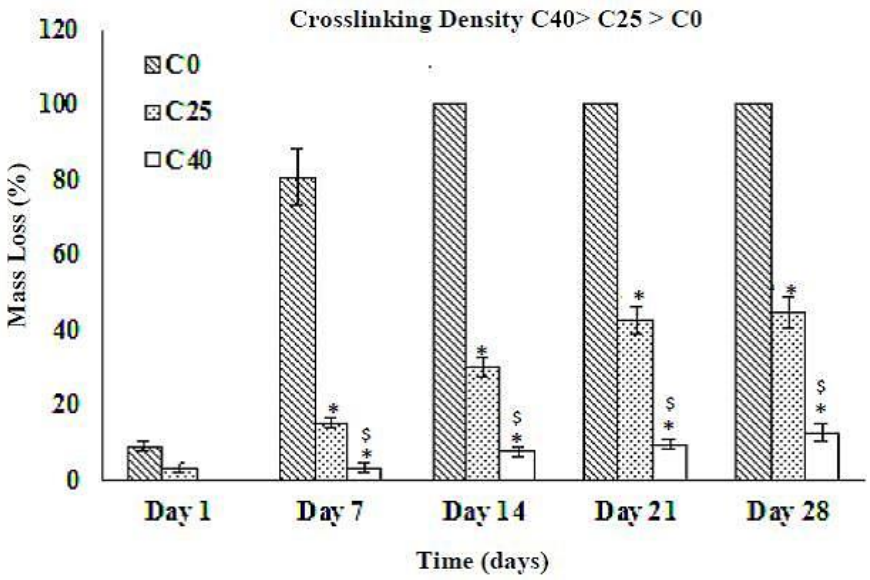
The degradation behaviour of parent and hybrid scaffolds under the effect of different pH values (PBS, 37^{o}C, 28 days), are presented in the following sections.

4.3.1.1 Collagen scaffolds:

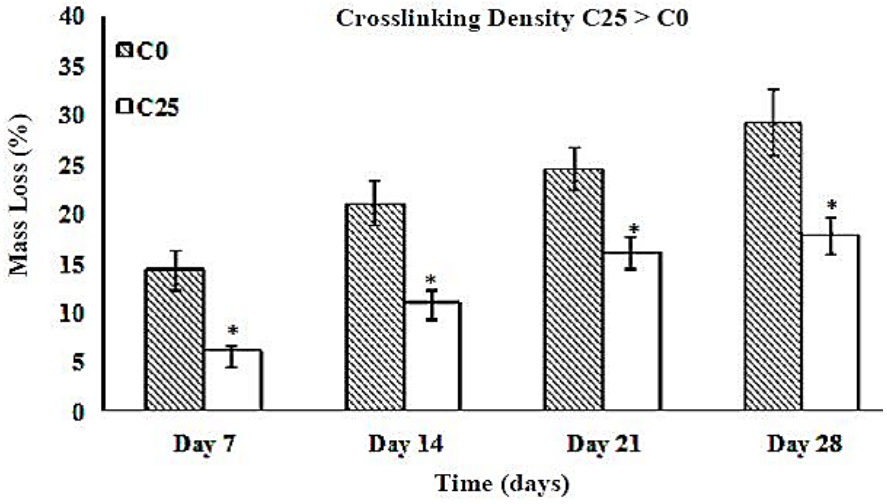
The increase in crosslinking density increases the degradation resistance of collagen network at pH 4.0, 7.4, and 10.0 as shown in figure 4.1A, figure 4.1B, and figure 4.1C respectively. Mass loss decreases as the crosslinking density increases at all three pH values. There is no mass loss for any composition at pH 7.4 and 10 on day 1 (figure 4.1B and figure 4.1C). The mass loss for sample C40 is almost negligible at pH 7.4 and 10.0. Similarly, C60 do not show any mass loss after 28 days at pH 4.0, 7.4 and 10.0 (data not shown). The comparison of the total mass loss of collagen networks at pH 4.0, 7.4 and 10.0 as a result of degradation is shown in table 4.1. The mass loss is highest for acidic pH and lowest for basic pH; order of degradation for collagen networks is as follows:

Acidic > Neutral > Basic

A


Crosslinking Density C40> C25 > C0
C0
C25
C40
Mass Loss (%)
120
100
80
60
40
20
0
Day 1
Day 7
Day 14
Day 21
Day 28
Time (days)

B


Crosslinking Density C25 > C0
C0
C25
Mass Loss (%)
40
35
30
25
20
15
10
5
0
Day 7
Day 14
Day 21
Day 28
Time (days)

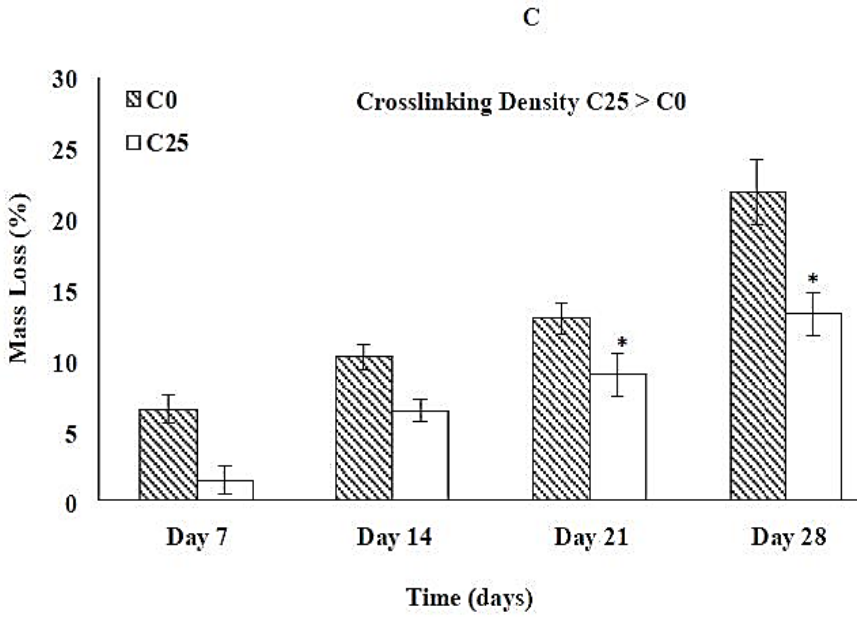


Fig 4.1: Effect of crosslinking density on the degradation behaviour of collagen scaffolds at (A) pH 4.0, (B) pH 7.4, and (C) pH 10. * and $ represent statistically significant values ($p < 0.05$) within collagen scaffolds on a given day as compared to C0 and C25 respectively.

Table 4.1: Summary of the total mass loss (%) of collagen scaffolds after 28 days in PBS at pH 4.0, 7.4, and 10.0. [a] and [b] represents statistically significant values ($p < 0.05$) within collagen scaffolds as compared to C0 and C25 respectively.

Sample ID	Effective crosslinking density (v_e, $\times 10^{-4}$ kg/m^3)	Total mass loss after 28 days (%)		
		pH 4.0	pH 7.4	pH 10.0
C0	0.4 ± 0.03	100 ± 0	29 ± 3	22 ± 2
C25	1.3 ± 0.2	45 ± 4 [a]	18 ± 2 [a]	13 ± 2
C40	2 ± 1 [a]	13 ± 2 [a, b]	0.3 ± 0 [a, b]	0.4 ± 0 [a, b]
C60	3.3 ± 0.4 [a, b]	0	0	0

4.3.1.2 HA scaffolds:

Similar to the collagen scaffolds, an increase in the crosslinking density increases the degradation resistance of HA scaffolds under acidic and physiological conditions as shown in figure 4.2A and figure 4.2B. HA networks exposed to pH 10.0 could not survive beyond day 1 (data not shown). As the EDC concentration is increased from 2 mM to 20 mM, the

crosslinking density also increases and the total mass loss decreases from 30 % to 17 % and 55% to 43% at pH 4.0 and pH 7.4 respectively (table 4.2). There is no mass loss for any composition on day 1 at pH 7.4 (figure 4.2B).

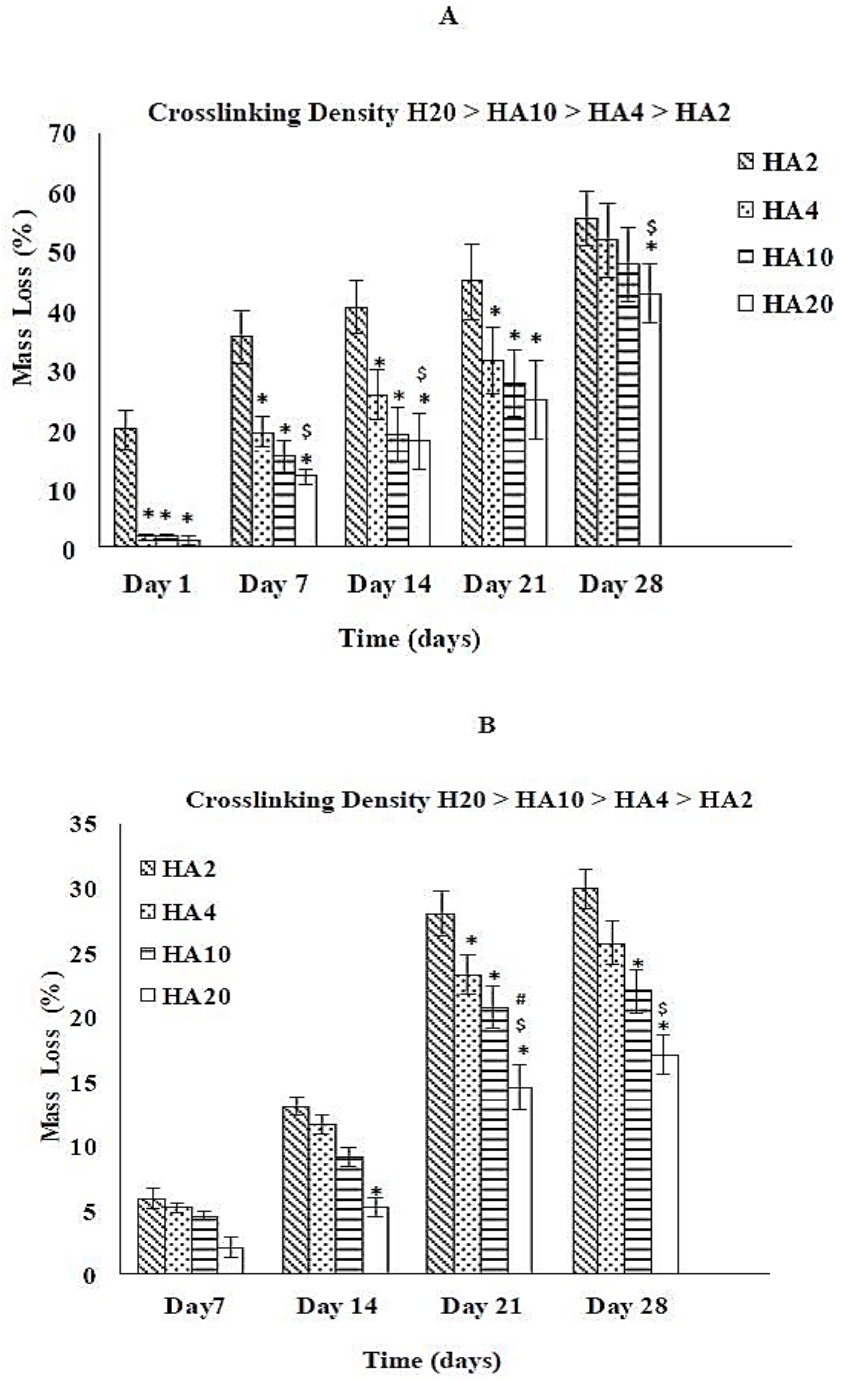


Figure 4.2: Effect of crosslinking density on the degradation behaviour of HA scaffolds (A) pH 4.0 and (B) pH 7.4. *, $ and # represent statistically significant values ($p < 0.05$) within HA scaffolds on a given day as compared to HA2, HA4, and HA10 respectively.

Table 4.2: Summary of the total mass loss (%) of HA networks after 28 days in PBS at pH 4.0, 7.4, and 10.0. [a], [b] and [c] represent statistically significant values ($p < 0.05$) within HA networks as compared to HA2, HA4, and HA10 respectively.

Sample ID	Effective crosslinking density (v_e, $\times 10^{-4}$ kg/m^3)	Total mass loss after 28 days (wt %)		
		pH 4.0	pH 7.4	pH 10.0
HA2	2 ± 0.3	30 ± 4	56 ± 5	100
HA4	2.5 ± 0.1	26 ± 1	52 ± 6	100
HA10	4.3 ± 0.1	22 ± 2 [a]	48 ± 6	100
HA20	17 ± 0.4 [a, b, c]	17 ± 2 [a, b]	43 ± 5 [a]	100

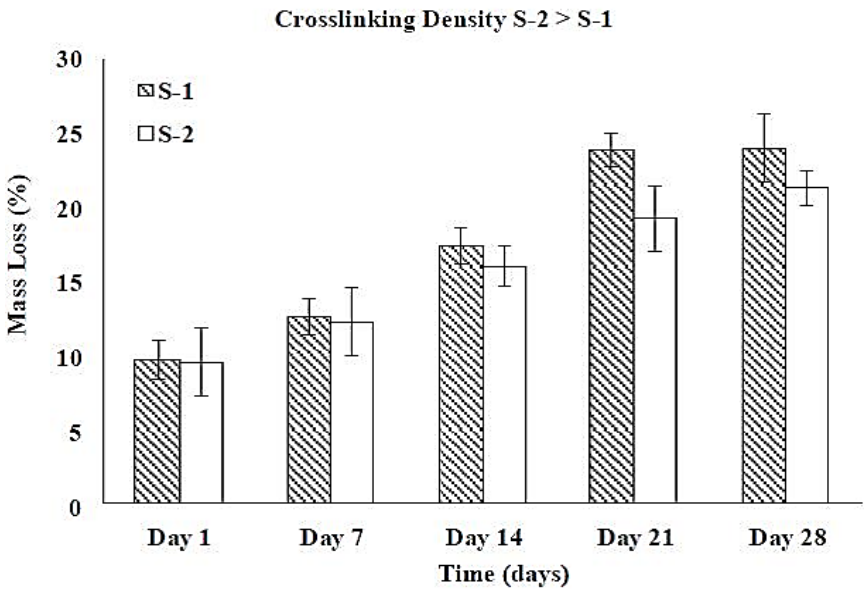
4.3.1.3 Collagen/HA hybrid scaffolds:

Degradation behaviour of collagen/HA hybrid scaffolds at pH 4.0, 7.4, and 10.0 is shown in figure 4.3A, 4.3B, and 4.3C respectively. While comparing the total mass loss of S-1 and S-2 under different pH as shown in table 4.3, mass loss is highest at pH 4.0 and lowest pH 10.0. There is no mass loss for any composition on day 1 at pH 10.0 (figure 4.3C). S-3 and S-4 do not show any mass loss until 28 days under all conditions. Table 4.3 suggests the order of degradation for collagen/HA hybrid scaffolds under non-enzymatic conditions as follows:

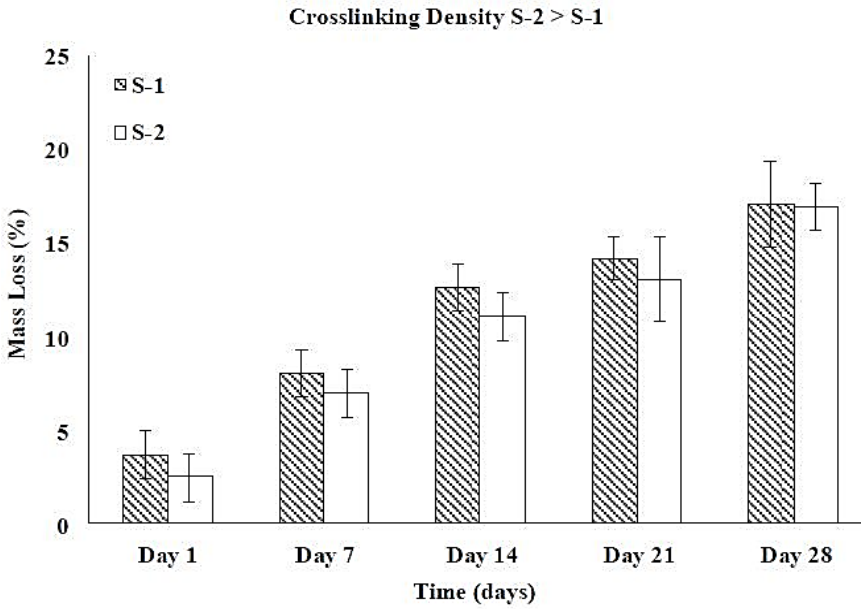
Acidic > Neutral > Basic

The total mass loss for collagen/HA hybrid scaffolds is less than the total mass loss for either collagen scaffold or HA scaffold. There is no significant difference in the mass loss between S-1 and S-2 under all conditions.

A


Crosslinking Density S-2 > S-1
S-1
S-2
Mass Loss (%)
30
25
20
15
10
5
0
Day 1
Day 7
Day 14
Day 21
Day 28
Time (days)

B


Crosslinking Density S-2 > S-1
S-1
S-2
Mass Loss (%)
25
20
15
10
5
0
Day 1
Day 7
Day 14
Day 21
Day 28
Time (days)

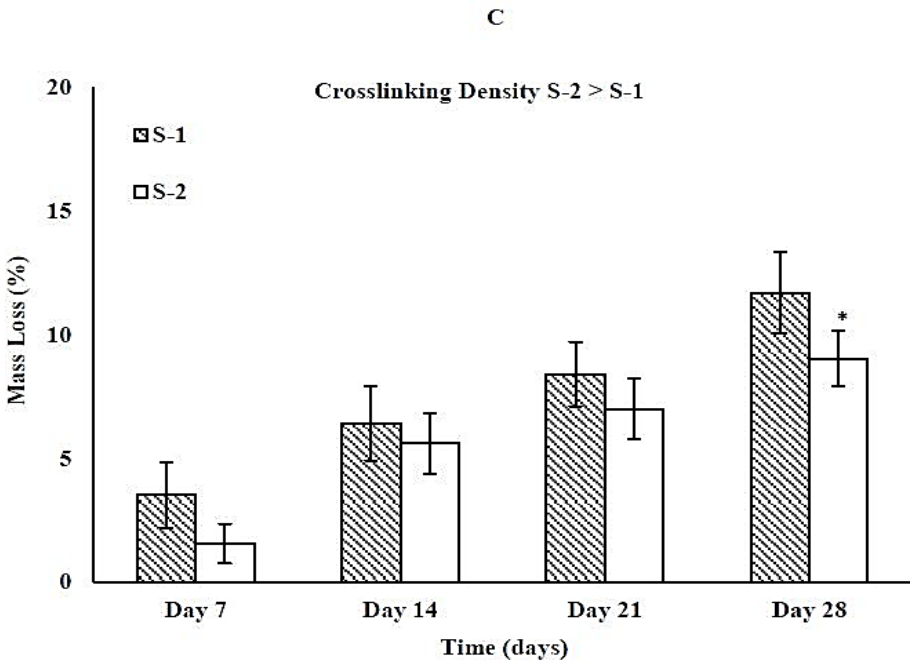


Figure 4.3: Effect of crosslinking density on the degradation behaviour of collagen/HA hybrid scaffolds at (A) pH 4.0, (B) pH 7.4, and (C) pH 10.0. S-3 and S-4 did not show any mass loss. * represent statistically significant values ($p < 0.05$) within collagen/HA hybrid scaffolds on a given day as compared to S-1.

Table 4.3: Summary of the total mass loss (%) of collagen/HA hybrid scaffolds after 28 days in PBS at pH 4.0, 7.4, and 10.0. There are no statistically significant differences ($p < 0.05$) among different groups at pH 4.0, pH 7.4, and pH 10.0 respectively.

Sample ID	Effective crosslinking density (v_e, $\times 10^{-4}$ kg/m^3)	Total mass loss after 28 days (wt %)		
		pH 4.0	pH 7.4	pH 10.0
S-1	0.8 ± 0.1	24 ± 2	17 ± 2	12 ± 3
S-2	0.9 ± 0.1	21 ± 3	17 ± 3	9 ± 2
S-3	5.0 ± 0.6 [f, g]	0	0	0
S-4	6.8 ± 0.7 [f, g, h]	0	0	0

4.3.2 Degradation behaviour under enzymatic conditions:

Figure 4.4 shows the degradation in the presence of collagenase at 37 ^{o}C (pH 7.4, 10U/ml) till 35 hours. C0 and C60, as controls, seem to span the range of the degradation behaviour of the hybrid scaffolds. C0 completely degrades in 10 hours but the mass loss for C60 is only 17% after 35 hours. S-1 shows a degradation behaviour similar to C0. S-2 shows a total mass loss of 46 % in 35 hours.

Figure 4.5 presents the case where hybrid scaffolds are degraded in the presence of hyaluronidase (10 U/ml, pH 7.4, 35 hours). HA2 and HA20 are run as controls and exhibit low degradation resistance. HA2 has survived for 2 hours whereas HA20 has degraded completely in 10 hours. S-1 and S-2 show total mass loss of around 19% and 25% respectively.

Figure 4.6 shows degradation behaviour of hybrid scaffolds under the combined effect of collagenase and hyaluronidase (10 U/ml of each, pH 7.4, 35 hours). The degradation rate is higher as compared to degradation under the effect of collagenase or hyaluronidase alone, as shown in figure 4.4 and 4.5. S-1 is digested completely in 10 hours, which is similar to the behaviour under the effect of collagenase only (figure 4.4). S-2 has a relatively higher degradation resistance and has shown a total mass loss of 60% in 35 hours. Collagenase and hyaluronidase alone or together have no effect on S-3 and S-4 and hence no appreciable mass loss could be measured for them. Taking figure 4.4, 4.5, 4.6 and data in table 4.4 together, the order of degradation rate of collagen/HA hybrid scaffolds in the presence of enzymes as can be defined as:

Collagenase + Hyaluronidase > Collagenase > Hyaluronidase

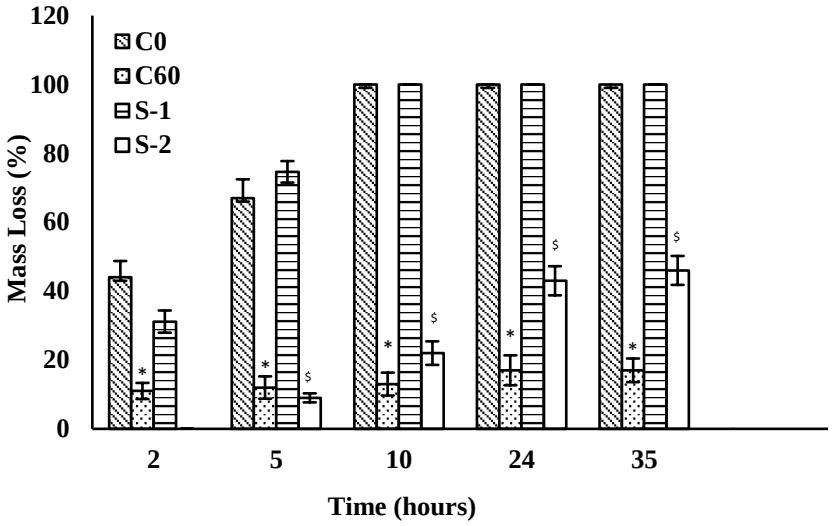


Figure 4.4: Degradation behaviour of collagen/HA based hybrid scaffolds in the presence of collagenase (10 U/ml, PBS pH 7.4, 35 hours). Collagen networks (C0 and C60) were degraded by respective enzymes as controls. * and $ represent the statistically significant values ($p < 0.05$) as compared to C0 and S-1 respectively within controls and hybrid scaffolds.

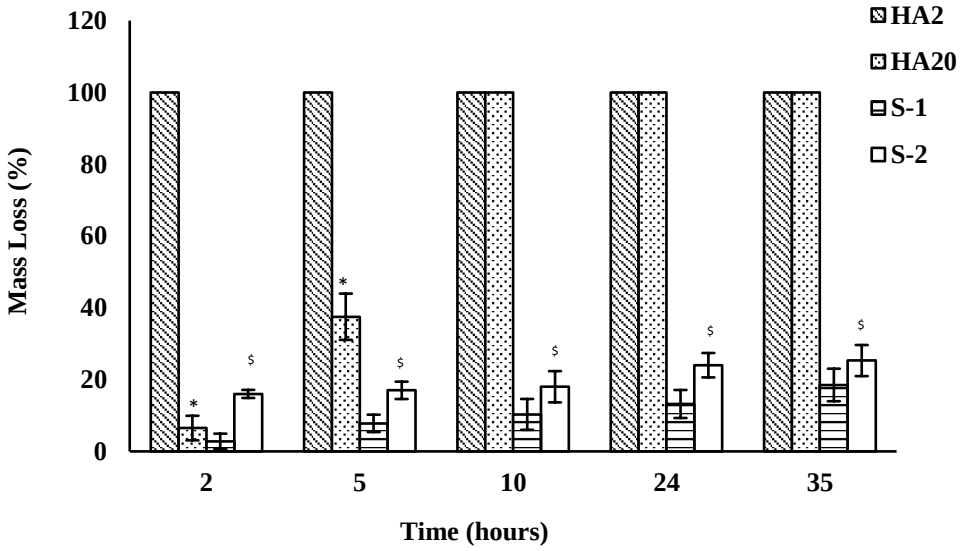


Figure 4.5: Degradation behaviour of collagen/HA hybrid scaffolds in the presence of hyaluronidase (10 U/ml, PBS pH 7.4, 35 hours). HA networks (HA2 and HA20) were degraded by respective enzymes as controls. * and $ represent the statistically significant values ($p < 0.05$) as compared to HA2 and S-1 respectively within controls and hybrid scaffolds.

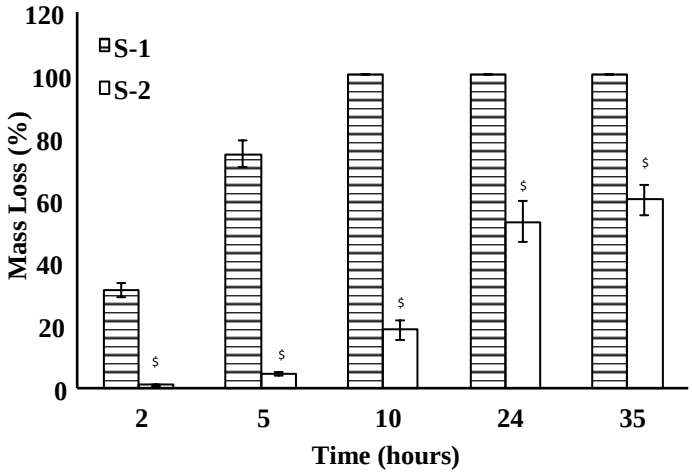


Figure 4.6: Degradation behaviour of collagen/HA hybrid scaffolds in the presence of collagenase and hyaluronidase (10 U/ml of each, PBS, pH 7.4) at 37 ºC for 35 hours. $ represents the statistically significant values ($p < 0.05$) as compared to S-1. S-3 and S-4 did not show any mass loss under given conditions.

Table 4.4: Effect of collagenase (10U/ml), hyaluronidase (10U/ml) and collagenase + hyaluronidase (10U/ml each of enzyme) on the total mass loss of scaffolds in PBS (pH 7.4, 37ºC, 35 hr). [a], [b], and [c] denotes the statistically significant differences ($p < 0.05$) among different groups in the presence of collagenase, hyaluronidase, and collagenase + hyaluronidase respectively.

	Weight loss (%) after 35 hours		
Sample ID	**Collagenase (10 U/ml)**	**Hyaluronidase (10 U/ml)**	**Collagenase + Hyaluronidase (10 U/ml each)**
C0	100	-	-
C60	17 ± 3 [a]	-	-
HA2	-	100	-
HA20	-	100	-
S-1	100	19 ± 5 [b]	100 [c]
S-2	46 ± 4 [a]	25 ± 4 [b]	60 ± 5 [c]
S-3	0	0	0
S-4	0	0	0

4.4 Discussion:

EDC/NHS crosslinking has increased the degradation resistance of the parent scaffolds when exposed to acidic, basic, and physiological environments as shown in figure 4.1 and figure 4.2. This is probably because of the engagement of the water interacting sites (– COOH, – NH_2) in the crosslinking process which could have increased the hydrophobicity of these polymers as discussed in chapter 3. Increase in hydrophobicity could slow down the degradation rate and hence less mass loss due to degradation[251, 342]. In the case of hybrid scaffolds, S-1 and S-2 showed similar degradation rate whereas S-3 and S-4 did not show any mass loss under non-enzymatic conditions. This behaviour can be attributed to the poor binding of non-crosslinked C0 network for HA network in S-1 and S-2 whereas the presence of highly crosslinked C60 network could hold the HA network in S-3 and S-4 as shown in figure 3.16B.

In this study, the pH dependence of the degradation behaviour of the parent networks and hybrid scaffolds has also been investigated. For instance, the rate of hydrolysis of the peptide (or amide) bond of collagen is higher at acidic pH [343, 344] and this could be the reason for the greatest mass loss of collagen scaffolds at pH 4.0 (figure 4.1A). On the other hand, HA is known to degrade through the deacetylation of the N-acetyl group (figure 1.15) at basic medium which could result in rapid degradation rates (figure 1.24) [216, 219]. This explains the greatest mass loss of the HA scaffolds at pH 10, as shown in figure 4.2B. Comparison of figure 4.1 and figure 4.3 suggests that the pH dependence of the degradation behaviour of the hybrid scaffolds follows that of the collagen scaffolds. This implies that the collagen network is abundantly present in the hybrid compositions and dominates the degradation behaviour of these scaffolds (figure 4.3). Furthermore, comparison of figure 4.1 and figure 4.2 shows that collagen network and HA network show contrasting behaviour with respect

to pH of the degrading medium. It can be inferred that pH-sensitive degradation of hybrid scaffolds can be tailored by choosing the primary network during fabrication.

Enzyme-assisted degradation studies of collagen/HA hybrid scaffolds have been informative for understanding the *in-vitro* degradation behaviour of these scaffolds. Collagenase and hyaluronidase have been chosen to target the collagen and HA networks, respectively. When exposed to collagenase, the presence of HA network did not enhance the degradation resistance of S-1 and S-2 significantly (figure 4.4). S-3 and S-4 showed high degradation resistance to collagenase which is most likely because of their higher crosslinking densities. Mass loss in all samples, in the presence of collagenase, could be attributed to the degradation of collagen network only. HA controls degraded quickly in the presence of hyaluronidase (figure 4.5). This may be partly due to the bulk erosion arising from the highly hydrophilic character of HA (table 3.5)[345] and partly due to the presence of hyaluronidase [346]. As the collagen is added to the HA network, degradation resistance towards hyaluronidase increases considerably as seen for S-1 and S-2. Mass loss of hybrid scaffolds in the presence of collagenase and hyaluronidase together is higher than the mass loss in the presence of collagenase or hyaluronidase alone (figure 4.6). This implies that the mass loss in figure 4.6 resulted from the degradation of both collagen and HA networks in hybrid scaffolds. S-3 and S-4 maintained their non-degradability under the given conditions due to the extensive entanglements between collagen and HA networks, as shown in the SEM and histology images in chapter 2 (figure 2.4 and figure 2.5).

Figure 4.7 (reproduced from figure 4.4 – figure 4.6) shows the effect of enzymatic environment on the degradation behaviour of S-2 as a case study. The degradation rate, as well as the total mass, is lowest when S-2 is exposed to hyaluronidase only. The total mass loss of S-2 as a result of degradation in the presence of both collagenase and hyaluronidase (60 %) is nearly equal to the sum of the mass loss resulting from collagenase (45 %) and that

of from hyaluronidase (25.3 %) as shown in table 4.4. This further supports the hypothesis that collagen forms the primary network while HA is present as a secondary network in the hybrid scaffolds.

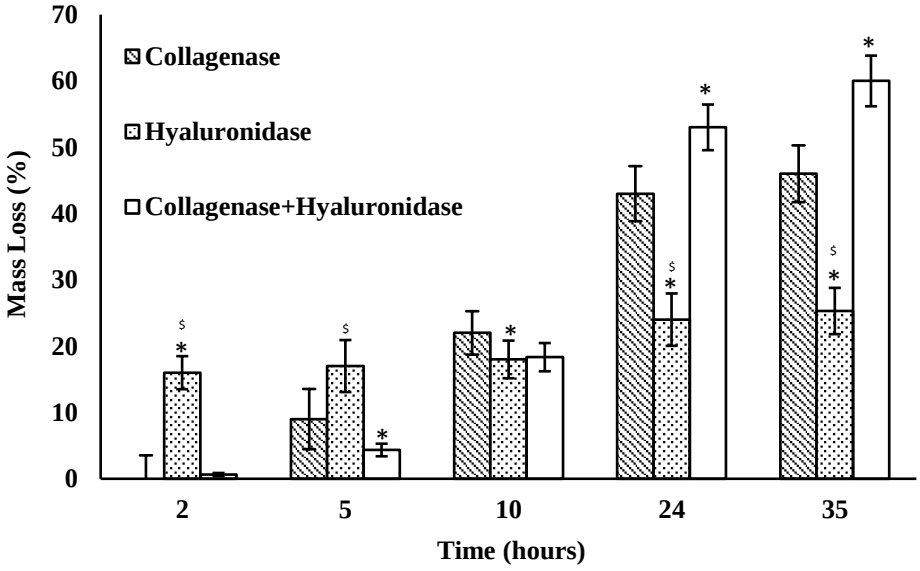


Figure 4.7: Case Study; degradation behaviour of S-2 in PBS (pH 7.4) at 37°C for 35 hours in the presence of collagenase (10U/ml), hyaluronidase (10U/ml), and under the combined action of both of these (10U/ml of each). * and $ represent the statistically significant values ($p < 0.05$) as compared to those in the presence of collagenase and collagenase + hyaluronidase respectively.

In general, scaffolds with higher crosslinking densities are more resistant towards degradation as compared to those with lower crosslinking densities[146, 176, 347]. Suri *et al* studied the degradation profiles of photo-patterned collagen/HA based interpenetrating polymer networks (IPNs) under similar conditions (10 U/ml of each enzyme in PBS, 37°C, 35 hours) and found that the composition even with highest crosslinked density was digested completely in 35 hours under the combined action of collagenase and hyaluronidase [347]. Collagen/HA hybrid scaffolds prepared through sequential EDC/NHS based crosslinking technique, reported in this thesis, not only showed a much lower mass loss but also some compositions (S-3 and S-4) were stable up to 35 hours (table 4.4).

The mechanism of enzyme assisted degradation can be understood by comparing the diameter of gyration (D_g) of the active enzyme and the distance between crosslinks points (ξ) as shown in table 4.5. At low crosslinking densities, D_g is smaller than ξ and mesh size of the target network is large enough to expose the backbone chain of the polymer (figure 4.8A). There is a high probability of the enzyme to cleave the backbone chain of the polymer. This results in a quick digestion of the polymer by the enzyme. However, as the crosslinking density increases, both ξ and M_c of the network decreases. As D_g approaches ξ, the access of enzyme to the backbone chain of the polymer is inhibited (figure 4.8B) [278, 348] and degradation rate is suppressed. If the crosslinking density is so high that ξ becomes smaller than D_g, degradation is stopped hypothetically (figure 4.8C). This agrees with the values presented in table 4.5. Collagenase (D_g = 4.8 nm) is likely to degrade the C0 more quickly than C60 which has a smaller ξ. The similar trend can be seen for hyaluronidase assisted degradation of the HA network. In the case of hybrid compositions, S-1 and S-2 show higher degradation rate because of the ξ values for both are within the range of the D_g of collagenase and hyaluronidase. ξ for S-3 and S-4 is low so the degradation rate for these compositions was even slower.

The average molecular weight between two crosslinks (M_c) could indicate the extent of mass loss of the network due to degradation. When a scission is made by the enzyme in a network with higher M_c value, it could result in a higher mass loss per scission as compared to the network with lower M_c value. In table 4.5, M_c value for C0 is highest and resulted in 100% mass loss in 35 hours whereas C60 with comparatively lower M_c value showed only 17% mass loss (table 4.4). Both HA2 and HA20 showed 100% mass loss in 35 hours despite their lower M_c values as compared to C0 and C60. This is probably due to their hydrophilic character, which dominates the degradation behaviour of HA networks. S-1 and S-2 with higher M_c values showed higher mass loss of 100% and 60% respectively as compared to S-

3 and S-4 with lower M_c values. S-3 and S-4 have similar M_c values as HA20, however, they did not show any mass loss. This indicates that hydrophobic character of collagen network controls the degradation behaviour of the hybrid scaffolds and hydrophilicity of HA network does not seem to influence their degradation behaviour.

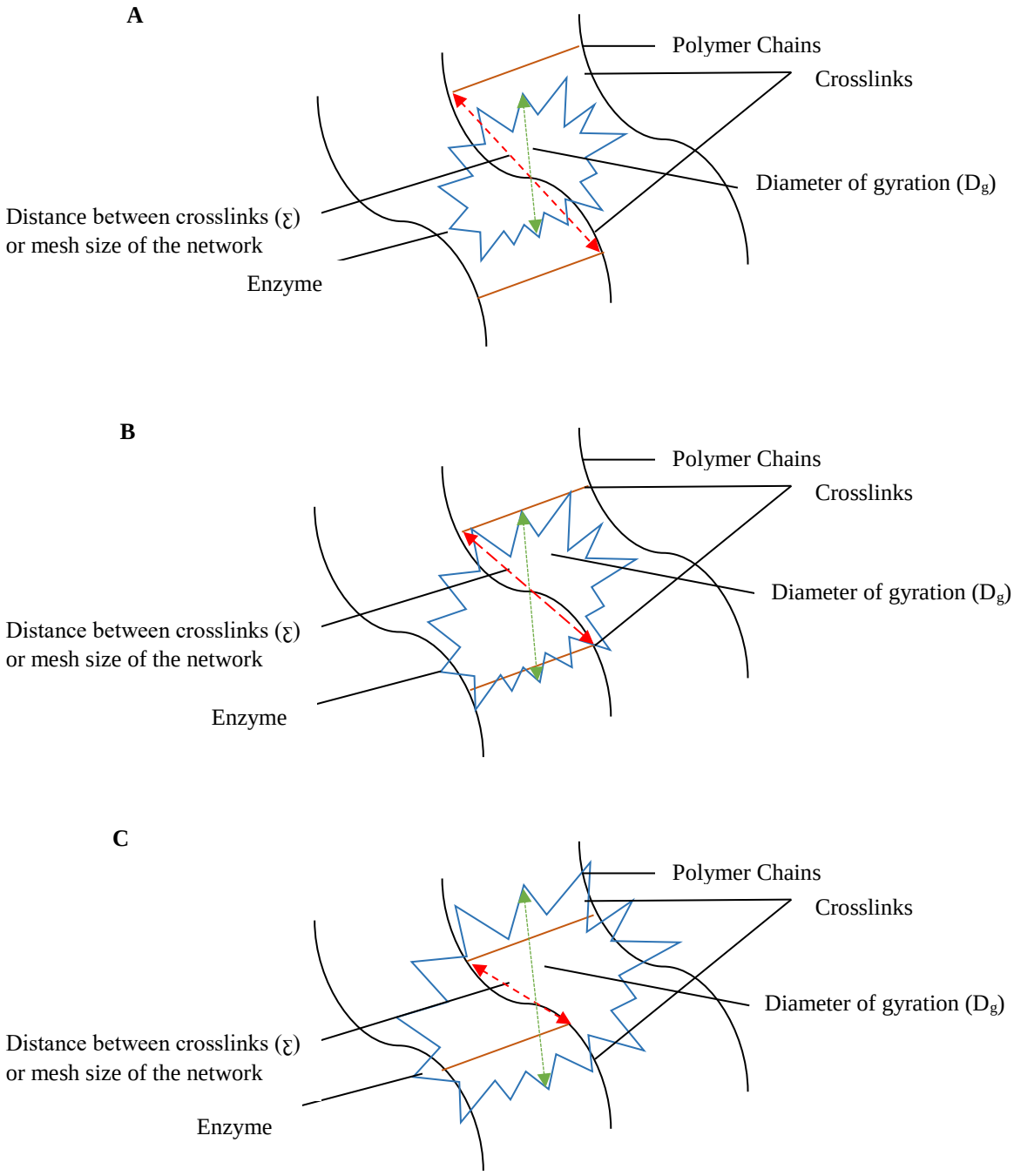


Figure 4.8: Schematic diagram for enzyme-assisted degradation of the crosslinked network (A) $\xi > D_g$, the degradation rate is high (B) $\xi \sim D_g$, the degradation rate is suppressed (C) $\xi < D_g$, degradation is stopped.

Table 4.5: Comparison of the diameter of gyration (D_g) or molecular weight (M_z) of the active enzymes with the average molecular weight (M_c) or average distance between the two crosslinks (ξ) in the target network.

Active Enzyme with approx. Molecular weight (M_z, kg/mol)	Diameter of gyration (D_g, nm)	Target Network	Distance between crosslinks points (ξ, nm) *	Average molecular weight between the two crosslinks ($M_c \times 10^2$ kg/mol)*
Collagenase (68-130)	4.8	C0	37 ± 3	32 ± 2.5
		C60	11 ± 1	4.1 ± 0.5
Hyaluronidase (55)	4.4	HA2	9.7 ± 1	6.4 ± 0.9
		HA20	2.4 ± 1	0.8 ± 0.2
Collagenase + Hyaluronidase		S-1	13 ± 1	16 ± 2.1
		S-2	10 ± 2	14 ± 2.4
		S-3	8.2 ± 3	0.7 ± 0.2
		S-4	7.3 ± 1	0.5 ± 0.1

* calculated from swelling studies using Flory-Rehner equation (Chapter 2, table 2.3B).

4.5 Conclusion:

In this chapter; the effect of pH, crosslinking density, and enzymatic activity on the degradation behaviour of the hybrid scaffolds have been studied. Collagen network and HA network show contrasting behaviour with respect to the pH of the degrading medium. This leads to the conclusion that the gross degradation response of collagen/HA hybrid scaffolds can be tuned by varying the collagen: HA network ratio (or choosing the primary network).

The increase in the concentration of EDC/NHS (or crosslinking density) increased the hydrophobicity of all compositions which delayed the mass loss due to degradation under all conditions. The partial mass loss occurred for hybrid scaffolds in either collagenase or hyaluronidase alone. Higher and accelerated mass loss resulted under the combined effect of collagenase and hyaluronidase. These observations further support the hypothesis that hybrid scaffolds are made up of independent networks of collagen and HA. Controlling the collagen: HA network ratio, as well as the crosslinking density of collagen/HA hybrid scaffolds, provide means to adjust the degradation rates for tissue engineering of organs other than heart valve leaflet. Also, pH-sensitive hybrid compositions can be designed for smart biomedical applications.

Degradation behaviour in physiological fluids can be quite different because of the involved cell activities. Therefore, the cell response of individual networks, as well as the resulting hybrid scaffolds, will be comprehended in chapter 5.

Chapter 5

Cell Response of Collagen/HA Hybrid Scaffolds

5.1 Introduction:

Cell response of scaffold helps to assess its *in-vivo* performance as an implant in service [26]. When an implant comes in contact with the biological tissue, the body registers a specific response to it. The body response depends on the nature of the material. If the presence of implant results in cell death in the surrounding tissue, the material is '*cytotoxic*' whereas the material is considered '*biocompatible*' if no negative response arises [349, 350].

Custom made cell-seeded scaffolds are aimed at the restoration of traumatized tissue [296, 351]. The choice of material for constructing the scaffold is important for the successful regeneration of any tissue. The material options for constructing the scaffold are narrowed down by the target tissue to be restored [352, 353]. The second important factor towards the complete makeup of an ideal tissue engineered heart valve (TEHV) is to select the right cell type as discussed in chapter 1 (section 1.3.6.4). Both endogenous adult progenitor cells and pluripotent stem cells are two promising candidates where they offer easy availability and ability to differentiate as shown in table 1.7[354-356]. Cardiosphere derived cells (CDCs) are a relatively newly discovered cardiac stem cells [357] which combine the features of both of the above cell lines and hence these have been selected as a cell source in this thesis. Therapeutic efficacy has been established in animal models [358, 359] and a clinical trial has also reported reduced area of damage in CDC-treated patients [360, 361].

In this chapter, CDCs response to collagen scaffolds and collagen/HA hybrid scaffolds in terms of cell attachment and proliferation has been studied by the alamarBlue® assay.

Bending modulus of CDCs-cultured hybrid scaffolds has been measured by self-deflection test according to the protocol outlined in chapter 3 (section 3.2.2.2). The visualization of the microstructure of CDCs-seeded collagen/HA hybrid scaffolds has been performed by scanning electron microscope (SEM).

5.2 Materials and methods:

5.2.1 CDCs harvest and isolation*:

CDCs were isolated from adult Sprague-Dawley rats (Harlan Laboratories, UK) and expanded, by the published protocols[358, 362, 363]. Firstly, the rat was killed by lethal injection of Euthatal® solution (Merial Animal Health Ltd, UK), and the heart was explanted, washed with Dulbecco's phosphate buffer saline (DPBS; Sigma-Aldrich Ltd, UK), and minced into small explants pieces in 0.05 % trypsin-EDTA (Life Technologies Ltd, UK). Explants were then plated onto fibronectin (Sigma-Aldrich Ltd, UK)-coated 60mm Petri dishes (Fisher Scientific Ltd, UK) with 1.5ml of complete explant medium (CEM), compromising Iscove's modified Dulbecco's medium (IMDM; Life Technologies Ltd, UK) supplemented with 20 % fetal bovine serum (Life Technologies Ltd, UK). 1 U/ml penicillin (Life Technologies Ltd, UK), 1ug/ml streptomycin (Life Technologies Ltd, UK) and 0.2mM L-glutamine (Life Technologies Ltd, UK), and incubated in a standard tissue culture incubator (BINDER GmbH, Germany) at 37^{o}C with 5 % CO_2. After approximately one week, small, round, phase bright cells grew out from the explants. Upon reaching 80 – 90 % confluency, these explant-derived cells (EDCs) were isolated from trypsin (Life Technologies Ltd, UK) and re-plated in poly-d-lysin (Sigma-Aldrich Ltd, UK)-coated 24-well plates (Corning Inc, USA) in cardiosphere growth medium (CGM) comprising 60 % Dulbecco's modified eagle medium

* performed by Dr. Arne Bruyneel, Department of Physiology, University of Oxford.

(DMEM; Life Technologies Ltd, UK), 30 % IMDM, 7% FBS, 2 % B-27® (Life Technologies Ltd, UK), 25ng/ml cardiotrophin (Peprotech EC Ltd, UK), 10ng/ml epidermal growth factor (EFG; Peprotech EC, UK), 20ng/ml basic fibroblast growth factor (FGF; Promega, UK) and 5 units thrombin (Sigma- Aldrich Ltd, UK). Cardiospheres formed after 2 – 3 days, at which time they were harvested by mechanical trituration and were plated in CEM in fibronectin-coated flasks to culture for CDCs. EDCs could be harvested from the explants for multiple times, in the experiments of this thesis second and third harvest cells were used at passages three to five.

5.2.2 CDCs culture on scaffolds:

Disc-shaped collagen/HA hybrid scaffolds along with collagen scaffolds (t = 1.5mm, d = 12.5mm) were prepared as outlined in chapter 2 (section 2.2.3). Before cell seeding, all scaffolds (n = 6) were sterilized by washing them three times, for 30 minutes each, with 100% ethanol and three times with DPBS. Then, they were placed in CEM. CDCs were harvested using trypsin, counted on a hemocytometer (Laboroptik GmbH, Germany) and diluted to 250,000 cells/ml. The scaffolds were placed in fibronectin-coated 24-well plates and cells were seeded by pipetting 200µL of the diluted cell suspension on the top of the scaffolds (50,000 cells per scaffold). The cells were cultured for 7 days at 37^{o}C with 5% CO_2. After the initial four hours of incubation, each well was supplemented with 800 µL more of CEM medium (to reach 1ml of the medium per well) and a total medium change was carried out every 48 hours.

5.2.3 Assessment of CDCs attachment and proliferation:

The attachment and proliferation of the CDCs were assessed with the alamarBlue® assay (AbD Serotec, UK). AlamarBlue® is an indicator dye that fluoresces in response to the

oxidation-reduction (REDOX) reactions in the cells. The amount of fluorescence corresponds to the metabolic activity of the cells and is proportional to the cell number [364]. Cell attachment was quantified on day 1 (20 hours after seeding), and cell proliferation was measured on day 4 and 7. On day 1, the scaffolds were first transferred into new 24-well plats and washed with DPBS (for 2×5 minutes). The culture medium in the old 24-well plates was removed, and the plates were also washed with DPBS (for 2×5 minutes). Fresh CEM supplemented with 10 % alamarBlue® was then added to both the old and new 24-well plates (1ml per well) and was incubated for three hours, to measure the proportion of cells attached on the scaffolds and left in the old plates respectively. On day 4 and 7, only the new plates containing scaffolds were incubated in the CEM-alamarBlue® solution. After the incubation, the supernatant was transferred into µClear black plates with a clear bottom (Greiner bio-one Ltd, UK). Fluorescence was measured using a FLUOstar Optima plate reader (BMG Labtech Ltd, UK) at 544/590 nm excitation/emission wavelengths. The percentage of alamarBlue® reduction, which represented the amount of the cells in the particular well, was calculated as the following:

% alamarBlue Reduction = [FI (Measured Well) – FI (Control)] / [FI (Max) – FI (Control)] Eq. 5.1

Where FI means the fluorescence intensity measured, FI (Control) was measured from the CEM-alamarBlue® solution that was incubated in empty wells, and FI (Max) was measured from the CEM-alamarBlue® solution that was treated on a dark heat block at 90ºC for 3 hours, which was considered to have reached 100% reduction [364]. The cell attachment ratio was calculated as the ratio of the number of cells on the scaffolds to the total number of cells on day 1[365]:

% Attachment = [% alamarBlue reduction (scaffold) / % alamarBlue reduction (scaffold) + % alamarBlue reduction (well)] ×100% Eq. 5.2

5.2.4 Scanning electron microscopy (SEM):

Cell morphologies were characterized using scanning electron microscopy (SEM) JSM840F (JEOL Ltd, Japan) at an accelerating voltage of 4kV. Scaffolds seeded with cells were fixed at day 7 in 4% paraformaldehyde (PFA; Sigma- Aldrich Ltd, UK) overnight at 4^{o}C. Samples were then dehydrated through exposure to a gradient of alcohol (30%, 50%, 70%, 90% and 100%) followed by hexamethyldisilazane (HDMS; Sigma-Aldrich Ltd, UK), and were air-dried. All specimens were coated with 3mm thick platinum by a 208HR sputter coater (Cressington Scientific Instruments Ltd, UK) before observation. Unseeded scaffolds were also studied by SEM as controls.

5.2.5 Self-deflection bending test:

Self-deflection bending tests were performed on CDCs-seeded scaffolds according to the protocol described in chapter 3 (section 3.2.2.2). Initial mass (M_{dry}) of the samples (n = 5) were measured. All four compositions of collagen/HA hybrid scaffolds were seeded with CDCs from the rat heart. The culture was continued for 28 days at physiological conditions (37^{o}C, 5% CO_2) with a feed of fresh media at regular intervals. On day 28, the samples were removed from cell-culture media as shown in figure 5.1 and allowed to drain on a wire mesh for one min. Final mass (M_{wet}) of the samples were recorded, and water uptake ratio (U) was calculated using the Eq. 3.1. Samples were then clamped over a span of 20 mm and allowed to self-deflect as shown in figure 3.3. The deflection was recorded by a camera (450D, 50mm, F1.8, Canon, Japan) and measured with the aid of Image J (National Institutes of Health, USA) [306]. The deflection (D) is determined by Eq. 3.2. Bending modulus of the CDCs-seeded scaffolds can be calculated using water uptake ratio, U, by Eq. 5.3.

$$E_{cell.bend} = 5ql^4/384DI = 5UM_{dry}gl^3/384DI \qquad Eq.\ 5.3$$

Where g = gravitational acceleration

l = span distance

I = the second moment of inertia

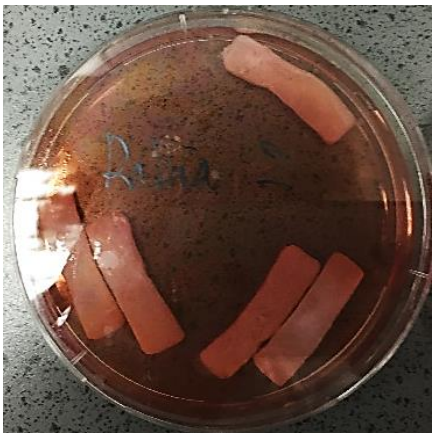


Figure 5.1: CDCs cultured rectangular collagen/HA interlaced scaffolds in culture medium for self-deflection bending tests.

5.2.6 Statistical analysis *:

The data for cell attachment and self-deflection bending test (figure 5.2, figure 5.3, and table 5.3) have been analyzed using one-way ANOVA, with a Bonferroni's posthoc whereas the data for cell proliferation (figure 5.4 and figure 5.5) have been analyzed using a two-way ANOVA with repeated measures and a Bonferroni's posthoc test. The probability of 95 % ($p < 0.05$) has been taken as statistically significant. Six samples have been analyzed for each group.

* performed by Prof. Carolyn Carr, Department of Physiology, University of Oxford.

5.3 Results:

5.3.1 CDCs attachment:

For collagen scaffolds, % CDCs attachment for C0 (50 %) is significantly higher than C25, C40, and C60 as shown in figure 5.2. However, there is no significant difference among the crosslinked collagen compositions i.e. C25, C40, and C60. For hybrid scaffolds, there is no significant difference in cell attachment between C0 (control) and S-1 as shown in figure 5.3. Also, the cell attachment for C0 and S-1 is significantly higher than S-2, S-3, and S-4. There is no significant difference among S-2, S-3, and S-4.

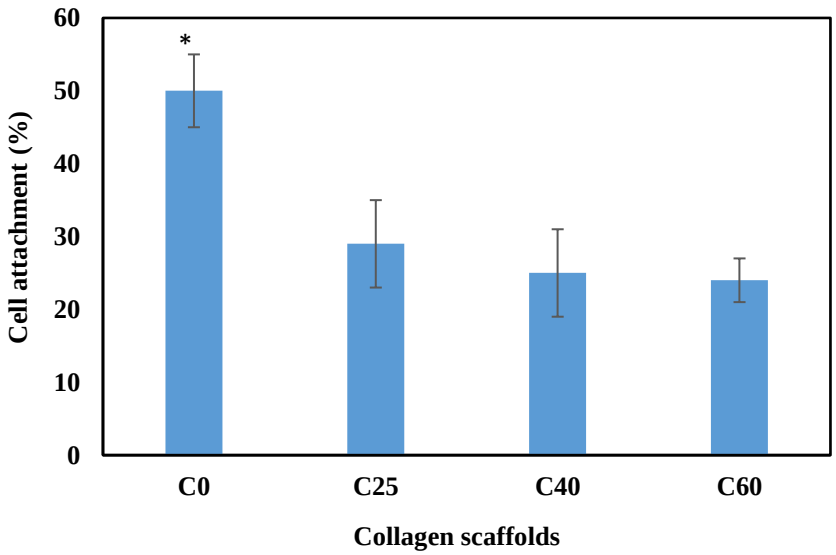


Figure 5.2: CDCs attachment on collagen scaffolds after 20 hours (day 1). * indicates statistically significant differences ($p < 0.05$) among the groups of different compositions.

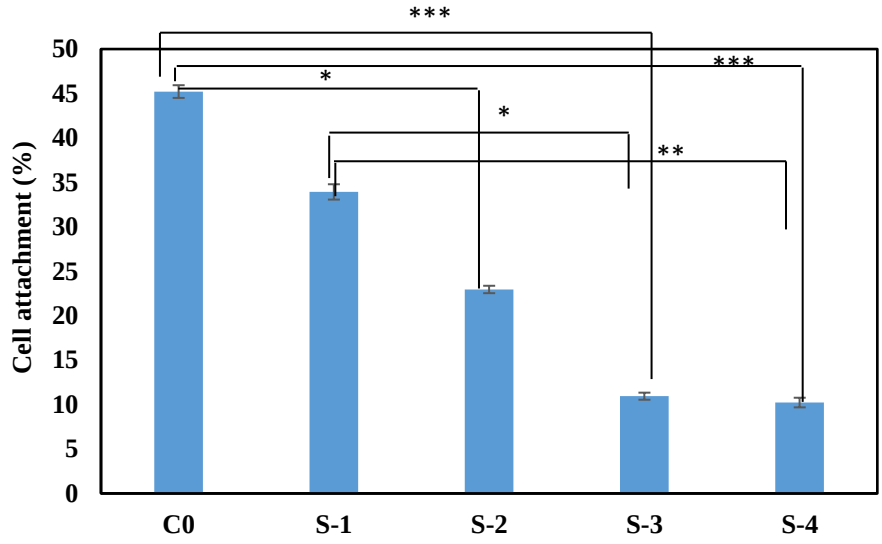


Figure 5.3: CDCs attachment on collagen/HA hybrid scaffolds after 20 hours (day 1). *, **, and * denotes the statistically significant difference with $p < 0.05$, $p < 0.01$, and $p < 0.001$ respectively.**

5.3.2 CDCs proliferation:

For collagen networks, there is a significant difference in cell proliferation on day 7 as compared to day 4 for all groups of samples (figure 5.4A). When comparing various groups of samples on a given day, CDCs proliferation is higher on C0 as compared to C40 and C60 on day 4. Similarly, CDC proliferation is greater on C0 and C25 as compared to C60 on day 7 (figure 5.4B). The extent of CDCs proliferation can be estimated by taking the ratio of % of CDCs attachments on different time points (table 5.1). CDCs proliferation ratio ranges from 3.5 to 1.1 on day 4 whereas it ranges from almost 9 to 6.2 on day 7. CDCs proliferation ratio is highest for C0 (e.g. 9) whereas it is lowest for C60 (e.g. 6.2) on day 7.

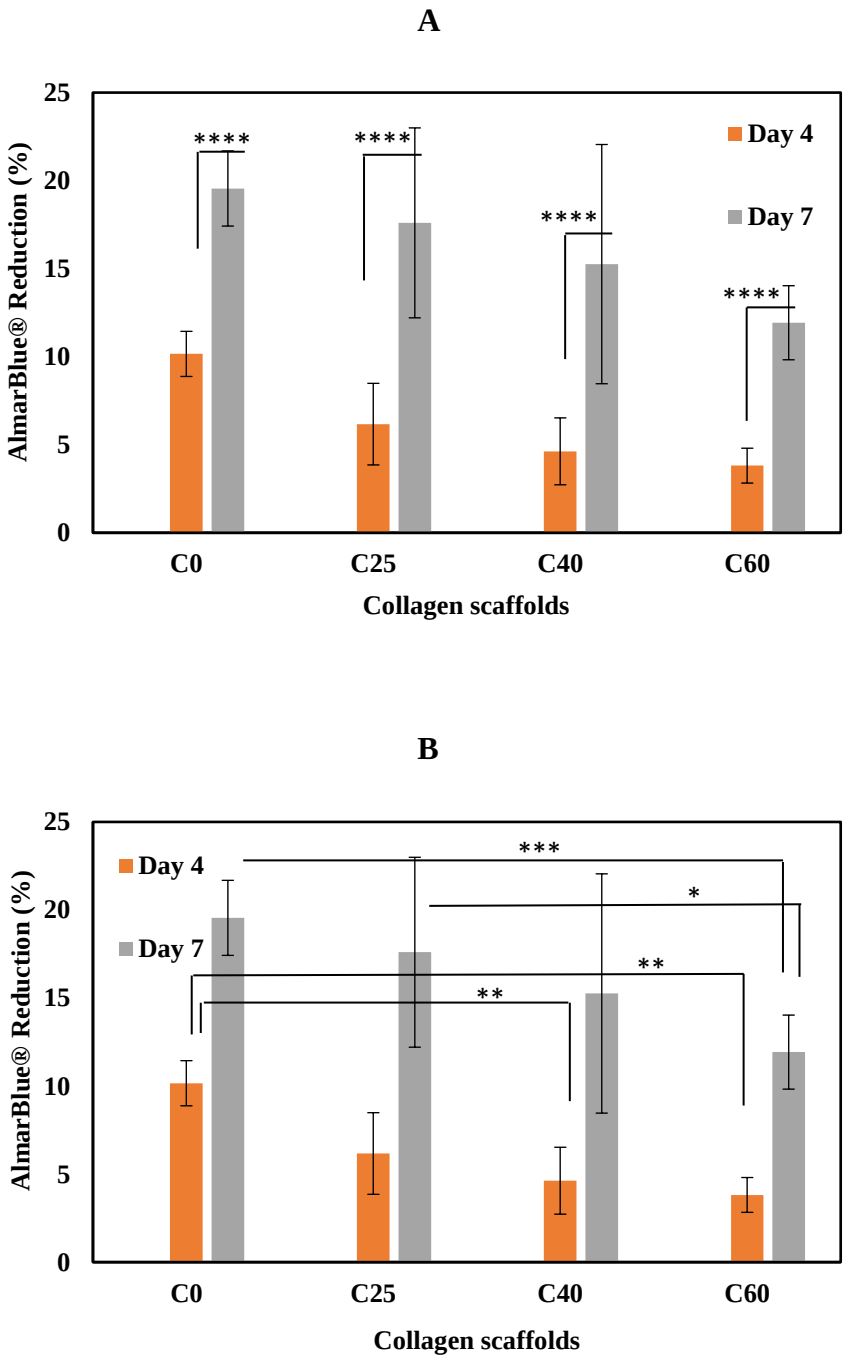


Figure 5.4: Proliferation of CDCs on collagen scaffolds on day 4 and day 7. (A) comparison between different days within a given composition (B) comparison of the various compositions on a given day. *, **, *, and **** denotes the statistically significant difference with $p < 0.05$, $p < 0.01$, $p < 0.001$, and $p < 0.0001$ respectively.**

Table 5.1: Percentage of alamarBlue® reduction for collagen scaffolds on day 4 and day 7 normalized to day 1. **, *, and **** denotes the statistically significant difference with $p < 0.01$, $p < 0.001$, and $p < 0.0001$ respectively. [a] and [b] represents statistically significant values of cross-linking density within collagen scaffolds as compared to C0 and C25 respectively.**

Sample ID	Effective crosslinking density (v_e, $\times 10^{-4}$ kg/m^3)	D_4/D_1	D_7/D_1
C0	0.4 ± 0.3	3.5 ± 0.6***	9 ± 1.3****
C25	1.3 ± 0.2	2.7 ± 0.6**	8 ± 2.3****
C40	2 ± 1 [a]	2.7 ± 0.4**	7.3 ± 1.9****
C60	3.3 ± 0.4 [a, b]	1.1 ± 0.3	6.2 ± 1.0****

Similar experiments have been performed on all collagen/HA hybrid scaffolds for 7 days. Non-crosslinked collagen scaffolds (C0) have been run as a control. The difference of proliferation between day 4 and day 7 is significant for S-3 and S-4 (figure 5.5A). When comparing different groups of samples on a given day (figure 5.5B), CDC proliferation for C0 on day 4 and day 7 is significantly higher than all hybrid scaffolds. On day 4, S-1 is significantly higher than S-3 and S-4. There is no significant difference among hybrid scaffolds on day 7. The extent of CDCs proliferation in terms of CDCs relative ratios on day 4 and day 7 has been presented in table 5.2. D_4/D_1 and D_7/D_1 decrease through S-1 to S-4. For example, D_4/D_1 ranges from 3.4 to 2.1 and D_7/D_1 ranges from 6.4 to 5.5. These values are lower as compared to those for collagen scaffolds (table 5.1).

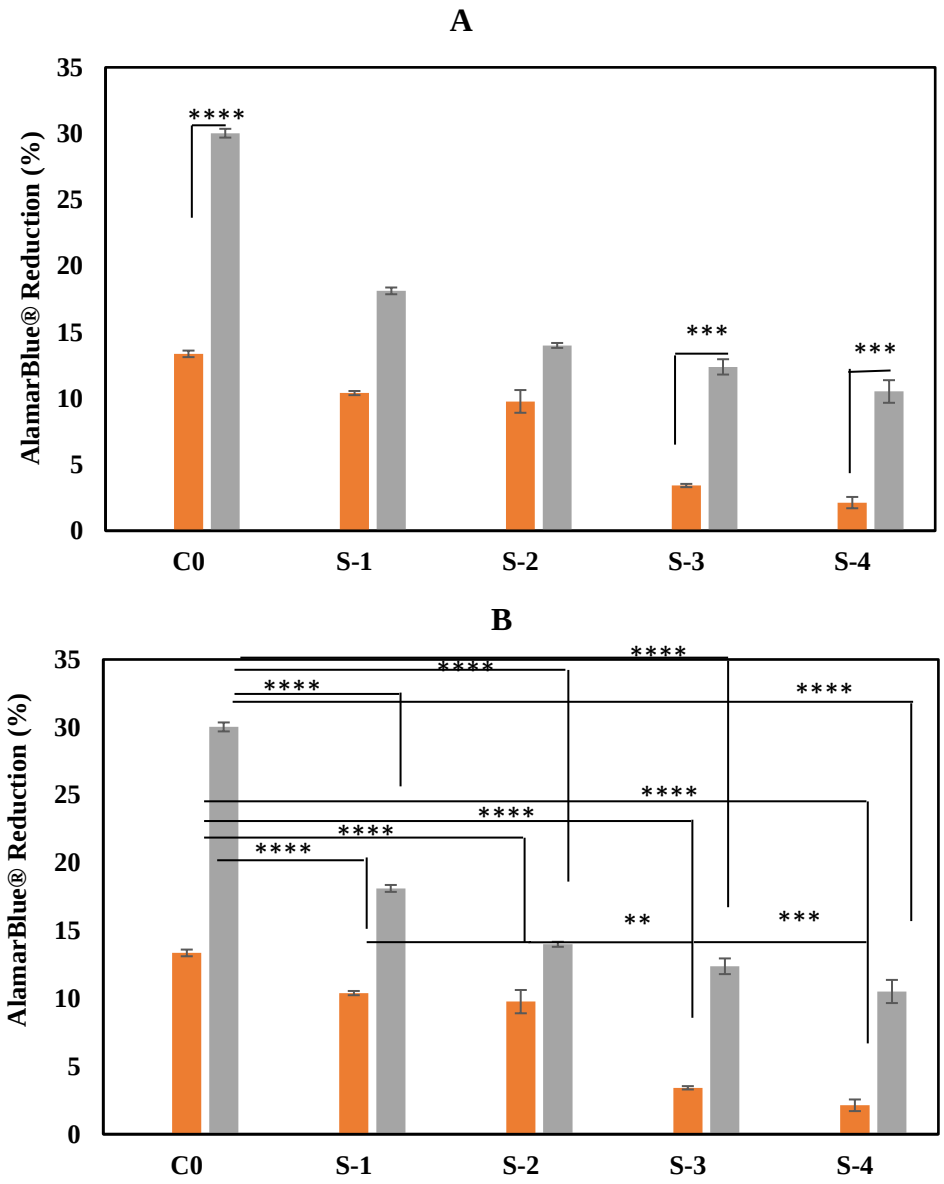


Figure 5.5: CDCs proliferation on collagen/HA hybrid scaffolds on day 4 and day 7. (A) comparison between different days within a given composition (B) comparison between compositions on a given day. *, **, *, and **** denotes the statistically significant difference with $p < 0.05$, $p < 0.01$, $p < 0.001$, and $p < 0.0001$ respectively.**

Table 5.2: Percentage of alamarBlue® reduction for collagen/HA hybrid scaffolds on day 4 and day 7 normalized to day 1. *, **, *, and **** denotes the statistically significant difference with $p < 0.05$, $p < 0.01$, $p < 0.001$, and $p < 0.0001$ respectively. [f], [g], and [h] represent statistically significant values of crosslinking density within hybrid scaffolds as compared to S-1, S-2, and S-3 respectively.**

Sample ID	Effective crosslinking density (v_e, $\times 10^{-4}$ kg/m^3)	D_4/D_1	D_7/D_1
S-1	0.8 ± 0.3	3.4 ± 0.8**	6.4 ± 0.1
S-2	0.9 ± 0.3	3.0 ± 0.2**	6.4 ± 0.8
S-3	1.8 ± 0.5 [f, g]	2.2 ± 0.1	5.5 ± 0.1
S-4	2.4 ± 0.3 [f, g, h]	2.1 ± 0.2	5.5 ± 0.2

5.3.3 Scanning electron microscopy (SEM):

Figure 5.6 shows the representative SEM images of hybrid scaffolds (unseeded and seeded). C0 (unseeded and seeded) has also been studied for comparison. Figure 5.6 (A, B) shows that CDCs are able to attach and proliferate on the surface of the non-crosslinked collagen scaffold (C0). The secondary HA network appears as a fine parallel mesh across the diameter of primary collagen pores in S-1 and S-2 (figure 5.6C and 5.6E). Figure 5.6 (D) and 5.6 (F) show that CDCs are attached to the surfaces of S-1 and S-2 respectively, however, HA mesh present in the microstructure of the unseeded scaffolds (figure 5.6C and 5.6E) is absent in seeded scaffolds. Unseeded S-3 and S-4 show a tightly packed microstructure as shown in figure 5.6 (G) and figure 5.6 (I) respectively. As can be seen in figure 5.6 (H) and figure 5.6 (J), few CDCs are attached to the surfaces of S-3 and S-4 respectively. HA network in S-3 and S-4 is only partially degraded till day 7 (figure 5.6H and figure 5.6J).

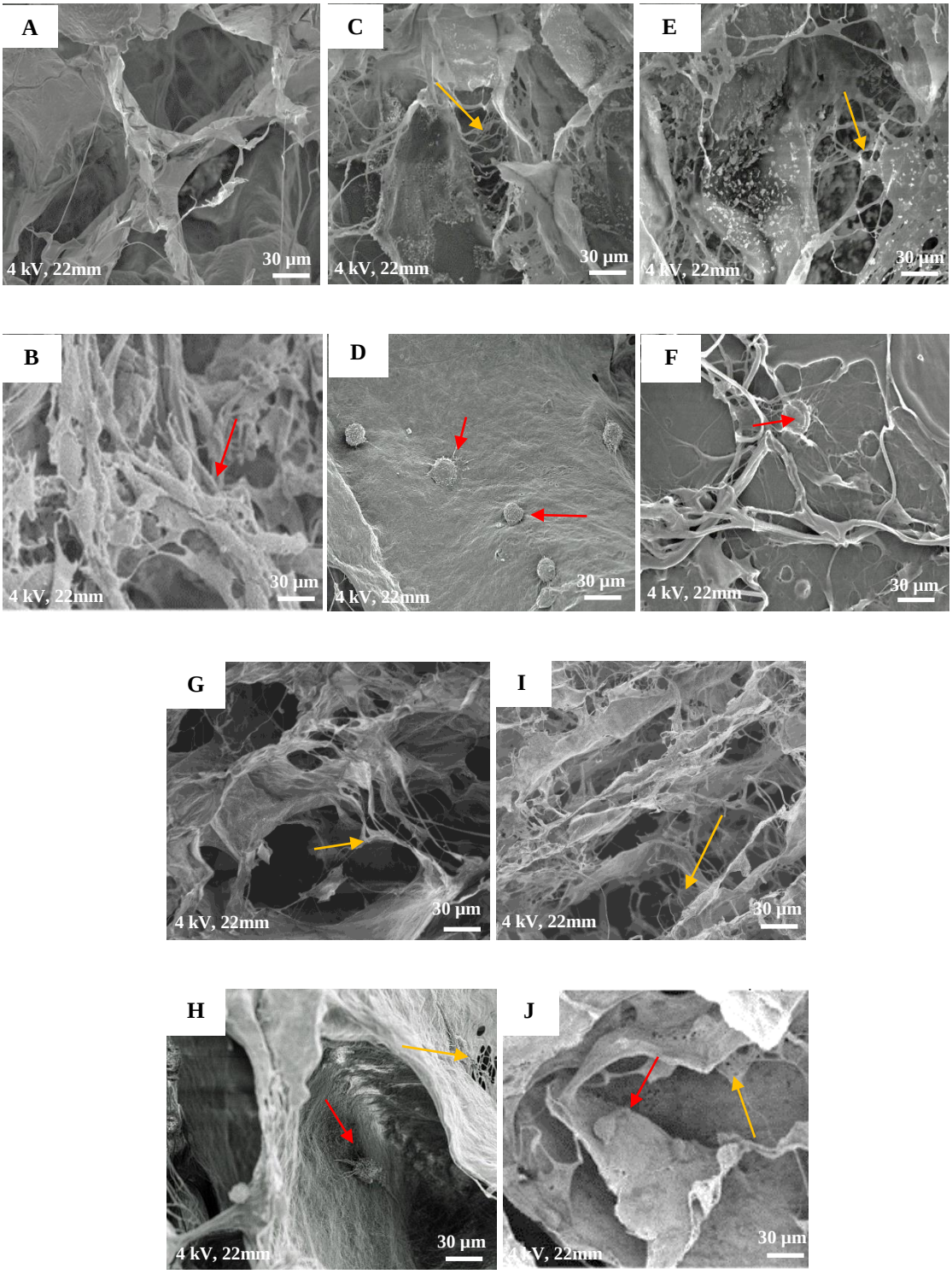


Figure 5.6: SEM images of unseeded and seeded collagen (A, B), unseeded and seeded S-1 (C, D), unseeded and seeded S-2 (E, F), unseeded and seeded S-3 (G, H), and unseeded and seeded S-4 (I, J) on day 7. Red arrows point towards CDCs attached to the surface of the scaffold. Yellow arrows point towards secondary HA network.

5.3.4 Self-deflection bending test:

$E_{cell.bend}$ values of hybrid scaffolds have been summarized in table 5.3. $E_{cell.bend}$ for collagen scaffolds and S-1 could not be measured because samples were not able to survive for 28 days during cell culture. Please note that U and $E_{wet.bend}$ for hybrid scaffolds have already been measured and discussed in chapter 3 (section 3.2.2, table 3.2). Comparison of $E_{cell.bend}$ and $E_{wet.bend}$ shows that $E_{cell.bend} > E_{wet.bend}$. $E_{cell.bend}$ for S-2, S-3, and S-4 increase by 50% as compared to their $E_{wet.bend}$. Also, $E_{cell.bend}$ values for S-3 and S-4 are significantly higher than that of S-2 whereas there is no significant difference between S-3 and S-4.

Table 5.3: Summary of cell-cultured ($E_{cell.bend}$) bending modulus (kPa) of hybrid scaffolds. [d], [e], and [f] represent statistically significant values within hybrid scaffolds as compared to S-1, S-2, and S-3 respectively.

Sample ID	Effective crosslinking density (v_e, kmol/m^3)	Water Uptake Ratio (U) %	Bending Modulus (kPa)	
			Wet $E_{wet.bend}$	Cell-cultured $E_{cell.bend}$
S-1	0.8 ± 0.1	2039 ± 39	1 ± 0.2	-
S-2	0.9 ± 0.1	2011 ± 33	1 ± 0.3	2 ± 0.3
S-3	5.0 ± 0.6 [d, e]	1097 ± 24 [d, e]	2 ± 0.3 [d, e]	5 ± 0.2 [e]
S-4	6.8 ± 0.7 [d, e, f]	984 ± 24 [d, e]	3 ± 0.2 [d, e, f]	6 ± 0.4 [e]

5.4 Discussion:

CDCs have been selected as the cell source in this study to assess the biocompatibility of collagen/HA hybrid scaffolds. CDCs tend to attach to all groups of samples (collagen scaffolds and hybrid scaffolds) as indicated by alamarBlue® reduction (figure 5.2 and figure

5.3). However, the attachment of CDCs decreases with increasing the crosslinking density of the scaffold in general. Comparing figure 5.2 with 5.3 shows that the attachment is higher for collagen scaffolds as compared to hybrid scaffolds. This behaviour can be explained by recalling from chapter 2 that crosslinking density increases with increasing the EDC concentration. CDCs are able to attach to the scaffolds through collagen binding receptors (α_1, α_2, α_3) and HA binding receptors (CD44)[361]. The presence of glycine is particularly important for the detection of collagen receptors such as $\alpha_1\beta_1$ and $\alpha_2\beta_1$ [366]. A crosslink is formed between carboxylate anions (present on aspartic and glycine) and free primary amino groups (present on hydroxylysine)[288, 367]. EDC crosslinking engages the integrin-binding arginine-glycine-aspartic acid (RGD) motifs in the crosslinking process which would make these sites unavailable for cell attachment.

Comparison of figure 5.4 and 5.5 shows that proliferation is also higher for collagen scaffolds as compared to hybrid scaffolds. CDCs proliferation seems to follow the similar behaviour to CDCs attachment i.e. decrease in proliferation rate with increasing the crosslinking density (figure 5.4 and figure 5.5). This suggests that CDCs proliferation is also affected by crosslinking density of the scaffold. Whereas CDCs attachment is influenced by the crosslinking density of the scaffold due to the number of available cell-attachment sites. It is also important to note that although the HA molecule contains CDCs-binding sites, however, incorporation of the crosslinked HA network does not seem to contribute to the cell attachment and proliferation behaviour of hybrid scaffolds. Figure 5.3 shows that only a small number of CDCs attach to S-3 and S-4 and therefore the rate of proliferation is also low as shown in figure 5.5. This also agrees with the observations from SEM imaging (figure 5.6H and figure 5.6J) which show the presence of only few CDCs on S-3 and S-4. It is probably the effect of denser entanglements between collagen and HA chains in hybrid compositions as it could mask the free cell-binding sites (figure 5.6G and figure 5.6I). This

may explain the decline of CDCs activities (attachment and proliferation) with increasing the crosslinking density among collagen scaffolds as well as the hybrid scaffolds.

There is significant variation in alamarBlue® reduction among the scaffold compositions on day 4 (blue and gray lines) as compared to day 7 (yellow and orange lines) as shown in figure 5.7. It is likely that the surfaces of all scaffolds could have been covered with ECM gradually over the course of time. Fresh ECM deposited by attached CDCs may change surface properties of the scaffold and hence the rate of proliferation which could explain less variation in cell proliferation rates on day 7.

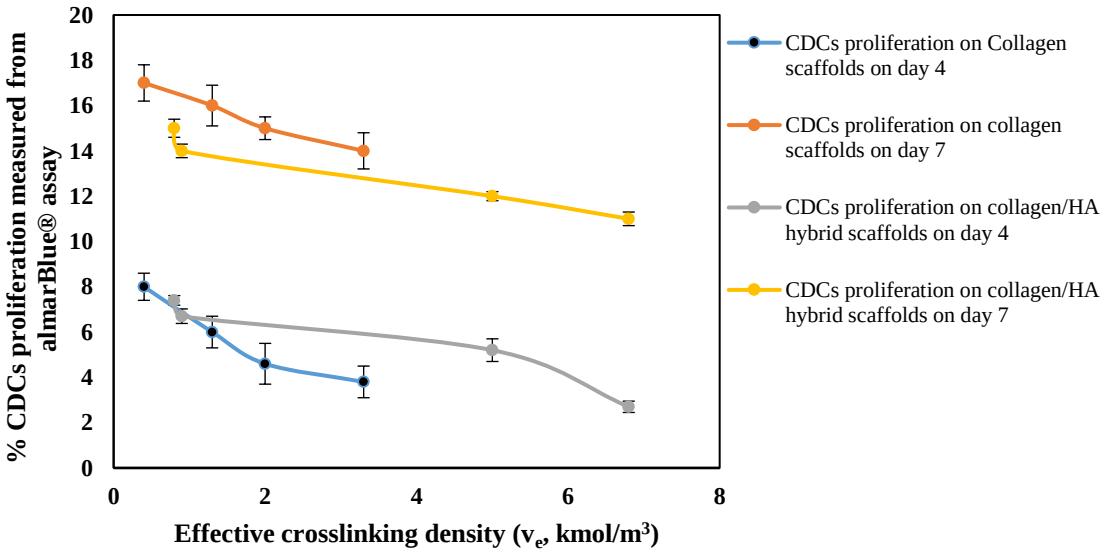


Figure 5.7: CDCs proliferation on collagen and collagen/HA hybrid scaffolds as a function of crosslinking density (replotted from figure 5.4 and figure 5.5).

Cell response of a scaffold may also be affected by microstructural features such as pore size [368-370] which should be large enough to provide room for cell attachment[371]. The favorable pore size range varies with respect to the specific tissue to be regenerated [372] and it should be in the range of 30 – 100 µm for cardiac tissue regeneration [280, 281]. It has also been shown in chapter 2 that EDC crosslinking has reduced the pore size of collagen and hybrid scaffolds due to the post-crosslinking volume shrinkage (Δv) and incorporation of secondary HA network (table 2.5). CDCs attachment on the hybrid scaffolds decreases despite the fact that

pore size is within the permissible range of 66 – 126 µm as shown in figure 5.7. This suggests that decrease in cell attachment is probably because of the fewer available cell binding sites resulting from an increase in crosslinking density and pore size does not seem to have an effect in this study.

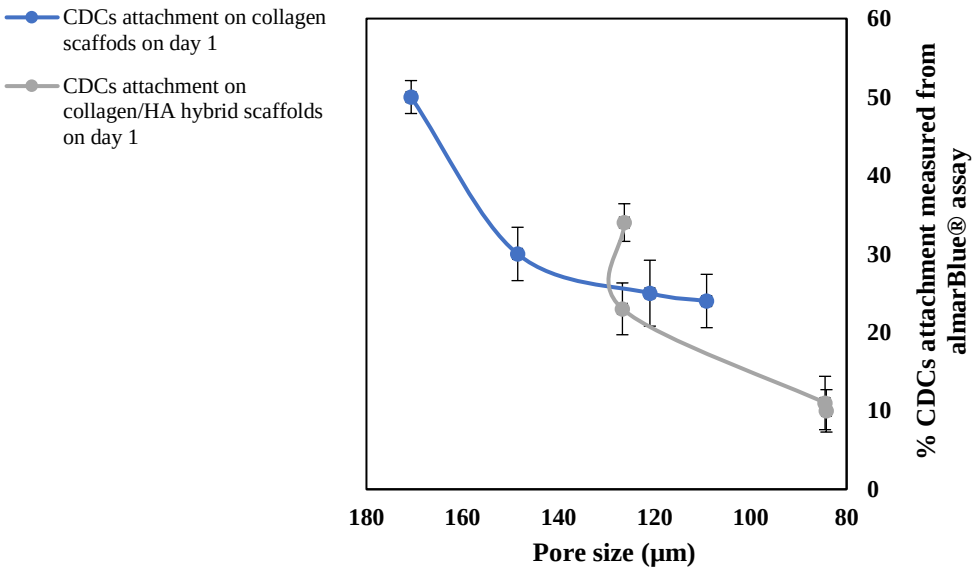


Figure 5.8: CDCs attachment on collagen networks and collagen/HA hybrid scaffolds as a function of pore size (replotted from figure 5.2 and figure 5.3).

A number of cell types such as endothelial cells (EC), smooth muscles cells (SMC), and cardiomyocytes (CMs) are sensitive to the stiffness of the host biomaterial. The proliferation of such cell lines increases with increasing the stiffness of the substrate [373, 374]. CDCs, in this study, show a contrasting behaviour where proliferation on hybrid scaffolds decreases with increasing wet bending modulus or stiffness as shown in figure 5.9. This is most probably due to the fewer cells attached to the scaffolds on day 1 which in turn is affected by the availability of the fewer cell-binding sites (or high crosslinking density). It can be inferred that proliferation of CDCs is more sensitive to crosslinking density and not to the stiffness of scaffold.

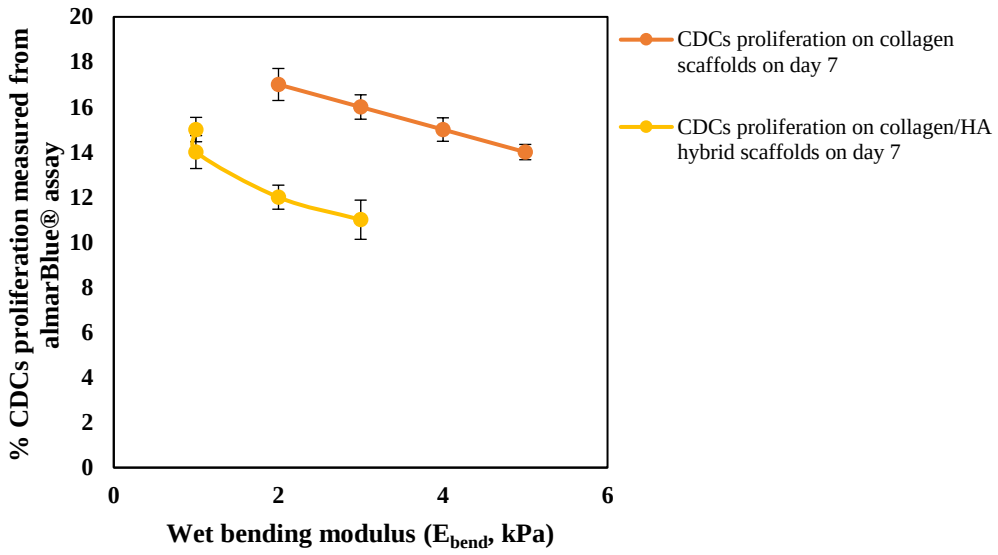


Figure 5.9: CDCs proliferation on collagen and collagen/HA hybrid scaffolds as a function of wet bending modulus (replotted from figure 5.4 and figure 5.5).

Figure 5.10 shows a comparison of CDCs proliferation on hybrid scaffolds and their mass loss due to degradation occurring in the culture medium. Enzyme-assisted degradation behaviour of hybrid scaffolds, discussed in chapter 4, can be approximated to their possible mass loss in cell culture medium (figure 4.6). Evidence of degradation process in the culture medium can also be seen in the SEM images of CDCs seeded S-1 and S-2 after 7 days (figure 5.5D, 5.5F) where the HA network has been degraded completely. CDCs proliferation is high for S-1 and S-2 and so is its mass loss due to degradation (figure 5.10). Low crosslinking densities of these compositions could leave enough free cell-motifs for either cell interaction (in the case of cell culture) or water interaction (in the case of degradation)[251]. On the other hand, high crosslinking densities of S-3 and S-4 have significantly reduced the mass loss whereas proliferation rates are also quite low due to the lack of attachment sites as shown in figure 5.10. Delayed degradation of S-3 and S-4 have possibly increased the life spans of these compositions in the culture medium.

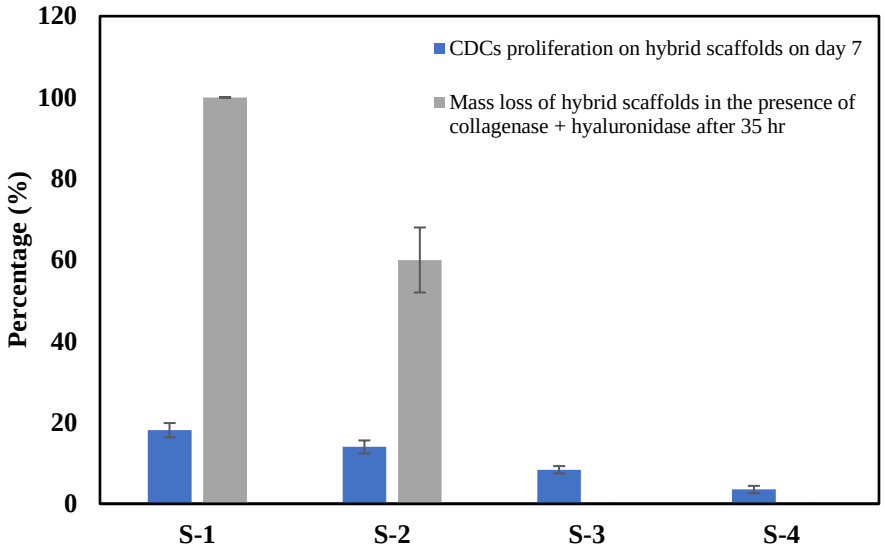


Figure 5.10: Comparison of CDCs proliferation and mass loss due to degradation in culture medium for hybrid scaffolds (reproduced from figure 4.6 and figure 5.5).

$E_{cell.bend}$ values in table 5.3 for hybrid compositions can be explained by considering ECM deposition by CDCs on scaffolds and degradation of the scaffolds in competition simultaneously[375, 376] as shown in figure 5.11. Higher proliferation rates for S-1 should result in greater ECM deposition and increase in the bending modulus. However, its degradation rate is probably much higher than the rate of ECM deposition (due to proliferating CDCs) which has resulted in the failure of S-1 (figure 5.11A). The proliferation rate of S-2 is similar to that of S-1 on day 7 as shown in figure 5.10. S-2 has not only survived the cell culture medium for 28 days but also has shown a little increase in bending modulus possibly due to slower degradation rate (figure 5.11B). On the other hand, most of the ECM deposited for S-3 and S-4 contribute towards the increase of bending modulus due to the small compensations for mass losses due to degradation (figure 5.11C). Above observations suggest that ECM deposition does not merely increase the bending modulus but it is also compensating at the same time for the mass loss due to on-going degradation. Therefore, increase in the bending modulus for any of the hybrid compositions is the net result of the dynamics of mass loss due to degradation and mass gain due to ECM deposition.

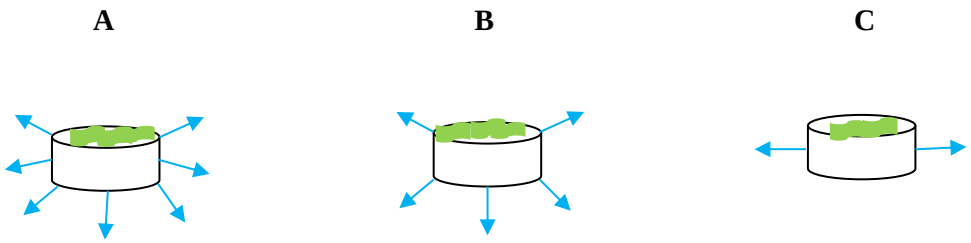


Figure 5.11: Schematic of the mass loss due to degradation (blue arrows) in culture medium vs the ECM deposition (green mass) by proliferating CDCs for hybrid scaffolds (A) degradation rate > ECM deposition, S-1 scaffolds disintegrate (B) degradation rate ≥ ECM deposition, S-2 scaffolds survive and show small increase in bending modulus (C) degradation rate < ECM deposition, S-3, and S-4 scaffolds show significant increase in bending modulus.

5.5 Conclusion:

It ha been shown that CDCs attachment and proliferation is influenced by the crosslinking density of the scaffold (or the number of available cell-binding sites). Cell attachment and proliferation are independent of pore size and stiffness of the scaffold respectively. ECM deposition by the proliferating cells could change the proliferation rate by day 7. It can be concluded that CDCs may change the local environment in the culture medium and the physical/mechanical properties of the hybrid scaffold have less effect on the CDCs behaviour after one week.

CDCs culture on hybrid scaffolds for 28 days has resulted in an increase in the bending modulus in wet condition possibly due to the ECM production. This suggests that mechanical properties of hybrid scaffolds can be increased by cell culturing provided its degradation rate is slowed down. Delayed degradation of scaffold would allow the proliferating CDCs enough time to produce sufficient quantities of ECM within the body of the scaffold. Thus, CDCs-collagen/HA combination has potential to serve as a sustainable cell-material system for aortic valve repair. In addition, variation in the crosslinking density provides a simple approach to tailor the bio-mechanical properties of the proposed hybrid scaffolds for other tissue engineering applications.

Chapter 6

Summary and Conclusions

6.1 Overview:

The aim of this thesis has been to develop and characterize collagen type I and hyaluronic acid (HA) based hybrid scaffolds as a potential tissue engineered heart valve (TEHV). A modified crosslinking route based on carbodiimide chemistry (EDC/NHS) has been developed for the fabrication of the proposed hybrid scaffolds. The sequential route of crosslinking has yielded hybrid scaffolds consisting of non-interacting networks of collagen type I and HA. Furthermore, these scaffolds have revealed interlaced microstructures resembling natural heart valve extracellular matrix (ECM). It has also been shown that the mechanical properties and degradation rate of these scaffolds could be tailored by controlling the crosslinking density. Such scaffolds have the potential to fill the existing gaps for a potential TEHV such as controlled degradation rate, mechanical strength in physiological conditions, and heterogeneous microstructure.

6.2 Summary:

Chapter 1 has highlighted the limitation of current heart valve replacements with a discussion on the recent progress related to TEHVs. Anatomy of the aortic heart valve and the surrounding tissue as well as the biomechanical functioning of the aortic valve have been discussed as background to the topic. It has also justified the choice of materials and technique chosen in this thesis.

Mechanical and bioprosthetic valves have been in clinical use for 4 decades to restore the traumatized heart valve[377, 378]. Mechanical valves require the lifetime intake of

anticoagulation drugs whereas bioprosthetic valves are at a risk of calcification which can cause valve leakage[379]. In addition, these alternatives do not have the capacity to remodel themselves and are not suitable for pediatric patients[380, 381]. Like replacement/repair strategies for other organs, tissue engineering has also influenced heart valve restoration where TEHVs have shown the potential to overcome the current limitations as discussed in **chapter 1** (section 1.3.6).

Synthetic and natural polymers are being investigated to validate their potential for successful regeneration of the heart valve[22, 382]. Synthetic polymer based scaffolds may not be biocompatible and have uncontrolled degradation rates. Natural polymers based scaffolds are biocompatible but have shown so far inadequate mechanical strength[26, 383]. Collagen type I and HA are the natural polymers found in the form of an interlaced heterogeneous microstructure in the heart valve ECM[52, 384] and therefore have been selected in this thesis.

Various crosslinking approaches are available today to increase the mechanical properties of the natural polymers[385, 386]. Physical crosslinking techniques involve the use of heat (dehydrothermal treatment, DHT) or radiations (ultraviolet, UV) which can destroy the triple helix structure of collagen[387, 388]. Chemical crosslinking techniques, in comparison, such as EDC/NHS have been known to yield higher and uniform crosslinking density without denaturation [389, 390]. EDC/NHS have been widely used as crosslinking agents for collagen and HA based scaffolds for tissue engineering of skin, cartilage, and eye but its use has been limited to prepare scaffolds with homogenous microstructures[204, 391, 392]. All attempts to prepare scaffolds with heterogeneous microstructures have involved the use of EDC/NHS coupled with either DHT or UV radiation[384, 393, 394]. Therefore, an EDC/NHS based crosslinking route could be developed to yield heterogeneous scaffolds based on natural polymers without the risk of denaturation.

Chapter 2 has demonstrated the EDC/NHS based crosslinking technique developed in this work. Our technique has utilized EDC for the crosslinking of both collagen type I and HA but in a multi-step sequential manner to avoid the crosslinking between collagen type I and HA (figure 2.2). FTIR (figure 2.5) and TGA (figure 2.8) of the resultant hybrid scaffolds have shown that no new phase has been formed between collagen type I and HA and no evidence has been found for the denaturation of triple helix structure of collagen. SEM images of hybrid scaffolds (figure 2.4) have shown HA mesh sitting inside collagen network pores whereas alcian blue/PAS-stained samples (figure 2.5) have revealed grey and blue interlaced bands of collagen type I and HA respectively.

Analysis of swelling data using Flory-Rehner equation (Eq. 2.2) has shown that crosslinking densities of collagen and HA networks increase with increasing EDC concentration. Also, crosslinking densities for hybrid compositions are found to be higher than their parent collagen type I network and lower than their parent HA network (table 2.3). The pore size of collagen network decrease from 170 ± 20 µm to 109 ± 13 µm with an increase in crosslinking density. Also, the pore size of primary collagen network decreases further from 126 ± 4 µm to 66 ± 2 µm with the incorporation of HA network in the hybrid compositions (table 2.5). This could be due to the volume shrinkage (Δv) arising from the crosslinks formed between the adjacent polymer (collagen or HA) strands[277-279] (figure 2.14). Thus, the range of pore size of hybrid scaffolds is within the recommended range for vascularization (30 – 100 µm) [395, 396] which indicates their potential for valve tissue regeneration. Hybrid scaffolds also offer a wide range of pore size (66 – 126 µm) which could be exploited for the regeneration of other tissues such as cartilage with an optimized pore size in the range (70 – 120 µm)[397].

The potential of hybrid scaffolds to mechanically qualify as TEHVs has been studied and discussed in **chapter 3**. It has been shown that E_{comp}, E_{bend}, G`, and G´´ range from 35 ± 5

kPa to 95 ± 5 kPa, 154 ± 12 kPa to 1660 ± 7 kPa, 16 ± 2 kPa to 113 ± 6 kPa, and 3 ± 1 to 10 ± 2 kPa respectively in the dry state (table 3.1 – table 3.3). Moduli for collagen and HA networks have increased probably due to the restricted movement of the crosslinked polymer chains (figure 3.13). The incorporation of crosslinked HA network has further increased the hindrance to polymer chain movements which has increased the mechanical moduli for hybrid compositions (figure 3.14). The decrease in tan δ from 0.1 to 0.09, in the dry state, also supports this reasoning.

In the wet state, $E_{wet.bend}$, G`, and G´´ range from 1 ± 0.3 kPa to 5 ± 0.1 kPa, 7 ± 2 kPa to 55 ± 4 kPa, and 2 ± 0.4 to 9 ± 2 respectively (table 3.2 and table 3.4). Wet mechanical moduli, for collagen and hybrid scaffolds, are 50 – 700 times less than those of in the dry state as shown in figure 6.1 and figure 6.2 respectively. For all compositions in dry and wet conditions, G´ ≥ G`` which shows the elastic character of parent collagen network as well as the hybrid scaffolds. In hybrid scaffolds, higher water absorption by HA chains has been reflected by their U ratios (table 3.2) as compared to collagen only scaffolds. Absorbed water could act as a lubricant easing the sliding of polymer chains and the decreasing $E_{wet.bend}$, G`, G´´, and tan δ in the wet condition.

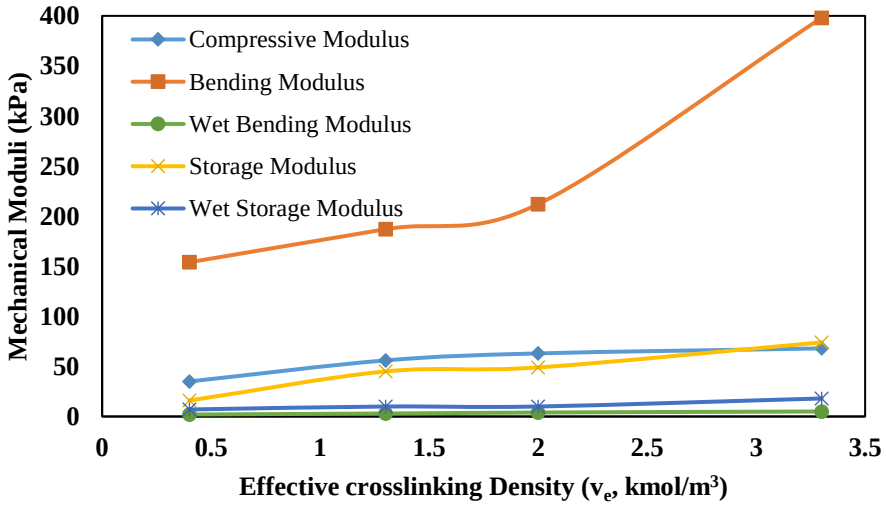


Figure 6.1: Effect of crosslinking density on the mechanical moduli of collagen network (data replotted from table 3.1 – table 3.4, chapter 3).

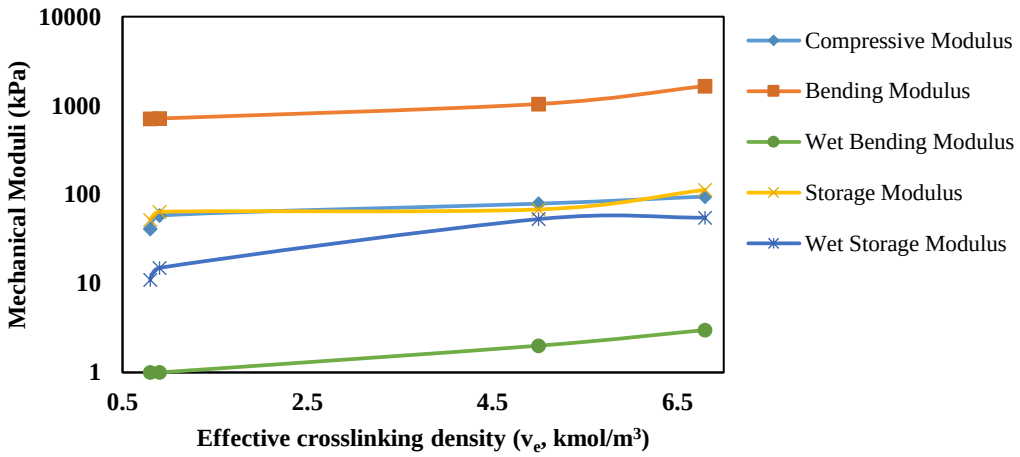


Figure 6.2: Effect of crosslinking density on the mechanical moduli of hybrid scaffolds (data replotted from table 3.1 – table 3.4, chapter 3).

The range of E_{bend}, reported in this study (154 – 1660 kPa), exceeds that of the porcine aortic valve leaflet (PAVL, 150 – 200 kPa) and matches that of the human aortic valve leaflet (HAVL, 1220 kPa in systole) as shown in table 3.6[69, 96, 398]. The range of G´ (16 – 113 kPa dry, 7 – 55 kPa wet) and tan δ in wet condition (0.38 – 0.1) also matches and exceeds G´ (0.54 – 10.5 kPa)[399] and tan δ (0.3 – 0.4)[399, 400] of HAVL as shown in table 3.7. Comparison of various mechanical properties of the hybrid scaffolds with those of HAVL (table 3.6 – table 3.7) has shown that two out of the four proposed compositions among hybrid scaffolds, S-3 and S-4, qualify mechanically to replace HAVL.

Degradation behaviour of scaffold under various conditions could be helpful in predicting its *in-vivo* life as TEHV[330-332]. Degradation behaviours of the parent networks and the resulting hybrid scaffolds under non-enzymatic (PBS, 37°C, 28 days) and enzymatic (PBS, 37°C, 10 U/ml of each of collagenase and hyaluronidase, 35 hrs) conditions have been studied in **chapter 4**. Experiments conducted under non-enzymatic conditions has compared the mass loss of samples under acidic, basic, and physiological pH values. It has been shown that the mass loss decreases with increasing the crosslinking density for all compositions

under all conditions (figure 4.1 – figure 4.3). Engagement of water-interacting sites in the crosslinking process possibly increase the hydrophobicity[401, 402] and hence the degradation resistance of all compositions. Collagen networks have shown 100 % mass loss under acidic conditions (pH 4.0) due to the highest rate of hydrolysis of the peptide bond[344] whereas HA networks have shown 100 % mass loss under basic conditions (pH 10.0) due to deacetylation of the N-acetyl group[216, 219].

Similar to collagen networks, S-1 (24 %) and S-2 (21 %) have shown the highest mass loss under acidic conditions among hybrid scaffolds which suggest the presence of collagen as the primary network which seems to dominate the degradation behaviour of scaffolds. This mass loss is also less than the those of the parent networks as shown in table 4.1 (100 % for C0) and table 4.3 (30 % for HA2). Also, S-3 and S-4 have not shown any mass loss. This could be the effect of the extensive chain entanglements between the two networks, as shown in SEM and histology images (figure 2.10 and figure 2.11), which would mask available water-interacting sites for hybrid scaffolds and increase the degradation resistance.

Mass loss, in the presence of enzymes, has decreased with increasing the crosslinking density for all compositions (figure 4.4 – figure 4.5). In addition to the engagement of the water-interacting sites, increase in crosslinking density for a given network also decrease the mesh size (ξ) of the network (table 2.3) which could limit the access of enzyme to the polymer backbone (figure 4.8). Highest mass loss values have been observed for S-1 (100 %) and S-2 (60 %) under the combined effect of collagenase and hyaluronidase as compared to the either enzyme alone (table 4.4). This supports the hypothesis that hybrid scaffolds are composed of two polymer networks which could be targeted by the specific enzymes at the same time and could result in the highest mass loss (figure 4.8A). No mass loss has been observed for S-3 and S-4 till 35 hours. Higher crosslinking densities of collagen type I and

HA networks in S-3 and S-4 (table 2.3) probably have reduced ε even further where enzymes could not access the backbone of polymer chains (figure 4.8C).

Cardiosphere derived cells (CDCs) have been chosen as cell source due to their presence in the heart[403, 404] and hence their response has reflected the biocompatibility potential of hybrid scaffolds as TEHV as discussed in **chapter 5**. CDCs have attached on all scaffolds including collagen controls and hybrid compositions, however, cell affinity of collagen networks (50 – 20 %) has been better than hybrid scaffolds (30 – 12 %). It could be due to the reason that higher crosslinking densities of hybrid scaffolds would result in the engagement of cell-attachment sites and make them unavailable for cell-attachment[251] (figure 5.2 and figure 5.3). Due to the higher cell attachment ratios, collagen scaffolds have shown higher proliferation rates (10 – 5 %) as compared to hybrid scaffolds (7 – 3 %) on day 4 as shown in figure 5.4 and figure 5.5 respectively. These ranges have suggested that cell proliferation depends on the number of CDCs attached on day 1 and not on the crosslinking density of the scaffolds. On day 7, there has been no significant difference in the cell proliferation rates among hybrid compositions (18 – 12 %) and among collagen scaffolds (19 – 13 %). It could be due to ECM deposition by the proliferating cells till day 7 which would minimize the effect of initially attached cells. The presence of CDCs on hybrid scaffolds on day 7 has also been confirmed by SEM images (figure 5.6). It has also been shown that cell behaviours are independent of the pore sizes and bending stiffness of the scaffolds (figure 5.8 and figure 5.9).

The effect of CDCs culturing on the bending moduli ($E_{cell.bend}$) has been measured by self-deflection test (Eq. 3.4). All compositions except S-1 has shown an increase in $E_{cell.bend}$ (2 ± 0.3 kPa to 6 ± 0.4) after 28 days of CDCs culturing as compared to their $E_{wet.bend}$ (1 ± 0.3 kPa to 3 ± 0.2 kPa) in the non-seeded condition. S-1 could not survive the course of the experiment (28 days) probably due to the rapid degradation rate (figure 5.10) whereas an

increase in $E_{cell.bend}$ for S-2, S-3, and S-4 could be attributed to the deposition of the fresh ECM by the proliferating cells (figure 5.11 and figure 5.12).

6.3 Conclusions:

6.3.1 Assessment of hybrid scaffolds as TEHV:

The properties of hybrid scaffolds, as archived in this thesis, have been assessed against the criterion for a TEHV in table 6.1. S-1 has shown the highest cell - compatibility (50 % of cells were attached), lowest mechanical properties (table 3.1 – table 3.4), and could not survive in culture medium probably due to low degradation resistance (table 4.3 – table 4.4). S-2 has shown better degradation resistance as compared to S-1 and survived in the culture medium for 28 days, however, it has failed to show a significant increase in the mechanical properties (table 3.2). Hence it is concluded that S-1 and S-2 cannot be considered as suitable candidates for designing a TEHV.

Table 6.1: Assessment of the properties of hybrid scaffolds to design TEHV. ✓ shows that composition fulfills the criteria for a certain property to design a TEHV whereas × shows that composition does not fulfill the criteria of a certain property to design a TEHV.

Composition	Mechanical properties	Degradation resistance	Cell-compatibility	*In-vitro* survival
S-1	×	×	✓	×
S-2	×	✓	✓	✓
S-3	✓	✓	✓	✓
S-4	✓	✓	✓	✓

On the other hand, S-3 and S-4 have not only mechanically matched with the heart valve tissue (table 3.6) but their highest degradation resistance (no mass loss under non-enzymatic and enzymatic conditions) has also resulted in longer survival periods (28 days) in the culture medium. Proliferation rates for these compositions have been low (5 – 7 %) till day 7 which could be improved (will be discussed in future work). Nevertheless, slow degradation coupled with increased *in-vitro* bending modulus ($E_{cell.bend}$) for S-3 and S-4 could minimize the chances of pre-mature *in-vivo* failure of the resultant TEHV. Therefore, S-3 and S-4 can be regarded as the 'close-fit' compositions for designing a TEHV among hybrid scaffolds.

6.3.2 Achievements of the thesis:

The main achievement(s)/contribution(s) to the current state of the art, made by this piece of work, are outlined as follows:

6.3.2.1 Development of a new crosslinking approach:

In this thesis, a sequential crosslinking technique based on EDC/NHS have been applied to collagen type I and HA without denaturation. To the best of the authors' knowledge, this is the first report for the synthesis of heterogeneous microstructures from collagen type I and HA by a crosslinking route entirely based on chemical crosslinking agents. It is concluded that our crosslinking technique is flexible and can be applied to various water-soluble polymers to prepare heterogeneous scaffolds for a wide range of engineering applications in general and for tissue engineering of organs requiring heterogeneous scaffolds in particular.

6.3.2.2 Aortic valve leaflet ECM mimicking scaffolds:

Sequential nature of our crosslinking technique has yielded heterogeneous scaffolds. Microstructural characterization of these scaffolds has revealed interlaced chains of collagen and HA on microscale which is similar to the fibrosa layer in the aortic valve leaflet ECM.

Furthermore, these scaffolds have the potential to be developed into the tri-layer structure of the leaflet which will be discussed in chapter 7.

6.3.2.3 Mechanically matching scaffolds:

Mechanical properties (compressive modulus, bending modulus, and dynamic moduli) of hybrid scaffolds, reported here, have matched and exceeded those of HAVL. These values are also higher than those of reported for collagen and HA based scaffolds in literature. Provided that the sinus and aortic wall are stiffer than the aortic valve leaflet[399, 405], hybrid scaffolds have the potential to be further developed into an integrated design mimicking the entire aortic root (including leaflets).

6.3.2.4 Tailorable properties:

Degradation data from **chapter 4** supports the data on mechanical properties from **chapter 3** that the addition of HA network has not only increased the mechanical properties of hybrid scaffolds but also have maintained some of these properties in the wet condition. The extent of increase in the mechanical properties of hybrid scaffolds by incorporating HA network depends on the crosslinking densities of the individual networks. Similarly, degradation behviours of hybrid scaffolds have been governed by the degradation behaviours of the individual networks. Therefore, our crosslinking technique successfully has produced hybrid scaffolds with tailorable mechanical and degradation behaviours. A wide spectrum of mechanical moduli and degradation behaviours could be achieved by simply varying the crosslinking densities of individual networks. The properties of these scaffolds can be optimized in future for other tissue engineering applications.

6.3.2.5 Understanding the microstructure-property relationship for hybrid scaffolds:

Investigations into mechanical properties, degradation behaviours, and cell response of hybrid scaffolds have provided a deeper understanding of their structure-property relationship. Appropriate mechanisms have been proposed in **chapter 3, 4, and 5** to explain the effects of crosslinking density as well as interlaced microstructure on the mechanical properties, degradation behaviours, and biocompatibility of the hybrid scaffolds. Furthermore, data reported on these properties will serve as a guideline for the future designs of TEHV based on collagen type I and HA.

6.3.2.6 A preliminary model for an ideal TEHV:

Thus, this thesis has proposed a basic model for TEHV based on interlaced collagen type I/HA hybrid scaffolds. These scaffolds have shown an ECM mimicking interlaced microstructure. In addition, controlled degradation, mechanical matching with HAVL, and reasonable cell compatibility have indicated the potential of these scaffolds to be further developed as an ideal TEHV. The recommendations for improvement in the proposed hybrid scaffolds will be discussed in chapter 7.

Chapter 7

Future Work

This chapter presents suggestions and ideas for the areas that could be usefully studied further.

7.1 Mimicking the native valve:

This work has focused on collagen type I and hyaluronic acid (HA) based hybrid scaffolds whereas 10% of the dry mass of the heart valve is comprised of a third polymer elastin[82, 406] as discussed in chapter 1 (section 1.3.3.3). Incorporation of elastin into hybrid scaffolds could more closely mimic the native aortic valve.

The crimped structure of collagen in fibrosa allows large strains during diastole as discussed in chapter 1 (figure 1.7). Therefore, the addition of a crimping pattern on the surface should increase the extensibility of hybrid scaffolds. This could be achieved by casting collagen slurry in a patterned mold before freeze drying.

Cross-sections of valve leaflet consist of fibrosa, spongiosa, and ventricularis as shown in figure 7.1. Collagen/HA hybrid scaffolds, reported here, with collagen forming the primary network have shown microstructure similar to fibrosa. Our crosslinking technique could also be utilized for the fabrication of hybrid scaffolds with HA and elastin forming primary networks to replicate spongiosa and ventricularis respectively to replicate the tri layer structure.

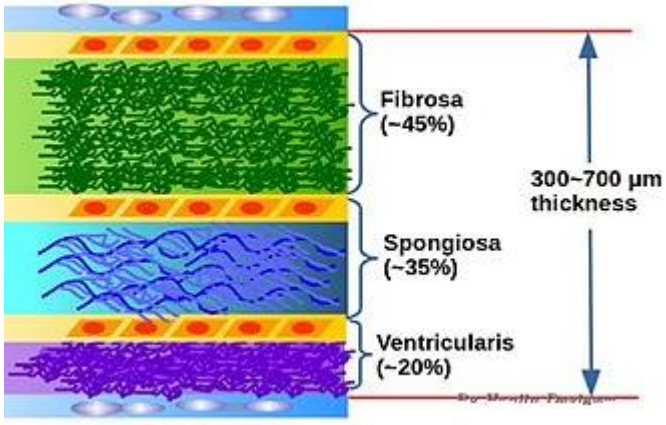


Figure 7.1: tri-layer microstructure of aortic valve leaflet showing interlaced chains of collagen, GAGs, and elastin in fibrosa, spongiosa, and ventricularis respectively.

However, tri-layered scaffolds may be at the risk of delamination during mechanical loading because of the difference in the bending moduli of the three layers[407]. To overcome this limitation, the tri-layered structure should be replaced by scaffold with a graded composition. Graded scaffolds for cartilage repair have been shown to minimize the effects of mechanical mismatching across different layers [408, 409]. This approach can be adopted to prepare graded scaffolds with collagen-rich phase, HA-rich phase, and elastin-rich phase which will potentially replicate fibrosa, spongiosa, and ventricularis respectively as shown in figure 7.2.

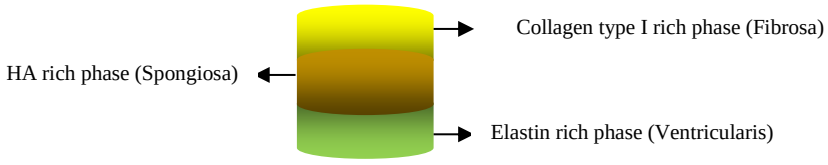


Figure 7.2: Hybrid scaffold with the graded composition for mimicking tri-layer microstructure of heart valve leaflet.

Collagen, glycosaminoglycans (GAGs), and elastin are present in the heart valve leaflet in the form of interpenetrating chains interlaced on molecular levels (nano-scale)[21, 55] as shown

in figure 7.1. A scaffold made up of these polymers in the form of interpenetrating polymer networks (IPNs) could have the potential to more closely match the microstructure of the native leaflet[21]. A number of research articles have claimed to synthesize and characterize IPNs formatted scaffolds. However, they lack the evidence for the nano-scale interlacing between polymer chains[410-414]. Collagen/HA hybrid scaffolds developed, in this thesis, revealed interlaced chains of polymers on the micro-scale (figure 2.10 and figure 2.11). Hence, there is a need to either modify an existing or develop a new characterization technique which can distinguish between the two different polymer networks on the molecular (nano) scale. Visualization under a specialized electron microscope and small angle neutron scattering (SANS) can be helpful in validating the nano-scale interactions between polymer networks in the proposed hybrid scaffolds[415-417].

7.2 Anisotropic mechanical properties:

A heterogeneous microstructure can lead to the anisotropy in mechanical properties of the heart valve leaflet [418] as discussed in chapter 1 (section 1.3.5.1, figure 1.8). Mechanical characterizations performed in this work (chapter 3) represent scaffolds' response in the circumferential direction only and an investigation of mechanical properties in the radial direction will reveal useful information.

Tensile deformation, an important mode in the valve dynamics[69, 419], could not be studied here. Therefore, uniaxial and biaxial (circumferential and radial) tensile properties of hybrid scaffolds should be performed in future.

It has been shown in chapter 5 that cell proliferation on the hybrid scaffold may increase or decrease the mechanical properties in wet conditions depending on its degradation rate (section 5.4, figure 5.11). The study of change of mechanical moduli over the course of

degradation and/or cell proliferation will be useful in understanding the dynamics of biomechanical stability of these hybrid scaffolds.

Comparison of data on mechanical properties of the biological valves from different studies is less reliable because of variations in testing methods[69, 151]. In general, testing procedures for the characterization of the mechanical properties of the native heart valves and substitutive scaffolds should be standardized.

7.3 Restoring the cell-attachment sites:

The mechanical properties and degradation resistance reached maximum values for S-3 and S-4 (table 3.1-table 3.5, table 4.1-table 4.3). However, these compositions suffered from low CDCs attachment and proliferation rates due to the lack of cell-attachment sites (table 5.2 and table 5.4). Studies have shown that the addition of synthetic RGD motifs on scaffolds can restore their cell-attachment sites[420-422] as shown in figure 7.3. Therefore, the standard protocol should be optimized to incorporate the RGD motifs on the surface of these hybrid scaffolds.

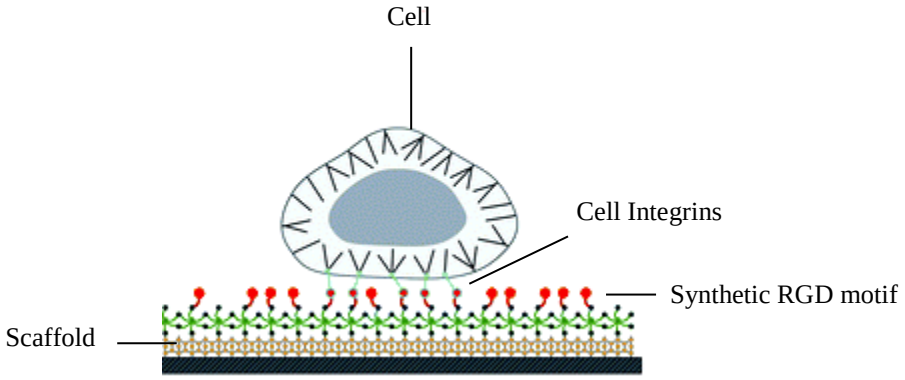


Figure 7.3: Attachment of synthetic RGD-peptides can restore the cell affinity of the scaffolds.

7.4 Cell-culture under dynamic conditions:

Differentiation behaviour of CDCs on hybrid scaffolds could not be studied because of time limitations. Cardio-sphere derived cells (CDCs) resemble stem cells and have the capacity to differentiate into the endothelial cell (EC) and smooth muscle cells (SMCs)[423, 424]. Growth factors such as vascular endothelial growth factor (VEGF) and fibroblast growth factor-inducible 14 (Fn14) could be tested as they have been reported to stimulate the stem cells differentiation into target cells[425, 426]. Additionally, electrical and mechanical stimuli could be tested to accelerate the ECM formation[427, 428].

References

1. E. Braunwald: 'Heart disease: a textbook of cardiovascular medicine', 1997, Saunders.
2. M. B. Gravanis: 'Cardiovascular disorders: pathogenesis and pathophysiology', 1993, Mosby-Year Book.
3. F. G. Estafanous, P. G. Barash, and J. G. Reves: 'Cardiac anesthesia: principles and clinical practice', 2001, Lippincott Williams & Wilkins.
4. T. Ichim: 'Stem cell therapy for cardiac valvular dysfunction', 2007, US Patent No. 20080050347.
5. I. Vesely: 'Heart valve tissue engineering', *Circulation research*, 2005, **97**(8), 743-755.
6. F. Barili, L. Dainese, V. K. Topkara, P. Biglioli, and G. Polvani: 'The future of human valve allografts: bioengineering and stem cells', *Artificial organs*, 2005, **29**(11), 923-923.
7. A. Krian, J. M. Matloff, and D. M. Nicoloff: 'Advancing the Technology of Bileaflet Mechanical Heart Valves', 2012, Steinkopff.
8. R. Lanza, R. Langer, and J. P. Vacanti: 'Principles of Tissue Engineering', 2000, Elsevier Science.
9. L. P. Dasi, H. A. Simon, P. Sucosky, and A. P. Yoganathan: 'Fluid mechanics of artificial heart valves', *Clinical and experimental pharmacology and physiology*, 2009, **36**(2), 225-237.
10. P. Zilla, J. Brink, P. Human, and D. Bezuidenhout: 'Prosthetic heart valves: catering for the few', *Biomaterials*, 2008, **29**(4), 385-406.
11. J. C. Chambers, J. Somerville, S. Stone, and D. N. Ross: 'Pulmonary autograft procedure for aortic valve disease long-term results of the pioneer series', *Circulation*, 1997, **96**(7), 2206-2214.
12. A. E. Abbas: 'Aortic Stenosis: Case-Based Diagnosis and Therapy', 2015, Springer, 2015.
13. D. L. Wise: 'Encyclopedic Handbook of Biomaterials and Bioengineering: v. 1-2. Applications', 1832; 1995, CRC Press, 1995.
14. J. B. Lakier, F. Khaja, D. J. Magilligan, and S. Goldstein: 'Porcine xenograft valves. Long-term (60-89-month) follow-up', *Circulation*, 1980, **62**(2), 313-318.

15. W. Vongpatanasin, L. D. Hillis, and R. A. Lange: 'Prosthetic heart valves', *New England Journal of Medicine*, 1996, **335**(6), 407-416.
16. P. Bloomfield: 'Choice of heart valve prosthesis', *Heart*, 2002, **87**(6), 583-589.
17. L. Iop and G. Gerosa: 'Guided Tissue Regeneration in Heart Valve Replacement: From Preclinical Research to First-in-Human Trials', *BioMed Research International*, 2015, **2015**, 432901.
18. S. Brose, R. Autschbach, M. Engel, T. Rauch, and F. Rauch: 'Patient adapted valve selection: biological vs. mechanical heart valve replacement in aortic valve diseases', *Zeitschrift fur Kardiologie*, 2001, **90**(Suppl 6), 48-57.
19. S. Dittrich, V. V. Alexi-Meskishvili, A. C. Yankah, I. Dähnert, R. Meyer, R. Hetzer, and P. E. Lange: 'Comparison of porcine xenografts and homografts for pulmonary valve replacement in children', *The Annals of thoracic surgery*, 2000, **70**(3), 717-722.
20. J. C. J. Sun, M. J. Davidson, A. Lamy, and J. W. Eikelboom: 'Antithrombotic management of patients with prosthetic heart valves: current evidence and future trends', *The Lancet*, **374**(9689), 565-576.
21. R. Nazir: 'Collagen–hyaluronic acid based interpenetrating polymer networks as tissue engineered heart valve', *Materials Science and Technology*, 2016, 1-12.
22. K. Mendelson and F. J. Schoen: 'Heart valve tissue engineering: concepts, approaches, progress, and challenges', *Annals of biomedical engineering*, 2006, **34**(12), 1799-1819.
23. M. R. Erik J. Suuronen: 'Biomaterials for Cardiac Regeneration', 323; 2014, Springer, 2014.
24. R. D. W. Ren-Ke Li: 'Cardiac Regeneration and Repair: Biomaterials and Tissue Engineering', 486; 2014, Elsevier, 2014.
25. F. E. Smit and P. M. Dohmen: 'Cardiovascular tissue engineering: where we come from and where are we now?', *Medical science monitor basic research*, 2015, **21**, 1.
26. B. Dhandayuthapani, Y. Yoshida, T. Maekawa, and D. S. Kumar: 'Polymeric scaffolds in tissue engineering application: a review', *International Journal of Polymer Science*, 2011, **2011**.
27. B. D. Ulery, L. S. Nair, and C. T. Laurencin: 'Biomedical applications of biodegradable polymers', *Journal of polymer science Part B: polymer physics*, 2011, **49**(12), 832-864.

28. D. T. Simionescu, J. Chen, M. Jaeggli, B. Wang, and J. Liao: 'Form Follows Function: Advances in Trilayered Structure Replication for Aortic Heart Valve Tissue Engineering', *Journal of healthcare engineering*, 2012, **3**(2), 179-202.
29. X. Zhang, B. Xu, D. S. Puperi, Y. Wu, J. L. West, and K. J. Grande-Allen: 'Application of Hydrogels in Heart Valve Tissue Engineering', *Journal of long-term effects of medical implants*, 2015, **25**(0), 105-134.
30. J. Sun, S. Vijayavenkataraman, and H. Liu: 'An Overview of Scaffold Design and Fabrication Technology for Engineered Knee Meniscus', *Materials*, 2017, **10**(1), 29.
31. Z. Izadifar, X. Chen, and W. Kulyk: 'Strategic Design and Fabrication of Engineered Scaffolds for Articular Cartilage Repair', *Journal of Functional Biomaterials*, 2012, **3**(4), 799-838.
32. D. Y. Cheung, B. Duan, and J. T. Butcher: 'Current Progress in Tissue Engineering of Heart Valves: Multiscale Problems, Multiscale Solutions', *Expert opinion on biological therapy*, 2015, **15**(8), 1155-1172.
33. R. J. Brady: 'The Cardiovascular System', 1970, Prentice Hall PTR.
34. A. Singh and I. Singh: 'Anatomy and Physiology for Paramedicals', 2008, Jaypee Brothers,Medical Publishers Pvt. Limited.
35. S. S. Mader: 'Inquiry Into Life', 1999, McGraw-Hill Higher Education.
36. D. Alon: 'Heart Valve Repair and Replacement', 2016, US Patent 20,160,120,645.
37. R. H. Anderson: 'Clinical anatomy of the aortic root', *Heart*, 2000, **84**(6), 670-673.
38. M. Loukas, E. Bilinsky, S. Bilinsky, C. Blaak, R. S. Tubbs, and R. H. Anderson: 'The anatomy of the aortic root', *Clinical anatomy (New York, N.Y.)*, 2014, **27**(5), 748-756.
39. E. I. Charitos and H.-H. Sievers: 'Anatomy of the aortic root: implications for valve-sparing surgery', *Annals of Cardiothoracic Surgery*, 2013, **2**(1), 53.
40. S. Y. Ho: 'Structure and anatomy of the aortic root', *European Heart Journal-Cardiovascular Imaging*, 2009, **10**(1), i3-i10.
41. M. Underwood, G. El Khoury, D. Deronck, D. Glineur, and R. Dion: 'The aortic root: structure, function, and surgical reconstruction', *Heart*, 2000, **83**(4), 376-380.
42. K. L. Weind, C. G. Ellis, and D. R. Boughner: 'The aortic valve blood supply', *The Journal of heart valve disease*, 2000, **9**(1), 1-7; discussion 7-8.
43. P. Nataf and E. Lansac: 'Dilation of the thoracic aorta: medical and surgical management', *Heart*, 2006, **92**(9), 1345-1352.

44. J. Z. Goldfinger, J. L. Halperin, M. L. Marin, A. S. Stewart, K. A. Eagle, and V. Fuster: 'Thoracic Aortic Aneurysm and Dissection', *Journal of the American College of Cardiology*, 2014, **64**(16), 1725-1739.
45. A. Tsamis, J. T. Krawiec, and D. A. Vorp: 'Elastin and collagen fibre microstructure of the human aorta in ageing and disease: a review', *Journal of the Royal Society Interface*, 2013, **10**(83), 20121004.
46. L. S. Lilly: 'Pathophysiology of Heart Disease: A Collaborative Project of Medical Students and Faculty', 2012, Wolters Kluwer Health.
47. M. D. Morash, W. H. Pearce, and J. S. T. Yao: 'Surgery of the Aorta and Its Body Branches', 2009, People's Medical Publishing House-USA.
48. R. E. Clark and E. H. Finke: 'Scanning and light microscopy of human aortic leaflets in stressed and relaxed states', *J Thorac Cardiovasc Surg*, 1974, **67**(5), 792-804.
49. A. G. Kidane, G. Burriesci, P. Cornejo, A. Dooley, S. Sarkar, P. Bonhoeffer, M. Edirisinghe, and A. M. Seifalian: 'Current developments and future prospects for heart valve replacement therapy', *Journal of Biomedical Materials Research Part B: Applied Biomaterials*, 2009, **88**(1), 290-303.
50. C. M. Otto: 'Evaluation and management of chronic mitral regurgitation', *New England Journal of Medicine*, 2001, **345**(10), 740-746.
51. C. Martin and W. Sun: 'Biomechanical characterization of aortic valve tissue in humans and common animal models', *Journal of Biomedical Materials Research Part A*, 2012, **100**(6), 1591-1599.
52. S. Hinderer, S. L. Layland, and K. Schenke-Layland: 'ECM and ECM-like materials — Biomaterials for applications in regenerative medicine and cancer therapy', *Advanced Drug Delivery Reviews*, 2016, **97**, 260-269.
53. M. Bäck, T. C. Gasser, J.-B. Michel, and G. Caligiuri: 'Biomechanical factors in the biology of aortic wall and aortic valve diseases', *Cardiovascular research*, 2013, **99**(2), 232-241.
54. M. S. Sacks, W. D. Merryman, and D. E. Schmidt: 'On the biomechanics of heart valve function', *Journal of biomechanics*, 2009, **42**(12), 1804-1824.
55. C. E. Eckert, R. Fan, B. Mikulis, M. Barron, C. A. Carruthers, V. M. Friebe, N. R. Vyavahare, and M. S. Sacks: 'On the Biomechanical Role of Glycosaminoglycans in the Aortic Heart Valve Leaflet', *Acta biomaterialia*, 2013, **9**(1), 4653-4660.
56. J. A. Stella, J. Liao, and M. S. Sacks: 'Time-dependent biaxial mechanical behavior of the aortic heart valve leaflet', *Journal of biomechanics*, 2007, **40**(14), 3169-3177.

57. S. Hinderer, J. Seifert, M. Votteler, N. Shen, J. Rheinlaender, T. E. Schäffer, and K. Schenke-Layland: 'Engineering of a bio-functionalized hybrid off-the-shelf heart valve', *Biomaterials*, 2014, **35**(7), 2130-2139.
58. I. Vesely and R. Noseworthy: 'Micromechanics of the fibrosa and the ventricularis in aortic valve leaflets', *Journal of Biomechanics*, 1992, **25**(1), 101-113.
59. B. Stelt: 'Tissue engineering of aortic valves'.
60. J. Lincoln, A. W. Lange, and K. E. Yutzey: 'Hearts and bones: shared regulatory mechanisms in heart valve, cartilage, tendon, and bone development', *Developmental biology*, 2006, **294**(2), 292-302.
61. I. Vesely: 'The role of elastin in aortic valve mechanics', *Journal of biomechanics*, 1997, **31**(2), 115-123.
62. R. M. Buchanan and M. S. Sacks: 'Interlayer micromechanics of the aortic heart valve leaflet', *Biomechanics and modeling in mechanobiology*, 2014, **13**(4), 813-826.
63. T. A. Drake and M. Pang: 'Effects of interleukin-1, lipopolysaccharide, and streptococci on procoagulant activity of cultured human cardiac valve endothelial and stromal cells', *Infection and immunity*, 1989, **57**(2), 507-512.
64. J. T. Butcher and R. M. Nerem: 'Valvular endothelial cells and the mechanoregulation of valvular pathology', *Philosophical Transactions of the Royal Society B: Biological Sciences*, 2007, **362**(1484), 1445-1457.
65. P. M. Taylor, P. Batten, N. J. Brand, P. S. Thomas, and M. H. Yacoub: 'The cardiac valve interstitial cell', *The International Journal of Biochemistry & Cell Biology*, 2003, **35**(2), 113-118.
66. A. C. Liu, V. R. Joag, and A. I. Gotlieb: 'The Emerging Role of Valve Interstitial Cell Phenotypes in Regulating Heart Valve Pathobiology', *The American Journal of Pathology*, 2007, **171**(5), 1407-1418.
67. I. El-Hamamsy, M. H. Yacoub, and A. H. Chester: 'Neuronal regulation of aortic valve cusps', *Current vascular pharmacology*, 2009, **7**(1), 40-46.
68. M. S. Sacks, W. David Merryman, and D. E. Schmidt: 'On the biomechanics of heart valve function', *Journal of biomechanics*, 2009, **42**(12), 1804-1824.
69. A. Hasan, K. Ragaert, W. Swieszkowski, Š. Selimović, A. Paul, G. Camci-Unal, M. R. Mofrad, and A. Khademhosseini: 'Biomechanical properties of native and tissue engineered heart valve constructs', *Journal of Biomechanics*, 2014, **47**(9), 1949-1963.

70. M. Thubrikar, W. C. Piepgrass, J. D. Deck, and S. P. Nolan: 'Stresses of natural versus prosthetic aortic valve leaflets in vivo', *The Annals of thoracic surgery*, 1980, **30**(3), 230-239.
71. G. W. Christie and B. G. Barratt-Boyes: 'Mechanical properties of porcine pulmonary valve leaflets: how do they differ from aortic leaflets?', *The Annals of thoracic surgery*, 1995, **60**, S195-S199.
72. B. V. Rego and M. S. Sacks: 'A functionally graded material model for the transmural stress distribution of the aortic valve leaflet', *Journal of Biomechanics*, 2017, **54**, 88-95.
73. A. C. Yankah, M. H. Yacoub, and R. Hetzer: 'Cardiac Valve Allografts: Science and Practice', 2012, Steinkopff.
74. G. Ailawadi and I. L. Kron: 'Catheter Based Valve and Aortic Surgery', 2016, Springer New York.
75. P. L. Gould, A. Cataloglu, and R. E. Clark: 'Mathematical modelling of human aortic valve leaflets', *Applied Mathematical Modelling*, 1976, **1**(1), 33-36.
76. Y. Dabiri, J. Ronsky, I. Ali, A. Basha, A. Bhanji, and K. Narine: 'Effects of Leaflet Design on Transvalvular Gradients of Bioprosthetic Heart Valves', *Cardiovascular engineering and technology*, 2016, **7**(4), 363-373.
77. J. M. Mattson, R. Turcotte, and Y. Zhang: 'Glycosaminoglycans contribute to extracellular matrix fiber recruitment and arterial wall mechanics', *Biomechanics and modeling in mechanobiology*, 2017, **16**(1), 213-225.
78. W. Cole, D. Chan, A. Hickey, and D. Wilcken: 'Collagen composition of normal and myxomatous human mitral heart valves', *Biochem. J*, 1984, **219**, 451-460.
79. K. Kunzelman, R. Cochran, S. Murphree, W. Ring, E. Verrier, and R. Eberhart: 'Differential collagen distribution in the mitral valve and its influence on biomechanical behaviour', *J. Heart Valve Dis.*, 1993, **2**(2), 236-244.
80. K. Murata: 'Acidic glycosaminoglycans in human heart valves', *J. Mol. Cell. Cardiol.*, 1981, **13**(3), 281-292.
81. N. Sasaki and S. Odajima: 'Stress-strain curve and young's modulus of a collagen molecule as determined by the X-ray diffraction technique', *Journal of Biomechanics*, 1996, **29**(5), 655-658.
82. P. Fratzl: 'Collagen: Structure and Mechanics', 2008, Springer US.

83. J. Leeson-Dietrich, D. Boughner, and I. Vesely: 'Porcine pulmonary and aortic valves: a comparison of their tensile viscoelastic properties at physiological strain rates', *The Journal of heart valve disease*, 1995, **4**(1), 88-94.
84. T. Jiao, R. J. Clifton, G. L. Converse, and R. A. Hopkins: 'Measurements of the effects of decellularization on viscoelastic properties of tissues in ovine, baboon, and human heart valves', *Tissue Engineering Part A*, 2011, **18**(3-4), 423-431.
85. Zhilei L. Shen, H. Kahn, R. Ballarini, and Steven J. Eppell: 'Viscoelastic Properties of Isolated Collagen Fibrils', *Biophysical Journal*, 2011, **100**(12), 3008-3015.
86. A. Borzacchiello, L. Russo, B. M. Malle, K. Schwach-Abdellaoui, and L. Ambrosio: 'Hyaluronic Acid Based Hydrogels for Regenerative Medicine Applications', *BioMed Research International*, 2015, **2015**, 12.
87. M. N. Collins and C. Birkinshaw: 'Physical properties of crosslinked hyaluronic acid hydrogels', *Journal of Materials Science: Materials in Medicine*, 2008, **19**(11), 3335-3343.
88. D. Collin, P. Lavalle, J. M. Garza, J.-C. Voegel, P. Schaaf, and P. Martinoty: 'Mechanical Properties of Cross-Linked Hyaluronic Acid/Poly-(l-lysine) Multilayer Films', *Macromolecules*, 2004, **37**(26), 10195-10198.
89. C. Chun, D. Y. Lee, J.-T. Kim, M.-K. Kwon, Y.-Z. Kim, and S.-S. Kim: 'Effect of molecular weight of hyaluronic acid (HA) on viscoelasticity and particle texturing feel of HA dermal biphasic fillers', *Biomaterials Research*, 2016, **20**(1), 24.
90. A. Balguid, M. P. Rubbens, A. Mol, R. A. Bank, A. J. Bogers, J. P. Van Kats, B. A. De Mol, F. P. Baaijens, and C. V. Bouten: 'The role of collagen cross-links in biomechanical behavior of human aortic heart valve leaflets—relevance for tissue engineering', *Tissue engineering*, 2007, **13**(7), 1501-1511.
91. E. Gentleman, A. N. Lay, D. A. Dickerson, E. A. Nauman, G. A. Livesay, and K. C. Dee: 'Mechanical characterization of collagen fibers and scaffolds for tissue engineering', *Biomaterials*, 2003, **24**(21), 3805-3813.
92. F. Silver: 'Biomaterials, Medical Devices and Tissue Engineering: An Integrated Approach: An integrated approach', 2012, Springer Netherlands.
93. C. R. Carlisle, C. Coulais, and M. Guthold: 'The mechanical stress-strain properties of single electrospun collagen type I nanofibers', *Acta Biomater*, 2010, **6**(8), 2997-3003.

94. C. Carlisle, C. Coulais, and M. Guthold: 'The mechanical stress–strain properties of single electrospun collagen type I nanofibers', *Acta biomaterialia*, 2010, **6**(8), 2997-3003.
95. R. Gnyaneshwar, R. K. Kumar, and K. R. Balakrishnan: 'Dynamic analysis of the aortic valve using a finite element model', *The Annals of thoracic surgery*, 2002, **73**(4), 1122-1129.
96. K. Balachandran, P. Sucosky, and A. P. Yoganathan: 'Hemodynamics and Mechanobiology of Aortic Valve Inflammation and Calcification', *International Journal of Inflammation*, 2011, **2011**.
97. L. Yang, K. O. van der Werf, C. F. C. Fitié, M. L. Bennink, P. J. Dijkstra, and J. Feijen: 'Mechanical Properties of Native and Cross-linked Type I Collagen Fibrils', *Biophysical Journal*, 2008, **94**(6), 2204-2211.
98. D. W. Kitzman, D. G. Schloz, P. T. Hagen, D. M. Ilstrup, and W. D. Edwards: 'Age-related changes in normal human hearts during the first 10 decades of life. Part II (maturity): a quantitative anatomic study of 765 specimens from subjects 20 to 99 years old', Mayo Clinic Proceedings, 1988, Elsevier, 137-146.
99. E. M. Culav, C. H. Clark, and M. J. Merrilees: 'Connective tissues: Matrix composition and its relevance to physical therapy', *Physical Therapy*, 1999, **79**(3), 308-319.
100. R. M. Wasserman: 'Institutional Research Healthcare & Biotechnology Initiation Report', 2010.
101. Brinckmann, J. Brinckmann, H. Notbohm, and P. K. Müller: 'Collagen : primer in structure, processing and assembly', 2005, Berlin, Springer.
102. E. Baer, J. Cassidy James, and A. Hiltner: 'Hierarchical Structure of Collagen Composite Systems', in 'Viscoelasticity of Biomaterials', 2-23; 1992, American Chemical Society.
103. E. Baer, J. J. Cassidy, and A. Hiltner: 'Hierarchical structure of collagen composite systems: lessons from biology', *Pure and applied chemistry*, 1991, **63**(7), 961-973.
104. S. Ricard-Blum and F. Ruggiero: 'The collagen superfamily: from the extracellular matrix to the cell membrane', *Pathol. Biol.*, 2005, **53**(7), 430-442.
105. A. M. Cribb and J. E. Scott: 'Tendon response to tensile stress - an ultrastructural investigation of collagen-proteoglycans interactions in stressed tendon', *Journal of Anatomy*, 1995, **187**, 423-428.

106. J. Gosline, M. Lillie, E. Carrington, P. Guerette, C. Ortlepp, and K. Savage: 'Elastic Proteins: Biological Roles and Mechanical Properties', *Philosophical Transactions: Biological Sciences*, 2002, **357**(1418), 121-132.

107. F. L. Wuyts and et al.: 'Elastic properties of human aortas in relation to age and atherosclerosis: a structural model', *Physics in Medicine and Biology*, 1995, **40**(10), 1577.

108. G. W. Christie: 'Anatomy of aortic heart valve leaflets: the influence of glutaraldehyde fixation on function', *European Journal of Cardio-Thoracic Surgery*, 1992, **6**(SUPPL. 1), S25-S33.

109. T. Q. Lee: 'Structure and function of ligamnets and tendons', *Basic Orthopaedic Biomechanics & Mechano-biology*, 2005, 301.

110. J. Fraser, T. Laurent, and U. Laurent: 'Hyaluronan: its nature, distribution, functions and turnover', *J. Intern. Med.*, 1997, **242**(1), 27-33.

111. B. P. Toole: 'Hyaluronan in morphogenesis', Seminars in cell & developmental biology, 2001, Elsevier, 79-87.

112. B. P. Toole: 'Hyaluronan: from extracellular glue to pericellular cue', *Nat. Rev. Cancer*, 2004, **4**(7), 528-539.

113. E. A. Balazs and T. C. Laurent: 'Chemistry, biology and medical applications of hyaluronan and its derivatives', 1998.

114. G. D. Prestwich and K. P. Vercruysse: 'Profiles therapeutic applications of hyaluronic acid and hyaluronan derivatives', *Pharm. Sci. Technolo. Today*, 1998, **1**(1), 42-43.

115. J. E. Dixon, G. Osman, G. E. Morris, H. Markides, M. Rotherham, Z. Bayoussef, A. J. El Haj, C. Denning, and K. M. Shakesheff: 'Highly efficient delivery of functional cargoes by the synergistic effect of GAG binding motifs and cell-penetrating peptides', *Proceedings of the National Academy of Sciences*, 2016, **113**(3), E291-E299.

116. Y. Luo, K. R. Kirker, and G. D. Prestwich: 'Cross-linked hyaluronic acid hydrogel films: new biomaterials for drug delivery', *Journal of controlled release*, 2000, **69**(1), 169-184.

117. T. Segura, B. C. Anderson, P. H. Chung, R. E. Webber, K. R. Shull, and L. D. Shea: 'Crosslinked hyaluronic acid hydrogels: a strategy to functionalize and pattern', *Biomaterials*, 2005, **26**(4), 359-371.

118. C. E. Schanté, G. Zuber, C. Herlin, and T. F. Vandamme: 'Chemical modifications of hyaluronic acid for the synthesis of derivatives for a broad range of biomedical applications', *Carbohydrate polymers*, 2011, **85**(3), 469-489.
119. X. Z. Shu, Y. Liu, Y. Luo, M. C. Roberts, and G. D. Prestwich: 'Disulfide cross-linked hyaluronan hydrogels', *Biomacromolecules*, 2002, **3**(6), 1304-1311.
120. Y. D. Park, N. Tirelli, and J. A. Hubbell: 'Photopolymerized hyaluronic acid-based hydrogels and interpenetrating networks', *Biomaterials*, 2003, **24**(6), 893-900.
121. C. Nishi, N. Nakajima, and Y. Ikada: 'In vitro evaluation of cytotoxicity of diepoxy compounds used for biomaterial modification', *J. Biomed. Mater. Res.*, 1995, **29**(7), 829-834.
122. A. Ramamurthi and I. Vesely: 'Smooth muscle cell adhesion on crosslinked hyaluronan gels', *J. Biomed. Mater. Res.*, 2002, **60**(1), 195-205.
123. M. A. Serban, G. Yang, and G. D. Prestwich: 'Synthesis, characterization and chondroprotective properties of a hyaluronan thioethyl ether derivative', *Biomaterials*, 2008, **29**(10), 1388-1399.
124. V. Crescenzi, A. Francescangeli, A. Taglienti, D. Capitani, and L. Mannina: 'Synthesis and partial characterization of hydrogels obtained via glutaraldehyde crosslinking of acetylated chitosan and of hyaluronan derivatives', *Biomacromolecules*, 2003, **4**(4), 1045-1054.
125. M. Chytil and M. Pekař: 'Effect of new hydrophobic modification of hyaluronan on its solution properties: Evaluation of self-aggregation', *Carbohydr. Polym.*, 2009, **76**(3), 443-448.
126. S. Oerther, A. C. Maurin, E. Payan, P. Hubert, F. Lapicque, N. Presle, J. Dexheimer, P. Netter, and F. Lapicque: 'High interaction alginate–hyaluronate associations by hyaluronate deacetylation for the preparation of efficient biomaterials', *Biopolymers*, 2000, **54**(4), 273-281.
127. O. Jeon, S. J. Song, K.-J. Lee, M. H. Park, S.-H. Lee, S. K. Hahn, S. Kim, and B.-S. Kim: 'Mechanical properties and degradation behaviors of hyaluronic acid hydrogels cross-linked at various cross-linking densities', *Carbohydr. Polym.*, 2007, **70**(3), 251-257.
128. X. Xu, A. K. Jha, D. A. Harrington, M. C. Farach-Carson, and X. Jia: 'Hyaluronic acid-based hydrogels: from a natural polysaccharide to complex networks', *Soft Matter*, 2012, **8**(12), 3280-3294.

129. G. Orlando: 'Regenerative Medicine Applications in Organ Transplantation', 2013, Elsevier Science.
130. N. Pallua and C. V. Suschek: 'Tissue Engineering: From Lab to Clinic', 2010, Springer Berlin Heidelberg.
131. X. Jia and K. L. Kiick: 'Hybrid multicomponent hydrogels for tissue engineering', *Macromolecular bioscience*, 2009, **9**(2), 140-156.
132. H. Yamaoka, H. Asato, T. Ogasawara, S. Nishizawa, T. Takahashi, T. Nakatsuka, I. Koshima, K. Nakamura, H. Kawaguchi, and U. i. Chung: 'Cartilage tissue engineering using human auricular chondrocytes embedded in different hydrogel materials', *J. Biomed. Mater. Res. A*, 2006, **78**(1), 1-11.
133. S. Suri and C. E. Schmidt: 'Cell-laden hydrogel constructs of hyaluronic acid, collagen, and laminin for neural tissue engineering', *Tissue Eng Part A*, 2010, **16**(5), 1703-1716.
134. J. Sun, W. Xiao, Y. Tang, K. Li, and H. Fan: 'Biomimetic interpenetrating polymer network hydrogels based on methacrylated alginate and collagen for 3D pre-osteoblast spreading and osteogenic differentiation', *Soft Matter*, 2012, **8**(8), 2398-2404.
135. A. Maleki, A.-L. Kjøniksen, and B. Nyström: 'Characterization of the chemical degradation of hyaluronic acid during chemical gelation in the presence of different cross-linker agents', *Carbohydrate research*, 2007, **342**(18), 2776-2792.
136. C. Williams, E. Budina, W. L. Stoppel, K. E. Sullivan, S. Emani, S. M. Emani, and L. D. Black: 'Cardiac extracellular matrix–fibrin hybrid scaffolds with tunable properties for cardiovascular tissue engineering', *Acta biomaterialia*, 2015, **14**, 84-95.
137. T. G. Kim, H. J. Chung, and T. G. Park: 'Macroporous and nanofibrous hyaluronic acid/collagen hybrid scaffold fabricated by concurrent electrospinning and deposition/leaching of salt particles', *Acta Biomater.*, 2008, **4**(6), 1611-1619.
138. A. Shapira, R. Feiner, and T. Dvir: 'Composite biomaterial scaffolds for cardiac tissue engineering', *International Materials Reviews*, 2016, **61**(2), 127-146.
139. S. Heydarkhan-Hagvall, K. Schenke-Layland, A. P. Dhanasopon, F. Rofail, H. Smith, B. M. Wu, R. Shemin, R. E. Beygui, and W. R. MacLellan: 'Three-dimensional electrospun ECM-based hybrid scaffolds for cardiovascular tissue engineering', *Biomaterials*, 2008, **29**(19), 2907-2914.

140. H. Davis and J. Leach: 'Hybrid and composite biomaterials in tissue engineering', *Topics in Multifunctional Biomaterials and Devices, Department of Biomedical Eng., University of California*, 2008.
141. R. Jin, L. M. Teixeira, P. Dijkstra, C. Van Blitterswijk, M. Karperien, and J. Feijen: 'Enzymatically-crosslinked injectable hydrogels based on biomimetic dextran–hyaluronic acid conjugates for cartilage tissue engineering', *Biomaterials*, 2010, **31**(11), 3103-3113.
142. X. Xin, A. Borzacchiello, P. Netti, L. Ambrosio, and L. Nicolais: 'Hyaluronic-acid-based semi-interpenetrating materials', *Journal of Biomaterials Science, Polymer Edition*, 2004, **15**(9), 1223-1236.
143. G. H. Hudalla and W. L. Murphy: 'Mimicking the Extracellular Matrix: The Intersection of Matrix Biology and Biomaterials', 2015, Royal Society of Chemistry.
144. F. Bonafè, M. Govoni, E. Giordano, C. M. Caldarera, C. Guarnieri, and C. Muscari: 'Hyaluronan and cardiac regeneration', *Journal of biomedical science*, 2014, **21**(1), 1.
145. R. Jin, L. Moreira Teixeira, P. Dijkstra, C. van Blitterswijk, M. Karperien, and J. Feijen: 'Enzymatically-crosslinked injectable hydrogels based on biomimetic dextran–hyaluronic acid conjugates for cartilage tissue engineering', *Biomaterials*, 2010, **31**(11), 3103-3113.
146. Y. Guo, T. Yuan, Z. Xiao, P. Tang, Y. Xiao, Y. Fan, and X. Zhang: 'Hydrogels of collagen/chondroitin sulfate/hyaluronan interpenetrating polymer network for cartilage tissue engineering', *J. Mater. Sci. Mater. Med.*, 2012, **23**(9), 2267-2279.
147. R. C. Dutta, M. Dey, A. K. Dutta, and B. Basu: 'Competent processing techniques for scaffolds in tissue engineering', *Biotechnology Advances*, 2017, **35**(2), 240-250.
148. S. Wu, B. Duan, X. Qin, and J. T. Butcher: 'Living nano-micro fibrous woven fabric/hydrogel composite scaffolds for heart valve engineering', *Acta Biomaterialia*, 2017, **51**, 89-100.
149. H. V. Almeida, B. N. Sathy, I. Dudurych, C. T. Buckley, F. J. O'Brien, and D. J. Kelly: 'Anisotropic Shape-Memory Alginate Scaffolds Functionalized with Either Type I or Type II Collagen for Cartilage Tissue Engineering', *Tissue Engineering Part A*, 2017, **23**(1-2), 55-68.
150. N. Celikkin, C. Rinoldi, M. Costantini, M. Trombetta, A. Rainer, and W. Święszkowski: 'Naturally derived proteins and glycosaminoglycan scaffolds for

tissue engineering applications', *Materials Science and Engineering: C*, 2017, **42** (3), 684-689.

151. A. Hasan, J. Saliba, H. P. Modarres, A. Bakhaty, A. Nasajpour, M. R. Mofrad, and A. Sanati-Nezhad: 'Micro and nanotechnologies in heart valve tissue engineering', *Biomaterials*, 2016, **103**, 278-292.
152. F. Lee and M. Kurisawa: 'Formation and stability of interpenetrating polymer network hydrogels consisting of fibrin and hyaluronic acid for tissue engineering', *Acta Biomater.*, 2013, **9**(2), 5143-5152.
153. N. Shanmugasundaram, P. Ravichandran, P. Neelakanta Reddy, N. Ramamurty, S. Pal, and K. Panduranga Rao: 'Collagen–chitosan polymeric scaffolds for the in vitro culture of human epidermoid carcinoma cells', *Biomaterials*, 2001, **22**(14), 1943-1951.
154. J. Zhu and R. E. Marchant: 'Design properties of hydrogel tissue-engineering scaffolds', 2011.
155. P. Khoshakhlagh and M. J. Moore: 'Photoreactive interpenetrating network of hyaluronic acid and Puramatrix as a selectively tunable scaffold for neurite growth', *Acta Biomater.*, 2015, **16**, 23-34.
156. D. A. Prawel, H. Dean, M. Forleo, N. Lewis, J. Gangwish, K. C. Popat, L. P. Dasi, and S. P. James: 'Hemocompatibility and Hemodynamics of Novel Hyaluronan–Polyethylene Materials for Flexible Heart Valve Leaflets', *Cardiovasc. Eng. Technol.*, 2013, **5**(1), 70-81.
157. A. Kheradvar, E. M. Groves, L. P. Dasi, S. H. Alavi, R. Tranquillo, K. J. Grande-Allen, C. A. Simmons, B. Griffith, A. Falahatpisheh, C. J. Goergen, M. R. K. Mofrad, F. Baaijens, S. H. Little, and S. Canic: 'Emerging Trends in Heart Valve Engineering: Part I. Solutions for Future', *Ann. Biomed. Eng.*, 2014, **43**(4), 833-843.
158. A. L. Barnes, P. G. Genever, S. Rimmer, and M. C. Coles: 'Collagen–poly (N-isopropylacrylamide) hydrogels with tunable properties', *Biomacromolecules*, 2016, **17**(3), 723-734.
159. A. Sionkowska, J. Skopinska-Wisniewska, M. Gawron, J. Kozlowska, and A. Planecka: 'Chemical and thermal cross-linking of collagen and elastin hydrolysates', *Int. J. Biol. Macromol.*, 2010, **47**(4), 570-577.
160. K. S. Weadock, E. J. Miller, L. D. Bellincampi, J. P. Zawadsky, and M. G. Dunn: 'Physical crosslinking of collagen fibers: comparison of ultraviolet irradiation and

dehydrothermal treatment', *Journal of biomedical materials research*, 1995, **29**(11), 1373-1379.

161. M. Madaghiele, E. Calò, L. Salvatore, V. Bonfrate, D. Pedone, M. Frigione, and A. Sannino: 'Assessment of collagen crosslinking and denaturation for the design of regenerative scaffolds', *Journal of Biomedical Materials Research Part A*, 2016, **104**(1), 186-194.
162. R. Alessandro, V. Brucato, L. Rimondini, and G. Spadaro: 'I materiali biocompatibili per la medicina / Biomaterials for Medicine: Atti del Convegno Nazionale della Società Italiana Biomateriali. Palermo, 2-4 luglio 2014', 2014, Universitas Studiorum.
163. M. G. Haugh, M. J. Jaasma, and F. J. O'Brien: 'The effect of dehydrothermal treatment on the mechanical and structural properties of collagen-GAG scaffolds', *Journal of Biomedical Materials Research Part A*, 2009, **89**(2), 363-369.
164. S. Sethuraman, U. M. Krishnan, and A. Subramanian: 'Biomaterials and Nanotechnology for Tissue Engineering', 2016, CRC Press.
165. M. P. Ohan and M. G. Dunn: 'Glucose stabilizes collagen sterilized with gamma irradiation', *Journal of Biomedical Materials Research Part A*, 2003, **67**(4), 1188-1195.
166. N. Inoue, M. Bessho, M. Furuta, T. Kojima, S. Okuda, and M. Hara: 'A novel collagen hydrogel cross-linked by gamma-ray irradiation in acidic pH conditions', *Journal of Biomaterials Science, Polymer Edition*, 2006, **17**(8), 837-858.
167. L. M. Roa: 'XIII Mediterranean Conference on Medical and Biological Engineering and Computing 2013: MEDICON 2013, 25-28 September 2013, Seville, Spain', 2013, Springer International Publishing.
168. D. T. Cheung, N. Perelman, D. Tong, and M. E. Nimni: 'The effect of γ-irradiation on collagen molecules, isolated α-chains, and crosslinked native fibers', *Journal of Biomedical Materials Research Part A*, 1990, **24**(5), 581-589.
169. W. Q. Sun and P. Leung: 'Calorimetric study of extracellular tissue matrix degradation and instability after gamma irradiation', *Acta Biomater.*, 2008, **4**(4), 817-826.
170. J. F. Kennedy, G. O. Phillips, and P. A. Williams: 'Sterilisation of tissues using ionizing radiations', 2005, Taylor & Francis.
171. N. Davidenko, D. V. Bax, C. F. Schuster, R. W. Farndale, S. W. Hamaia, S. M. Best, and R. E. Cameron: 'Optimisation of UV irradiation as a binding site conserving

method for crosslinking collagen-based scaffolds', *Journal of Materials Science. Materials in Medicine*, 2016, **27**, 14.

172. H. Niknejad and R. Mahmoudzadeh: 'Comparison of Different Crosslinking Methods for Preparation of Docetaxel-loaded Albumin Nanoparticles', *Iranian Journal of Pharmaceutical Research : IJPR*, 2015, **14**(2), 385-394.
173. S. Dumitriu and V. Popa: 'Polymeric Biomaterials: Structure and Function', 2013, CRC Press.
174. J. E. Lee, J. C. Park, Y. S. Hwang, J. K. Kim, J. G. Kim, and H. Suh: 'Characterization of UV-irradiated dense/porous collagen membranes: morphology, enzymatic degradation, and mechanical properties', *Yonsei Medical Journal*, 2001, **42**(2), 172-179.
175. J. Baier Leach, K. A. Bivens, C. W. Patrick Jr, and C. E. Schmidt: 'Photocrosslinked hyaluronic acid hydrogels: natural, biodegradable tissue engineering scaffolds', *Biotechnology and bioengineering*, 2003, **82**(5), 578-589.
176. M. D. Brigham: 'Collagen and hyaluronic acid interpenetrating polymer networks for tissue engineering', Massachusetts Institute of Technology, 2007.
177. M. D. Brigham, A. Bick, E. Lo, A. Bendali, J. A. Burdick, and A. Khademhosseini: 'Mechanically robust and bioadhesive collagen and photocrosslinkable hyaluronic acid semi-interpenetrating networks', *Tissue Eng Part A*, 2008, **15**(7), 1645-1653.
178. T. Scheibel: 'Recombinant mussel byssus protein', 2007, US Patent No. EP1787995 A1.
179. N. E. Fedorovich, M. H. Oudshoorn, D. van Geemen, W. E. Hennink, J. Alblas, and W. J. Dhert: 'The effect of photopolymerization on stem cells embedded in hydrogels', *Biomaterials*, 2009, **30**(3), 344-353.
180. C. G. Williams, A. N. Malik, T. K. Kim, P. N. Manson, and J. H. Elisseeff: 'Variable cytocompatibility of six cell lines with photoinitiators used for polymerizing hydrogels and cell encapsulation', *Biomaterials*, 2005, **26**(11), 1211-1218.
181. P. Puttawibul, J. Meesane, and S. Benjakul: 'Preparation and characterization of type I collagen/PVA hybrid biomimetic hydrogels scaffold for wound healing', Biomedical Engineering International Conference (BMEiCON), 2012, 2012, IEEE, 1-4.
182. V. J. Ferrans, T. Xenakis, R. A. Hopkins, S. L. Hilbert, M. Jones, P. L. Lange, and L. J. Wolfinbarger: 'Cardiac Reconstructions with Allograft Valves', 2012, Springer New York.

183. R. Sidwell and M. Thomson: 'Concise Paediatrics, Second Edition', 2009, Arnold.
184. L. O. Damink, P. Dijkstra, M. Van Luyn, P. Van Wachem, P. Nieuwenhuis, and J. Feijen: 'Glutaraldehyde as a crosslinking agent for collagen-based biomaterials', *J. Mater. Sci. Mater. Med.*, 1995, **6**(8), 460-472.
185. M. Kikuchi, H. N. Matsumoto, T. Yamada, Y. Koyama, K. Takakuda, and J. Tanaka: 'Glutaraldehyde cross-linked hydroxyapatite/collagen self-organized nanocomposites', *Biomaterials*, 2004, **25**(1), 63-69.
186. J.-i. Kawahara, K. Ishikawa, T. Uchimaru, and H. Takaya: 'Chemical cross-linking by glutaraldehyde between amino groups: its mechanism and effects', in 'Polymer Modification', 119-131; 1997, Springer.
187. T.-H. Nguyen and B.-T. Lee: 'Fabrication and characterization of cross-linked gelatin electro-spun nano-fibers', *J Biomed Sci Eng*, 2010, **3**(12), 1117.
188. C.-S. Ko, J.-P. Huang, C.-W. Huang, and I. Chu: 'Type II collagen-chondroitin sulfate-hyaluronan scaffold cross-linked by genipin for cartilage tissue engineering', *J. Biosci. Bioeng.*, 2009, **107**(2), 177-182.
189. L. P. Yan, Y. J. Wang, L. Ren, G. Wu, S. G. Caridade, J. B. Fan, L. Y. Wang, P. H. Ji, J. M. Oliveira, and J. T. Oliveira: 'Genipin-cross-linked collagen/chitosan biomimetic scaffolds for articular cartilage tissue engineering applications', *J. Biomed. Mater. Res. A*, 2010, **95**(2), 465-475.
190. R. A. A. Muzzarelli, M. El Mehtedi, C. Bottegoni, A. Aquili, and A. Gigante: 'Genipin-Crosslinked Chitosan Gels and Scaffolds for Tissue Engineering and Regeneration of Cartilage and Bone', *Marine Drugs*, 2015, **13**(12), 7314-7338.
191. C. Yang: 'Enhanced physicochemical properties of collagen by using EDC/NHS-crosslinking', *Bull. Mater. Sci.*, 2012, **35**(5), 913-918.
192. A. Sionkowska: 'Current research on the blends of natural and synthetic polymers as new biomaterials: Review', *Progress in Polymer Science*, 2011, **36**(9), 1254-1276.
193. K. Nam, T. Kimura, and A. Kishida: 'Controlling Coupling Reaction of EDC and NHS for Preparation of Collagen Gels Using Ethanol/Water Co-Solvents', *Macromolecular bioscience*, 2008, **8**(1), 32-37.
194. L. Calderon, E. Collin, M. Murphy, D. O'Halloran, and A. Pandit: 'Type II collagen-hyaluronan hydrogel-a step towards a scaffold for intervertebral disc tissue engineering', 2010.
195. B. Hafemann, K. Ghofrani, H.-G. Gattner, H. Stieve, and N. Pallua: 'Cross-linking by 1-ethyl-3-(3-dimethylaminopropyl)-carbodiimide (EDC) of a collagen/elastin

membrane meant to be used as a dermal substitute: effects on physical, biochemical and biological features in vitro', *J. Mater. Sci. Mater. Med.*, 2001, **12**(5), 437-446.

196. J. Shepherd, S. Ghose, S. Kew, A. Moavenian, S. M. Best, and R. E. Cameron: 'Effect of fiber crosslinking on collagen-fiber reinforced collagen–chondroitin-6-sulfate materials for regenerating load-bearing soft tissues', *J. Biomed. Mater. Res. A*, 2013, **101**(1), 176-184.
197. N. Vrana, N. Builles, H. Kocak, P. Gulay, V. Justin, M. Malbouyres, F. Ruggiero, O. Damour, and V. Hasirci: 'EDC/NHS cross-linked collagen foams as scaffolds for artificial corneal stroma', *J. Biomater. Sci., Polym. Ed.*, 2007, **18**(12), 1527-1545.
198. Y. Tabata, M. Miyao, M. Ozeki, and Y. Ikada: 'Controlled release of vascular endothelial growth factor by use of collagen hydrogels', *J. Biomater. Sci., Polym. Ed.*, 2000, **11**(9), 915-930.
199. B. A. Harley, J. H. Leung, E. C. Silva, and L. J. Gibson: 'Mechanical characterization of collagen–glycosaminoglycan scaffolds', *Acta Biomater.*, 2007, **3**(4), 463-474.
200. R. A. Hortensius and B. A. Harley: 'The use of bioinspired alterations in the glycosaminoglycan content of collagen–GAG scaffolds to regulate cell activity', *Biomaterials*, 2013, **34**(31), 7645-7652.
201. M. G. Haugh, C. M. Murphy, R. C. McKiernan, C. Altenbuchner, and F. J. O'Brien: 'Crosslinking and mechanical properties significantly influence cell attachment, proliferation, and migration within collagen glycosaminoglycan scaffolds', *Tissue Engineering Part A*, 2011, **17**(9-10), 1201-1208.
202. N. Davidenko, J. Campbell, E. Thian, C. Watson, and R. E. Cameron: 'Collagen–hyaluronic acid scaffolds for adipose tissue engineering', *Acta biomaterialia*, 2010, **6**(10), 3957-3968.
203. K. Weadock, R. M. Olson, and F. H. Silver: 'Evaluation of collagen crosslinking techniques', *Biomaterials, medical devices, and artificial organs*, 1983, **11**(4), 293-318.
204. J. Shepherd, D. Bax, S. Best, and R. Cameron: 'Collagen-Fibrinogen Lyophilised Scaffolds for Soft Tissue Regeneration', *Materials*, 2017, **10**(6), 568.
205. C. O. Au and I. Thorn: 'Applications of Wet-End Paper Chemistry', 2013, Springer Netherlands.
206. M. Jafari-Sabet, H. Nasiri, and R. Ataee: 'The Effect of Cross-Linking Agents and Collagen Concentrations on Properties of Collagen Scaffolds', *Journal of Archives of Military Medicine*, 2016, **4**(4).

207. L. S. M. Teixeira, J. Feijen, C. A. van Blitterswijk, P. J. Dijkstra, and M. Karperien: 'Enzyme-catalyzed crosslinkable hydrogels: emerging strategies for tissue engineering', *Biomaterials*, 2012, **33**(5), 1281-1290.

208. F. Lee, J. E. Chung, and M. Kurisawa: 'An injectable hyaluronic acid–tyramine hydrogel system for protein delivery', *Journal of Controlled Release*, 2009, **134**(3), 186-193.

209. T. Wu, Y. Li, and D. S. Lee: 'Chitosan-based composite hydrogels for biomedical applications', *Macromolecular Research*, 2017, 1-9.

210. N. Reddy, R. Reddy, and Q. Jiang: 'Crosslinking biopolymers for biomedical applications', *Trends in Biotechnology*, **33**(6), 362-369.

211. C. N. Grover, R. E. Cameron, and S. M. Best: 'Investigating the morphological, mechanical and degradation properties of scaffolds comprising collagen, gelatin and elastin for use in soft tissue engineering', *Journal of the mechanical behavior of biomedical materials*, 2012, **10**, 62-74.

212. L. Ma, C. Gao, Z. Mao, J. Zhou, and J. Shen: 'Enhanced biological stability of collagen porous scaffolds by using amino acids as novel cross-linking bridges', *Biomaterials*, 2004, **25**(15), 2997-3004.

213. P. Ducheyne, K. Healy, D. E. Hutmacher, D. W. Grainger, and C. J. Kirkpatrick: 'Comprehensive Biomaterials', 2011, Elsevier Science.

214. S. C. Gad and S. Gad-McDonald: 'Biomaterials, Medical Devices, and Combination Products: Biocompatibility Testing and Safety Assessment', 2015, CRC Press.

215. S.-N. Park, J.-C. Park, H. O. Kim, M. J. Song, and H. Suh: 'Characterization of porous collagen/hyaluronic acid scaffold modified by 1-ethyl-3-(3-dimethylaminopropyl) carbodiimide cross-linking', *Biomaterials*, 2002, **23**(4), 1205-1212.

216. J. Patterson, R. Siew, S. W. Herring, A. S. Lin, R. Guldberg, and P. S. Stayton: 'Hyaluronic acid hydrogels with controlled degradation properties for oriented bone regeneration', *Biomaterials*, 2010, **31**(26), 6772-6781.

217. V. Zapotocky, M. Pospisilova, K. Janouchova, D. Svadlak, J. Batova, J. Sogorkova, M. Cepa, J. Betak, V. Stepankova, R. Sulakova, J. Kulhanek, T. Pitucha, J. Vranova, G. Duffy, and V. Velebny: 'Fabrication of biodegradable textile scaffold based on hydrophobized hyaluronic acid', *International Journal of Biological Macromolecules*, 2017, **95**, 903-909.

218. J. Patterson, R. Siew, S. W. Herring, A. S. P. Lin, R. Guldberg, and P. S. Stayton: 'Hyaluronic acid hydrogels with controlled degradation properties for oriented bone regeneration', *Biomaterials*, 2010, **31**(26), 6772-6781.
219. H. Mojarradi: 'Coupling of substances containing a primary amine to hyaluronan via carbodiimide-mediated amidation', 2010.
220. M. Fröhlich, W. L. Grayson, L. Q. Wan, D. Marolt, M. Drobnic, and G. Vunjak-Novakovic: 'Tissue Engineered Bone Grafts: Biological Requirements, Tissue Culture and Clinical Relevance', *Current stem cell research & therapy*, 2008, **3**(4), 254-264.
221. S. Pashneh-Tala, S. MacNeil, and F. Claeyssens: 'The Tissue-Engineered Vascular Graft—Past, Present, and Future', *Tissue Engineering. Part B, Reviews*, 2016, **22**(1), 68-100.
222. S. Jana, R. T. Tranquillo, and A. Lerman: 'Cells for tissue engineering of cardiac valves', *Journal of Tissue Engineering and Regenerative Medicine*, 2016, **10**(10), 804-824.
223. Y. Ikada: 'Challenges in tissue engineering', *Journal of the Royal Society Interface*, 2006, **3**(10), 589-601.
224. B. Duan, E. Kapetanovic, L. A. Hockaday, and J. T. Butcher: 'Three-dimensional printed trileaflet valve conduits using biological hydrogels and human valve interstitial cells', *Acta Biomaterialia*, 2014, **10**(5), 1836-1846.
225. U. A. Stock and J. P. Vacanti: 'Tissue engineering: current state and prospects', *Annual review of medicine*, 2001, **52**, 443-451.
226. Q. Chen, A. Bruyneel, C. Carr, and J. Czernuszka: 'Bio-mechanical properties of novel bi-layer collagen-elastin scaffolds for heart valve tissue engineering', *Procedia Engineering*, 2013, **59**, 247-254.
227. T. C. Flanagan and A. Pandit: 'Living artificial heart valve alternatives: a review', *Eur Cell Mater*, 2003, **6**(1), 28-45.
228. K. Takahashi and S. Yamanaka: 'Induction of Pluripotent Stem Cells from Mouse Embryonic and Adult Fibroblast Cultures by Defined Factors', *Cell*, **126**(4), 663-676.
229. A. Ratcliffe and L. E. Niklason: 'Bioreactors and bioprocessing for tissue engineering', *Ann N Y Acad Sci*, 2002, **961**, 210-215.
230. N. Plunkett and F. J. O'Brien: 'Bioreactors in tissue engineering', *Technology and health care : official journal of the European Society for Engineering and Medicine*, 2011, **19**(1), 55-69.

231. L. E. Freed, F. Guilak, X. E. Guo, M. L. Gray, R. Tranquillo, J. W. Holmes, M. Radisic, M. V. Sefton, D. Kaplan, and G. Vunjak-Novakovic: 'Advanced tools for tissue engineering: scaffolds, bioreactors, and signaling', *Tissue Eng*, 2006, **12**(12), 3285-3305.

232. L. Buttafoco, P. Engbers-Buijtenhuijs, A. A. Poot, P. J. Dijkstra, I. Vermes, and J. Feijen: 'Physical characterization of vascular grafts cultured in a bioreactor', *Biomaterials*, 2006, **27**(11), 2380-2389.

233. H. Park, B. L. Larson, M. E. Kolewe, G. Vunjak-Novakovic, and L. E. Freed: 'Biomimetic scaffold combined with electrical stimulation and growth factor promotes tissue engineered cardiac development', *Exp. Cell Res.*, 2014, **321**(2), 297-306.

234. J. S. Wendel, L. Ye, P. Zhang, R. T. Tranquillo, and J. J. Zhang: 'Functional consequences of a tissue-engineered myocardial patch for cardiac repair in a rat infarct model', *Tissue Eng Part A*, 2014, **20**(7-8), 1325-1335.

235. C. Best, E. Onwuka, V. Pepper, M. Sams, J. Breuer, and C. Breuer: 'Cardiovascular tissue engineering: preclinical validation to bedside application', *Physiology*, 2016, **31**(1), 7-15.

236. A. Y. Lee, N. Mahler, C. Best, Y.-U. Lee, and C. K. Breuer: 'Regenerative implants for cardiovascular tissue engineering', *Translational Research*, 2014, **163**(4), 321-341.

237. G. Vunjak-Novakovic: 'Tissue engineering of the heart: An evolving paradigm', *The Journal of Thoracic and Cardiovascular Surgery*, 2017, **153**(3), 593-595.

238. T. Freyman, I. Yannas, and L. Gibson: 'Cellular materials as porous scaffolds for tissue engineering', *Progress in Materials Science*, 2001, **46**(3), 273-282.

239. S. J. Hollister: 'Porous scaffold design for tissue engineering', *Nature materials*, 2005, **4**(7), 518-524.

240. G. Camci-Unal, D. Cuttica, N. Annabi, D. Demarchi, and A. Khademhosseini: 'Synthesis and characterization of hybrid hyaluronic acid-gelatin hydrogels', *Biomacromolecules*, 2013, **14**(4), 1085-1092.

241. D. W. Kitzman, D. G. Schloz, P. T. Hagen, D. M. Ilstrup, and W. D. Edwards: 'Age-related changes in normal human hearts during the first 10 decades of life. Part II (maturity): a quantitative anatomic study of 765 specimens from subjects 20 to 99 years old', Mayo Clinic Proceedings, 1988, Elsevier, 137-146.

242. T. Lu, Y. Li, and T. Chen: 'Techniques for fabrication and construction of three-dimensional scaffolds for tissue engineering', *International journal of nanomedicine*, 2013, **8**, 337.
243. H.-W. Kang, Y. Tabata, and Y. Ikada: 'Fabrication of porous gelatin scaffolds for tissue engineering', *Biomaterials*, 1999, **20**(14), 1339-1344.
244. P. F. Gratzer and J. M. Lee: 'Control of pH alters the type of cross-linking produced by 1-ethyl-3-(3-dimethylaminopropyl)-carbodiimide (EDC) treatment of acellular matrix vascular grafts', *Journal of biomedical materials research*, 2001, **58**(2), 172-179.
245. Z. Grabarek and J. Gergely: 'Zero-length crosslinking procedure with the use of active esters', *Analytical biochemistry*, 1990, **185**(1), 131-135.
246. P. Buijtenhuijs, L. Buttafoco, A. A. Poot, W. F. Daamen, T. H. Van Kuppevelt, P. J. Dijkstra, R. A. De Vos, L. M. T. Sterk, B. R. Geelkerken, and J. Feijen: 'Tissue engineering of blood vessels: characterization of smooth-muscle cells for culturing on collagen-and-elastin-based scaffolds', *Biotechnology and applied biochemistry*, 2004, **39**(2), 141-149.
247. C. Picart, R. Elkaim, L. Richert, F. Audoin, Y. Arntz, M. Da Silva Cardoso, P. Schaaf, J. C. Voegel, and B. Frisch: 'Primary Cell Adhesion on RGD-Functionalized and Covalently Crosslinked Thin Polyelectrolyte Multilayer Films', *Advanced Functional Materials*, 2005, **15**(1), 83-94.
248. W. Friess: 'Collagen–biomaterial for drug delivery', *European Journal of Pharmaceutics and Biopharmaceutics*, 1998, **45**(2), 113-136.
249. K. H. Gustavson: 'Chemistry and reactivity of collagen', 1956.
250. R. Zeeman: 'Cross-linking of collagen-based materials', 1998, Universiteit Twente.
251. N. Davidenko, C. Schuster, D. Bax, N. Raynal, R. Farndale, S. Best, and R. Cameron: 'Control of crosslinking for tailoring collagen-based scaffolds stability and mechanics', *Acta biomaterialia*, 2015, **25**, 131-142.
252. C.-M. Hsieh, Y.-W. Huang, M.-T. Sheu, and H.-O. Ho: 'Biodistribution profiling of the chemical modified hyaluronic acid derivatives used for oral delivery system', *International journal of biological macromolecules*, 2014, **64**, 45-52.
253. R. S. H. Wong, M. Ashton, and K. Dodou: 'Effect of crosslinking agent concentration on the properties of unmedicated hydrogels', *Pharmaceutics*, 2015, **7**(3), 305-319.

254. M. N. Collins and C. Birkinshaw: 'Investigation of the swelling behavior of crosslinked hyaluronic acid films and hydrogels produced using homogeneous reactions', *Journal of applied polymer science*, 2008, **109**(2), 923-931.
255. Q. Xing, K. Yates, C. Vogt, Z. Qian, M. C. Frost, and F. Zhao: 'Increasing mechanical strength of gelatin hydrogels by divalent metal ion removal', *Scientific reports*, 2014, **4**.
256. S. Balaghi: 'Development of Rheo-Additives and their Applications in Food Technology', 2015, epubli GmbH.
257. I. M. Watt: 'The Principles and Practice of Electron Microscopy', 1997, Cambridge University Press.
258. A. Bandyopadhyay and S. Bose: 'Characterization of Biomaterials', 2013, Elsevier Science.
259. S. Yamabayashi: 'Periodic acid-Schiff-alcian blue: a method for the differential staining of glycoproteins', *The Histochemical journal*, 1987, **19**(10-11), 565-571.
260. J. D. Bancroft and M. Gamble: 'Theory and Practice of Histological Techniques', 2008, Churchill Livingstone.
261. M. R.W.: 'Alcian blue techniques for the histochemical study of acidic carbohydrates', *J Histochem and Cytochem*, 1956, 403-407.
262. G. Gauglitz and D. S. Moore: 'Handbook of Spectroscopy, 4 Volume Set', 2014, Wiley.
263. B. C. Smith: 'Fundamentals of Fourier Transform Infrared Spectroscopy, Second Edition', 2011, CRC Press.
264. P. Gabbott: 'Principles and Applications of Thermal Analysis', 2008, Wiley.
265. M. M. Coleman and P. C. Painter: 'Fundamentals of Polymer Science: An Introductory Text, Second Edition', 1998, Taylor & Francis.
266. X. Wang, D. Li, W. Wang, Q. Feng, F. Cui, Y. Xu, X. Song, and M. van der Werf: 'Crosslinked collagen/chitosan matrix for artificial livers', *Biomaterials*, 2003, **24**(19), 3213-3220.
267. F. Bonnier, S. Rubin, L. Ventéo, C. Krishna, M. Pluot, B. Baehrel, M. Manfait, and G. Sockalingum: 'In-vitro analysis of normal and aneurismal human ascending aortic tissues using FT-IR microspectroscopy', *Biochimica et Biophysica Acta (BBA)-Biomembranes*, 2006, **1758**(7), 968-973.
268. F. J. L. Everaerts: 'A novel approach in cross-linking of bioprosthetic heart valves', 2007, University of Twente.

269. B. C. Smith: 'Infrared spectral interpretation: a systematic approach', 1998, CRC press.
270. F. Everaerts, M. Torrianni, M. Hendriks, and J. Feijen: 'Biomechanical properties of carbodiimide crosslinked collagen: influence of the formation of ester crosslinks', *Journal of Biomedical Materials Research Part A*, 2008, **85**(2), 547-555.
271. E. Baslé, N. Joubert, and M. Pucheault: 'Protein Chemical Modification on Endogenous Amino Acids', *Chemistry & Biology*, 2010, **17**(3), 213-227.
272. S.-N. Park, J.-C. Park, H. O. Kim, M. J. Song, and H. Suh: 'Characterization of porous collagen/hyaluronic acid scaffold modified by 1-ethyl-3-(3-dimethylaminopropyl)carbodiimide cross-linking', *Biomaterials*, 2002, **23**(4), 1205-1212.
273. A. Martínez, M. Blanco, N. Davidenko, and R. Cameron: 'Tailoring chitosan/collagen scaffolds for tissue engineering: Effect of composition and different crosslinking agents on scaffold properties', *Carbohydrate polymers*, 2015, **132**, 606-619.
274. G. Tronci, A. Doyle, S. J. Russell, and D. J. Wood: 'Structure-property-function relationships in triple-helical collagen hydrogels', MRS Proceedings, 2013, Cambridge Univ Press, 145-150.
275. L. B. Koh, M. M. Islam, D. Mitra, C. W. Noel, K. Merrett, S. Odorcic, P. Fagerholm, W. B. Jackson, B. Liedberg, J. Phopase, and M. Griffith: 'Epoxy Cross-Linked Collagen and Collagen-Laminin Peptide Hydrogels as Corneal Substitutes', *Journal of Functional Biomaterials*, 2013, **4**(3), 162-177.
276. L. Cahalan, P. T. Cahalan, B. Fouache, M. Hendriks, M. W. Torrianni, and M. Verhoeven: 'A method of crosslinking collagen-based material and bioprosthetic devices produced therefrom', 1999, Google Patents.
277. J. F. Mano: 'Biomimetic approaches for biomaterials development', 2013, John Wiley & Sons.
278. C. Vasile: 'Environmentally Degradable Materials based on Multicomponent Polymeric Systems', 2009, CRC Press.
279. M. McKegney, I. Taggart, and M. Grant: 'The influence of crosslinking agents and diamines on the pore size, morphology and the biological stability of collagen sponges and their effect on cell penetration through the sponge matrix', *Journal of Materials Science: Materials in Medicine*, 2001, **12**(9), 833-844.

280. E. Ruvinov, S. Cohen, and Y. Sapir: 'Cardiac Tissue Engineering: Principles, Materials, and Applications', 2012, Morgan & Claypool.
281. N. A. Peppas and M. V. Sefton: 'Molecular and Cellular Foundations of Biomaterials', 2004, Elsevier / Academic Press.
282. M. Amri, M. Firdaus, M. Fauzi, S. R. Chowdhury, N. Fadilah, W. Wan Hamirul, M. Reusmaazran, B. Aminuddin, and B. Ruszymah: 'Cytotoxic evaluation of biomechanically improved crosslinked ovine collagen on human dermal fibroblasts', *Bio-medical materials and engineering*, 2014, **24**(4), 1715-1724.
283. R. G. Paul and A. J. Bailey: 'Chemical stabilisation of collagen as a biomimetic', *The Scientific World Journal*, 2003, **3**, 138-155.
284. A. Botzki: 'Structure-based design of hyaluronidase inhibitors', 2004.
285. Y.-t. Wei, F.-z. Cui, and W.-m. Tian: 'Fabrication and characterization of hyaluronic-acid-based antigen sensitive degradable hydrogel', *Frontiers of Materials Science in China*, 2009, **3**(4), 353-358.
286. S. K. Hahn, R. Ohri, and C. M. Giachelli: 'Anti-calcification of bovine pericardium for bioprosthetic heart valves after surface modification with hyaluronic acid derivatives', *Biotechnology and Bioprocess Engineering*, 2005, **10**(3), 218-224.
287. J. S. Pieper, T. Hafmans, J. H. Veerkamp, and T. H. van Kuppevelt: 'Development of tailor-made collagen-glycosaminoglycan matrices: EDC/NHS crosslinking, and ultrastructural aspects', *Biomaterials*, 2000, **21**(6), 581-593.
288. N. Davidenko, C. F. Schuster, D. V. Bax, N. Raynal, R. W. Farndale, S. M. Best, and R. E. Cameron: 'Control of crosslinking for tailoring collagen-based scaffolds stability and mechanics', *Acta Biomaterialia*, 2015, **25**, 131-142.
289. E. Sachlos and J. Czernuszka: 'Making tissue engineering scaffolds work. Review: the application of solid freeform fabrication technology to the production of tissue engineering scaffolds', *Eur Cell Mater*, 2003, **5**(29), 39-40.
290. G. E. Tatagiri, G. Collins, and M. Jaffe: 'Spinning of collagen fibers and characterizing thermal, mechanical, tensile and structural properties', Bioengineering Conference, 2004. Proceedings of the IEEE 30th Annual Northeast, 2004, IEEE, 134-135.
291. M. N. Collins and C. Birkinshaw: 'Hyaluronic acid based scaffolds for tissue engineering—A review', *Carbohydrate polymers*, 2013, **92**(2), 1262-1279.
292. C. Englert, T. Blunk, R. Müller, S. S. von Glasser, J. Baumer, J. Fierlbeck, I. M. Heid, M. Nerlich, and J. Hammer: 'Bonding of articular cartilage using a combination

of biochemical degradation and surface cross-linking', *Arthritis Res Ther*, 2007, **9**(3), R47.

293. A. Gandaglia, A. Bagno, F. Naso, M. Spina, and G. Gerosa: 'Cells, scaffolds and bioreactors for tissue-engineered heart valves: a journey from basic concepts to contemporary developmental innovations', *European Journal of Cardio-Thoracic Surgery*, 2011, **39**(4), 523-531.
294. B. Ward, S. Brown, and P. Krebsbach: 'Bioengineering strategies for regeneration of craniofacial bone: a review of emerging technologies', *Oral diseases*, 2010, **16**(8), 709-716.
295. G. G. Walmsley, A. T. Cheung, M. S. Hu, H. P. Lorenz, and M. T. Longaker: 'Osteogenic Differentiation of Adipose-Derived Stromal Cells: Advancements and Future Directions for Bone Tissue Engineering', *Science Proceedings*, 2016, **3**.
296. F. J. O'Brien: 'Biomaterials & scaffolds for tissue engineering', *Materials Today*, 2011, **14**(3), 88-95.
297. S. J. Hollister, R. Maddox, and J. M. Taboas: 'Optimal design and fabrication of scaffolds to mimic tissue properties and satisfy biological constraints', *Biomaterials*, 2002, **23**(20), 4095-4103.
298. D. W. Hutmacher: 'Scaffolds in tissue engineering bone and cartilage', *Biomaterials*, 2000, **21**(24), 2529-2543.
299. N. J. Driessen, A. Mol, C. V. Bouten, and F. P. Baaijens: 'Modeling the mechanics of tissue-engineered human heart valve leaflets', *Journal of biomechanics*, 2007, **40**(2), 325-334.
300. S. L. Hilbert, F. J. Schöen, and V. J. Ferrans: 'Biomechanics: Allograft Heart Valves', in 'Cardiac Reconstructions with Allograft Tissues', 210-212; 2005, Springer.
301. L. Ma, C. Gao, Z. Mao, J. Zhou, J. Shen, X. Hu, and C. Han: 'Collagen/chitosan porous scaffolds with improved biostability for skin tissue engineering', *Biomaterials*, 2003, **24**(26), 4833-4841.
302. J. Ma, H. Wang, B. He, and J. Chen: 'A preliminary in vitro study on the fabrication and tissue engineering applications of a novel chitosan bilayer material as a scaffold of human neofetal dermal fibroblasts', *Biomaterials*, 2001, **22**(4), 331-336.
303. D. Wiltz, C. A. Arevalos, L. R. Balaoing, A. A. Blancas, M. C. Sapp, X. Zhang, and K. J. Grande-Allen: 'Extracellular Matrix Organization, Structure, and Function', in 'Calcific Aortic Valve Disease', (ed. E. Aikawa), Ch. 01; 2013, Rijeka, InTech.

304. Q. Chen: 'Collagen-based scaffolds for heart valve tissue engineering', University of Oxford, 2013.
305. Q. Chen, A. Bruyneel, K. Clarke, C. Carr, and J. Czernuszka: 'Collagen-based Scaffolds for potential application of heart valve tissue engineering', *J Tissue Sci Eng*, 2012, **11**, 003.
306. Q. Chen: 'Collagen-based scaffolds for heart valve tissue engineering ', Doctrol thesis, University of Oxford, 2013.
307. P. Davis, S. Huang, L. Ambrosio, D. Ronca, and L. Nicolais: 'A biodegradable composite artificial tendon', *Journal of Materials Science: Materials in Medicine*, 1992, **3**(5), 359-364.
308. L. J. Gibson and M. F. Ashby: 'Cellular solids: structure and properties', 1999, Cambridge university press.
309. N. C. Mat and F. K. Awam: 'Analysis and Design of Simply Supported Beam with Lateral Restained at Load Application Point by Using Microsoft Excel 2007 for Eurocode 3', 2011, Universiti Teknologi Malaysia.
310. U. R. Acharya, K. P. Joseph, N. Kannathal, C. M. Lim, and J. S. Suri: 'Heart rate variability: a review', *Medical and biological engineering and computing*, 2006, **44**(12), 1031-1051.
311. Q. L. Loh and C. Choong: 'Three-Dimensional Scaffolds for Tissue Engineering Applications: Role of Porosity and Pore Size', *Tissue Engineering. Part B, Reviews*, 2013, **19**(6), 485-502.
312. G. O. Shonaike and S. G. Advani: 'Advanced Polymeric Materials: Structure Property Relationships', 2003, CRC Press.
313. I. Fernández Farrés, R. J. A. Moakes, and I. T. Norton: 'Designing biopolymer fluid gels: A microstructural approach', *Food Hydrocolloids*, 2014, **42, Part 3**, 362-372.
314. R. R. R. Vincent, B. W. Mansel, A. Kramer, K. Kroy, and M. A. K. Williams: 'Micro-rheological behaviour and nonlinear rheology of networks assembled from polysaccharides from the plant cell wall', *New Journal of Physics*, 2013, **15**(3), 035002.
315. K. Urdl, A. Kandelbauer, W. Kern, U. Müller, M. Thebault, and E. Zikulnig-Rusch: 'Self-healing of densely crosslinked thermoset polymers—A critical review', *Progress in Organic Coatings*, 2017, **104**, 232-249.

316. G. J. Papakonstantopoulos, F. J. Feher, C. L. Alwardt, and B. J. Lee: 'Rubber composition having a crosslink distribution, its preparation and article with component', 2017, US Patent No. 20150274945 A1.
317. J. Lam, N. F. Truong, and T. Segura: 'Design of cell–matrix interactions in hyaluronic acid hydrogel scaffolds', *Acta biomaterialia*, 2014, **10**(4), 1571-1580.
318. S. P. Zustiak, Y. Wei, and J. B. Leach: 'Protein–hydrogel interactions in tissue engineering: Mechanisms and applications', *Tissue Engineering Part B: Reviews*, 2012, **19**(2), 160-171.
319. S. Ebnesajjad: 'Handbook of biopolymers and biodegradable plastics: properties, processing and applications', 2012, William Andrew.
320. M. Sewell-Loftin, Y. W. Chun, A. Khademhosseini, and W. D. Merryman: 'EMT-inducing biomaterials for heart valve engineering: taking cues from developmental biology', *Journal of cardiovascular translational research*, 2011, **4**(5), 658-671.
321. D. Mavrilas and Y. Missirlis: 'An approach to the optimization of preparation of bioprosthetic heart valves', *Journal of biomechanics*, 1991, **24**(5), 331-339.
322. W. D. Merryman, H.-Y. S. Huang, F. J. Schoen, and M. S. Sacks: 'The effects of cellular contraction on aortic valve leaflet flexural stiffness', *Journal of biomechanics*, 2006, **39**(1), 88-96.
323. D. S. Puperi, R. W. O'Connell, Z. E. Punske, Y. Wu, J. L. West, and K. J. Grande-Allen: 'Hyaluronan hydrogels for a biomimetic spongiosa layer of tissue engineered heart valve scaffolds', *Biomacromolecules*, 2016, **17**(5), 1766-1775.
324. L. Polo-Corrales, M. Latorre-Esteves, and J. E. Ramirez-Vick: 'Scaffold Design for Bone Regeneration', *Journal of nanoscience and nanotechnology*, 2014, **14**(1), 15-56.
325. J. L. Drury and D. J. Mooney: 'Hydrogels for tissue engineering: scaffold design variables and applications', *Biomaterials*, 2003, **24**(24), 4337-4351.
326. R. Lanza, R. Langer, and J. P. Vacanti: 'Principles of Tissue Engineering', 2011, Elsevier Science.
327. U. Meyer, T. Meyer, J. Handschel, and H. P. Wiesmann: 'Fundamentals of Tissue Engineering and Regenerative Medicine', 2009, Springer Berlin Heidelberg.
328. J. Henkel, M. A. Woodruff, D. R. Epari, R. Steck, V. Glatt, I. C. Dickinson, P. F. Choong, M. A. Schuetz, and D. W. Hutmacher: 'Bone regeneration based on tissue engineering conceptions—a 21st century perspective', *Bone research*, 2013, **1**(3), 216.

329. L. Zhang, J. Hu, and K. A. Athanasiou: 'The role of tissue engineering in articular cartilage repair and regeneration', *Critical Reviews™ in Biomedical Engineering*, 2009, **37**(1-2).

330. H. S. Azevedo and R. L. Reis: 'Understanding the enzymatic degradation of biodegradable polymers and strategies to control their degradation rate', *Biodegradable systems in tissue engineering and regenerative medicine. Boca Raton, FL: CRC Press*, 2005, **177201**.

331. K. A. Blackwood, N. Bock, T. R. Dargaville, and M. Ann Woodruff: 'Scaffolds for growth factor delivery as applied to bone tissue engineering', *International Journal of Polymer Science*, 2012, **2012**.

332. T. Garg, O. Singh, S. Arora, and R. Murthy: 'Scaffold: a novel carrier for cell and drug delivery', *Critical Reviews™ in Therapeutic Drug Carrier Systems*, 2012, **29**(1).

333. Z. Aguilar: 'Nanomaterials for Medical Applications', 2012, Elsevier.

334. R. Narayan, M. Singh, and J. McKittrick: 'Advances in Bioceramics and Biotechnologies: Ceramic Transactions', 2010, Wiley.

335. C. Engineer, J. Parikh, and A. Raval: 'Review on hydrolytic degradation behavior of biodegradable polymers from controlled drug delivery system', *Trends Biomater Artif Organs*, 2011, **25**(2), 79-85.

336. L. Yildirimer, A. Buanz, S. Gaisford, E. L. Malins, C. R. Becer, N. Moiemen, G. M. Reynolds, and A. M. Seifalian: 'Controllable degradation kinetics of POSS nanoparticle-integrated poly (ε-caprolactone urea) urethane elastomers for tissue engineering applications', *Scientific reports*, 2015, **5**.

337. R. Splinter: 'Handbook of Physics in Medicine and Biology', 2010, CRC Press.

338. S. O. Adeosun, G. I. Lawal, and O. P. Gbenebor: 'Characteristics of Biodegradable Implants', *Journal of Minerals and Materials Characterization and Engineering*, 2014, **2014**.

339. R. L. Reis, N. M. Neves, J. F. Mano, M. E. Gomes, A. P. Marques, and H. S. Azevedo: 'Natural-Based Polymers for Biomedical Applications', 2008, Elsevier Science.

340. L. E. Gerweck and K. Seetharaman: 'Cellular pH gradient in tumor versus normal tissue: potential exploitation for the treatment of cancer', *Cancer research*, 1996, **56**(6), 1194-1198.

341. I. F. Tannock and D. Rotin: 'Acid pH in tumors and its potential for therapeutic exploitation', *Cancer research*, 1989, **49**(16), 4373-4384.
342. C. L. Chapman and T. U. o. T. a. A. B. Engineering: 'Gas Permeation Through Nanoporous Polycarbonate Track-etched Membranes: Pulsed Plasma Polymerization of Thin Coatings to Modulate Gas Permeability', 2007, University of Texas at Arlington.
343. B. Testa and J. M. Mayer: 'Hydrolysis in Drug and Prodrug Metabolism', 2003, Wiley.
344. R. G. Compton, C. H. Bamford, and C. F. H. Tipper: 'Ester Formation and Hydrolysis and Related Reactions', 1972, Elsevier Science.
345. A. S. Hoffman: 'Hydrogels for biomedical applications', *Advanced drug delivery reviews*, 2012, **64**, 18-23.
346. S. Zhong, D. Campoccia, P. Doherty, R. Williams, L. Benedetti, and D. Williams: 'Biodegradation of hyaluronic acid derivatives by hyaluronidase', *Biomaterials*, 1994, **15**(5), 359-365.
347. S. Suri and C. E. Schmidt: 'Photopatterned collagen–hyaluronic acid interpenetrating polymer network hydrogels', *Acta Biomaterialia*, 2009, **5**(7), 2385-2397.
348. J. C. Salamone: 'Polymeric Materials Encyclopedia, Twelve Volume Set', 1996, Taylor & Francis.
349. K. C. Dee, D. A. Puleo, and R. Bizios: 'An Introduction to Tissue-Biomaterial Interactions', 2003, Wiley.
350. B. D. Ratner, A. S. Hoffman, F. J. Schoen, and J. E. Lemons: 'Biomaterials Science: An Introduction to Materials in Medicine', 2012, Elsevier Science.
351. J. P. Fisher, A. G. Mikos, J. D. Bronzino, and D. R. Peterson: 'Tissue Engineering: Principles and Practices', 2012, Taylor & Francis.
352. E. Fiumana: 'Stem Cells as a therapy for myocardial infarction in animal models', 2008.
353. D. F. Williams: '25 Tissue engineering: the multidisciplinary epitome of hope and despair', *Studies in multidisciplinarity*, 2005, **3**, 483-524.
354. D. Schmidt and S. P. Hoerstrup: 'Tissue engineered heart valves based on human cells', *Swiss medical weekly*, 2006, **136**(39-40), 618-623.
355. L.-C. Hsiao, C. Carr, K.-C. Chang, S.-Z. Lin, and K. Clarke: 'Stem cell-based therapy for ischemic heart disease', *Cell transplantation*, 2013, **22**(4), 663-675.

356. J. E. Dixon, E. Dick, D. Rajamohan, K. M. Shakesheff, and C. Denning: 'Directed Differentiation of Human Embryonic Stem Cells to Interrogate the Cardiac Gene Regulatory Network', *Mol Ther*, 2011, **19**(9), 1695-1703.

357. R. R. Smith, L. Barile, H. C. Cho, M. K. Leppo, J. M. Hare, E. Messina, A. Giacomello, M. R. Abraham, and E. Marbán: 'Regenerative potential of cardiosphere-derived cells expanded from percutaneous endomyocardial biopsy specimens', *Circulation*, 2007, **115**(7), 896-908.

358. C. A. Carr, D. J. Stuckey, J. J. Tan, S. C. Tan, R. S. Gomes, P. Camelliti, E. Messina, A. Giacomello, G. M. Ellison, and K. Clarke: 'Cardiosphere-derived cells improve function in the infarcted rat heart for at least 16 weeks–an MRI study', *PloS one*, 2011, **6**(10), e25669.

359. S.-T. Lee, A. J. White, S. Matsushita, K. Malliaras, C. Steenbergen, Y. Zhang, T.-S. Li, J. Terrovitis, K. Yee, and S. Simsir: 'Intramyocardial injection of autologous cardiospheres or cardiosphere-derived cells preserves function and minimizes adverse ventricular remodeling in pigs with heart failure post-myocardial infarction', *Journal of the American College of Cardiology*, 2011, **57**(4), 455-465.

360. R. R. Makkar, R. R. Smith, K. Cheng, K. Malliaras, L. E. Thomson, D. Berman, L. S. Czer, L. Marbán, A. Mendizabal, and P. V. Johnston: 'Intracoronary cardiosphere-derived cells for heart regeneration after myocardial infarction (CADUCEUS): a prospective, randomised phase 1 trial', *The Lancet*, 2012, **379**(9819), 895-904.

361. R. R. Smith, E. Marbán, and L. Marbán: 'Enhancing retention and efficacy of cardiosphere-derived cells administered after myocardial infarction using a hyaluronan-gelatin hydrogel', *Biomatter*, 2013, **3**(1), e24490.

362. E. Messina, L. De Angelis, G. Frati, S. Morrone, S. Chimenti, F. Fiordaliso, M. Salio, M. Battaglia, M. V. Latronico, and M. Coletta: 'Isolation and expansion of adult cardiac stem cells from human and murine heart', *Circulation research*, 2004, **95**(9), 911-921.

363. J. J. Tan, C. A. Carr, D. J. Stuckey, G. M. Ellison, E. Messina, A. Giacomello, and K. Clarke: 'Isolation and Expansion of Cardiosphere-Derived Stem Cells', *Current Protocols in Stem Cell Biology*, 2011, 2C. 3.1-2C. 3.12.

364. S. A: 'alamarBlue Technical Datasheet', 2008.

365. A. Yahyouche, X. Zhidao, J. T. Czernuszka, and A. Clover: 'Macrophage-mediated degradation of crosslinked collagen scaffolds', *Acta biomaterialia*, 2011, **7**(1), 278-286.

366. C. G. Knight, L. F. Morton, A. R. Peachey, D. S. Tuckwell, R. W. Farndale, and M. J. Barnes: 'The Collagen-binding A-domains of Integrins α1β1 and α2β1recognize the same specific amino acid sequence, GFOGER, in native (Triple-helical) collagens', *Journal of Biological Chemistry*, 2000, **275**(1), 35-40.
367. C. N. Grover, J. H. Gwynne, N. Pugh, S. Hamaia, R. W. Farndale, S. M. Best, and R. E. Cameron: 'Crosslinking and composition influence the surface properties, mechanical stiffness and cell reactivity of collagen-based films', *Acta biomaterialia*, 2012, **8**(8), 3080-3090.
368. C. M. Murphy, G. P. Duffy, A. Schindeler, and F. J. O'brien: 'Effect of collagen-glycosaminoglycan scaffold pore size on matrix mineralization and cellular behavior in different cell types', *Journal of Biomedical Materials Research Part A*, 2016, **104**(1), 291-304.
369. J. Y. Wong, J. B. Leach, and X. Q. Brown: 'Balance of chemistry, topography, and mechanics at the cell–biomaterial interface: Issues and challenges for assessing the role of substrate mechanics on cell response', *Surface Science*, 2004, **570**(1), 119-133.
370. X. Q. Brown, K. Ookawa, and J. Y. Wong: 'Evaluation of polydimethylsiloxane scaffolds with physiologically-relevant elastic moduli: interplay of substrate mechanics and surface chemistry effects on vascular smooth muscle cell response', *Biomaterials*, 2005, **26**(16), 3123-3129.
371. A. G. Mikos and J. S. Temenoff: 'Formation of highly porous biodegradable scaffolds for tissue engineering', *Electronic Journal of Biotechnology*, 2000, **3**(2), 23-24.
372. K. Leong, C. Chua, N. Sudarmadji, and W. Yeong: 'Engineering functionally graded tissue engineering scaffolds', *Journal of the mechanical behavior of biomedical materials*, 2008, **1**(2), 140-152.
373. A. Marsano, R. Maidhof, L. Q. Wan, Y. Wang, J. Gao, N. Tandon, and G. Vunjak-Novakovic: 'Scaffold stiffness affects the contractile function of three-dimensional engineered cardiac constructs', *Biotechnology progress*, 2010, **26**(5), 1382-1390.
374. B. N. Mason, J. P. Califano, and C. A. Reinhart-King: 'Matrix stiffness: A regulator of cellular behavior and tissue formation', in 'Engineering Biomaterials for Regenerative Medicine', 19-37; 2012, Springer.
375. P. X. Ma and J. Elisseeff: 'Scaffolding In Tissue Engineering', 2005, CRC Press.
376. J. Locker: 'Transcription Factors', 2000, Taylor & Francis.

377. F. M. Berg: 'Health risks associated with weight loss and obesity treatment programs', *Journal of Social Issues*, 1999, **55**(2), 277-297.
378. J. G. Copeland, R. G. Smith, F. A. Arabia, P. E. Nolan, G. K. Sethi, P. H. Tsau, D. McClellan, and M. J. Slepian: 'Cardiac replacement with a total artificial heart as a bridge to transplantation', *New England Journal of Medicine*, 2004, **351**(9), 859-867.
379. J. Chikwe, F. Filsoufi, and A. F. Carpentier: 'Prosthetic valve selection for middle-aged patients with aortic stenosis', *Nature Reviews Cardiology*, 2010, **7**(12), 711-719.
380. S. S. Khan, A. Trento, M. DeRobertis, R. M. Kass, M. Sandhu, L. S. Czer, C. Blanche, S. Raissi, G. P. Fontana, and W. Cheng: 'Twenty-year comparison of tissue and mechanical valve replacement', *The Journal of thoracic and cardiovascular surgery*, 2001, **122**(2), 257-269.
381. J. R. Fuchs, B. A. Nasseri, and J. P. Vacanti: 'Tissue engineering: a 21st-century solution to surgical reconstruction', *The Annals of thoracic surgery*, 2001, **72**(2), 577-591.
382. P. Fong, T. Shin'oka, R. I. Lopez-Soler, and C. Breuer: 'The use of polymer based scaffolds in tissue-engineered heart valves', *Progress in Pediatric Cardiology*, 2006, **21**(2), 193-199.
383. S. Ravi, Z. Qu, and E. L. Chaikof: 'Polymeric Materials for Tissue Engineering of Arterial Substitutes', *Vascular*, 2009, **17**(Suppl 1), S45-S54.
384. R. Nazir: 'Collagen–hyaluronic acid based interpenetrating polymer networks as tissue engineered heart valve', *Materials Science and Technology*, 2016, **32**(9), 871-882.
385. J. De Boer, C. Van Blitterswijk, P. Thomsen, J. Hubbell, R. Cancedda, J. D. de Bruijn, A. Lindahl, J. Sohier, and D. F. Williams: 'Tissue Engineering', 2008, Elsevier Science.
386. O. Olatunji: 'Natural Polymers: Industry Techniques and Applications', 2015, Springer International Publishing.
387. X. Yu, C. Tang, S. Xiong, Q. Yuan, Z. Gu, Z. Li, and Y. Hu: 'Modification of collagen for biomedical applications: a review of physical and chemical methods', *Current Organic Chemistry*, 2016, **20**(17), 1797-1812.
388. A. Nakada, K. Shigeno, T. Sato, T. Hatayama, M. Wakatsuki, and T. Nakamura: 'Optimal dehydrothermal processing conditions to improve biocompatibility and

durability of a weakly denatured collagen scaffold', *Journal of Biomedical Materials Research Part B: Applied Biomaterials*, 2016.

389. V. Charulatha and A. Rajaram: 'Influence of different crosslinking treatments on the physical properties of collagen membranes', *Biomaterials*, 2003, **24**(5), 759-767.
390. S. Rimdusit, K. Somsaeng, P. Kewsuwan, C. Jubsilp, and S. Tiptipakorn: 'Comparison of gamma radiation crosslinking and chemical crosslinking on properties of methylcellulose hydrogel', *Engineering Journal*, 2012, **16**(4), 15-28.
391. C. A. Acevedo, E. Sánchez, P. Díaz-Calderón, J. J. Blaker, J. Enrione, and F. Quero: 'Synergistic effects of crosslinking and chitosan molecular weight on the microstructure, molecular mobility, thermal and sorption properties of porous chitosan/gelatin/hyaluronic acid scaffolds', *Journal of Applied Polymer Science*, 2017, **134**(18).
392. M. Osmond, S. M. Bernier, M. B. Pantcheva, and M. D. Krebs: 'Collagen and collagen-chondroitin sulfate scaffolds with uniaxially aligned pores for the biomimetic, three-dimensional culture of trabecular meshwork cells', *Biotechnology and Bioengineering*, 2017, **114**(4), 915-923.
393. J. Kozlowska and A. Sionkowska: 'Effects of different crosslinking methods on the properties of collagen-calcium phosphate composite materials', *Int J Biol Macromol*, 2015, **74**, 397-403.
394. J. Kozlowska, A. Sionkowska, A. M. Osyczka, and M. Dubiel: 'Stabilizing effect of carbodiimide and dehydrothermal treatment crosslinking on the properties of collagen/hydroxyapatite scaffolds', *Polymer International*, 2017, **66**(8), 1164-1172.
395. T. Tokatlian, C. Cam, and T. Segura: 'Non-viral DNA delivery from porous hyaluronic acid hydrogels in mice', *Biomaterials*, 2014, **35**(2), 825-835.
396. C. Smadar, R. Emil, and S. Yulia: 'Cardiac Tissue Engineering: Principles, Materials, and Applications', 200; 2012, Morgan & Claypool.
397. B. Balakrishnan and R. Banerjee: 'Biopolymer-Based Hydrogels for Cartilage Tissue Engineering', *Chemical Reviews*, 2011, **111**(8), 4453-4474.
398. W. D. Merryman, H. Y. Huang, F. J. Schoen, and M. S. Sacks: 'The effects of cellular contraction on aortic valve leaflet flexural stiffness', *J Biomech*, 2006, **39**(1), 88-96.
399. T. Jiao, R. J. Clifton, G. L. Converse, and R. A. Hopkins: 'Measurements of the Effects of Decellularization on Viscoelastic Properties of Tissues in Ovine, Baboon, and Human Heart Valves', *Tissue Engineering. Part A*, 2012, **18**(3-4), 423-431.

400. T. Jiao, R. J. Clifton, G. L. Converse, and R. A. Hopkins: 'Measurements of the effects of decellularization on viscoelastic properties of tissues in ovine, baboon, and human heart valves', *Tissue Eng Part A*, 2012, **18**(3-4), 423-431.

401. A. Kusumi and K. Suzuki: 'Toward understanding the dynamics of membrane-raft-based molecular interactions', *Biochimica et Biophysica Acta (BBA) - Molecular Cell Research*, 2005, **1746**(3), 234-251.

402. C. Silioc, A. Maleki, K. Zhu, A.-L. Kjøniksen, and B. Nyström: 'Effect of Hydrophobic Modification on Rheological and Swelling Features during Chemical Gelation of Aqueous Polysaccharides', *Biomacromolecules*, 2007, **8**(2), 719-728.

403. T. H. Kasai-Brunswick, A. R. d. Costa, R. A. Q. Barbosa, B. Farjun, F. C. P. Mesquita, D. Silva dos Santos, I. P. Ramos, G. Suhett, G. V. Brasil, S. T. d. Cunha, J. O. R. Brito, J. d. A. Passipieri, A. B. Carvalho, and A. C. Campos de Carvalho: 'Cardiosphere-derived cells do not improve cardiac function in rats with cardiac failure', *Stem Cell Research & Therapy*, 2017, **8**, 36.

404. R. E. Redgrave, S. Tual-Chalot, B. J. Davison, E. Singh, D. Hall, M. M. Amirrasouli, D. Gilchrist, A. Medvinsky, and H. M. Arthur: 'Cardiosphere-Derived Cells Require Endoglin for Paracrine-Mediated Angiogenesis', *Stem Cell Reports*, 2017, **8**(5), 1287-1298.

405. N. Gundiah, P. B. Matthews, R. Karimi, A. Azadani, J. Guccione, T. S. Guy, D. Saloner, and E. E. Tseng: 'Significant material property differences between the porcine ascending aorta and aortic sinuses', *The Journal of heart valve disease*, 2008, **17**(6), 606-613.

406. G. W. Hastings: 'Cardiovascular Biomaterials', 2012, Springer London.

407. N. Masoumi, N. Annabi, A. Assmann, B. L. Larson, J. Hjortnaes, N. Alemdar, M. Kharaziha, K. B. Manning, J. E. Mayer, and A. Khademhosseini: 'Tri-layered elastomeric scaffolds for engineering heart valve leaflets', *Biomaterials*, 2014, **35**(27), 7774-7785.

408. P. J. da Silva Bartolo, M. A. Jorge, F. da Conceicao Batista, H. A. Almeida, J. M. Matias, J. C. Vasco, J. B. Gaspar, M. A. Correia, N. C. Andre, and N. F. Alves: 'Virtual and Rapid Manufacturing: Advanced Research in Virtual and Rapid Prototyping', 2007, CRC Press.

409. A. A. Shetty, S. J. Kim, N. Nakamura, and M. Brittberg: 'Techniques in Cartilage Repair Surgery', 2014, Springer Berlin Heidelberg.

410. L. Bidault, M. Deneufchatel, M. Hindié, C. Vancaeyzeele, O. Fichet, and V. Larreta-Garde: 'Fibrin-based interpenetrating polymer network biomaterials with tunable biodegradability', *Polymer*, 2015, **62**, 19-27.

411. H. T. Peng, L. Martineau, and P. N. Shek: 'Hydrogel–elastomer composite biomaterials: 1. Preparation of interpenetrating polymer networks and in vitro characterization of swelling stability and mechanical properties', *Journal of Materials Science: Materials in Medicine*, 2007, **18**(6), 975-986.

412. A. Chan, P. Boughton, A. Ruys, and M. Oyen: 'An interpenetrating network composite for a regenerative spinal disc application', *Journal of the mechanical behavior of biomedical materials*, 2017, **65**, 842-848.

413. N. Naseri, B. Deepa, A. P. Mathew, K. Oksman, and L. Girandon: 'Nanocellulose-Based Interpenetrating Polymer Network (IPN) Hydrogels for Cartilage Applications', *Biomacromolecules*, 2016, **17**(11), 3714-3723.

414. W. Liu, C. Deng, C. R. McLaughlin, P. Fagerholm, N. S. Lagali, B. Heyne, J. C. Scaiano, M. A. Watsky, Y. Kato, R. Munger, N. Shinozaki, F. Li, and M. Griffith: 'Collagen-phosphorylcholine interpenetrating network hydrogels as corneal substitutes', *Biomaterials*, 2009, **30**(8), 1551-1559.

415. B. Hammouda: 'SANS from polymers—review of the recent literature', *Journal of Macromolecular Science®, Part C: Polymer Reviews*, 2010, **50**(1), 14-39.

416. Y. Mao, K. Liu, C. Zhan, L. Geng, B. Chu, and B. S. Hsiao: 'Characterization of Nanocellulose Using Small-Angle Neutron, X-ray, and Dynamic Light Scattering Techniques', *The Journal of Physical Chemistry B*, 2017, **121**(6), 1340-1351.

417. R. C. Masters, A. J. Pearson, T. S. Glen, F.-C. Sasam, L. Li, M. Dapor, A. M. Donald, D. G. Lidzey, and C. Rodenburg: 'Sub-nanometre resolution imaging of polymer-fullerene photovoltaic blends using energy-filtered scanning electron microscopy', *Nature communications*, 2015, **6**.

418. M. S. Sacks and A. P. Yoganathan: 'Heart valve function: a biomechanical perspective', *Philosophical Transactions of the Royal Society B: Biological Sciences*, 2007, **362**(1484), 1369-1391.

419. T. V. Lam: 'The mechanical properties of native porcine aortic and pulmonary heart valve leaflets', University of Pittsburgh, 2005.

420. S. L. Bellis: 'Advantages of RGD peptides for directing cell association with biomaterials', *Biomaterials*, 2011, **32**(18), 4205-4210.

421. M. Tallawi, E. Rosellini, N. Barbani, M. G. Cascone, R. Rai, G. Saint-Pierre, and A. R. Boccaccini: 'Strategies for the chemical and biological functionalization of scaffolds for cardiac tissue engineering: a review', *Journal of the Royal Society Interface*, 2015, **12**(108), 20150254.
422. M. J. Cooke, S. R. Phillips, D. S. Shah, D. Athey, J. H. Lakey, and S. A. Przyborski: 'Enhanced cell attachment using a novel cell culture surface presenting functional domains from extracellular matrix proteins', *Cytotechnology*, 2008, **56**(2), 71-79.
423. R. Duelen and M. Sampaolesi: 'Stem Cell Technology in Cardiac Regeneration: A Pluripotent Stem Cell Promise', *EBioMedicine*, 2017, **16**, 30-40.
424. M. T. Alrefai, D. Murali, A. Paul, K. M. Ridwan, J. M. Connell, and D. Shum-Tim: 'Cardiac tissue engineering and regeneration using cell-based therapy', *Stem Cells and Cloning : Advances and Applications*, 2015, **8**, 81-101.
425. F. Colazzo, A. H. Chester, P. M. Taylor, and M. H. Yacoub: 'Induction of mesenchymal to endothelial transformation of adipose-derived stem cells', *The Journal of heart valve disease*, 2010, **19**(6), 736-744.
426. W. Huang, D. Z. Xiao, Y. Wang, Z. X. Shan, X. Y. Liu, Q. X. Lin, M. Yang, J. Zhuang, Y. Li, and X. Y. Yu: 'Fn14 promotes differentiation of human mesenchymal stem cells into heart valvular interstitial cells by phenotypic characterization', *Journal of cellular physiology*, 2014, **229**(5), 580-587.
427. C. Gualandi: 'Porous Polymeric Bioresorbable Scaffolds for Tissue Engineering', 2011, Springer Berlin Heidelberg.
428. V. Nedovic and R. Willaert: 'Applications of Cell Immobilisation Biotechnology', 2005, Springer Netherlands.